Key innate immune components controlling intracellular infection

Benard, E.L.

Key innate immune components controlling intracellular infection

Erica L. Benard

Printed and bound by: Wöhrmann print service

ISBN: 978-94-6203-657-4

Key innate immune components controlling intracellular infection

Proefschrift

Ter verkrijging van
de graad van Doctor aan de Universiteit Leiden
op gezag van Rector Magnificus prof.mr. C.J.J.M. Stolker,
volgens besluit van het College voor Promoties
te verdedigen op donderdag 25 september 2014
klokke 13.45 uur

door

Erica L. Benard
geboren te Westville, Zuid Afrika
op 5 maart 1986

Promotiecommissie:

Promotor:	Prof. Dr. H.P. Spaink	
Co-promotor:	Dr. A.H. Meijer	
Overige leden:	Prof. Dr. C.J. ten Cate	
	Prof. Dr. T.H.M. Ottenhoff	(Leids Universitair Medisch Centrum)
	Prof. Dr. Ir. G.F. Wiegertjes	(Wageningen University)
	Dr. P.M. Elks	(University of Sheffield)

Table of contents

Chapter 1	Outline of the thesis	***11***
Chapter 2	Infection of zebrafish embryos with intracellular bacterial pathogens	***17***
Chapter 3	A morpholino knockdown screen for genes involved in mycobacterium infection	***35***
Chapter 4	Time-resolved transcriptome profiling of the zebrafish host innate immune response to mycobacterium infection	***59***
Chapter 5	Phagocytosis of mycobacteria by zebrafish macrophages is dependent on the scavenger receptor Marco, a key control factor of pro-inflammatory signalling	***97***
Chapter 6	The macrophage-expressed perforins Mpeg1 and Mpeg1.2 have anti-bacterial functions in zebrafish	***125***
Chapter 7	Summary and discussion	***159***
	Samenvatting	***169***
	List of publications	***173***
	Curriculum vitae	***175***

“Science knows no country, because knowledge belongs to humanity, and is the torch which illuminates the world”

- Louis Pasteur

Chapter 1

Outline of the thesis

Zebrafish as a model for innate immunity studies

The zebrafish is an excellent model to study vertebrate innate immunity. Zebrafish embryos are fertilised externally and develop an innate immune system within the first days after fertilisation. The first innate immune cell type to develop is the macrophage, which is already functional in one-day-old zebrafish embryos. At this stage, macrophages are capable of phagocytosing pathogens and tissue debris. Neutrophils are the second innate immune cell type to develop and produce anti-microbial proteins within their characteristic granules by 2 days post fertilisation. These cells are the first responders to inflammatory stimuli and are also efficient scavengers of bacteria in infected tissues. The first immature T-cells can be detected in four day old larvae, but it takes several weeks before zebrafish also have antibody-producing B-cells and a fully functional adaptive immune system. Using the zebrafish as a host model has several advantages. Firstly, the temporal separation of innate and adaptive immunity allows us to study the isolated function of innate immune factors during infection. Secondly, various transgenic lines are available that have fluorescently labelled macrophages, neutrophils, or other immune cell types, and the behaviour of these cells can be imaged in real-time and with excellent resolution during the early life stages when zebrafish are transparent. Thirdly, the recently published sequenced genome of the zebrafish allows us to apply state-of-the-art RNA sequencing techniques to study gene expression profiles. Fourthly, many genetic tools are available to create temporary knockdowns or permanent mutations of genes of interest. All these tools combined make the zebrafish embryo an ideal model host to study the function of innate immune genes during pathogenic infections.

Mycobacterial infection studies in zebrafish

The zebrafish has become a well-accepted model to study the function of innate immunity during mycobacterial infection. Mycobacteria are the causative agents of life-threatening human diseases, including tuberculosis and leprosy. Infection with *Mycobacterium marinum*, a natural pathogen of fish and a close relative of the human pathogen *Mycobacterium tuberculosis*, leads to granuloma formation in zebrafish embryos, the key hallmark of tuberculosis. Using *M. marinum* infection in zebrafish embryos led to the discovery that innate immune factors are sufficient to initiate granuloma formation, a process that was previously thought to develop only in the presence of adaptive immunity. Furthermore, research in zebrafish has changed the view of the tuberculous granuloma, which had been historically regarded strictly as a host defence structure, but is now known to play an important role in the dissemination and expansion of mycobacterial infection (Ramakrishnan, Nat Rev Immunol 12:352, 2012). These findings illustrate the importance of using various host models to contribute to our understanding of mycobacterial pathogenesis. Zebrafish models for a wide variety of other pathogens have also been established and their use is leading to new mechanistic insights into host-pathogen interactions and is inspiring novel therapeutic strategies for infectious disease treatment (Meijer et al., Cell Microbiol 16:39, 2014).

Overview of this thesis

This thesis is focused on the innate immune defence mechanisms responsible for controlling mycobacterial growth after infection. In addition to *M. marinum,* another intracellular bacterial pathogen, *Salmonella typhimurium*, is used as a comparative model. To study the host immune responses to infection, the pathogens are delivered into the embryo by various injection techniques to create a rapid, systemic infection or a localised infection. Chapter 2 demonstrates a bacterial preparation protocol for injection, various injection techniques, and techniques for confocal imaging. We also provide representative results for the used injection methods demonstrating their versatility.

To identify candidate genes that play a role in controlling *M. marinum* infection during the early stage of infection while granulomas are formed, a morpholino knockdown screen was performed which is described in chapter 3. Morpholinos are specifically designed molecules that block correct translation of RNA of a gene of interest which leads to a dysfunctional or non-functional protein. The candidate genes used in this screen were chosen based on previous transcriptome data of zebrafish embryonic macrophages and *M. marinum* infection studies. The screen started with seventeen candidate genes and resulted in five positive hits: four leading to an increased infection and one leading to a decreased infection after knockdown. The detailed function of three of the five positive hit genes are further described in the following chapters of this thesis.

To provide a detailed description of the host's innate immune response to *M. marinum* infection, zebrafish gene expression levels were analysed by RNA sequencing at various time points during infection ranging from 2 hours until 5 days after infection and correlated with imaging data of the process of pathogenesis. These results are presented in chapter 4 where an early-, mid- and late-phase immune response to *M. marinum* is characterised. One of the transcription factors that we found to be induced during the early- and late-phase of infection is *atf3* (*a*ctivating *t*ranscription *f*actor *3*). Knockdown of *atf3* in the zebrafish embryo resulted in an increased migration of leukocytes towards local inflammation sites and a decreased bacterial burden, indicating that that the induction of *atf3* during *M. marinum* infection antagonises an effective innate immune control of this pathogen.

Directly after infection, immune cells detect the presence of pathogen-associated molecular patterns on the surface of microbes. Scavenger receptors on the cell surface of macrophages play an important role in this process through their ability to not only bind microbial ligands, but also induce phagocytosis. In chapter 5, it is demonstrated that the scavenger receptor Marco (macrophage receptor with collagenous structure) is a key player in the rapid phagocytosis of *M. marinum* and we use gene expression analysis in combination with gene knockdown studies to show that it is also essential

in the establishment of an initial transient pro-inflammatory response to *M. marinum* infection.

Once phagocytosed, *M. marinum* is capable of avoiding killing mechanisms of the host cell and can continue to grow within macrophages. This is the period when Membrane Attack Complex/Perforin (MACPF) proteins are involved in killing intracellular bacteria by their pore-forming activities. In **chapter 6**, we reveal the regulatory mechanisms and function of two macrophage specific genes, *mpeg1* and *mpeg1.2* (**m**acro**p**hage **e**xpressed **g**ene **1.2**), and illustrate that both genes encode proteins with MACPF domains. Combined results of infection experiments with *M. marinum* and *S. typhimurium* during knockdown conditions of *mpeg1* and *mpeg1.2* support their anti-bacterial function.

The findings presented in this thesis are summarised and discussed in **chapter 7**. The results complement knowledge obtained from other model organisms by providing new insights into both counteracting and supporting mechanisms underlying the innate immune response. An overview is presented of the key players in innate immune defences identified in this study. This overview highlights how an integrated study of transcriptional responses and morpholino knockdown studies can rapidly lead to functional information of a group of key genes involved in the innate immune defence system.

Chapter 2

Infection of zebrafish embryos with intracellular bacterial pathogens

Erica L. Benard[1], Astrid M. van der Sar[2], Felix Ellett[3], Graham J. Lieschke[3], Herman P. Spaink[1], Annemarie H. Meijer[1]

[1] Institute of Biology Leiden, Leiden University
[2] Medical Microbiology and Infection Control, VU University Medical Center
[3] Australian Regenerative Medicine Institute, Monash University

Journal of Visualized Experiments, 2012

Abstract

Zebrafish (*Danio rerio*) embryos are increasingly used as a model for studying the function of the vertebrate innate immune system in host-pathogen interactions [1]. The major cell types of the innate immune system, macrophages and neutrophils, develop during the first days of embryogenesis prior to the maturation of lymphocytes that are required for adaptive immune responses. The ease of obtaining large numbers of embryos, their accessibility due to external development, the optical transparency of embryonic and larval stages, a wide range of genetic tools, extensive mutant resources and collections of transgenic reporter lines, all add to the versatility of the zebrafish model. *Salmonella enterica* serovar Typhimurium *(S. typhimurium)* and *Mycobacterium marinum* can reside intracellularly in macrophages and are frequently used to study host-pathogen interactions in zebrafish embryos. The infection processes of these two bacterial pathogens are interesting to compare because *S. typhimurium* infection is acute and lethal within one day, whereas *M. marinum* infection is chronic and can be imaged up to the larval stage [2, 3]. The site of micro-injection of bacteria into the embryo (fig. 1) determines whether the infection will rapidly become systemic or will initially remain localized. A rapid systemic infection can be established by micro-injecting bacteria directly into the blood circulation via the caudal vein at the posterior blood island or via the Duct of Cuvier, a wide circulation channel on the yolk sac connecting the heart to the trunk vasculature. At 1 dpf, when embryos at this stage have phagocytically active macrophages but neutrophils have not yet matured, injecting into the blood island is preferred. For injections at 2-3 dpf, when embryos also have developed functional (myeloperoxidase-producing) neutrophils, the Duct of Cuvier is preferred as the injection site. To study directed migration of myeloid cells towards local infections, bacteria can be injected into the tail muscle, otic vesicle, or hindbrain ventricle [4-6]. In addition, the notochord, a structure that appears to be normally inaccessible to myeloid cells, is highly susceptible to local infection [7]. A useful alternative for high-throughput applications is the injection of bacteria into the yolk of embryos within the first hours after fertilization [8]. Combining fluorescent bacteria and transgenic zebrafish lines with fluorescent macrophages or neutrophils creates ideal circumstances for multi-color imaging of host-pathogen interactions. This video article will describe detailed protocols for intravenous and local infection of zebrafish embryos with *S. typhimurium* or *M. marinum* bacteria and for subsequent fluorescence imaging of the interaction with cells of the innate immune system. The video can be viewed at:

http://www.jove.com/video/3781/infection-of-zebrafish-embryos-with-intracellular-bacterial-pathogens

Protocol Text

1) Prepare injection needles

1.1) Prepare borosilicate glass microcapillary injection needles (Harvard Apparatus, 300038, 1 mm O.D. × 0.78 mm I.D.) using a micropipette puller device (Sutter Instruments Inc., Flaming/Brown p-97 with the following settings for a longer tip: air pressure 400; heat 610; pull 40; velocity 50; time 30 and with the following settings for a shorter tip: air pressure 500; heat 510; pull 100; velocity 200; time 60).

1.2) Break off the needle tip with fine tweezers to obtain a tip opening diameter of 5-10 µm. It is advisable to bevel the needle tip opening under a 45 degrees angle with a microgrinder (Narishige Inc., EG-400) to yield a sharper tip. This will facilitate puncturing the epidermal layer and thus result in more reproducible injections with less tissue damage than with blunt needles. Longer tipped needles are preferred for caudal vein (step 5) and Duct of Cuvier (step 6.1) injections and shorter tipped needles are preferred for the other injection protocols (steps 6.2-6.6).

2) Prepare *S. typhimurium* inoculum

2.1) Plate out *S. typhimurium* from a -80°C glycerol stock onto LB agar plates (with appropriate antibiotics to select for fluorescence expression vectors) and incubate overnight at 37°C.

2.2) Pick individual fluorescently positive colonies and resuspend them to the desired concentration (see protocols 5 and 6) in sterile phosphate-buffered saline (PBS), optionally containing 0.085% (v/v) phenol red (Sigma-Aldrich) to aid visualization of the injection process. Directly use the fresh suspension for the injection or prepare glycerol stocks. To prepare glycerol stocks, spin down the freshly made injection stock with the desired concentration of bacteria and concentrate the stock by resuspending the pellet in half the starting volume in sterile 20% (v/v) glycerol (Sigma-Aldrich) in PBS. Store the glycerol stock at -80˚C. Dilute the glycerol stock 1:1 (v/v) prior to injection in sterile PBS, optionally containing 0.17% phenol red.

2.3) Vortex the bacterial suspension well to avoid clumping.

2.4) Load the inoculum into the microcapillary needle using a microloader tip (Eppendorf, 5242956.003).

2.5) Due to the relatively large size of *S. typhimurium* bacteria and their bright Ds-RED fluorescence when using the pGMDs3 expression vector [3] (strain available upon request), individual bacterial cells can easily be counted with a fluorescence stereomicroscope in order to set the injection dose. To this end, inject 1 nL into a drop of PBS on an agar plate, count the fluorescent bacteria, and calculate the injection volume that is required

to obtain the desired bacterial dose (preferably keep the injection volume between 1-2 nL). Inject the embryos with *S. typhimurium* via the selected route (see protocols 5 and 6).

3) Prepare *M. marinum* inoculum

3.1) Keep the *M. marinum* strain growing on Difco Middlebrook 7H10 agar (BD and company) supplemented with 10% oleic acid-albumin-dextrose-catalase (OADC, BD and company), 0.5% glycerol, and with appropriate antibiotics to select for fluorescence expression vectors (strains available upon request [9]), so there is always a fresh stock.

3.2) Pick a colony of *M. marinum* and resuspend it in Difco Middlebrook 7H9 broth (BD and company) supplemented with 10% albumin-dextrose-catalase (ADC, BD and company) and 0.05% Tween 80 (Sigma-Aldrich) and the appropriate antibiotics. Check that the optical density (OD) at 600 nm is 0.2 - 0.3 and let it grow statically overnight at 28.5˚C. The generation time of *M. marinum* is approximately 4-6 h, varying according to the strain.

3.3) Measure the OD at 600 nm again on the day of injections. An OD600 of 1 corresponds to approximately 10^8 *M. marinum*/mL (this may vary according to the bacterial strain used and thus should be based on a growth curve for the particular strain).

3.4) Harvest the bacteria when they are in logarithmic phase (do not let the OD600 exceed 1.00) by centrifuging and washing them three times in sterile PBS.

3.5) Measure the OD600 again of the bacterial suspension in PBS, spin down, and resuspend the bacteria to the desired concentration (see protocols 5 and 6) in PBS or in 2% Polyvinylpyrrolidone (PVP40) in PBS (w/v), which improves homogeneity of the bacterial suspension. Phenol red (Sigma-Aldrich) may be added to a concentration of 0.085% to aid visualization of the injection process. Directly use the fresh suspension for the injection or prepare glycerol stocks. To prepare glycerol stocks spin down the freshly made injection stock with the desired concentration of bacteria and concentrate the stock by resuspending the pellet in half the starting volume in sterile 20% glycerol in PBS. Store the glycerol stock at -80˚C. Dilute the glycerol stock 1:1 (v/v) in sterile PBS, optionally containing 4% PVP40 and/or 0.17% phenol red.

4) Prepare zebrafish embryos for injections

4.1) Set up zebrafish breeding pairs and collect embryos as shown in [10]. Keep embryos in a Petri dish filled with egg water (60 µg/mL Sea salts; ca. 60 embryos/dish) and incubate at 28.5°C.

4.2) If required, add 0.003% *N*-Phenylthiourea (PTU, Sigma-Aldrich) to the egg water when the embryos are approximately 12 hpf to prevent melanization.

4.3) Around 24 hours post fertilization (hpf), dechorionate the embryos with fine tweezers (Fine Science Tools Inc., Dumont #5 Forceps - Inox Biology).

4.4) Keep the embryos in a Petri dish filled with egg water and with a layer of 1% agarose on the bottom to prevent embryos from sticking to the plastic surface.

4.5) Anesthetize the embryos with 200 µg/mL buffered 3-aminobenzoic acid (Tricaine, Sigma-Aldrich) approximately 10 min prior to injections.

5) Intravenous injection of bacteria into one-day old embryos

5.1) Stage the embryos at 28 hpf [11] by checking for consistent blood circulation, beginning of pigmentation in the eye, a straight tail, and the heart being positioned just ventrally to the eye.

5.2) Anesthetize the embryos, see step 4.5.

5.3) Load the needle with the bacterial inoculum using a microloader tip.

5.4) Mount the loaded needle onto a micromanipulator (Sutter Instrument, MM-33) connected to a stand (World precision Instruments, M10L magnetic stand) and position it under a stereo microscope (Leica M50, achromat 1x objective 0,15 NA, transmitted light base TL ST). Set the injection time to 0.2 s and the compensation pressure to 15 hPa (Eppendorf, Femtojet). Adjust the injection pressure between 700 and 900 hPa to obtain the correct injection volume for the needle used. Adjust the drop size to match the desired diameter with the help of a scale bar on a microscope slide or in the ocular. For size determination the drop can be injected into mineral oil on a microscope slide, or the size can be estimated by injecting into the air, which leaves the drop hanging on the needle tip. The radius of a drop of 1 nL is 0.062 mm ($V = 4/3\ \pi\ r^3$).

5.5) Set the micromanipulator with the loaded needle into the correct position prior to injecting (i.e. approximately at a 45° angle with respect to the injection plate surface) and only move it back and forth to inject.

5.6) The anesthetized embryos are pipetted onto a flat 1% agarose injecting plate and excess egg water is removed, allowing surface tension to hold the embryos in place during injections. Use a hair loop tool (fig. 2) to line up the embryos. Orientate the injection plate by hand during injections to place the embryos into the preferred position for inserting the needle, i.e. with their tails pointing towards the needle tip.

5.7) Place the needle tip directly above the caudal vein close to the urogenital opening (fig. 1A), pierce the periderm with the needle tip and inject the desired dose of bacteria; we use ca. 250 cfu of *S. typhimurium* wild type (wt) strain SL1027, containing the Ds-RED expression vector pGMDs3, and ca. 120 cfu of *M. marinum* strain Mma20. The injected bacterial suspension will follow the blood flow through the caudal vein towards the

heart. Monitor if the injection was performed correctly by checking for an expanding volume of the vascular system directly after the pulse [2]. For dose-response experiments, 2-3 consecutive injections can be performed without extracting the needle.

5.8) Frequently check that the injection volume remains the same during the experiment. To provide a control for the consistency of the injections throughout the experiment, inject a drop of bacteria directly into a sterile PBS drop on bacterial growth medium after approximately every 30th embryo injection. Plate out this drop and count the bacterial colonies after incubation to determine the colony forming units (cfu) in the injection volume.

5.9) Use a fluorescent stereomicroscope (protocol 7) to observe individual fluorescent *S. typhimurium* cells circulating in the bloodstream directly after injection, and discard embryos that are not properly injected. Individual fluorescent *M. marinum* bacteria cannot be observed by stereo fluorescence microscopy directly after injections, but fluorescent aggregates of infected cells should be visible by 2 days post infection (dpi).

6) Alternative routes of infection

6.1) Duct of Cuvier injection: line up anesthetized embryos (2-3 dpf) on a flat 1% agarose injecting plate as for caudal vein injections (see 5.6). Orientate the injection plate by hand during injections to place the embryos into the preferred position for inserting the needle, i.e. diagonally under a 45˚ angle so that the Duct of Cuvier can be approached by the needle tip from the dorsal side of the embryo (fig. 1B). Insert the needle into the starting point of the Duct of Cuvier just dorsal to the location where the duct starts broadening over the yolk sac and inject 100-200 bacteria (1-3 nL). The injection is correct if the volume within the duct expands directly after the pulse and the yolk sac is not ruptured. As for caudal vein injections (see 5.7), several consecutive injections can be performed without extracting the needle.

6.2) Hindbrain ventricle injection: line up anesthetized embryos (32 hpf) on a flat 1% agarose injecting plate such that the embryos are positioned with their dorsal side towards the needle tip. Insert the needle into the hindbrain ventricle from an anterior position without touching the neuroepithelium (fig. 1C) and inject 20-100 bacteria (0.5-1 nL). To practise the procedure, use a fluorescent dye (such as Texas-Red Dextran) as shown in [13].

6.3) Tail muscle injection: position anesthetized embryos (1-2 dpf) as for caudal vein injections (see 5.6). Adjust the micromanipulator with the loaded needle to an angle of approximately 65° with respect to the injection plate surface. Inject a bacterial suspension (0.5-1 nL) containing 20- 50 cfu into the muscle above the urogenital opening (fig. 1D) without causing damage to the notochord or blood vessels.

6.4) Otic vesicle injection: position anesthetized embryos (2-3 dpf) as for caudal vein injections (see 5.6). Adjust the micromanipulator with the loaded needle to an angle of approximately 65° with respect to the injection plate surface. Inject approximately 20 bacteria (0.5 nL) into the otic vesicle (fig. 1E) with low pressure to avoid local tissue rupture.

6.5) Notochord injection: line up anesthetized embryos (1-2 dpf) on a flat 1% agarose injecting plate such that the embryos are positioned with their tail pointing away from the needle tip. Insert the needle through the tail muscle tissue into the notochord (fig. 1F) and inject approximately 20-50 bacteria (maximal 0.5 nL). Take care not to inject too much volume to avoid rupture of the notochord.

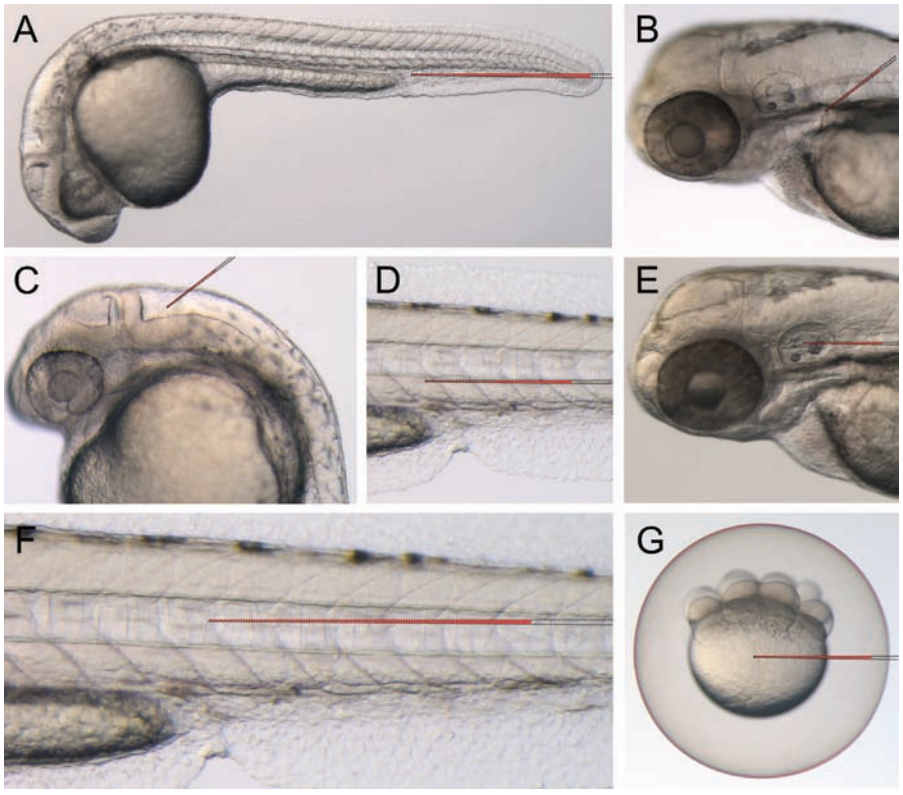

Figure 1. Overview of injection methods used for establishing systemic or local infections in zebrafish embryos. (A-B) Intravenous injections for establishing a rapid systemic infection are performed into the caudal vein at the posterior blood island at 1 dpf (A) or into the Duct of Cuvier at 2-3 dpf (B). (C-E) Local injections for studying macrophage and neutrophil chemotaxis are performed into the hindbrain ventricle at 1 dpf (C), the tail muscle at 1-2 dpf (D) or the otic vesicle at 2-3 dpf (E). (F) Injections to create an infection apparently inaccessible to phagocytes are performed into the notochord at 1-2 dpf. (G) Injections to create an early systemic infection with slow growing bacteria such as *M. marinum* can be performed into the yolk at the 16-1000 cell stage. All images were taken with a Leica M165C, PLANAPO 1.0x connected to a Leica DFC420 camera (Leica 10446307 0.8x).

6.6) Yolk injection: position eggs containing embryos at the 16 to 1000 cell stage on a 1% agarose injecting plate with rectangular or *V*-shaped channels made with a channel mold [12] or online at http://zfin.org/zf_info/zfbook/chapt5/5.1.html. Pierce the needle through the chorion into the center of the yolk (fig. 1G) and inject 20-40 bacteria (1-2 nL). The use of 2% PVP40 carrier solution for the bacterial suspension (see step 3.5) is important to prevent early bacterial spread into the embryo.

7) Stereo imaging of the infection

7.1) Anesthetize the infected embryos in a 1% agarose layered Petri dish covered with egg water containing Tricaine (see 4.5).

7.2) Align the embryos in the correct position for imaging under a fluorescence stereo microscope with a hair loop tool (fig. 2). Before the swim bladder has inflated (1-5 dpf), the embryos will lie flat on their sides enabling lateral view imaging.

7.3) If a different position than the lateral view is required, mount the embryos in 1.5% methyl cellulose. Manipulate the embryo into the required position with a hair loop tool (fig. 2).

7.4) Return the embryos to egg water after imaging.

8) Confocal imaging of the infection

8.1) Place a drop of Low Melting Point agarose (Lonza Inc., 1.5% (w/v) in egg water) on the glass bottom of a WillCo-dish (WillCo Wells, GWSt-5040) if an inverted confocal microscope is used, or on a single cavity depression slide (Agar Scientific, L4090) if an upright confocal microscope is used.

8.2) Place the anesthetized embryo into the agarose drop with limited amount of egg water and manipulate the embryo into position with a hair loop tool (fig. 2). When using an inverted microscope it is important that the embryo's region of interest is flat against the glass bottom of the imaging dish. An upright microscope can be used in combination with water immersion or long distance dry objectives and the embryo should be positioned such that the region of interest is as close to the objective as possible.

8.3) Let the agarose solidify and submerge the agarose drop in egg water containing Tricaine (see 4.5). If an upright microscope is used, place a glass cover slip on top of the depression cavity (do not allow air bubbles to form).

8.4) Sequentially acquire fluorescence and transmission images.

8.5) Carefully remove the agarose from the embryo with fine tweezers and place the embryo back into egg water if it is required for further experiments.

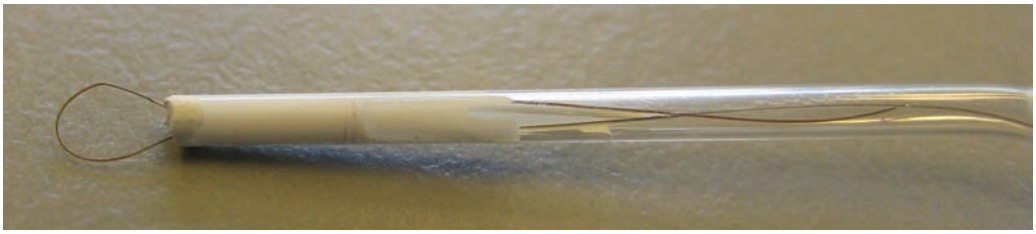

Figure 2. Hair loop tool. A piece of human hair is inserted as a loop into the opening of a Pasteur pipet and fixed in place with super glue or with Tipp-Ex. This provides a convenient tool for gently manipulating fragile zebrafish embryos.

Representative results

Injection of *Salmonella typhimurium* or *Mycobacterium marinum* bacteria into the blood island of embryos at 1 dpf results in the rapid phagocytosis by macrophages. The *mpeg1* gene has recently been identified as a faithful marker of embryonic macrophages, colocalizing with the well-established macrophage marker *csfr1* (*fms*) and not overlapping with neutrophil markers such as *mpx* (*mpo*) and *lyz* [4, 14]. For live imaging of bacterial phagocytosis we used transgenic lines in which the *mpeg1* promoter drives fluorescent protein expression in macrophages [14]. These transgenic lines either have the *mpeg1* promoter fused directly to the *gfp* gene, or employ a two-component system where the *mpeg1* promoter drives expression of the yeast Gal4 transcription factor that activates a second transgene with the Gal4 recognition sequence (UAS, upstream activating sequence) fused to the *kaede* gene. When the blood island injection (protocol 5; fig. 1A) is performed correctly, the bacteria will immediately flow through the blood circulation and spread throughout the embryo. Dissemination of the relatively large and brightly fluorescent Ds-RED labeled *S. typhimurium* bacteria can be imaged directly with a stereo fluorescence microscope (fig. 3A), and confocal imaging at 2 hpi shows that many bacteria are phagocytosed by fluorescent macrophages (fig. 3B-C). The injection of as little as 25 cfu of wild type *S. typhimurium* bacteria will result in a lethal infection, while a similar dose of bacteria of an avirulent strain, such as Ra, can be cleared by the embryonic immune system [3]. An injection dose of 250 cfu was used to determine transcriptional responses to *S. typhimurium* infection in the zebrafish embryo and demonstrated the induction of a strong pro-inflammatory gene expression response [15]. In contrast, the intravenous injection of *M. marinum* bacteria does not elicit a strong pro-inflammatory response, but leads to a persistent infection where infected macrophages form tight aggregates that are considered as the initial stages of granulomas, which are the hallmark of tuberculosis [2]. Confocal imaging of such a granuloma-like aggregate in the *tg*(*mpeg1:EGFP)* line at 5 dpi shows the intracellular growth of mCherry-labeled *M. marinum* bacteria inside the green fluorescent macrophages (fig. 3D-E).

Other routes of infection are useful for different purposes. Bacteria can be injected into the hindbrain ventricle at 32 hpf (fig. 1C), which is a compartment devoid of macrophages. Injection of 20-100 mCherry-labeled *M. marinum* bacteria into this

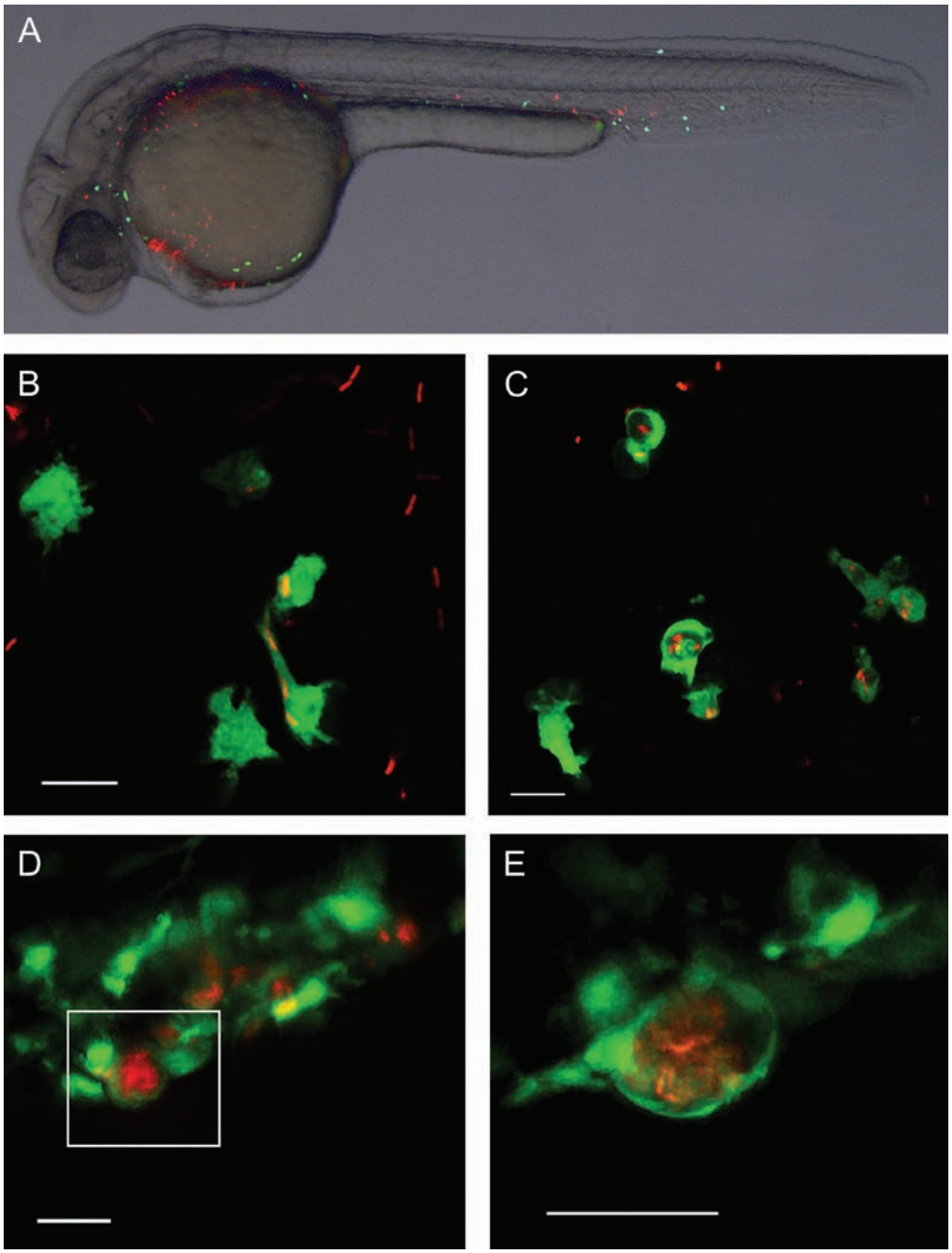

Figure 3. Intravenous injections of red fluorescent *Salmonella typhimurium* and *Mycobacterium marinum.* Ds-RED-labeled *S. typhimurium* SL1027 bacteria (A-C) and mCherry-labeled *M. marinum* Mma20 bacteria (D-E) were injected into the blood island of *tg(uas:kaede/mpeg1:gal4)* (A-C) or *tg(mpeg1:EGFP)* (D-E) zebrafish embryos at 28 hpf (D-E). (A) Stereo-fluorescence and bright-field overlay image showing dissemination of *S. typhimurium* in the blood circulation at

Figure 3 continued: 2 hpi (Leica MZ16FA microscope with Leica DFC420C camera). (B-C) Confocal z-stack projections showing red *S. typhimurium* bacteria phagocytosed by green macrophages at 2 hpi (Leica TCS SPE, HCX APO objective 40x 0.8 NA). Bacteria that are still extracellular can also be observed. (D) Confocal z-stack projection showing a granuloma-like aggregate containing *M. marinum* Mma20-infected and uninfected macrophages at 5 dpi (Leica TCS SPE, HCX APO 40x 0.8 NA). Macrophages in green and bacteria in red. (E) Confocal z-stack projection of an individual macrophage (green) with intracellular *M. marinum* bacteria (red). The area depicted in D by the white rectangle was imaged with a higher magnification objective (Leica TCS SPE, HCX PL APO 63x 1.2 NA). Scalebars: 20 µm.

compartment leads to the rapid infiltration by macrophages that phagocytose the bacteria (fig. 4A). Another method to study the directed migration of innate immune cells is injection of bacteria into the tail muscle (fig. 1D). However, tail muscle injections also cause tissue damage that by itself elicits some attraction of leukocytes. Such a wounding response can be avoided when carefully injecting a small volume (0.5-1 nL) into the otic vesicle (fig. 1E). As shown here by using the *tg(mpx:EGFP)i114* [16], injection of approximately 20 cfu of *S. typhimurium* into the otic vesicle leads to the attraction of neutrophils at 3 hpi (fig. 4D), while this response is not observed in PBS control injections (fig. 4E). The notochord, which appears to be resistant to infiltration by leukocytes, is a permissive compartment for the growth of *M. marinum* mutants that are strongly attenuated when injected in other tissues [7]; (fig. 4F). Finally, early injection of *M. marinum* into the yolk of embryos at the 16 to 1000 cell stage (fig. 1G) provides an alternative method to achieve a systemic infection. Following yolk injection of a dose of 20-40 cfu, *M. marinum* bacteria spread over several days into the embryonic tissues and form granuloma-like aggregates similar to those observed upon the conventional intravenous injection method [8]; (fig. 4G). The yolk injection method is not suitable for *S. typhimurium* infection, because its rapid growth in the yolk causes early lethality. The yolk infection method for *M. marinum* infection will be useful for high-throughput applications since it can be automated using an injection robot [8].

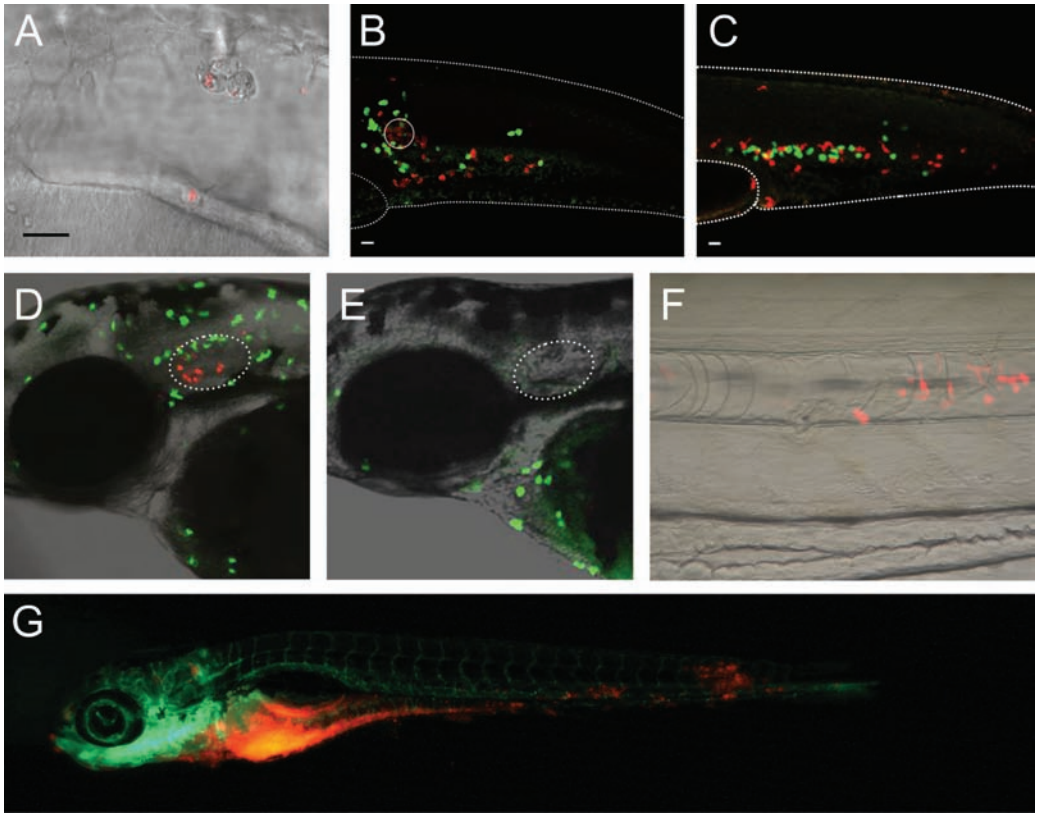

Figure 4. Alternative routes for infection of zebrafish embryos. (A) mCherry-labeled *M. marinum* Mma20 bacteria were injected into the hindbrain ventricle at 32 hpf. Fluorescence and transmission overlay image showing mCherry-labeled bacteria phagocytosed by macrophages at 5 hpi (Leica TCS SPE, HCX PL FLUO TAR 40.0x 0.7 NA). (B) *S. typhimurium* was injected into the tail muscle at 1 dpf. Attraction of myeloid cells to the injection site (white circle) is shown at 3 hpi by fluorescent in situ hybridization [4], (C) whereas in uninjected embryos there are normally no myeloid cells at this morphological site. Although the embryos do not contain mature neutrophils at this stage, two populations of myeloid cells can be distinguished, one expressing the macrophage marker *mfap4* (red) and one expressing the neutrophil marker *mpx* (green) (Leica TCS SPE, HC PL FLUOTAR 10.0x 0.3 NA). Fluorescence of the bacteria is lost after the in situ hybridization procedure. (D) Ds-RED-labeled *S. typhimurium* bacteria were injected into the otic vesicle of *tg(mpx:EGFP)i114* zebrafish at 2 dpf. Stereo-fluorescence and bright-field overlay image show that *mpx:EGFP* labeled neutrophils cells are attracted to the infected otic vesicle (dotted ellipse) at 3 hpi, (E) whereas control injection of PBS into the otic vesicle of *tg(mpx:EGFP)* zebrafish does not show attraction of neutrophils to the uninfected otic vesicle (dotted ellipse) (Leica MZ16FA with Leica DFC420C camera). (F) mCherry-labeled *M. marinum* bacteria of the attenuated E11 *eccCb1*::tn mutant strain [17] were injected into the notochord at 1 dpf. Proliferation inside the notochord was imaged at 5 dpi (Leica MZ16FA microscope with DC500 camera). (G) mCherry-labeled *M. marinum* E11 bacteria were injected into the yolk of 16-cell stage zebrafish embryos of the *tg(fli1a:EGFP)* line that expresses *gfp* in endothelial cells of blood and lymph vessels. Formation of granuloma-like aggregates of infected cells in the tail region is observed at 5 dpi (Leica MZ16FA microscope with Leica DFC420C camera; image from[8]).

Discussion

The infection methods described in this article are frequently used to study the function of host innate immunity genes or bacterial virulence genes [1]. The intravenous micro-injection methods (protocols 5 and 6.1) are used most often for such studies. The caudal vein at the posterior blood island is the most convenient location for intravenous injection of 1-day-old embryos. As the caudal vein becomes more difficult to penetrate at later stages, we prefer the Duct of Cuvier as intravenous injection site for embryos at 2-3 dpf. In all cases it is critical to inject the embryos with consistent numbers of bacteria, which should be checked by plating injection inocula for cfu counting. The following aspects must be considered to achieve reproducible injections. Firstly, it is essential to have high-quality glass microcapillary injection needles. If the needle tip is too large, the injection will create a puncture hole large enough for bleeding to occur and the injected bacteria will flow out of the blood circulation. Secondly, bacteria must be injected directly into the blood circulation. If the needle tip is not inside the vein or if injection fluid spreads into the yolk sac extension, the embryo must be discarded from the experiment. Thirdly, using PVP40 as a carrier for injecting *M. marinum* will assist in preventing the bacteria from sinking in the glass needle. PVP40 improves the homogeneity of the suspension, resulting in more reproducible inocula throughout the duration of injections. PVP40 may also be used for *S. typhimurium* injections, but here it is less important because the larger size and bright fluorescence of the bacteria allows a visual control over the injection inoculum during experiments. For practising the injections we recommend the use of phenol red dye (1% v/v) or 1 µm fluorescent spheres available in different colors (Invitrogen). Once the technique is mastered, it takes approximately 30 minutes to inject 50-100 embryos, including the time required for aligning the embryos on agarose plates and adjusting the bacterial injection volume.

While intravenous injections into the blood island (protocol 5) or into the duct of Cuvier (protocol 6.1) are most commonly used, the alternative routes of infection described in this video article have proved useful to study macrophage and neutrophil chemotaxis (protocols 6.2, 6.3, and 6.4), to study growth of attenuated bacterial strains (protocol 6.5), and to adapt the zebrafish infection model for high-throughput applications (protocol 6.6) [4-8]. The described micro-injection methods can also be applied for injections of viruses [18, 19], fungal spores [14, 20] or protozoan parasites (Maria Forlenza, personal communication). A useful addition to the injection procedures described in this video article is a recently described procedure for subcutaneous injection of bacteria into zebrafish embryos [21]. This procedure was applied to study phagocytosis of bacteria by neutrophils, which were found to efficiently engulf bacteria on tissue surfaces but, in contrast to macrophages, were virtually unable to phagocytose bacteria upon injection into the blood or into fluid-filled body cavities. For subcutaneous injections embryos are positioned similar as for the tail muscle injections described in this video article, but the needle is inserted just under the skin to inject the bacteria over a somite.

It is important to consider that micro-injection is essentially an artificial route of infection. However, early embryos are highly resistant to external exposure to bacterial pathogens. In fact, immersion assays, where embryos are bathed in a bacterial suspension, are not reproducible in our hands [22]. While some embryos may become infected upon immersion, we have observed a large variation in mortality rates and in the expression of inflammatory marker genes between individual embryos in such assays. The micro-injection methods described in this article achieve reproducible infections and are particularly useful to study bacterial interactions with host innate immune cells. An efficient approach to quantify bacterial infection in individual embryos is to analyze the fluorescent images of infected embryos with custom-made, dedicated pixel quantification software [17, 23]. This approach has been shown to correlate well with results of cfu counts after plating of infected embryos. Similarly, relative changes in leukocyte numbers per embryo have been quantified by digital image analysis in transgenic leukocyte fluorophore reporter lines; this approach would be applicable to quantifying the host leukopoietic response to infection[24].

The function of host innate immune genes can be investigated efficiently *in vivo* by combining the described infection models with morpholino knockdown. Morpholinos are synthetic antisense oligonucleotides that target specific RNAs and reduce the expression of the gene products when injected into 1-cell stage zebrafish embryos as shown in other video articles in this journal [10, 25]. In morpholino knockdown studies, it is of great importance that all embryo groups to be compared are staged correctly prior to bacterial injections. This is especially important because embryos have a developing immune system that becomes increasingly competent over time.

There are several transgenic reporter lines currently available to distinguish the major innate immune subsets, macrophages and neutrophils, in zebrafish embryos. The *mpx* and *lyz* promoters have been used to generate neutrophil reporter lines [16, 26, 27], and the *csf1r* (*fms*) and *mpeg1* promoters were used to produce macrophage reporters [14, 28]. While *csf1r* (*fms*) is additionally expressed in xanthophores, *mpeg1* expression is exclusively in macrophages. As shown in this video article, the recently developed *mpeg1* reporter lines are highly useful to image bacterial phagocytosis by macrophages.

Table of specific reagents

Reagent	Supplier	Catalogue number
Phenol Red	Sigma	P0290
Glycerol	Sigma-Aldrich	228210
Difco Middlebrook 7H10 agar	Becton, Dickenson and Company	262710
BBL Middlebrook OADC Enrichment	Becton, Dickenson and Company	211886
Difco Middlebrook 7H9 Broth	Becton, Dickenson and Company	271310
BBL Middlebrook ADC Enrichment	Becton, Dickenson and Company	211887
Tween 80	Sigma-Aldrich	P1754
Polyvinylpyrrolidone (PVP40)	Calbiochem, Merck KGaA	529504
N-Phenylthiourea (PTU)	Sigma-Aldrich	P7629
Ethyl 3-aminobenzoate methanesulfonate salt (Tricaine)	Sigma-Aldrich	A5040
Methyl cellulose	Sigma-Aldrich	M0387
SeaPlaque Agarose (low melting point agarose)	Lonza Inc.	50100
FluoSpheres (1.0 µm, red fluorescent (580/605))	Invitrogen	F8821
FluoSpheres (1.0 µm, yellow-green fluorescent (505/515))	Invitrogen	F8823

Acknowledgements

The authors would like to thank Chao Cui, Floor de Kort, Esther Stoop and Ralph Carvalho for images in Figure 4, Ulrike Nehrdich and Davy de Witt for fish care, and other lab members for helpful discussions. This work is supported by the Smart Mix Program of the Netherlands Ministry of Economic Affairs and the Ministry of Education, Culture and Science, the European Commission 7th framework project ZF-HEALTH (HEALTH-F4-2010-242048), the European Marie-Curie Initial Training Network FishForPharma (PITN-GA-2011-289209), and by the Australian NHMRC (637394). The Australian Regenerative Medicine Institute is supported by grants from the State Government of Victoria and the Australian Government.

References

1. Meijer, A.H. & Spaink, H.P. Host-pathogen interactions made transparent with the zebrafish model. *Curr Drug Targets* **12**, 1000-1017 (2011).

2. Davis, J.M. *et al.* Real-time visualization of mycobacterium-macrophage interactions leading to initiation of granuloma formation in zebrafish embryos. *Immunity* **17**, 693-702 (2002).

3. van der Sar, A.M. *et al.* Zebrafish embryos as a model host for the real time analysis of Salmonella typhimurium infections. *Cell Microbiol* **5**, 601-611 (2003).

4. Zakrzewska, A. *et al.* Macrophage-specific gene functions in Spi1-directed innate immunity. *Blood* **116**, e1-11 (2010).

5. Le Guyader, D. *et al.* Origins and unconventional behavior of neutrophils in developing zebrafish. *Blood* **111**, 132-141 (2008).

6. Herbomel, P., Thisse, B. & Thisse, C. Ontogeny and behaviour of early macrophages in the zebrafish embryo. *Development* **126**, 3735-3745 (1999).

7. Alibaud, L. *et al.* A Mycobacterium marinum TesA mutant defective for major cell wall-associated lipids is highly attenuated in Dictyostelium discoideum and zebrafish embryos. *Mol Microbiol* **80**, 919-934 (2011).

8. Carvalho, R. *et al.* A high-throughput screen for tuberculosis progression. *PLoS One* **6**, e16779 (2011).

9. van der Sar, A.M., Spaink, H.P., Zakrzewska, A., Bitter, W. & Meijer, A.H. Specificity of the zebrafish host transcriptome response to acute and chronic mycobacterial infection and the role of innate and adaptive immune components. *Mol Immunol* **46**, 2317-2332 (2009).

10. Rosen, J.N., Sweeney, M.F. & Mably, J.D. Microinjection of zebrafish embryos to analyze gene function. *J Vis Exp* (2009).

11. Kimmel, C.B., Ballard, W.W., Kimmel, S.R., Ullmann, B. & Schilling, T.F. Stages of embryonic development of the zebrafish. *Dev Dyn* **203**, 253-310 (1995).

12. Westerfield, M. (ed.) *The Zebrafish Book. A Guide for the Laboratory Use of Zebrafish (Brachydanio rerio)*. (The University of Oregon Press, Eugene, 1993).

13. Gutzman, J.H. & Sive, H. Zebrafish brain ventricle injection. *J Vis Exp* (2009).

14. Ellett, F., Pase, L., Hayman, J.W., Andrianopoulos, A. & Lieschke, G.J. mpeg1 promoter transgenes direct macrophage-lineage expression in zebrafish. *Blood* **117**, e49-56 (2011).

15. Stockhammer, O.W., Zakrzewska, A., Hegedus, Z., Spaink, H.P. & Meijer, A.H. Transcriptome profiling and functional analyses of the zebrafish embryonic innate immune response to Salmonella infection. *J Immunol* **182**, 5641-5653 (2009).

16. Renshaw, S.A. *et al.* A transgenic zebrafish model of neutrophilic inflammation. *Blood* **108**, 3976-3978 (2006).

17. Stoop, E.J. *et al.* Zebrafish embryo screen for mycobacterial genes involved in the initiation of granuloma formation reveals a newly identified ESX-1 component. *Dis Model Mech* **4**, 526-536 (2011).

18. Levraud, J.P. *et al.* Identification of the zebrafish IFN receptor: implications for the origin of the vertebrate IFN system. *Journal of immunology* **178**, 4385-4394 (2007).

19. Levraud, J.P., Colucci-Guyon, E., Redd, M.J., Lutfalla, G. & Herbomel, P. In vivo analysis of zebrafish innate immunity. *Methods Mol Biol* **415**, 337-363 (2008).

20. Brothers, K.B. Biobanking in pediatrics: the human nonsubjects approach. *Per Med* **8**, 79 (2011).

21. Colucci-Guyon, E., Tinevez, J.Y., Renshaw, S.A. & Herbomel, P. Strategies of professional phagocytes in vivo: unlike macrophages, neutrophils engulf only surface-associated microbes. *J Cell Sci* **124**, 3053-3059 (2011).

22. van Soest, J.J.S., O. W. ; Ordas, A.; Bloemberg, G. V.; Spaink, H. P.; Meijer, A. H. Comparison of static immersion and intravenous injection systems for exposure of zebrafish embryos to the natural pathogen *Edwardsiella tarda*. *BMC Immunology* (2011, In press).

23. Adams, K.N. *et al.* Drug tolerance in replicating mycobacteria mediated by a macrophage-induced efflux mechanism. *Cell* **145**, 39-53 (2011).

24. Ellett, F.L., G.J. Computational quantification of fluorescent leukocyte numbers in zebrafish embryos. *Methods in Enzymology* (2011, In press).

25. Yuan, S. & Sun, Z. Microinjection of mRNA and morpholino antisense oligonucleotides in zebrafish embryos. *J Vis Exp* (2009).

26. Mathias, J.R. *et al.* Resolution of inflammation by retrograde chemotaxis of neutrophils in transgenic zebrafish. *J Leukoc Biol* **80**, 1281-1288 (2006).

27. Hall, C., Flores, M.V., Storm, T., Crosier, K. & Crosier, P. The zebrafish lysozyme C promoter drives myeloid-specific expression in transgenic fish. *BMC Dev Biol* **7**, 42 (2007).

28. Gray, C. *et al.* Simultaneous intravital imaging of macrophage and neutrophil behaviour during inflammation using a novel transgenic zebrafish. *Thromb Haemost* **105**, 811-819 (2011).

Chapter 3

A morpholino knockdown screen for genes involved in mycobacterium infection

Erica L. Benard [1], Peter I. Racz [1], Alexander E. Nezhinsky [2], Fons J. Verbeek [2], Herman P. Spaink [1], Annemarie H. Meijer [1]

[1] Molecular Cell Biology, Leiden University
[2] Section Imaging and Bioinformatics, Leiden Institute for Advanced Computer Science, Leiden University

Abstract

Zebrafish infection with *Mycobacterium marinum* is a well characterised animal model for human tuberculosis. Based on previous transcriptome data of zebrafish embryonic macrophages and infection studies, we selected genes for a knockdown screen to identify host genes involved in controlling mycobacterial growth during early stages of infection when granulomas are being formed. The level of infection in zebrafish embryos could be assessed by using specifically designed software that calculates the *M. marinum* fluorescent pixel count per embryo. This screen resulted in 7 hits of the 17 candidate genes tested that repeatedly led to an increased or decreased *M. marinum* infection load after a morpholino-based knockdown and 5 of these results could be reproduced by using a second morpholino with different target sites indicating their high specificity. Of these candidate hits, the transcription factor gene *atf3*, knockdown led to reduced infection, while knockdown of the other hits led to increased infection, including the perforin gene *mpeg1*, the scavenger receptor genes *cd36* and *marco*, and the signalling mediator gene *creld2*. RNA deep sequencing analysis of uninfected and infected samples of both morphants of *creld2* showed that although no general immune-deficiency was observed, a specific down-regulation of a group of apolipoprotein genes was detected. Further in-depth analysis of these genes will contribute to a better understanding of the innate immune response to mycobacterial infection and the mechanisms involved in granuloma formation.

Introduction

Mycobacterium tuberculosis is the cause of tuberculosis in humans. One third of individuals of the world population is infected with this pathogen and there is an increasing occurrence of multidrug resistant strains of *M. tuberculosis* [1], which highlights that understanding the mechanistic basis of host-pathogen interactions underlying tuberculosis has important medical implications. In order to address this topic, a combination of functional genomics approaches and modern cell biology are required in animal models that mimic the human disease. *Mycobacterium marinum* is the closest genetic relative of the *M. tuberculosis* complex and a natural pathogen of fish. Similar to human tuberculosis, *M. marinum* infected fish develop latency with survival of the pathogen in caseating granulomas, which are tight aggregates of infected and non-infected macrophages and other immune cells [2, 3]. Infecting the optically transparent zebrafish embryo with fluorescent bacteria allows us to monitor the infection *in vivo* and follow granuloma formation in real time [4].

A major benefit of using zebrafish embryos as a host for studying gene function is the use of research tools for reverse genetics by knocking down a target gene with, for instance, morpholinos. Morpholinos consist of antisense oligonucleotides, usually 25 nucleotides long, with bases connected to a morpholine ring structure as the backbone,

making them very stable. They can be designed to either block translation initiation in the cytosol (by targeting the 5' UTR or the first 25 bases of coding sequence) or they can modify pre-mRNA splicing in the nucleus (by targeting splice junctions or splice regulatory sites). Unfortunately, the use of morpholinos can also produce off-target effects (non-antisense effects due to interactions with structures other than gene transcripts) which can induce an aspecific phenotype. The exact underlying mechanisms of off-target effects are not completely understood, however, the phenotypes are often the result of p53-dependent neural toxicity [5] or a more extreme toxicity with severe overall deformity [6, 7]. The advantage of using a morpholino approach over a knockout approach, such as ENU mutagenesis, is that knockdown of the selected gene can be rapidly achieved in any transgenic or wildtype zebrafish line, whereas generating a stable mutant zebrafish line requires extensive labour and time. Furthermore, in the case of studies of essential genes, knockdown of which leads to lethality, translation-blocking morpholino knockdown can give complementary information because it can also lead to knockdown of maternally inherited mRNAs. Therefore, if applied with appropriate controls, morpholinos remain a powerful tool.

To investigate which genes play a role during *M. marinum* infection, we set up a morpholino knockdown screen in zebrafish to identify genes involved in susceptibility or resistance to mycobacterial infection. The target genes studied in this research were selected for their specific expression in macrophage cells, for their infection-inducible or -repressible expression during *M. marinum* infection, or for their suggested function based on literature. This selection process resulted in seventeen candidate genes to screen, in addition to *spi1b* (also called *pu.1*) which is known to be required for leukocyte development, as a positive control [8]. The selection included several macrophage-specific genes (such as *cd53*, *coro1a*, *mpeg1*, *marco*, and *mfap4*) previously shown to be expressed downstream of the highly conserved Spi1b transcription factor [9] or expressed in macrophages of *mpeg1* transgenic reporter lines (unpublished). These genes were considered to be promising candidates because two other Spi1-regulated genes (*cxcr3*.2 and *ptpn6*) were shown to be involved in infection with *M. marinum* [9, 10]. The selection also included infection-responsive genes, such as the transcription factor gene *atf3*, a gene shown to be required for optimal killing of bacteria by phagocytes in mice, *plac8* [11], and an immune-responsive gene with bactericidal activity of macrophage-lineage cells, *irg1*. The final selection of candidate genes for which morpholinos were designed is shown in Table 1.

Based on the initial screening results, a subset of candidate genes was selected for more detailed analyses and their role in mycobacterial infection was confirmed with additional morpholinos. The endoplasmic reticulum (ER) stress-inducible gene *cysteine-rich with EGF-like domains 2* (*creld2*) was selected as an example gene from the screen to confirm the specificity of the morpholino knockdown approach. Therefore, RNA sequencing was applied to further investigate the knockdown phenotype which was associated with a strongly increased mycobacterial burden. Notably, a group of genes

encoding apolipoproteins was down-regulated in absence or presence of infection in both *creld2* morphant groups.

Materials and methods

Zebrafish lines and handling of embryos

Zebrafish were handled in compliance with the local animal welfare regulations and were maintained according to standard protocols (zfin.org). The culture was approved by the local animal welfare committee (DEC) of the University of Leiden and all protocols adhered to the international guidelines specified by the EU Animal Protection Directive 2010/63/EU. The zebrafish line AB/TL was used in this study. Embryos were grown at 28.5-30°C in egg water (60 µg/ml Instant Ocean sea salts). For the duration of bacterial injections and imaging, embryos were kept under anaesthesia in egg water containing 200 µg/ml tricaine (Sigma-Aldrich). Embryos used for stereo fluorescence imaging were kept in egg water containing 0.003% 1-phenyl-2-thiourea (Sigma-Aldrich) to prevent melanisation.

Morpholino knockdown

Morpholino oligonucleotides (Gene Tools) were diluted to the desired concentration in 1x Danieau buffer (58 mM NaCl, 0.7 mM KCl, 0.4 mM $MgSO_4$, 0.6 mM $Ca(NO_3)_2$, 5.0 mM HEPES; pH 7.6) containing 1% phenol red (Sigma-Aldrich) and 1 nl was injected into the yolk at the 1-2 cell stage using a Femtojet injector (Eppendorf). An overview of the used morpholino sequences, exon-intron boundary sites, and concentrations can be found in Table 1. As a control, the standard control morpholino (Gene Tools) was used at the same concentrations as the other morpholinos.

Infection experiments

Embryos were staged at 24 hours post fertilisation (hpf) by morphological criteria and manually dechorionated. *M. marinum* infections were performed using the Mma20 strain expressing mCherry in a pSMT3 vector [12]. *M. marinum* was prepared as described previously, injected into the blood circulation at 28 hpf, and plated during injections to confirm the number of colony forming units (cfu's) injected [13].

RNA isolation, DNase treatment and RT-PCR

Whole embryo RNA isolation and removal of residual genomic DNA was performed as described in [14]. Morpholino knockdown was verified by RT-PCR with the SuperScript® One-Step RT-PCR System (Invitrogen, #10928-034) using 50 ng DNAse treated RNA template. RT-PCR primers for knockdown verification can be found in Table 2.

RNA for deep sequencing analysis was isolated using QIAzol lysis reagent and purified using the Rneasy MinElute Cleanup kit (QIAGEN Benelux B.V., Venlo, Netherlands). RNA sequencing was performed as previously described [15].

Chemically induced inflammation assay

Copper sulphate was administered via the egg water ($CuSO_4$ (Merck, #1027910250), 10 uM, 2 hours treatment at 28°C) [16]. Embryos were washed in egg water three times and fixed in 4% paraformaldehyde in phosphate buffered saline (PBS) overnight at 4°C.

Immunohistochemistry

Identification of leukocytes was performed by immuno-labelling with the leukocyte specific anti-L-plastin antibody and Alexa568-conjugated secondary antibody [17].

Image analysis

Fluorescence images were taken with a Leica MZ16FA stereo fluorescence microscope equipped with a DFC420C digital colour camera. In *M. marinum* infection experiments, bacterial pixel counts were obtained with stereo fluorescence images and analysed using dedicated pixel quantification software [18]. An image can be made of one, two or three embryos and contains two channels: bright field and fluorescence. The software allows the user to allocate the number of embryos per image and it selects the fluorescence channel for analysis. Images of non-infected embryos are used to set the threshold level for background fluorescence and the number of fluorescent pixels per embryo is determined for each group of morphants or control embryos. This is performed for all groups of embryos and the results are written to a comma-separated file for statistical analysis.

Statistical analysis

All data (mean ± SEM) were analysed using unpaired, two-tailed t-tests for comparisons between two groups (ns, no significant difference; *, $p<0.05$; **, $p<0.01$; ***, $p<0.001$). For RNA deep sequencing, significant differences were calculated by DESeq analysis of transcript count data (*=fold change>2, $p<0.05$).

Gene synteny, protein alignment and homology

Gene synteny of *creld2* was analysed with Genomicus, version 75.01 [19]. Multiple protein alignment performed with ClustalW2 [20]. Amino acid identity and similarity percentages were determined using UniProt CLUSTAL O(1.2.0) multiple sequence alignment.

Results

Morpholino screen workflow

To study the effect of our selected genes on the development of *M. marinum* infection we chose to use a morpholino knockdown approach as a rapid screen while zebrafish from an ENU mutagenesis screen were being sequenced (Hubrecht and Sanger Institutes). We primarily used morpholinos targeting exon-intron boundaries of the pre-mRNA to block correct splicing. Splice-blocking sites were preferentially chosen to delete an exon encoding a functional domain of the protein or creating an early stop codon. Similarly, when an intron was included this introduced an early stop codon. When no splice blocking sites could be determined, a translational-blocking morpholino was designed. The specificity of the morpholinos was checked via BLAST (Ensembl) and the optimal concentration was determined by titrating the dose. The ideal dose of morpholino was set at the highest concentration that elicited no detectable off-target effects [21, 22] yet still produced an effective knockdown of the target gene. Efficient splice modification was determined by reverse-transcriptase polymerase chain reaction (RT-PCR) showing a band shift after gel electrophoresis of RT-PCR products.

After injecting the morpholinos into 1-2 cell staged embryos (fig. 1A), the morphants and their control embryos were treated with PTU at 12 hpf to prevent melanisation, then at 24 hpf they were dechorionated, staged according to morphological criteria [23] and subsequently infected via the blood island with 150-200 cfu of mCherry-expressing Mma20 bacteria (fig. 1B). Fluorescence images of the infected embryos at 4 days post infection (dpi) were created (fig. 1C) to assess the bacterial burden with dedicated pixel quantification software [18, 24]. A subset of these candidate genes yielding a significantly higher or lower bacterial pixel count compared to the standard control group were selected for more detailed analysis and their role in mycobacterial granuloma formation was confirmed with additional morpholinos targeting different intron-exon boundaries (fig. 1D).

During the first phase of the morpholino screen we observed slight differences between the pre-calculated cfu value and the actual injected cfu value that was determined by plating aliquots of the injection dose. Therefore, to enhance consistency within different experiments of the morpholino screen, we tested whether using aliquots of glycerol stocks of *M. marinum* stored at -80°C would enable a more consistent cfu number for injection. To test this, we used the *creld2* morphants that we showed during the first phase of the morpholino screen to have a reliable significant effect on the levels of infection generated by liquid cultured *M. marinum* and injected the morphants with two sources of *M. marinum*: a 7H9 liquid culture stock grown at 28.5°C overnight to logarithmic phase and a glycerol stock [13]. Image analysis at 4 dpi showed that the *creld2* morphants only showed a significant difference when injected with the liquid culture (fig. 2A) and not with the glycerol stock (fig. 2B) of *M. marinum*. In addition,

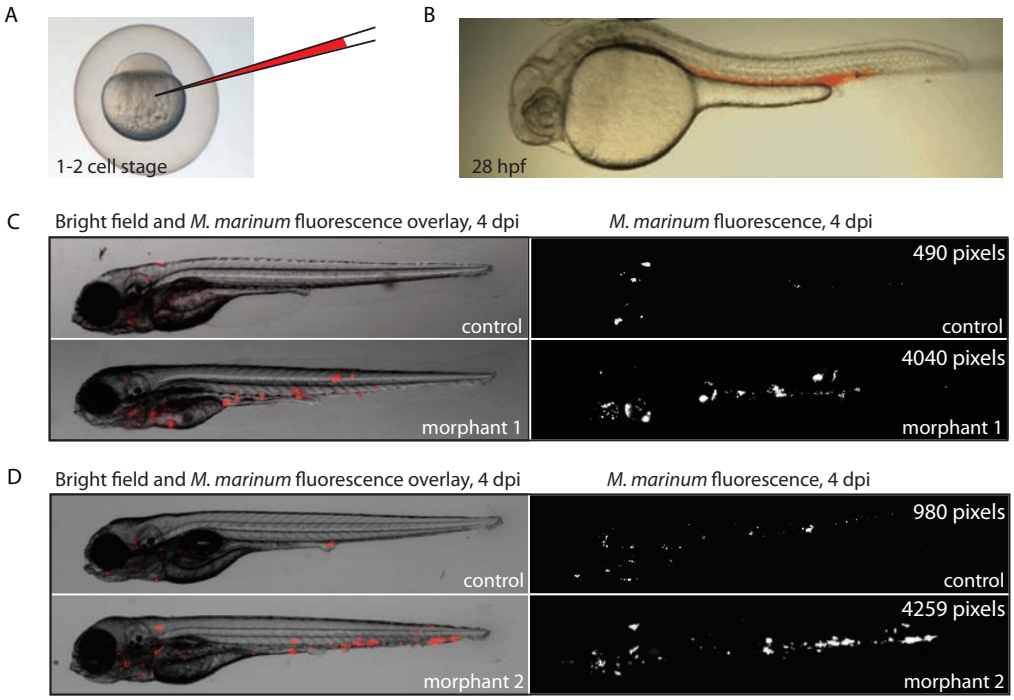

Figure 1. Overview of screen workflow. (A) Morpholinos are micro-injected into 1-2 cell stage AB/TL embryos. (B) Morphant and control embryos are injected with mCherry-expressing *M. marinum* bacteria (150-200 cfu) in 2% PVP. The injection substance contains 1% phenol red for visual support of correct injection into the blood circulation at 28 hpf. Image is still from [13]. (C and D) Images of an infected control (top) and morphant (bottom) embryo injected with the (C) first morpholino and the (D) second morpholino of the same gene (example used is from knockdown of *creld2*). Left hand images are overlays of bright field and mCherry-fluorescence channel of *M. marinum* and right images are the mCherry-fluorescence channel with fluorescence depicted as white pixels. *M. marinum* fluorescence levels as determined using dedicated pixel quantification software [18, 39] are indicated in the top right corner of the images.

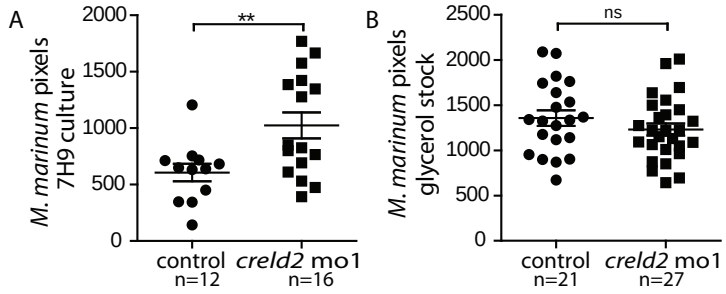

Figure 2. Infection with 7H9 liquid cultured *M. marinum* leads to increased bacterial burden in *creld2* morphants. Morphants of *creld2* and their controls only show a significant increase in *M. marinum* pixel count after injection with (A) 7H9 liquid cultured *M. marinum* and not after injection with (B) glycerol stock *M. marinum*. Bacterial burden was quantified by determining the number of fluorescent bacterial pixels with dedicated software.

when determining cfu numbers the colonies of the liquid culture *M. marinum* grew sufficiently for counting at 4 dpi, while the colonies of the glycerol stock *M. marinum* grew with a delay and could only be counted at 7 dpi. This experiment was repeated with morphants of *myeloid differentiation factor 88* (*myd88*), encoding an adaptor protein in Toll-like receptor (TLR) and interleukin-1 receptor signalling. Mutation or knockdown of this gene is known to lead to a severely increased bacterial load [25, 26]. Similar to knockdown of *creld2*, significant differences were only observed in the morphants injected with bacteria from liquid cultured *M. marinum* (data not shown) and not in morphants injected with bacteria from glycerol stock. Considering that morpholino effects are attenuated over time, we concluded that the more rapid growth of bacteria from liquid culture is better compatible with the assessment of morpholino effects. This impelled us to perform the remaining part of the morpholino screen with the liquid cultured *M. marinum*.

From the selected candidate genes, *spi1b* (*pu.1*) was used as a positive control to validate the designed workflow of the screen. Knockdown of this transcription factor gene causes a lack of macrophages in embryos and these morphants have previously been shown to be highly susceptible to *M. marinum* infection [27]. This result was confirmed during our morpholino knockdown screen (table 1 and supplementary fig. 1A).

Morpholino screen results

After initial screening of the first seventeen genes, seven positive hits were found that showed a significant difference in bacterial infection level and that was repeatable at least twice: one reducing *M. marinum* infection (*atf3)* and six increasing *M. marinum* infection (*cd36*, *marco*, *mpeg1*, *creld2*, *cd53*, *coro1a*) (table 1 and supplementary fig. 1). These seven positive hits were then re-tested with a second splice-blocking morpholino targeting a different exon-intron boundary or an ATG translational blocking morpholino (table 1 and supplementary table 2). This resulted in five hits that showed an infection phenocopy: *creld2*, *cd36*, *mpeg1*, *marco*, and *atf3*. Of these hits, *creld2* is further described below and *atf3, marco*, and *mpeg1* are further investigated in detail in the thesis Chapters 4, 5, and 6. Combined bacterial pixel count data for other morpholinos that showed consistent repeated effects on *M. marinum* infection are shown in supplementary fig. 1.

Detailed analysis of Creld2

The *creld2* gene shows high conservation between zebrafish (ENSDARG00000029071), humans (ENSG00000184164), mice (ENSMUSG00000023272), and rats (ENSRNOG00000004659) in terms of gene synteny and protein homology (supplementary fig. 3). SMART analysis of Creld2 protein reveals that it contains a signal peptide domain, a DUF3456 domain (TLR4 regulator and MIR-interacting saposin-like protein (MSAP)), an epidermal growth factor-like calcium binding domain, and a furin-like cysteine rich repeats domain (supplementary fig. 3B). When *creld2* was knocked down in zebrafish

Table 1. Results of morpholino screen

Gene symbol	Selection criteria	MO #	Screened # morphant/control	# Repeats	Significance	% *M. marinum* Pixel Count	Confirmed knockdown
spi1b	Positive control. Morphants have depleted macrophage population and have high susceptibility to *M. marinum* infection in zebrafish embryo model.	1	24/24	1	Yes, P<0.0001	**2181%**	Yes
atf3	Infection responsive; literature links with human TB and TLR signalling	1	321/392	3	Yes, P<0.0001	**46%**	Yes
		2	133/151	3	Yes, P<0.0001	**54%**	No
		3	95/112	2	Yes, P<0.0001	**31%**	N.A.
cd36	Infection responsive; literature link with human TB	1	174/135	4	Yes, P<0.0001	**220%**	Yes
		2	35/60	1	Yes, P=0.0014	**189%**	Yes
cd53	Macrophage specific; literature link with TNF signaling	1	128/117	3	Yes, P<0.0001	**469%**	No
		2	53/36	1	No	**233%**	N.A.
coro1a	Macrophage specific; literature link with human TB	1	30/30	2	Yes, P=0.0062	**617%**	No
		2	6/15	1	No	**390%**	No
creld2	Infection responsive; function in ER stress (important in infection)	1	288/215	5	Yes, P<0.0001	**236%**	Yes
		2	147/129	2	Yes, P<0.0001	**213%**	Yes
marco	Macrophage-specific; literature link with human TB	1	60/102	2	Yes, P<0.0001	**238%**	Yes
		2	109/73	2	Yes, P<0.0001	**213%**	Yes
mpeg1	Infection responsive; macrophage-specific	1	239/211	5	Yes, P<0.0001	**224%**	Yes
		2	158/141	3	Yes, P<0.0001	**536%**	Yes
cd180	Infection responsive; literature link with TLR signaling	1	79/167	3	No	**146%**	No
crel	Infection responsive; major transcription factor in innate immunity	1	16/31	1	No	**178,8%**	No
irg1l	Infection responsive; macrophage-specific	1	Phenotype	1			N.A.
irg1	Infection responsive; macrophage-specific	1	12/18	1	No	**72%**	No
lgals9l1	Macrophage-specific; literature link with human TB	1	Phenotype				N.A.
		2	Phenotype				N.A.
mfap4	Macrophage-specific; putative role in inflammation	1	51/51	2	No	**101%**	Yes
plac8.1	Infection responsive; literature on mouse infection models	1	26/12	1	No	**68%**	No
stat1a	Infection responsive; major transcription factor in innate immunity	1	41/15 and Phenotype	2	Yes, P<0.0001 and N.A.	**28%**	No
		2	Phenotype	1			N.A.
stat1b	Infection responsive; major transcription factor in innate immunity	1	Phenotype	2			N.A.

% Legend
<40
40-80
80-120
120-200
200-300
300-400
>500

* TB = tuberculosis, TLR = Toll-like receptor

Table 2. Description of used morpholinos.

Gene symbol	Ensembl ID	Target boundary site	Morpholino sequence 5' - 3'	Concentration [mM]
spi1b	ENSDARG00000000767	MO1 ATG	GATATACTGATACTCCATTGGTGGT	1
atf3	ENSDARG00000007823	MO1 intron2-exon3	GGACAGCCTGAAATAACAACATCTA	0.2
		MO2 intron3-exon4	CTTCTCAGACTCCTAAAGTCAAAAC	0.2
		MO3 ATG	GTGCTGAAGCATCATGCCGAAATCT	0.1
cd36	ENSDARG00000032639	MO1 exon2-intron2	CTATGAGGCCACAAATATTACCTGT	0.2
		MO2 exon3-intron3	TTTGAAATACATACTGCGACAGCAA	0.6
cd53	ENSDARG00000068233	MO1 intron5-exon6	AGCAACCAAACTGGTGAAAGAAGGA	0.1
		MO2 exon6-intron6	ATGTGAGAGCAGTATTACCTTATGC	0.1
coro1a	ENSDARG00000054610	MO1 exon3-intron3	ATGAAGTCCTTGTCACTCACCATGA	0.25
		MO2 exon4-intron4	TGGTTTCTGATGTGGTTTACCTGCA	0.25
creld2	ENSDARG00000029071	MO1 exon5-intron5	TGACAGTATTTTTGAATACCTTTGC	0.6
		MO2 exon2-intron2	CATTTTAATTTTCTTCTCACCTCGT	0.45
marco	ENSDARG00000059294	MO1 intron15-exon16	ACGGACCACTGATGAAGAAAAACAA	0.02
		MO2 exon3-intron3	TAACTAAAAGTACCTTGGCTTCCAC	0.3
mpeg1	ENSDARG00000055290	MO1 exon1-intron1	ATTTTGTACTTACTTGAACCCGTGC	0.2
		MO2 intron1-exon2	GGTTACGGACCTGAGAAACAAATTT	0.1
***cd180(2of2)* and *cd180(1of2)* ***	ENSDARG00000093750 and ENSDARG00000067536	MO1 exon1-intron1 and exon2-intron2	GGTTATTTAGCTTTGCTCACCTTGT	0.5
crel	ENSDARG00000055276	MO1 exon4-intron4	AAAAGATTGAACTTACGCAATGGCC	0.6
irg1	ENSDARG00000069844	MO1 intron3-exon4	GAGTGCACCTATAATATATATCCCA	Phenotype
irg1l	ENSDARG00000062788	MO1 intron2-exon3	TGCCACTGAAAACAGACAAGAGACA	N.A.
lgals9l1	ENSDARG00000025903	MO1 exon3-intron3	CGGAGTGAATGTACTTGTACCTTGT	Phenotype
		MO2 intron8-exon9	ATTATGCTGATGGAAGCAGCAAAAT	Phenotype
mfap4	ENSDARG00000090783	MO1 ATG	CGCCAAGAACAGCACGATTGCCATC	0.5
		MO2 exon3-intron3	TAAAGTCACACTCGTACCGTCCATC	0.2
plac8.1	ENSDARG00000043729	MO1 exon3-intron3	GCTATAAAGATACTAACCTCTATGT	0.5
plac8.2 *	ENSDARG00000094438	MO1 exon3-intron3	ACAGACAGACAGACATTCACCTGTA	0.25
		MO2 intron2-exon3	CCTAAGAAAAATACATGGTTGACGT	0.1
stat1a	ENSDARG00000006266	MO1 exon3-intron3	ATGTGGTCAACAGGCACCTGCAAGT	0.25
stat1b	ENSDARG00000076182	MO1 intron2-exon3	ATTCCCTGCAAACAACACTGACTAC	Phenotype
tnfrsf1a *	ENSDARG00000018569	MO1 intron2-exon2	TCCCTTCAAACTGTCCGTAAAGGGC	Inconclusive
		MO2 exon6-intron7	CTGCATTGTGACTTACTTATCGCAC	Inconclusive
tnfrsf1b *	ENSDARG00000070165	MO1 exon2-intron2	ATTCTTGTTTTATAACGTACCTGGT	Inconclusive
		MO2 exon3-intron3	CCTTTTTGTTTAAAACTCACCTTCT	Inconclusive

* *plac8.2*, *tnfrsf1a* and *tnfrsf1b* data is inconclusive (not consistent between repeated experiments) and is not shown in Table 1. Morpholino for *cd180* targets two paralogous genes: *cd180 (1of2)* and *cd180 (2of2).*

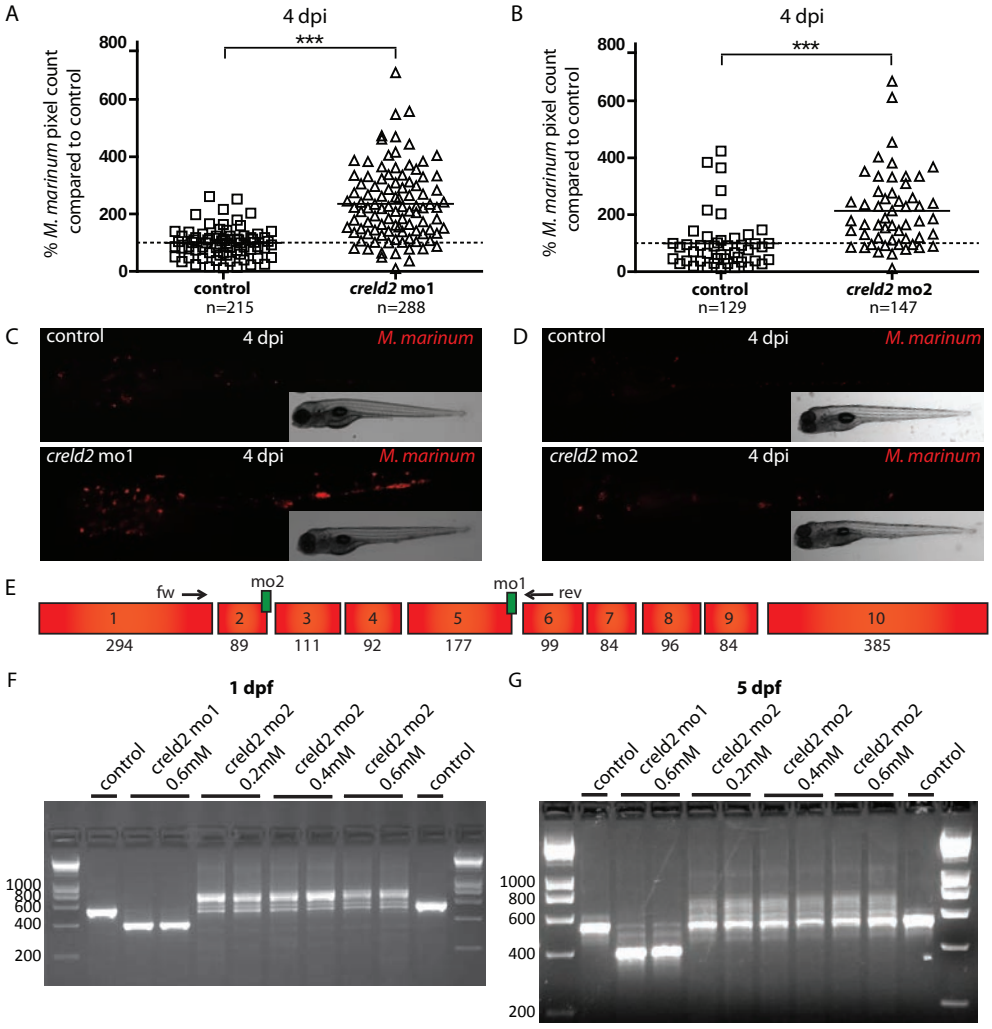

Figure 3. Knockdown of *creld2* with two separate morpholinos impairs control of *M. marinum* infection. AB/TL embryos were injected with different splice blocking morpholinos against *creld2* (mo1 or mo2) or with control morpholinos, subsequently injected with mCherry-expressing *M. marinum*, and infected embryos were imaged at 4 dpi. Graphs show combined representative results of *creld2* knockdown of 5 repeated independent experiments with (A) mo1 and 2 repeated independent experiments with (B) mo2. All pixel values of data points are compared against the average pixel value of the infected control embryos and presented as percentages. The mean ± SEM is indicated (n = number of embryos). (C and D) Representative stereo fluorescent images are shown below the graph of each experiment with an inlay of the bright field image of the same embryo. (E) Overview of the exon/intron structure of zebrafish *creld2* (ENSDARG00000029071) with base pair values given below the respective exon. Intron sizes are not depicted truly. Targeting sites of mo1, mo2, and forward and reverse primers of the RT-PCR reaction are also depicted. (F and G) Injection with both morpholinos against *creld2* generates sufficient knockdown as tested by RT-PCR. Gel electrophoresis shows a shift in fragment size of the PCR product of both morphants compared to controls (530 bp) at (F) 1 dpf and (G) 5 dpf.

embryos, it consistently led to an increased level of *M. marinum* fluorescence pixels at 4 dpi in over 200 screened embryos (Table 1 and fig. 3A+C). This infection phenotype could be phenocopied with a second morpholino (Table 1 and fig. 3B+D) and neither of the morphants showed any toxicity phenotypes (fig. 3C-D). By performing an RT-PCR with a forward primer located in exon 1 and a reverse primer located in exon 6, the knockdown of morpholino 1 (targeting exon2-intron2 boundary) and morpholino 2 (targeting exon5-intron5 boundary) (fig. 3E) was confirmed at 1 dpf (time point of *M. marinum* injection) and 5 dpf (time point of *M. marinum* pixel analysis) (fig. 3F-G).

To verify whether knocking down *creld2* has any effect on the capability of leukocytes to migrate towards a local inflammation site, an event that frequently occurs during granuloma formation, a chemical inflammation (ChIN) assay [16] was used. By treating embryos with copper sulphate, the hair cells of the neuromast along the lateral line of the zebrafish embryo are damaged which causes a local inflammation site, eventually leading to attraction of macrophages and neutrophils. The ChIN assay on *creld2* morphants and their control revealed no differences in the attraction of leukocytes to the inflammation sites (fig. 4).

To gain insight in whether the higher *M. marinum* infection could be caused by an immune-deficiency we performed RNA-Seq analysis of pools of uninfected and infected *creld2* morphants for both morpholinos and their controls at 4 dpi, the time point when granuloma-like structures have formed and *creld2* is still partially knocked down in both morphants. First, we focussed on a set of genes that are consistently induced during *M. marinum* infection (fig. 5). Although some differences with the control were noted, a clear immune-deficiency was not observed. A number of genes were similarly up- or down-regulated in both morphants, although not always significant in both cases. The genes that were slightly up-regulated in the morphants during infection included the general pro-inflammatory genes *il1b* and *cxcl-c1c,* the matrix metalloproteinases *mmp9* and *mmp13a* and the tissue inhibitor of matrix metalloproteinases *timp2b,* and the non-coding RNA *si:ch211-243g18.3*. The genes that were slightly down-regulated included *cyp1a*, *cyp24a1*, *hmox*, and *mfap4 (6 of 13)* (fig. 5).

When studying the total number of genes that were up- and down-regulated, both in uninfected and infected embryos, a substantial overlap could be observed between both morphants (fig. 6). Approximately 30% of all up-regulated genes in the uninfected samples (49 genes) and in the infected samples (52 genes) overlap between both morphants (fig. 6A). Furthermore, approximately 40% of all genes down-regulated in the uninfected samples (117 genes) and in the infected samples (114 genes) overlap between the two morphants (fig. 6B). When comparing these overlapping groups of the uninfected morphants with the infected morphants, 25% of the genes are identical in the up-regulated group (16 genes, listed in fig. 6A) and 30% of the genes are identical in the down-regulated group (55 genes, listed in fig. 6B).

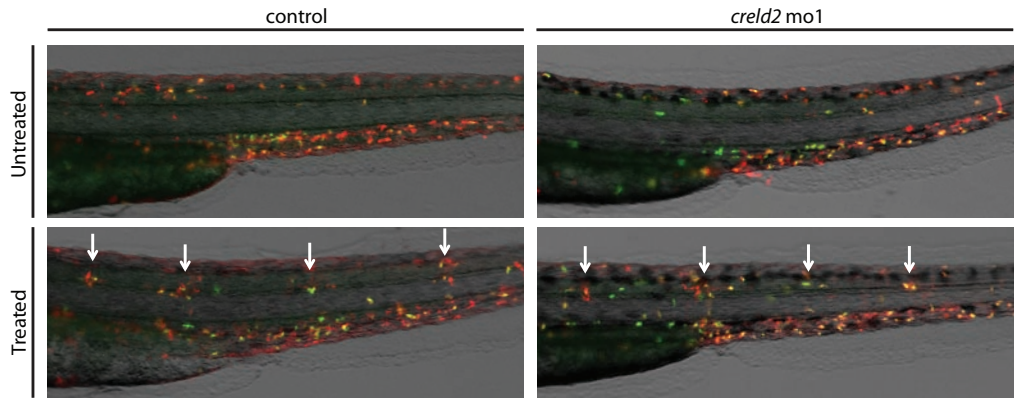

Figure 4. *creld2* does not play a role in leukocyte migration towards local inflammation. Representative images of untreated and copper sulphate treated control and *creld2* morphant (mo1) 3 dpf embryos. Embryos were immuno-labelled with Ab against the general leukocyte marker L-plastin (red signal) in combination with a neutrophil-specific Mpx TSA-staining (green signal). White arrows indicate accumulation of leukocytes at the local inflammation sites of the neuromasts due to chemically induced hair cell damage [16].

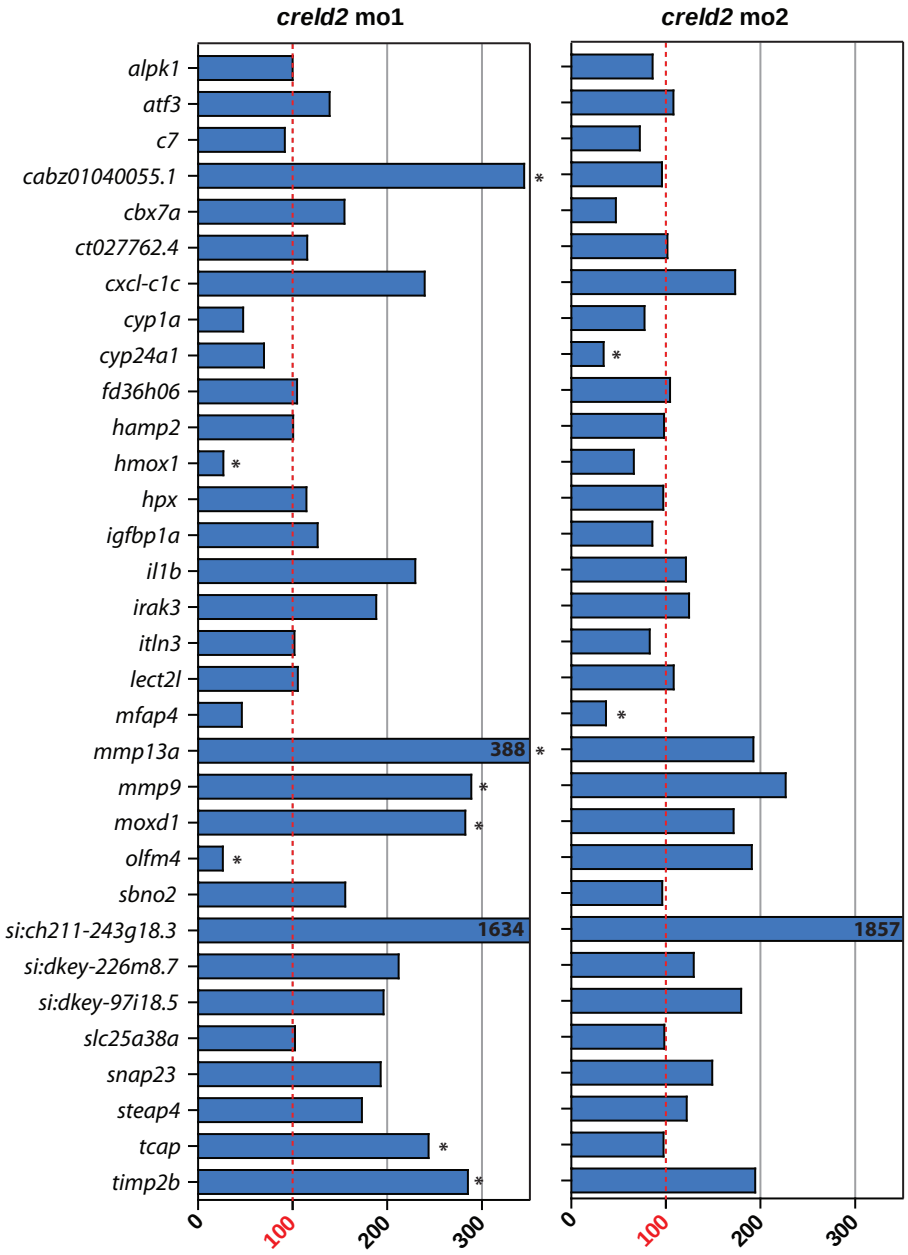

Figure 5. Effect of *creld2* knockdown on the innate immune response during *M. marinum* infection. Graphs show the effects of *creld2* mo1 and mo2 knockdown on a set of genes that showed reproducible induction by *M. marinum* infection in control embryos. The expression level of these genes under infection conditions of *creld2* deficiency is expressed as the percentage of the expression level in the corresponding infection conditions of the control embryos. Results are based on RNA-Seq analysis of pools of 30 infected and 30 uninfected embryos for each group. Embryos were injected with *M. marinum* Mma20 (250 cfu) or mock injected with 2% PVP, and RNA-Seq analysis was performed at 4 dpi. (*=fold change>2, $p<0.05$).

A

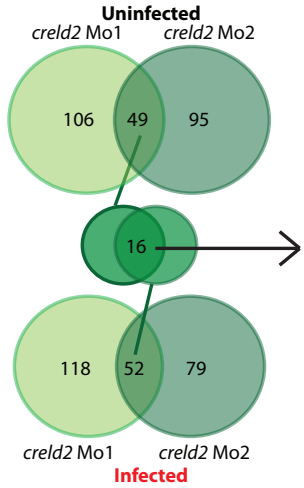

Up-regulated genes

Ensembl Gene ID	Associated Gene Name
ENSDARG00000087755	*afap1L1 (3 of 4)*
ENSDARG00000077389	*bx119910.6*
ENSDARG00000087080	*cabz01044356.1*
ENSDARG00000090805	*cr385054.2*
ENSDARG00000074879	*cr774186.2*
ENSDARG00000022614	*ddx43*
ENSDARG00000016713	*dhrs13l1*
ENSDARG00000070242	*enod1 (6 of 15)*
ENSDARG00000090425	*lrrtm2*
ENSDARG00000070801	*opa1*
ENSDARG00000078069	*rrm2*
ENSDARG00000009017	*scyl1 (1 of 2)*
ENSDARG00000094890	*si:ch211-163b2.4*
ENSDARG00000071644	*si:dkey-19a16.7*
ENSDARG00000094058	*si:dkeyp-118h3.1*
ENSDARG00000093888	*si:dkeyp-87e3.1*

B

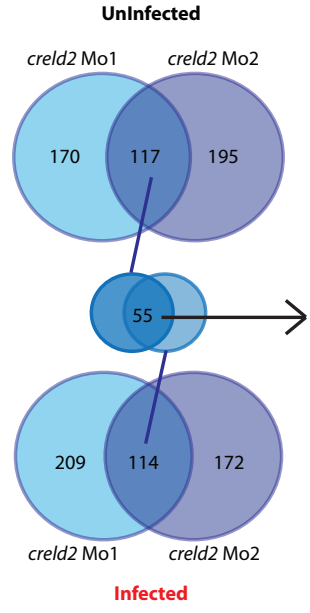

Down-regulated genes

Ensembl Gene ID	Associated Gene Name	Ensembl Gene ID	Associated Gene Name
ENSDARG00000016412	*agt*	ENSDARG00000052734	*hmgcra*
ENSDARG00000026764	*ahsg*	ENSDARG00000037533	*mep1b*
ENSDARG00000013856	*amy2a*	ENSDARG00000087851	*mrpl53 (2 of 2)*
ENSDARG00000020866	*apoa4 (1 of 4)*	ENSDARG00000055876	*msmo1*
ENSDARG00000094929	*apoa4 (4 of 4)*	ENSDARG00000009153	*pla2g1b*
ENSDARG00000042780	*apoba*	ENSDARG00000079544	*si:ch1073-464p5.5*
ENSDARG00000060350	*apod (3 of 3)*	ENSDARG00000075270	*si:ch211-233g6.8*
ENSDARG00000086370	*apoea*	ENSDARG00000053448	*si:ch211-251f6.6*
ENSDARG00000024503	*c6ast3*	ENSDARG00000087390	*si:ch211-5k11.12*
ENSDARG00000052578	*c6ast4*	ENSDARG00000045835	*si:dkey-14d8.6*
ENSDARG00000030254	*cbln9*	ENSDARG00000086849	*si:dkey-187k19.2*
ENSDARG00000043168	*cela1 (2 of 7)*	ENSDARG00000094215	*si:dkey-240n22.2*
ENSDARG00000041569	*ces2*	ENSDARG00000069189	*si:dkey-242h9.3*
ENSDARG00000041595	*ces3*	ENSDARG00000028784	*si:dkey-24p1.6*
ENSDARG00000073898	*ckap5*	ENSDARG00000077192	*slc15a1a*
ENSDARG00000043722	*cpa4*	ENSDARG00000090469	*sycn (1 of 2)*
ENSDARG00000021339	*cpa5*	ENSDARG00000023176	*tdo2b*
ENSDARG00000090899	*cr450711.2*	ENSDARG00000023151	*ucp1*
ENSDARG00000045089	*CRP*	ENSDARG00000036833	*upp2*
ENSDARG00000021172	*cyp2ad2*	ENSDARG00000093844	*zgc:136461*
ENSDARG00000042953	*cyp2n13*	ENSDARG00000030893	*zgc:154142*
ENSDARG00000042641	*cyp51*	ENSDARG00000095863	*zgc:161979*
ENSDARG00000056744	*ela2*	ENSDARG00000086569	*zgc:172051*
ENSDARG00000007276	*ela3l*	ENSDARG00000034403	*zgc:173443*
ENSDARG00000053526	*enpp7*	ENSDARG00000076221	*zgc:198419*
ENSDARG00000019532	*fads2*	ENSDARG00000009443	*zgc:92137*
ENSDARG00000090689	*hbbe1.2*	ENSDARG00000040282	*zgc:92590*
ENSDARG00000023656	*he1a*		

Figure 6. Overlap of genes up- and down-regulated in uninfected and infected *creld2* morphants. Significantly (A) up-regulated genes and (B) down-regulated genes in *creld2* mo1 samples (left circles in light colour) and mo2 samples (right circles in dark colour) of uninfected (top circles) and infected (bottom circles) embryos. The overlap of each group is shown as an overlap between each circle (Venn-diagram). Total overlap between overlapping genes of uninfected and infected embryos are indicated as small Venn-diagrams in the middle (16 up-regulated and 55 down-regulated genes). Lists of these genes are provided on the right with their Ensembl gene IDs and associated gene names.

Discussion

This study focussed on a knockdown screen to identify host genes that are involved in control of mycobacterial infection. We used a morpholino-based approach to knockdown a list of candidate genes and studied their effect on *M. marinum* infection, the natural pathogen of fish and a close relative of *M. tuberculosis*. Approximately 30% of the screened genes resulted in hits that when knocked down gave rise to a reproducible increase or decrease of *M. marinum* infection load which could be phenocopied with a second morpholino. The high number of hits is not surprising considering that all genes selected are either infection-responsive, expressed in macrophages, the immune cell that plays a major part in the infection process of *M. marinum*, or have been published to have a link with mycobacterial infection. In follow up work, functional analyses of three of the most interesting genes from this knockdown screen (*atf3, marco*, and *mpeg1*) have been performed to identify which step of the infection process is affected and which genes and pathways are influenced (Chapters 4, 5, and 6). Here, we investigated one of the hits from the screen, *creld2*, in more detail.

CRELD2 in mice is a glycoprotein of approximately 60-kDa that is localised not only in the ER and Golgi apparatus [28], but is also spontaneously secreted [29]. CRELD2 has been suggested to function as a signalling mediator and to be involved in processing and trafficking of proteins through the ER–Golgi apparatus and is also associated with ER stress-related diseases [28]. During *M. tuberculosis* infection, mycobacteria are capable of secreting early secreted Antigen of 6 kDa (ESAT-6) which in turn can induce ER stress [30], a response that occurs in macrophages of tuberculosis granulomas in areas where apoptotic cells accumulate in both mice and humans [31]. The *Creld2* gene is conserved between humans, mice, and zebrafish; however, the molecular features of Creld2 in either species are unknown. In zebrafish embryos, *in situ* hybridisation revealed that *creld2* (ENSDARG00000029071) is expressed at 1 dpf in the yolk syncytial layer (YSL), liver primordium and intestinal bulb, at 2 dpf in the intestinal bulb and liver, and at 5 dpf in the gut and liver [32]. We have also detected *creld2* expression in macrophage, neutrophil, and lymphocyte populations isolated from transgenic zebrafish larvae carrying fluorescent markers for these cell types (Rougeot et al., unpublished). To gain information about how gene expression is affected in *creld2* morphants during the *M. marinum* infection process, we used RNA sequencing technology (RNA-Seq) which revealed that knockdown of *creld2* pre-mRNA does not lead to a general immune deficiency: however, we observed consistent down-regulation of a group of apolipoprotein genes in both uninfected and infected embryos of both morphants. This is of interest because RNA-Seq analysis of a time course of *M. marinum* infection shows that these genes are collectively regulated in a dynamic pattern of alternating up- and down-regulation (chapter 4). Here we find that this same cluster of genes is down-regulated in both *creld2* morphant groups, either in the absence or in the presence of infection. Further study will be required to dissect the role of Creld2 in mycobacterial pathogenesis and the possible functional relationship with apolipoprotein-mediated lipid transport.

Great care was taken during our screen to avoid false-positive results caused by any off-target effects of the injected morpholinos. By first injecting a dose curve of a morpholino, we could optimise the concentration to prevent development of morphological phenotypes. Once a morpholino produced reproducible differences in *M. marinum* infection levels compared to the control embryos, a second morpholino was used to validate the observed infection phenotype. It is well documented that 15-20% of morpholinos produce non-specific toxic off-target effects [5, 6, 33] and we also encountered morpholinos that produced non-specific morphological phenotypes, even when injected at a very low dose, such as *stat1b*, *irg1l*, and *lgals9l1* (Table 1 and table 2). An additional disadvantage of morpholinos is their temporary knockdown effect which generally lasts for the first few days post fertilisation. The exact time period of knockdown can be studied by performing an RT-PCR (in the case of splice blocking morpholinos used in this study). Despite this temporary knockdown effect, different levels of *M. marinum* infections could be observed, both increased and decreased, in our morpholino screen which is most likely the result of an accumulated effect on mycobacterial growth during the first days of infection.

Despite the two previously mentioned disadvantages, morpholinos remain a rapid and convenient resource for knockdown of a gene of interest and can be used in any wild type or transgenic line of zebrafish, which is ideal for screening purposes. Once an interesting gene has been identified, more time can be invested into creating a mutant zebrafish line. While previously the identification of mutations in zebrafish relied mostly on random ENU mutagenesis, new techniques for targeted mutagenesis purpose have been developed rapidly over the last few years, which use custom nuclease-targeted genome engineering tools like zinc finger nucleases (ZFNs), transcription activator-like effector nucleases (TALENs), and the clustered regularly interspaced short palindromic repeats (CRISPR/Cas) system (reviewed in [34]). These techniques are less time consuming compared to traditional ENU mutagenesis because they do not need multiple outcrosses to reduce background mutations [35]. ZFNs, TALENs and CRISPR/Cas approaches can induce double-strand breaks in DNA that stimulate error-prone non-homologous end joining or homology-directed repair at specific genomic locations [36]. On the one hand, ZFNs proved to be difficult in production, have high costs, and modest efficacy in many applications. On the other hand, TALENs proved to be more easy to produce (open source), have low costs, and a reliably high activity. Recently, the CRISPR/Cas system has proven to also be applicable to zebrafish [37, 38] and although still in further development this system is very promising. It only requires as few as two plasmids, one containing a Cas9 sequence (encoding the Cas9 enzyme that generates a specific double-stranded DNA break) and the second containing the single guide template sequence which enables target recognition with its inserted 20 base pair spacer sequence. It is possible to synthesise this spacer commercially, integrate it into the single guide template plasmid, and synthesise the RNA. Alternatively to the use of the second plasmid, a synthetic template can be used to synthesise the guide RNA, thereby avoiding any cloning steps. Although all three of these targeted approaches

to create mutant zebrafish still can produce off-target effects, they can be an efficient tool to use during the next phase of detailed analysis of target genes identified in initial screens such as our morpholino screen for genes involved in mycobacterium infection.

References

1. Chiang, C.Y., Centis, R. & Migliori, G.B. Drug-resistant tuberculosis: past, present, future. *Respirology* **15**, 413-432 (2010).

2. Swaim, L.E. *et al.* Mycobacterium marinum Infection of Adult Zebrafish Causes Caseating Granulomatous Tuberculosis and Is Moderated by Adaptive Immunity. *Infection and Immunity* **74**, 6108-6117 (2006).

3. Parikka, M. *et al.* Mycobacterium marinum causes a latent infection that can be reactivated by gamma irradiation in adult zebrafish. *PLoS pathogens* **8**, e1002944 (2012).

4. Davis, J.M. *et al.* Real-time visualization of mycobacterium-macrophage interactions leading to initiation of granuloma formation in zebrafish embryos. *Immunity* **17**, 693-702 (2002).

5. Nasevicius, A. & Ekker, S.C. Effective targeted gene 'knockdown' in zebrafish. *Nat Genet* **26**, 216-220 (2000).

6. Ekker, S.C. & Larson, J.D. Morphant technology in model developmental systems. *Genesis* **30**, 89-93 (2001).

7. Woods, I.G. & Schier, A.F. Targeted mutagenesis in zebrafish. *Nat Biotechnol* **26**, 650-651 (2008).

8. Rhodes, J. *et al.* Interplay of Pu.1 and Gata1 Determines Myelo-Erythroid Progenitor Cell Fate in Zebrafish. *Developmental Cell* **8**, 97-108 (2005).

9. Zakrzewska, A. *et al.* Macrophage-specific gene functions in Spi1-directed innate immunity. *Blood* **116**, e1-11 (2010).

10. Kanwal, Z. *et al.* Deficiency in hematopoietic phosphatase ptpn6/Shp1 hyperactivates the innate immune system and impairs control of bacterial infections in zebrafish embryos. *J Immunol* **190**, 1631-1645 (2013).

11. Ledford, J.G., Kovarova, M. & Koller, B.H. Impaired host defense in mice lacking ONZIN. *Journal of immunology* **178**, 5132-5143 (2007).

12. van der Sar, A.M. *et al.* Mycobacterium marinum Strains Can Be Divided into Two Distinct Types Based on Genetic Diversity and Virulence. *Infection and Immunity* **72**, 6306-6312 (2004).

13. Benard, E.L. *et al.* Infection of zebrafish embryos with intracellular bacterial pathogens. *J Vis Exp* **pii: 3781. doi: 10.3791/3781** (2012).

14. Stockhammer, O.W., Zakrzewska, A., Hegedus, Z., Spaink, H.P. & Meijer, A.H. Transcriptome profiling and functional analyses of the zebrafish embryonic innate immune response to Salmonella infection. *J Immunol* **182**, 5641-5653 (2009).

15. Veneman, W.J. *et al.* A zebrafish high throughput screening system used for Staphylococcus epidermidis infection marker discovery. *BMC Genomics* **14**, 255 (2013).

16. d'Alençon, C.A. *et al.* A high-throughput chemically induced inflammation assay in zebrafish. *BMC Biology* **8**, 151 (2010).

17. Mathias, J.R. *et al.* Live imaging of chronic inflammation caused by mutation of zebrafish Hai1. *Journal of Cell Science* **120**, 3372-3383 (2007).

18. Nezhinsky A.E., V.F.J. Pattern recognition for high throughput zebrafish imaging using genetic algorithm optimization. *Lecture Notes in BioInformatics* **6282**, 301-312 (2010).

19. Louis, A., Muffato, M. & Roest Crollius, H. Genomicus: five genome browsers for comparative genomics in eukaryota. *Nucleic Acids Res* **41**, D700-705 (2013).

20. Larkin, M.A. *et al.* Clustal W and Clustal X version 2.0. *Bioinformatics* **23**, 2947-2948 (2007).

21. Ekker, S.C. Morphants: a new systematic vertebrate functional genomics approach. *Yeast* **17**, 302-306 (2000).

22. Eisen, J.S. & Smith, J.C. Controlling morpholino experiments: don't stop making antisense. *Development* **135**, 1735-1743 (2008).

23. Kimmel, C.B., Ballard, W.W., Kimmel, S.R., Ullmann, B. & Schilling, T.F. Stages of embryonic development of the zebrafish. *Dev Dyn* **203**, 253-310 (1995).

24. Stoop, E.J.M. *et al.* Zebrafish embryo screen for mycobacterial genes involved in the initiation of granuloma formation reveals a newly identified ESX-1 component. *Disease Models & Mechanisms* **4**, 526-536 (2011).

25. van der Vaart, M., van Soest, J.J., Spaink, H.P. & Meijer, A.H. Functional analysis of a zebrafish myd88 mutant identifies key transcriptional components of the innate immune system. *Dis Model Mech* **6**, 841-854 (2013).

26. Cambier, C.J. *et al.* Mycobacteria manipulate macrophage recruitment through coordinated use of membrane lipids. *Nature* **505**, 218-222 (2014).

27. Clay, H. *et al.* Dichotomous Role of the Macrophage in Early Mycobacterium marinum Infection of the Zebrafish. *Cell Host & Microbe* **2**, 29-39 (2007).

28. Oh-hashi, K. *et al.* CRELD2 is a novel endoplasmic reticulum stress-inducible gene. *Biochemical and biophysical research communications* **387**, 504-510 (2009).

29. Oh-hashi, K., Kunieda, R., Hirata, Y. & Kiuchi, K. Biosynthesis and secretion of mouse cysteine-rich with EGF-like domains 2. *FEBS letters* **585**, 2481-2487 (2011).

30. Choi, H.H. *et al.* Endoplasmic reticulum stress response is involved in Mycobacterium tuberculosis protein ESAT-6-mediated apoptosis. *FEBS letters* **584**, 2445-2454 (2010).

31. Seimon, T.A. *et al.* Induction of ER stress in macrophages of tuberculosis granulomas. *PloS one* **5**, e12772 (2010).

32. Thisse, B. & Thisse, C. Fast Release Clones: A High Throughput Expression Analysis. *ZFIN Direct Data Submission* (2004).

33. Heasman, J. Morpholino oligos: making sense of antisense? *Developmental biology* **243**, 209-214 (2002).

34. Blackburn, P.R., Campbell, J.M., Clark, K.J. & Ekker, S.C. The CRISPR system--keeping zebrafish gene targeting fresh. *Zebrafish* **10**, 116-118 (2013).

35. de Bruijn, E., Cuppen, E. & Feitsma, H. Highly Efficient ENU Mutagenesis in Zebrafish. *Methods in molecular biology* **546**, 3-12 (2009).

36. Gaj, T., Gersbach, C.A. & Barbas, C.F., 3rd ZFN, TALEN, and CRISPR/Cas-based methods for genome engineering. *Trends Biotechnol* **31**, 397-405 (2013).

37. Hwang, W.Y. *et al.* Efficient genome editing in zebrafish using a CRISPR-Cas system. *Nature biotechnology* **31**, 227-229 (2013).

38. Jao, L.E., Wente, S.R. & Chen, W. Efficient multiplex biallelic zebrafish genome editing using a CRISPR nuclease system. *Proc Natl Acad Sci U S A* **110**, 13904-13909 (2013).

39. Nezhinsky A.E., V.F.J. Efficient and Robust Shape Retrieval from Deformable Templates. *International Symposium on Leveraging Applications of Formal Methods* Part II, LNCS 7610 (T. Margaria, B. Steffen, and M. Merten (Eds.)), 42-55 (2012).

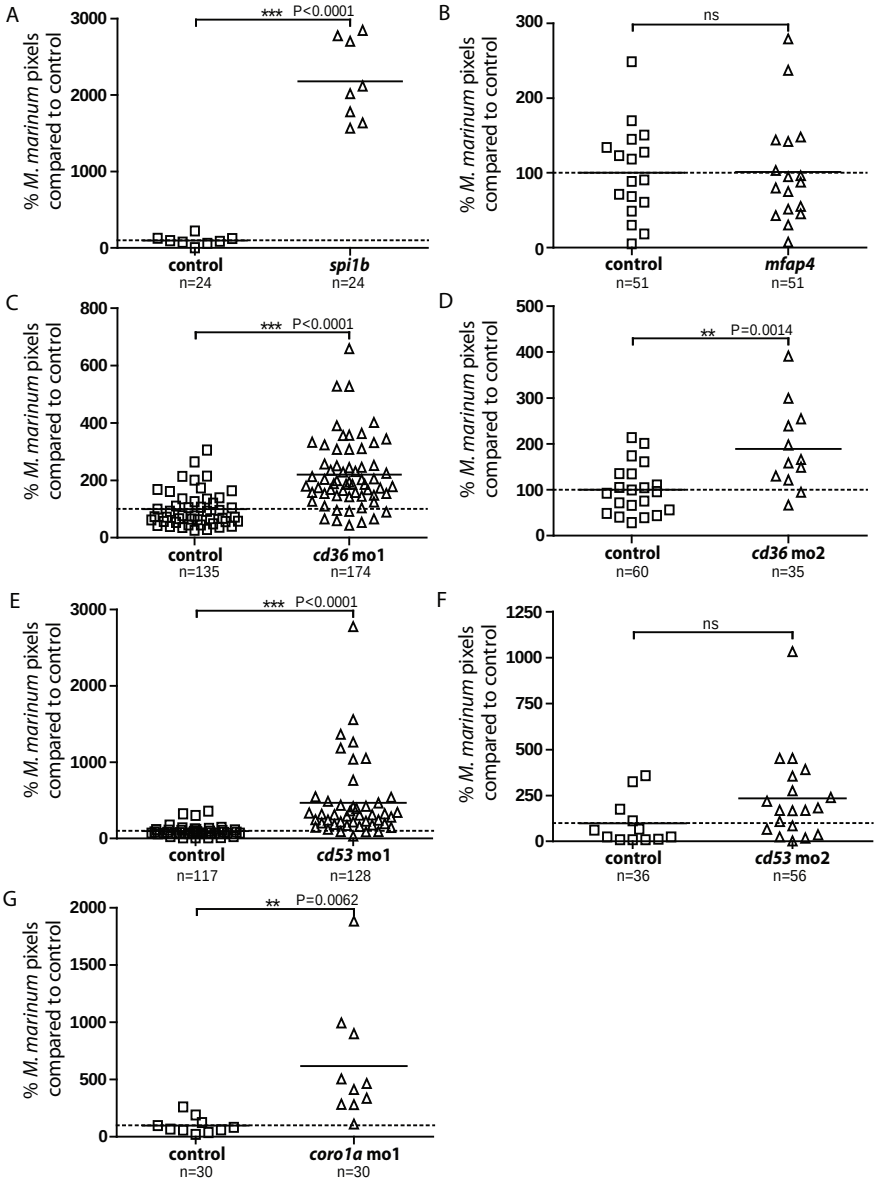

Supplementary figure 1. *M. marinum* pixel count results for morpholinos showing repeated consistent results. AB/TL embryos were injected with morpholinos against a target gene or with standard control morpholino, subsequently injected with mCherry-expressing *M. marinum*, and infected embryos were imaged at 4 dpi. Graphs show combined representative results of all experiments for knockdown of (A) *spi1b*, (B) *mfap4*, (C) *cd36* with morpholino 1, (D) *cd36* with morpholino 2, (E) *cd53* with morpholino 1, (F) *cd53* with morpholino 2, and (G) *coro1a* with morpholino 1. All pixel values of data points are compared against the average pixel value of the infected control embryos and presented as percentages. Results for knockdown of *atf3, marco*, and *mpeg1* can be found in thesis chapters 4, 5, and 6, respectively. The mean ± SEM is indicated (n = number of embryos).

A

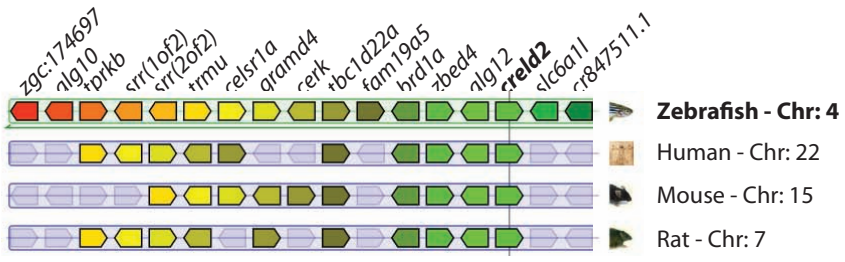

B

```
                                  Signal peptide                    DUF3456 (TLR4 regulator
mCRELD2          MHLLLAAAFGLL--LLLPPPGAVASRK-PTMCQRCRTLVDKFNQGMANTARKNFGGGNTA 57
rCRELD2          MHLLLAAGFGLL--LLLLPP-PAASKK-PTQCQRCRTLVDKFNQGMANTARKNFGGGNTA 56
hCRELD2          MRLPRRAALGLLPLLLLLPPAPEAAKK-PTPCHRCRGLVDKFNQGMVDTAKKNFGGGNTA 59
zCreld2          -MLLSCSIFRLFCIILLLQLGSIYTKDFTALCSTCRQLVDDFDKGLEKTAKQNFGGGNTA 59
                   *   : : *:  :**     .  ::. .: *  ** ***.*::*: .**::********
and MSAP)
mCRELD2          WEEKTLSKYEFSEIRLLEIMEGLCDSSDFECNQLLEQQEEQLEAWWQTLKKEHPNLFEWF 117
rCRELD2          WEEKTLSKYEFSEIRLLEIMEGLCDSSDFECNQLLEQQEEQLEAWWQSLKKDYPNLFEWF 116
hCRELD2          WEEKTLSKYESSEIRLLEILEGLCESSDFECNQMLEAQEEHLEAWWLQLKSEYPDLFEWF 119
zCreld2          WEERKLSKYETSEIRLTEILEGLCQSSNFECSHMLEENEEHLEAWWFKRKTKHPDLFKWF 119
                 ***:.***** ***** **:****:**:***.::** :**:*****   *..:*:**:**
                                  Epidermal growth factor-like domain
mCRELD2          CVHTLKACCLPGTYGPDCQECQGGSERPCSGNGYCSGDGSRQGDGSCQCHTGYKGPLCID 177
rCRELD2          CVRTLKACCLPGTYGPDCKECQGGSERPCSGNGYCSGDGSRQGDGSCQCHAGYKGPLCID 176
hCRELD2          CVKTLKVCCSPGTYGPDCLACQGGSQRPCSGNGHCSGDGSRQGDGSCRCHMGYQGPLCTD 179
zCreld2          CIETIKVCCPKGSFGPDCNTCIGGADRPCHGNGKCDGDGTRAGNGKCSCDEGYDGEFCLD 179
                 *:.*:*.**  *::****  * **::*** *** * .***:* *:*.* *. **.* :* *
                                                  Furin-like repeat
mCRELD2          CTDGFFSLQRNETHSICSACDESCKTCSGPSNKDCIQCEVGWAR-VEDACVDVDECAAET 236
rCRELD2          CMDGYFSLQRNETHSICLACDESCKTCSGPSNKDCVQCEVGWAR-VEDACVDVDECAAET 235
hCRELD2          CMDGYFSSLRNETHSICTACDESCKTCSGLTNRDCGECEVGWVL-DEGACVDVDECAAEP 238
zCreld2          CSDGYFNSLRNDTFFLCKECHESCVGCSGGTNQHCKECRNGWVKDQEGSCIDINECIKDP 239
                 * **:*.  **:*. :*  *.***  *** :*:.* :*. **.   *.:*:*::**   :.
                                                  Furin-like repeat
mCRELD2          SPCSDGQYCENVNGSYTCEDCDSTCVGCTGKGPANCKECIAGYTKESGQCTDIDECSLEE 296
rCRELD2          PPCSEAQYCENVNGSYICEECDSTCVGCTGKGPANCKECIAGYTKQSGQCADIDECSLEE 295
hCRELD2          PPCSAAQFCKNANGSYTCEECDSSCVGCTGEGPGNCKECISGYAREHGQCADVDECSLAE 298
zCreld2          APCSDDQYCLNTDGSFSCKACDIRCTGCKGDGASSCLNCADGYKDEEGTCTDIDECTEDP 299
                 .***  *:* *.:**: *: **  *.**.*.*...* :*  **   : * *:*:***:

mCRELD2          KACKRKNENCYNVPGSFVCVCPEGFEETEDACVQTAEGKVTE-ENPTQPPSREDL 350
rCRELD2          KACKRRNENCYNVPGSFVCVCPDGFEETEDACVQTAQSEVTE-ENPTQPLSHEDL 349
hCRELD2          KTCVRKNENCYNTPGSYVCVCPDGFEETEDACVPPAEAEATEGESPTQLPSREDL 353
zCreld2          ASCS-DNQHCLNTDGSFSC--------EEKVPAFNSEGAKTG-DSPEK---HEDL 341
                  :*   *::* *. **: *         *.. .  ::.  *  :.* :   :***
```

C

Identical / Similar	**z-Creld2**	m-CRELD2	r-CRELD2	h-CRELD2
z-Creld2	**100**	47	47	50
m-CRELD2	78	**100**	91	76
r-CRELD2	77	98	**100**	76
h-CRELD2	77	90	90	**100**

Supplementary figure 2. Conservation of vertebrate *creld2*. Genomic structure and sequence analysis of the zebrafish *creld2* gene. (A) Physical synteny of the region containing the *creld2* gene in zebrafish chromosome 4 (Chr: 4) with human chromosome 22 (Chr: 22), mouse chromosome 15 (Chr: 15), and rat chromosome 7 (Chr: 7). Seventeen genes are included in this figure, each represented by a unique coloured box. Surrounding *creld2* the genes *alg12*, *zbed4*, *brd1a*, *fam19a5*, *tbc1d22a*, *cerk*, *gramd4*, *celsr1a*, and *trmu* are arranged in the same

Supplementary figure 2 continued: order on zebrafish Chr: 4 as on the vertebrate species analysed (human, mouse, and rat). Coding direction of the genes is indicated by the pointed end. Pale blue symbols indicate non-syntenic genes. (B) Multiple alignment of the vertebrate Creld2 proteins. Grey boxes indicate the protein domains signal peptide, DUF3456 (TLR4 regulator and MIR-interacting saposin-like protein (MSAP)), Epidermal growth factor-like calcium binding domain, and furin-like cysteine rich repeats regions. *(asterisk) = single, fully conserved residue, : (colon) = conservation between groups of strongly similar properties - scoring > 0.5 in the Gonnet PAM 250 matrix, . (period) = conservation between groups of weakly similar properties - scoring =< 0.5 in the Gonnet PAM 250 matrix. (C) Homology of protein sequences was determined between zebrafish (zCreld2): ENSDARP00000048382; rat (rCRELD2): ENSRNOP00000006357; human (hCRELD2): ENSP00000332223; mouse (mCRELD2): ENSMUSP00000024042. Amino acid identity and similarity percentages were determined using UniProt CLUSTAL O(1.2.0) multiple sequence alignment.

Chapter 4

Time-resolved transcriptome profiling of the zebrafish host innate immune response to mycobacterium infection

Erica L. Benard, Julien Rougeot, Peter Racz, Herman P. Spaink, Annemarie H. Meijer

Manuscript in preparation

Abstract

Mycobacterium marinum infection in zebrafish embryos is a well-established infection model of mycobacterial pathogenesis. Zebrafish infected with this bacterium develop granulomas similar to *Mycobacterium tuberculosis* infection in humans and the formation of these pathological hallmarks can be visualised in detail in the transparent early larval life stages. To provide a detailed description of the host innate immune response to *M. marinum* infection, we analysed global gene expression levels at multiple time points during infection of zebrafish larvae and interrelated this with imaging data of the infection process and granuloma formation. Our RNA-Seq analysis revealed three distinct phases in the immune response. The early-phase response, during the first hours after phagocytosis of *M. marinum*, is characterised by rapid induction of several transcription factors and a subsequent transient peak of expression of genes linked to pro-inflammatory responses. This is followed by a mid-phase response around 1 day post infection, when expression levels of most genes return to uninfected control levels. Finally, a characteristic late-phase transcriptomal response is initiated when granuloma-like aggregates start forming. This is characterised by increasing expression levels of the same genes that were induced during early-phase and many other inflammation-associated genes. Throughout all phases, profound changes in genes associated with lipid metabolism occur. Notably, the expression profile of a group of apolipoprotein genes is the exact opposite of that of pro-inflammatory genes, showing down-regulation during the early- and late-phase and up-regulation during the mid-phase. In contrast to these dynamic changes in expression, complement components are up-regulated during the entire time course, also during the mid-phase, when other immune related genes show baseline levels. One of the transcription factor genes up-regulated during the early and late phases of infection is *activating transcription factor 3* (*atf3*), which in mice is known to function as a transcriptional repressor of genes involved in the immune response [1, 2]. Embryos in which *atf3* function is inhibited by morpholino treatment have an increased recruitment of macrophages and neutrophils to local inflammatory regions and are better able to control *M. marinum* infection. These results indicate that the induction of *atf3* during *M. marinum* infection antagonises an effective innate immune control of this pathogen.

Introduction

Mycobacterium tuberculosis is a highly successful human pathogen, estimated to have currently infected about one third of the human world population. Host cells express several innate immune pattern recognition receptors (PRRs), such as Toll-like receptors, NOD-like receptors, mannose receptors, scavenger receptors, and complement receptors, that function in the recognition of pathogen associated molecular patterns (PAMPs) of *M. tuberculosis* (reviewed in [3]).This recognition function of the innate immune system provides the first protective barrier of the host against *M. tuberculosis*

and collaborates with the adaptive immune response to control *M. tuberculosis* infection at later stages during infection. The immune response to *M. tuberculosis* infection is not only regulated by the host itself, but also manipulated by the mycobacteria to provide a suitable environment for proliferation, and also promote the immune-mediated responses required for the transmission of disease (reviewed in [4]).

Mycobacterium marinum, a close relative to *M. tuberculosis*, is a natural pathogen of fish and other cold-blooded animals. The genomes of both strains show that there is an *M. marinum* orthologue for 80% of all coding DNA sequences in *M. tuberculosis,* the averaged shared amino acid identity is 85% [5], and many virulence factors found in *M. tuberculosis* have homologous genes in *M. marinum* [6, 7]. Both *M. marinum* and *M. tuberculosis* are capable of surviving and replicating within macrophages. They avoid the bactericidal mechanisms of the macrophage by blocking phagosome-lysosome fusion and both species are also capable of escaping from the phagosome into the cytosol [8-12]. Furthermore, the hallmark of infection with both pathogens is the formation of granulomas, which are highly structured aggregates of infected and non-infected immune cells. Historically these granulomas were strictly regarded as host defence structures containing the infection, but recent insights implicate granulomas, especially the early stages, also in the expansion and dissemination of mycobacterial infection [13].

M. marinum infection of zebrafish shows remarkable resemblance to the human infection with *M. tuberculosis* because caseating granulomas form and latency develops [14, 15]. The transparent embryos and larvae of the zebrafish have become widely used for studying the initial stages of granuloma formation [16, 17]. These studies are facilitated by increasing numbers of fluorescent transgenic zebrafish lines that allow detailed visualisation of the host response towards *M. marinum* infection. *M. marinum* is recognised and phagocytosed extremely rapidly by primitive macrophages following injection into the blood circulation of the zebrafish embryo (Benard et al., chapter 5) [16]. Phagocytosis by macrophages has proven to be an important mechanism of innate immunity, as zebrafish embryos lacking functional leukocytes are not capable of restricting mycobacterial growth [18]. Despite the controlling mechanism of macrophages on the growth of *M. marinum*, this pathogen is still capable of growing restrictedly within these cells. Furthermore, *M. marinum* can direct macrophages to aggregate into granulomas by producing the virulence determinant RD1 (region of deletion 1)-dependent signal [19]. Subsequently, infected macrophages can be seen to leave primary granulomas, either via tissue migration or via the vasculature, and can then initiate secondary granulomas [20]. These events take place during the first few days of zebrafish embryo and early larval development, at which stages an active adaptive immune system is lacking [21]. Thus, the context of innate immunity appears to be sufficient for granuloma formation [16]. Knockdown of tumour necrosis factor receptor 1 (TR1) or knockout of myeloid differentiation factor 88 (*myd88*) have demonstrated the importance of innate immune control in the zebrafish embryo *M. marinum* infection model. In the absence of TNF signalling, *M. marinum* intracellular growth and granuloma formation were

accelerated and followed by necrotic death of overladen macrophages and breakdown of granulomas [22]. Similarly, knockout of *myd88* accelerated formation of granuloma-like aggregates and increased the bacterial burden, which was associated with lower induction of genes central to innate immunity [23].

To support the increasing use of the zebrafish embryo model for *M. marinum* infection, we aimed to provide a detailed time-resolved expression analysis of the innate immune response using RNA deep sequencing (RNA-Seq) technology. We therefore determined RNA-Seq profiles of *M. marinum* infected and non-infected embryos throughout a time course of infection every 2 hours from 2 to 8 hours post infection (hpi) and daily from 1 to 5 days post infection (dpi). To relate these expression profiles to different stages in the infection process, we visualised the host-pathogen interactions over the same time course using a fluorescent macrophage-specific transgenic line in combination with transgenic lines marking neutrophils and endothelial cells of the vascular and lymphatic system. In order to test whether our expression data has functional implications, we analysed the effect of morpholino knockdown of *activating transcription factor 3* (*atf3*) as it is one of a group of transcriptional regulators that showed a significant up-regulation at both early and late stages of infection. We provide evidence that knockdown of *atf3* leads to a decreased mycobacterial load as well as increased macrophage and neutrophil inflammatory migration.

Materials and methods

Zebrafish lines and handling of embryos

Zebrafish were handled in compliance with the local animal welfare regulations and were maintained according to standard protocols (zfin.org). The culture was approved by the local animal welfare committee (DEC) of the University of Leiden and all protocols adhered to the international guidelines specified by the EU Animal Protection Directive 2010/63/EU. Zebrafish lines used in this study included AB/TL, *Tg(fli1a:EGFP)* [24], *Tg(mpx:GFP)*^{i114} [25], *Tg(mpeg1:EGFP)*, and *Tg(mpeg1:mCherry-F)*^{UMSF001} [26]. Embryos were grown at 28.5-30°C in egg water (60 µg/ml Instant Ocean sea salts). For the duration of bacterial injections and imaging, embryos were kept under anaesthesia in egg water containing 200 µg/ml tricaine (Sigma-Aldrich). Embryos used for stereo fluorescence imaging were kept in egg water containing 0.003% 1-phenyl-2-thiourea (Sigma-Aldrich) to prevent melanisation.

Morpholino knockdown

Morpholino oligonucleotides (Gene Tools) were diluted to the desired concentration in 1x Danieau buffer (58 mM NaCl, 0.7 mM KCl, 0.4 mM $MgSO_4$, 0.6 mM $Ca(NO_3)_2$, 5.0 mM HEPES; pH 7.6) containing 1% phenol red (Sigma-Aldrich) and 1 nL was injected into the yolk at the 1-2 cell stage using a Femtojet injector (Eppendorf).

For knockdown of *atf3*, two splice blocking morpholinos were used, morpholino 1 targeting intron 2 – exon 3 and morpholino 2 targeting intron 3 – exon 4 boundaries (*atf3* mo1: 5'GGACAGCCTGAAATAACAACATCTA3', 0.2 mM and *atf3* mo2: 5'CTTCTCAGACTCCTAAAGTCAAAAC3', 0.2 mM) and one translation blocking morpholino (*atf3* ATG: 5'GTGCTGAAGCATCATGCCGAAATCT3', 0.1 mM). As a control the standard control morpholino from Gene Tools was used at the same concentrations as the other morpholinos.

Chemically induced inflammation

Copper sulphate ($CuSO_4$, 10 uM, 2 hours treatment) Merck, #1027910250) was administered via the egg water to induce cell death of neuromast hair cells [27].

Infection experiments

Mycobacterium marinum infections were performed using the wild type Mma20 strain expressing mCherry in a pSMT3 vector (250 cfu) [28] for RNA-Seq, qPCR analysis and imaging experiments. Additionally, when triple-fluorescence imaging was performed, the wildtype M strain expressing E2-Crimson in a pSMT3 vector (250 cfu) [15] was used. Both wild type strains are human isolates and AFLP-DNA fingerprint identifies them both as Cluster I strains which cause acute disease [28]. We observe a similar behaviour in embryonic infection with both wild type strains. Embryos were staged at 24 hpf by morphological criteria [29] and manually dechorionated. Bacteria were prepared and injected into the blood circulation at 28 hpf, and 2% PVP was injected as a control [30].

RNA isolation, cDNA synthesis, and expression analyses

Pools of 30 embryos for RNA isolation were snap frozen in liquid nitrogen and subsequently stored at -80°C. Time course RNA-Seq reactions were performed with four biological replicates. Embryos were homogenized in 0.7 ml of QIAzol® Reagent (Qiagen) and subsequently total RNA was extracted and on-column DNase digestion was performed with a miRNeasy Mini Kit (Qiagen) according to the manufacturer's instructions. RNA sequencing was performed as previously described with a minimum of 10 million reads per sample [31]. qPCR analysis was performed as described [32]. Primers for *il1b* and *mmp9* are described in [33], *apoa4* are described in [34], and *il8* are described in [32]. All data (mean ± SEM) were analysed using unpaired, two-tailed t-tests for comparisons between two groups (*, $p<0.05$; **, $p<0.01$; ***, $p<0.001$). For RNA deep sequencing, significant differences were calculated by DESeq analysis of transcript count data (*=fold change>2, $p<0.05$).

Proportional Venn diagrams were created with a Venn Diagram Generator (http://jura.wi.mit.edu/bioc/tools/venn.php). Gene ontology analysis was performed using DAVID v6.7 (http://david.abcc.ncifcrf.gov/home.jsp) [35]. Gene ontology terms are considered significant when the false-discovery rate was below 5%.

Knockdown of *atf3* with splice morpholino 1 and morpholino 2 was verified by RT-PCR with the SuperScript® One-Step RT-PCR System (Invitrogen, #10928-034) using 50 ng of DNAse treated RNA template. RT-PCR primers for *atf3* Mo1 knockdown verification were FW: 5'ATGTCCAACGGCATGAGCAC3'; REV: 5'GCGGTGTGTGTTGGTCCATT3'. The following adjustments were made to the PCR settings: 59.4°C for 30 seconds for the annealing step with 40 cycles of the PCR amplification. RT-PCR primers for *atf3* Mo2 knockdown verification were FW 5'ATTGTTGATGGGTGGGTGTTG3' RV: 5'TCCTCGATCTGAGCTTTCAGC3'. The following adjustments were made to the PCR settings: 54°C for 30 seconds for the annealing step with 1 min elongation at 72°C with 40 cycles. Morpholino 2 targets the intron3-exon4 boundary site leading to an intron inclusion (exon 4 is the last exon). The RT-PCR primers used were designed to amplify the retained third intron during *atf3* morpholino 2 knockdown. RNA from pools of 30 infected and uninfected *atf3* morphants and control embryos at 4 dpi (one biological replicate) was isolated as described above and RNA sequencing was performed as previously described [31].

Immunohistochemistry

Identification of neutrophils and macrophages was done by immuno-labelling with a leukocyte specific L-plastin antibody and Alexa568/488-conjugated secondary antibody, combined with neutrophil specific staining for myeloperoxidase activity [36].

Image analysis

Fluorescence images were taken with a Leica MZ16FA stereo fluorescence microscope equipped with a DFC420C digital colour camera. Overlay images of bright field and fluorescence stereomicroscopy and merged channel maximum intensity z-stack projections were made and stitched together in Fiji. In *M. marinum* infection experiments, bacterial pixel counts of stereo fluorescence images were analysed using dedicated pixel quantification software (Benard et al., chapter 6) and bacterial pixel counts of stitched confocal images of the tail regions of embryos were analysed with Fiji. E2-Crimson channels (8-bit) were made binary and the 'analyze particle' function was used to determine number of clusters and pixel values per image. All bacterial pixel count data (mean ± SEM) were analysed using unpaired, two-tailed t-tests for comparisons between two groups (***, $p<0.001$). Confocal images were taken on a Leica TCS SPE with a HC APO 20x 0.7 NA objective and a HCX APO 40x 0.8 NA objective or on a Zeiss LSM5 Exciter / AxioObserver with an HC APO 20x 0.7 NA objective.

Results

Timing of events during the *M. marinum* infection process in zebrafish embryos

In this study we used fluorescence markers to visualise the sequence of events during the first days of the mycobacterial pathogenesis in zebrafish embryos up to the early larval stage and interrelated this with a time-resolved RNA sequencing analysis of the host innate immune response. At 40 minutes post infection (mpi) after intravenous injection of a single cell suspension of *M. marinum* (250 colony forming units (cfu)) we observed that the bacteria are completely internalised by predominantly macrophages (*mpeg1:mCherry-F*) (fig. 1A) and at 2 hpi occasionally by neutrophils (*mpx:GFP*) around the site of injection (fig. 1B). Using a combination of transgenic markers for macrophages (*mpeg1:mCherry-F*) and endothelial cells (*fli1a:EGFP*) and E2-Crimson-expressing *M. marinum* we determined that between 6 hours post injection (hpi) and 1 day post injection (dpi) infected cells travel through the vascular system (fig. 1C-G, supplementary movie S1) and can occasionally be observed outside the blood circulation, adjacent to the duct of Cuvier (fig. 1E) and posterior to the transition of the caudal vein and artery (fig. 1G). However, the majority of the infected cells remain within the vasculature during these stages. At 2 dpi *M. marinum* infected macrophages can be observed within the caudal fin of the embryo (fig 1H). In addition, infected cells travel through the intersegmental vessels, the infection spreads from the caudal vein to the dorsal longitudinal lymphatic vessel, and *M. marinum* can also be seen outside the caudal vein (fig. 1I). Between 2 and 5 dpi clusters of *M. marinum* tend to stay in the same position, where they continue to grow and form tight infection structures. During this growth process the structures extend from inside the blood circulation to outside the vessels (fig. 1I-J).

The formation of granuloma-like structures becomes evident by comparing uninfected embryos (fig. 1K-O) with *M. marinum* infected embryos (fig. 1P-Y) obtained from double transgenic zebrafish carrying the macrophage marker *mpeg1:mCherry-F* and the neutrophil marker *mpx:GFP*. At 1 dpi the infected macrophages and uninfected neutrophils are still spread evenly and no clusters of cells can be seen (fig. 1P), quite similar to the macrophage and neutrophil distribution of uninfected embryos (fig. 1K). At 2 dpi the first clusters can be observed consisting of more infected and uninfected macrophages and a few uninfected neutrophils (fig. 1Q). At 3 dpi neutrophils are attracted to the forming tight aggregates of infected macrophages (fig. 1R) and infected neutrophils can be observed for the first time within the granuloma-like structures (supplementary fig. 1A). At 4 dpi the morphology of the infected macrophages changes to a more rounded shape (fig. 1S) and these cells contain a high level of bacterial fluorescence (fig. 1X), indicating that they are severely infected and this phenomenon is even more apparent at 5 dpi (fig. 1T) when the macrophage fluorescence markedly diminishes. At this stage the number of neutrophils surrounding the granuloma-like structure is increased again compared to the previous day and the granuloma structures start protruding the epithelial layer of the embryo (supplementary fig. 1B).

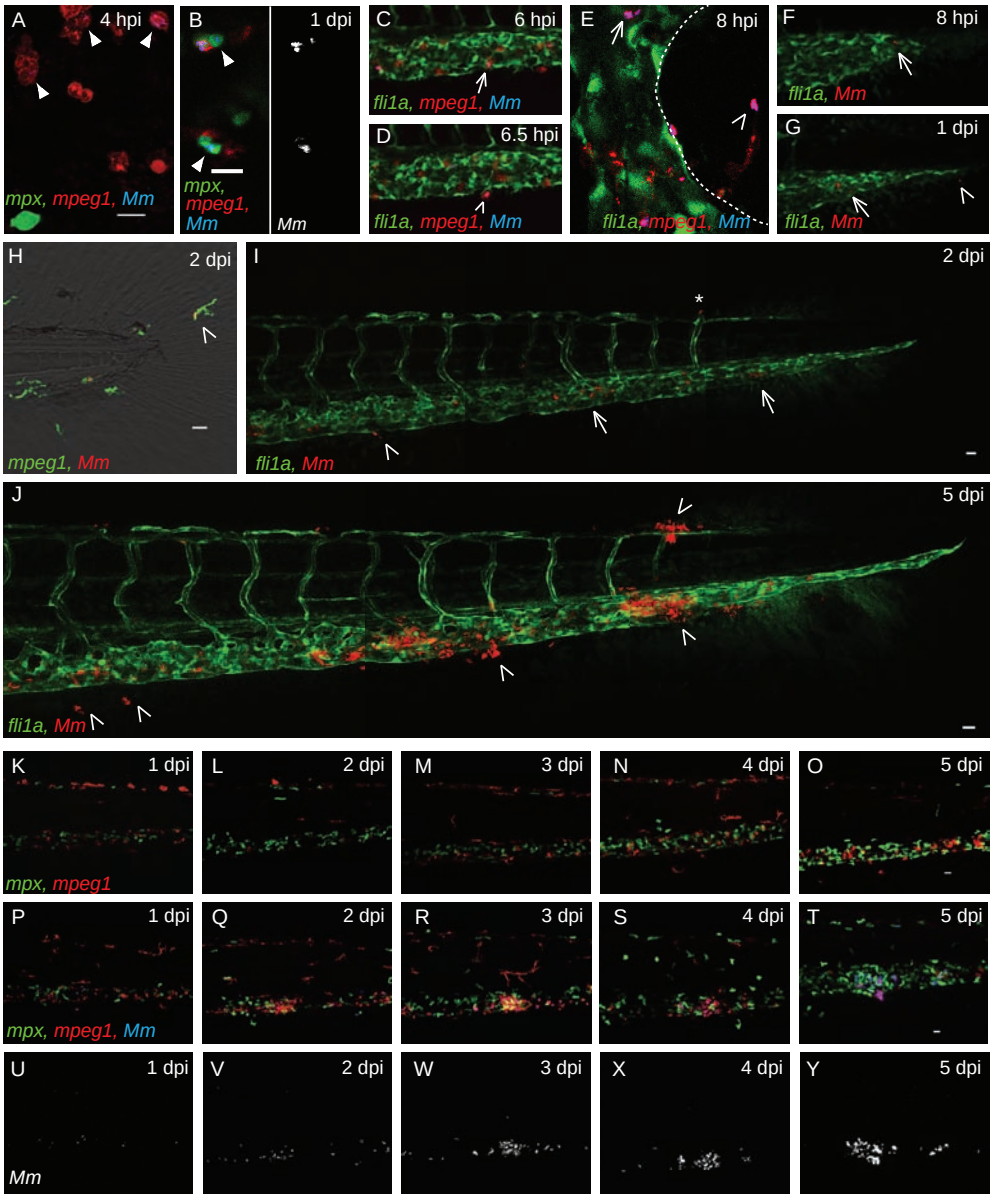

Figure 1. Overview of the *M. marinum* infection process imaged in zebrafish embryos. (A) E2-Crimson-expressing *M. marinum* bacterial infection in *Tg(mpeg1:mCherry-F)/Tg(mpx:GFP)* embryos at 4 hpi imaged at Duct of Cuvier site. Solid arrow heads indicate infected macrophages. (B) E2-Crimson-expressing *M. marinum* bacterial infection in *Tg(mpeg1:mCherry-F)/Tg(mpx:GFP)* embryos at caudal vein site. Left panel: overlay of all three fluorescence channels, right panel: E2-Crimson fluorescence channel with *M. marinum* fluorescence depicted as white pixels. Solid arrowheads indicate infected neutrophils. (C-E) E2-Crimson-expressing *M. marinum* bacterial infection in *Tg(fli1a:EGFP) / Tg(mpeg1:mCherry-F)* embryo imaged over time at (C–D and supplementary movie 1)) the caudal vein at 6 and 6.5 hpi and (E) the Duct of Cuvier site at 8 hpi. *M. marinum* infected macrophages (purple colour: double positive for mCherry and

Figure 1 continued: E2-Crimson) are observed both (arrows) inside and (pointed arrowheads) outside the vasculature. Dotted line in (E) indicates border of vasculature in Duct of Cuvier. (F-G) mCherry-expressing *M. marinum* bacterial infection in a *Tg(fli1a:EGFP)* embryo at the transition of the caudal vein and artery at (F) 8 hpi and (G) 1 dpi. *M. marinum* can be observed (arrow) inside and (pointed arrowhead) outside the vasculature. (H) mCherry-expressing *M. marinum* bacterial infection in a *Tg(mpeg1:EGFP)* embryo imaged at the posterior tail area. Merged image of bright field, GFP and mCherry channels show an infected macrophage (pointed arrowhead) located in the caudal fin. (I-J) mCherry-expressing *M. marinum* bacterial infection in a *Tg(fli1a:EGFP)* embryo imaged at the tail region at (I) 2 dpi and (J) 5 dpi. An *M. marinum* cluster can be seen (asterisk) in the dorsal longitudinal lymphatic vessel and various *M. marinum* clusters can be seen residing (arrow) within the caudal vein and (pointed arrowhead) outside the caudal vein at (I) 2 dpi. These clusters increase in size at (J) 5 dpi and clusters previously inside the caudal vein at 2 dpi are now observed (pointed arrowhead) outside the caudal vein. (K-O) Uninfected (mock injected) *Tg(mpx:GFP)/Tg(mpeg1:mCherry-F)* embryo tail region posterior to the urogenital opening imaged over a time course of (K) 1 dpi, (L) 2 dpi, (MI) 3 dpi, (N) 4 dpi and (O) 5 dpi. Images are z-stack projections of the merged channels of GFP and mCherry. (P-Y) E2-Crimson-labelled *M. marinum* bacterial infection in a *Tg(mpx:GFP)/Tg(mpeg1:mCherry-F)* embryo imaged in identical area as (K-O) uninfected embryo over time course of (P) 1 dpi, (Q) 2 dpi, (R) 3 dpi, (S) 4 dpi and (T) 5 dpi. Images are z-stack projections of the merged channels of GFP, mCherry and E2-Crimson. (U-Y) Z-stack projections of the E2-Crimson channel isolated from P-T and depicted as white pixels. Scale bars: 20 µm.

The profiles of the gene expression response to *M. marinum* infection can be divided into an early, mid, and late-phase

For a detailed characterisation of the host innate immune response during the course of *M. marinum* infection, we sampled pools of 30 embryos every 2 hours from 2 hpi to 8 hpi and daily from 1 dpi to 5 dpi. Four biological replicates of each time point were used for RNA sequencing and DeSeq was used for statistical comparison with mock-injected control embryos sampled at the same time points [37]. At 2 hpi, an immediate response to the infection was observed with 170 up-regulated genes and 64 down-regulated genes. Subsequently, over the time period between 4 hpi and 1 dpi, the total number of differently regulated genes was at least 3-fold lower (55 up and 33 down at 4 hpi, with a further decline between 6 hpi and 1 dpi (fig. 2A, table 1). Subsequently, an increase in up- and down-regulated genes was seen at 2 dpi (310 up and 459 down) which then decreased slightly at 3 dpi but continued to increase remarkably at 4 (1165 up and 748 down) and 5 dpi (1394 up and 668 down) when the embryos were highly infected.

Based on the apparent trend in gene regulation, we divide the transcriptional response in three main phases: an immediate early-phase with a clear response at 2 dpi and rapid decline at 4 hpi, a mid-phase response from 4 hpi to 1 dpi when there is low differential gene regulation, and a late-phase response, which starts from 2 dpi but is mainly characterised by a striking increase in differential gene expression at 4 and 5 dpi (fig. 2A). When we look at the overlap between different time points, we find that there is remarkable little overlap between consecutive time points of the series up to 4 dpi (table 1). For example, in the early phase only 13 up-regulated genes were overlapping between 2 hpi and 4 hpi, and there was no overlap of the down-regulated genes (fig. 2B). The only genes that were significantly up-regulated for each time point during 2 hpi until 8 hpi are the matrix metalloproteinase gene *mmp9* and a non-coding RNA (*si:dkey-97i18.5*). Hardly any overlap can be found when comparing two mid-phase stages (6 hpi with 1 dpi), during which a very low number of genes are differentially regulated (fig. 2B). This is quite the opposite when the final two time points of the late-phase time points are compared (4 dpi with 5 dpi), when a high overlap is evident between the up-regulated genes (table 1). Furthermore, there was also higher overlap between the earliest time point (2 hpi) and the latest time points (4 and 5 dpi). This is reflected in the results of gene ontology (GO) analysis using DAVID [35], which shows up-regulated biological process categories that are identified during both the early-phase and late-phase responses: response to bacterium and proteolysis (fig. 2C and supplementary table 1). In contrast, during the mid-phase response the category of lipid transport is exclusively detected at 1 dpi. Hexose metabolic process, oxygen transport, and muscle contraction are exclusively up-regulated at the beginning of the late phase at 2 dpi (fig. 2C). Notable at this time point was also the down-regulation of genes related to the GO-terms homeostatic process and DNA replication initiation. The up- and down-regulated gene groups at 2 dpi show that the transition between the mid-phase and late-phase in the infection process is associated with strong effects on the host metabolism.

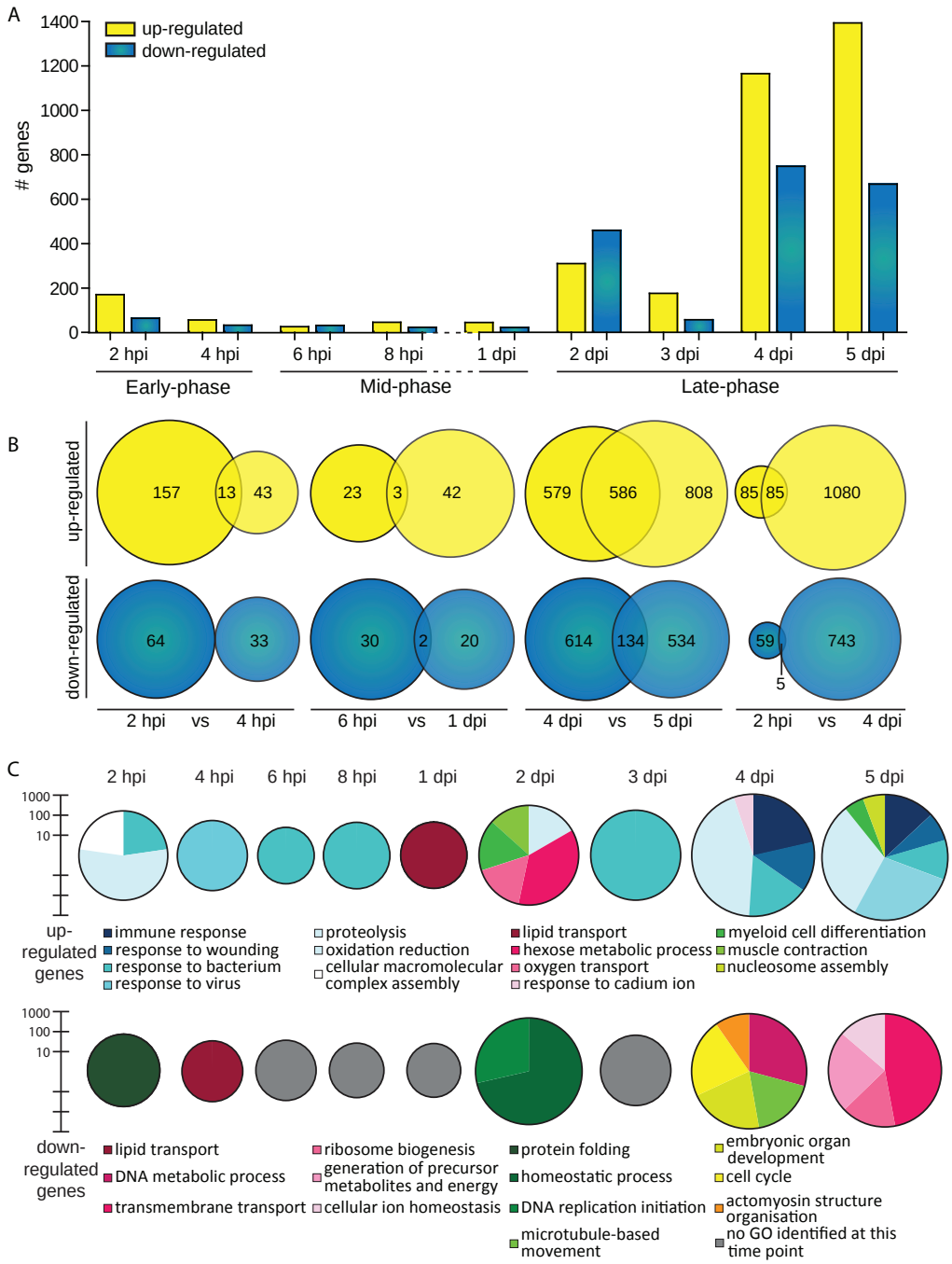

Figure 2. Overview of total number of genes differentially regulated in M. marinum infected embryos, their overlap between various time points and Gene ontology terms enriched per time point. AB/TL embryos were infected with *M. marinum* Mma20 strain at 1 dpf and their expression profiles were compared to their mock-injected control embryos at 2, 4, 6 and

Figure 2 continued: 8 hpi and 1, 2, 3, 4 and 5 dpi. (A) Overview of the total number of genes either significantly up-regulated (yellow) or down-regulated (blue) per time-point in the *M. marinum* infected samples compared to the uninfected control embryos. (B) Area-proportionate Venn-diagrams representing the overlap of both up-regulated and down-regulated genes during *M. marinum* infection. The time points compared are 2 hpi versus 4 hpi, 6 hpi versus 1 dpi, 4 dpi versus 5 dpi, and 2 hpi versus 4 dpi (respectively left versus right circle for each comparison). (C) Gene ontology terms identified per time point represented as pie charts. The diameter of each chart is proportional to the total number of genes up-regulated (top) or down-regulated (bottom) per time point. Colours illustrate the relative proportion of each identified gene ontology term. Genes without associated gene ontology term are not represented in the pie charts (except for time points with no gene ontologies identified).

Table 1: Overlap of genes up- and down-regulated during *M. marinum* time course infection.

# overlap UP	2 hpi	4 hpi	6 hpi	8 hpi	1 dpi	2 dpi	3 dpi	4 dpi	5 dpi
2 hpi	170	13	6	23	18	28	18	85	88
4 hpi		56	7	9	3	29	23	37	38
6 hpi			26	9	3	16	12	17	17
8 hpi				46	21	22	14	20	24
1 dpi					45	20	6	17	14
2 dpi						310	41	70	69
3 dpi							176	83	98
4 dpi								1165	586
5 dpi									1394

# overlap DOWN	2 hpi	4 hpi	6 hpi	8 hpi	1 dpi	2 dpi	3 dpi	4 dpi	5 dpi
2 hpi	64	0	2	3	1	8	4	5	6
4 hpi		33	1	2	2	1	0	6	1
6 hpi			32	2	2	1	0	2	1
8 hpi				23	3	7	0	2	3
1 dpi					22	9	5	3	3
2 dpi						459	6	40	29
3 dpi							57	14	7
4 dpi								748	134
5 dpi									668

There was no overlap between the time points in down-regulated biological process categories (fig 2C). In addition to the strong down-regulation response at 2 dpi, many down-regulated gene groups were detected at 4 and 5 dpi, with gene ontology terms mainly related to DNA and protein metabolism and transmembrane transport.

Detailed analysis of gene expression profiles

Following the global gene ontology analysis, we looked in more detail at the expression patterns of different functional groups of genes over the infection time course. This showed that a major part of the immediate early response to *M. marinum* infection at 2 hpi is the up-regulation of transcription factor genes (fig 3A). These included members of the activating transcription factor (ATF) family, the interferon regulatory factor (IRF) family, the CCAAT/enhancer binding protein family (CEBP), the AP-1 (FOS and JUN family), and the NFκB family. About half of these transcription factor genes were still up-regulated at 4 hpi, after which their expression levels returned to the uninfected control levels between 6 hpi to approximately 3 dpi only to become significantly induced again during the final stage of the late phase response at 4-5 dpi (fig 3A).

Pro-inflammatory cytokines produced by phagocytes, such as tumor necrosis factor alpha (TNF-α) and interleukin 1 beta (IL-1β), play an important role in control of mycobacterial infection. IL-1β expression is tightly controlled by a signal that can induce the expression of pro-IL-1β and a signal that results in the maturation of IL-1β via inflammasome-mediated cleavage by caspase-1 [38]. During *in vivo M. tuberculosis* infection in mice, it was shown that IL-1β is essential for MyD88-dependent host resistance [39]. In zebrafish, the presence of a MyD88-dependent signalling route leading to *il1b* induction has been demonstrated during *M. marinum* infection [23]. The zebrafish genome contains two homologs of the TNF-α gene (named *tnfa* and *tnfb*) [40] and it was demonstrated that a strict balance of TNF-α signalling is essential for control of *M. marinum* infection in zebrafish embryos [41]. During the *M. marinum* infection, up-regulation of *il1b* and both *tnf*-α genes can be observed as well as up-regulation of two chemokine genes, *il8* (*cxcl8*) and *cxcl-c1c*. Similar to its human counterpart, zebrafish *il8* has been shown to mediate neutrophil recruitment [42, 43] and *cxcl-c1c* is an *il8*-related chemokine that is also induced during Salmonella infection [32]. Analysis of the *M. marinum* infection time course shows that there are two apparent waves of significant up-regulation of pro-inflammatory cytokines, the first at 4 hpi when *il1b* , *tnfb* (tumor necrosis factor alpha b), *il8* and *cxcl-c1c* peak and the second at 3 – 5 dpi when *il8* and *cxcl-c1c* are first up-regulated at 3 dpi followed by the additional up-regulation of *il1b* at 4 dpi and *tnfa* (tumor necrosis factor alpha a) and *tnfb* at 4 dpi onwards. Induction of *il1b* and *il8* was confirmed with qPCR analysis (supplementary fig. 2F and G).

Matrix metalloproteinases (MMPs) have been implicated in tissue remodelling and cytokine processing [44]. In zebrafish, *mmp9* has been shown to play an important role during *M. marinum* infection by facilitating the recruitment of leukocytes to the site of infected macrophages (fig. 1P-T) [45]. *mmp9* as well as *mmp13a* were found to be significantly up-regulated at most time points during the course of infection (fig. 3C) and the observed up-regulation of *mmp9* was confirmed with qPCR analysis (supplementary fig. 2H). A similar pattern was observed for the expression of *tissue inhibitor of metalloproteinase 2b* (*timp2b*), presumably functioning to avoid excess tissue damage by inhibiting the strongly induced MMPs. TIMPs can bind in a non-covalent manner to the catalytic domain of MMPs, thus regulating their activity [46]. Other metalloproteinases, such as members of the ADAM (A Disintegrin And Metalloproteinase) family, were only up-regulated during the late-phase of infection (supplementary fig. 2A).

Remarkably, a group of 10 genes related to lipid metabolism and transport appeared to be co-regulated, showing strong fluctuations throughout the infection process. This group of 9 apolipoprotein genes and a fatty acid binding protein gene (*fabp1b.1*) was first up-regulated at 2 hpi and subsequently down-regulated at 4 hpi (fig. 3D), exactly coinciding with the transient peak in pro-inflammatory cytokine induction (fig. 3B)). The down-regulation of *apoa4* at the 4 dpi time point was confirmed with qPCR analysis (supplementary fig. 2I). After the down-regulation at 4 hpi, the gene group was notably up-regulated again between 8 hpi and 2 dpi, and subsequently showed another trend

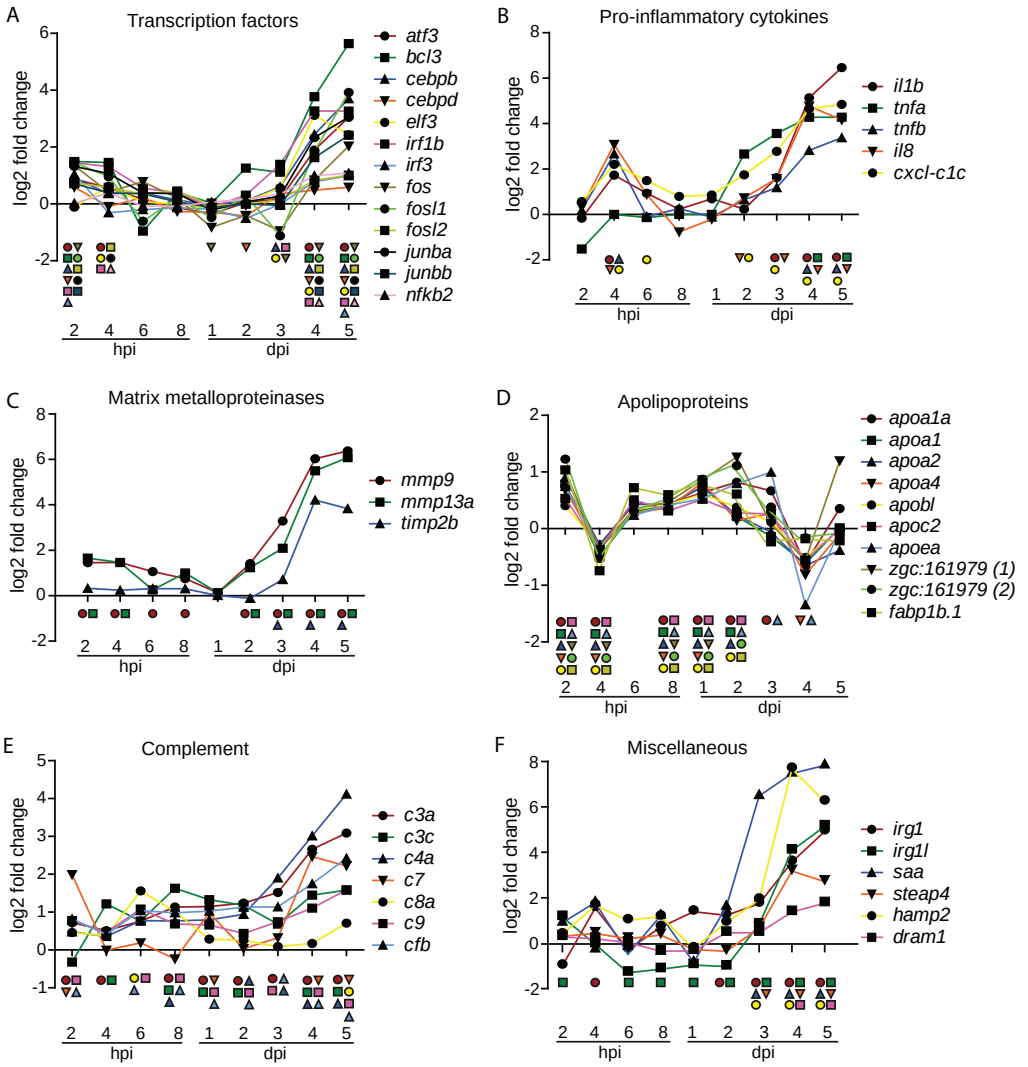

Figure 3. Overview of gene expression profiles during *M. marinum* infection. Gene expression levels of groups of selected genes during a time course of *M. marinum* infection are represented as log2 fold change values. Groups of genes represented are: (A) transcription factors; (B) pro-inflammatory cytokines and chemokine cxcl-c1c; (C) matrix metalloproteinases and inhibitor; (D) apolipoproteins; (E) complement components; (F) miscellaneous late-phase responses. Statistically significant data points (adjusted P-value <0.1) are indicated below the x-axis as the shape filled with the colour of the specific gene (see legend for gene shape and colour). Gene IDs and descriptions can be found in supplementary table 2. Only genes are shown for which differential expression was significant in at least one time point.

towards down-regulation at 4 dpi, but significant only for some genes in the group. The way these genes are regulated is quite remarkable because they are the few genes that are collectively up-regulated during the mid-phase period of the *M. marinum* infection time course, when differential expression of other genes is minimal.

Complement can be immediately activated in response to an invading pathogen and it has been reported that maternal complement components are present in zebrafish eggs [47]. Here, we observed that the expression levels of complement components such as *c3a*, *c7*, *c9,* and *cfb* are rapidly up-regulated by *M. marinum* infection at 2 hpi (fig. 3A). In the subsequent stages of infection different complement components continue to show up-regulated expression. Thus, this is one of the few up-regulated gene groups during the mid-phase, similar to the apolipoprotein gene group. However, in contrast to the apolipoprotein genes, expression of complement genes strongly increased during the late-phase of infection (4-5 dpi) (fig. 3A).

In addition to the above mentioned functional gene groups, we present in Fig. 3F the expression profiles of a miscellaneous group of genes that were previously shown to be important during infection, including: the genes for mitochondria-localising enzymes encoded by *immunoresponsive gene 1-like* (*irg1l*) and *immunoresponsive gene 1* (*irg1*), which was shown to augment bactericidal activity of macrophage-lineage cells by regulating β-oxidation-dependent mitochondrial ROS production [48]; the acute phase response gene *serum amyloid A* (*saa*), an apolipoprotein family member highly expressed in response to inflammation and tissue injury [49]; the metalloreductase gene *six transmembrane epithelial antigen of prostate 4* (*steap4*) (also known as *tumor necrosis factor alpha-induced protein 9* (*tnfaip9*) or *six-transmembrane protein of prostate 2* (*stamp2*), which was shown to play a role in integration of inflammatory and metabolic responses and previously linked with *M. marinum* expression in zebrafish [50-52]; the *hepcidin antimicrobial peptide 2* (*hamp2*) gene involved in microbial killing [53], and the autophagy modulator gene *DNA-damage regulated autophagy modulator 1* (*dram1)*, which our laboratory recently showed to protect against mycobacterial infection in zebrafish [54]. All these genes are strongly up-regulated during the late phase of infection at 4 and 5 dpi, while *irg1* and *irg1l* additionally show up- or down-regulated expression also at earlier time points (fig. 3F). Concomitant with the up-regulation of this miscellaneous group of genes during the late-phase of infection, three other groups of genes are up-regulated, namely a group of prostaglandin genes (supplementary fig. 2C), a group of genes coding for various negative regulators of the immune response (supplementary fig. 2D), and a group of NADH oxidase complex genes (supplementary fig. 2E).

Atf3 impairs control of bacterial growth

Activating transcription factor 3 (*atf3*) is one of the transcription factor genes that we observed to be up-regulated during the early-phase response at 2 and 4 hpi and during the late-phase response at 4 and 5 dpi (fig. 4A). Human ATF3 belongs to the cAMP responsive element-binding (CREB) protein family of transcription factors and is characterised as an immediate early response gene that is induced in cells exposed to a variety of stress stimuli [55]. We chose a morpholino knockdown approach to determine whether *atf3* has an effect on the bacterial growth of *M. marinum*. Knockdown of *atf3* with a splice blocking morpholino resulted in a significantly reduced bacterial burden at 4 dpi compared to the control embryos (fig. 4B and E; supplementary fig. 3A). This effect could be pheno-copied with a second splice blocking morpholino (fig. 4C and F; supplementary fig. 3B) and with a morpholino targeting the translational start site (fig. 4D and G). Since knockdown of *atf3* results in a better control of *M. marinum* infection, we conclude that the transcriptional up-regulation of *atf3* is not a host beneficial response in acute infection in zebrafish larvae.

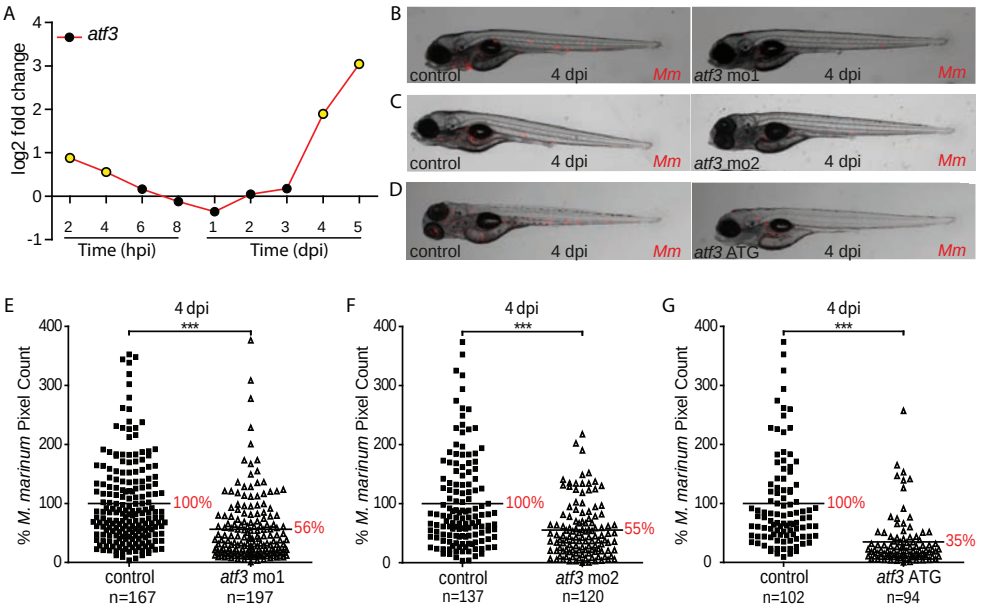

Figure 4. Regulation and function of *atf3* in promoting *M. marinum* infection. (A) Gene expression levels of *atf3* during *M. marinum* time course, represented as log2 fold change in RNA-Seq data compared with uninfected control. Light colouring of a data point indicates that *atf3* expression in infected embryos was significantly different from uninfected controls at this time point. (B-D) Representative overlay images of infected *atf3* (B) splice blocking morpholino 1 (mo1), (C) splice blocking morpholino 2 (mo2), (D) translation blocking morpholino (ATG) injected morphants and their infected standard control morpholino injected controls. (E-G) Bacterial burden of each group was quantified by determining the number of fluorescent bacterial pixels with dedicated software. Graphs show combined percentages of bacterial pixel counts of 3 (E-F) or 2 (G) repeated independent experiments with the standard control mean set to 100%. Each data point represents an individual embryo.

atf3 morphants show minor alterations in the immune response to *M. marinum* infection

To determine whether the morphants of *atf3* have a differently regulated immune response to *M. marinum* we performed RNA sequencing analysis on pools of infected and non-infected *atf3* morphants (splice blocking morpholino 1) and compared this to their control morpholino injected embryos at 4 dpi, a time point when partial knockdown is observed (supplementary fig. 3A) and the morphants have a significantly reduced bacterial burden (fig. 4B and E). We focussed this comparison on the set of genes previously identified during the RNA-Seq analysis of *M. marinum* infection time course (fig. 3). Under infected circumstances, the most notable difference in gene expression levels was in the apolipoprotein and complement gene groups, where all genes showed a lower expression trend in the infected *atf3* morphants compared to the infected control embryos, although only significant for a few of these genes, namely *apoea*, *zgc:161979* (apolipoproteins A-II family*), fabp1b.1*, and *c7.* In addition, in the miscellaneous gene group *hamp2* showed significantly lower expression in infected *atf3* morphants (supplementary fig. 4). The only gene of the set of genes previously selected to show an induction in infected *atf3* morphants compared to infected controls was *irg1l*. None of the genes previously mentioned were significantly up- or down-regulated in uninfected *atf3* morphants compared to uninfected control embryos with the exception of *c3c*, which was down-regulated (fold change 0.48, adjusted p-value 0.026). We also examined expression of pro-inflammatory cytokines and *mmp9* at 4 hpi by qPCR, but found no difference in the transient induction of these genes by infection at this time point or in their basal expression levels in the *atf3* morphants (data not shown). Thus, we conclude that loss of *atf3*, while significantly improving *M. marimum* growth control, had a relatively minor effect on the gene expression response to *M. marinum* infection.

Atf3 suppresses macrophage and neutrophil inflammatory migration

During *M*. *marinum* infection, macrophages and neutrophils are recruited to the site of granuloma formation (fig. 1P-T). Knockdown of *atf3* did not affect total numbers of macrophages and neutrophils (supplementary fig. 3C). We next determined if Atf3 affects the migration of leukocytes and used a chemically induced inflammatory (ChIN) assay [27] to test this on *atf3* morphants and their controls. When the neuromast hair cells of the lateral line were damaged by copper sulphate treatment in this assay, the *atf3* morphants showed increased numbers of both macrophages and neutrophils surrounding the damaged hair cells (fig. 5). This indicates that Atf3 plays an inhibiting role on the migration of leukocytes towards local inflammation sites.

To determine whether the observed increased attraction of macrophages and neutrophils towards inflammatory sites also occurs during *M. marinum* granuloma formation, we imaged *M. marinum* infected individual transgenic embryos with fluorescent macrophages *Tg*(*mpeg1:mCherry-F*) and neutrophils *Tg*(*mpx:GFP*) injected

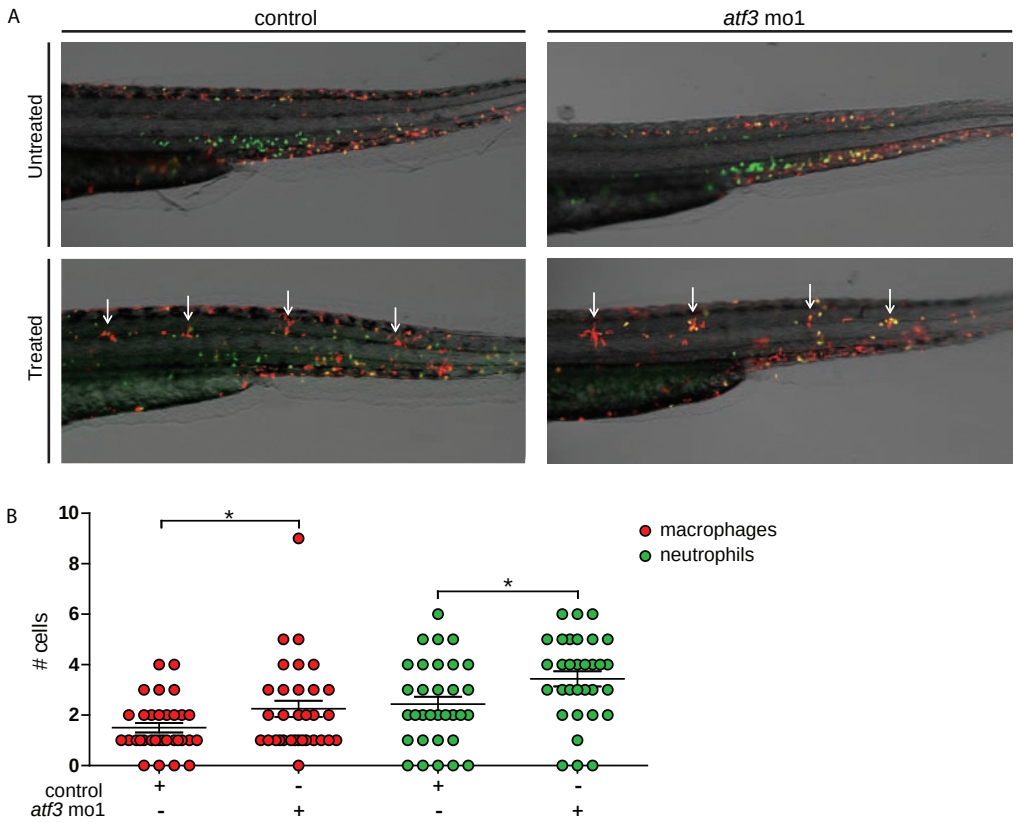

Figure 5. Atf3 inhibits macrophage and neutrophil migration to local inflammation sites. (A) Representative images of untreated and copper sulphate treated control and *atf3* mo1 morphant 3 dpf embryos. Embryos were immuno-labelled with Ab against the general leukocyte marker L-plastin (red signal) in combination with a neutrophil-specific Mpx TSA-staining (green signal). White arrows indicate accumulation of leukocytes at the local inflammation sites of the neuromasts. (B) Number of macrophages and neutrophils surrounding each neuromast site in the copper sulphate treated groups. Each data point represents cells surrounding one neuromast site of individual embryos (3 neuromast locations per embryo) and the mean ± SEM is indicated. Asterisks indicate significant differences (*, $p<0.1$) tested by unpaired t-test.

Figure 6. Detailed visualisation of granuloma formation in atf3 morphants. (A) Region imaged for visualising granuloma formation (red dotted rectangle). (B) Quantified levels of *M. marinum* pixels show that the imaged *atf3* morphant (C) has a decreased total pixel value and decreased number of clusters of *M. marinum* compared to the control embryo (C) in the tail region from 2 dpi onwards, indicating that this morphant is representative for the large pool of *atf3* morphants analysed in figure 4. (C) Merged channel z-stack projections of E2-Crimson-expressing *M. marinum* infection in an *atf3* morphant and a control embryo of the transgenic *Tg(mpeg1:mCherry-F)/Tg(mpx:GFP)* line at 4 hpi (single z-stack), 1 and 2 dpi (two stitched z-stacks), and 3 and 4 dpi (three stitched z-stacks). Macrophages are red, neutrophils are green and *M. marinum* is blue. Scale bars: 20 µm.

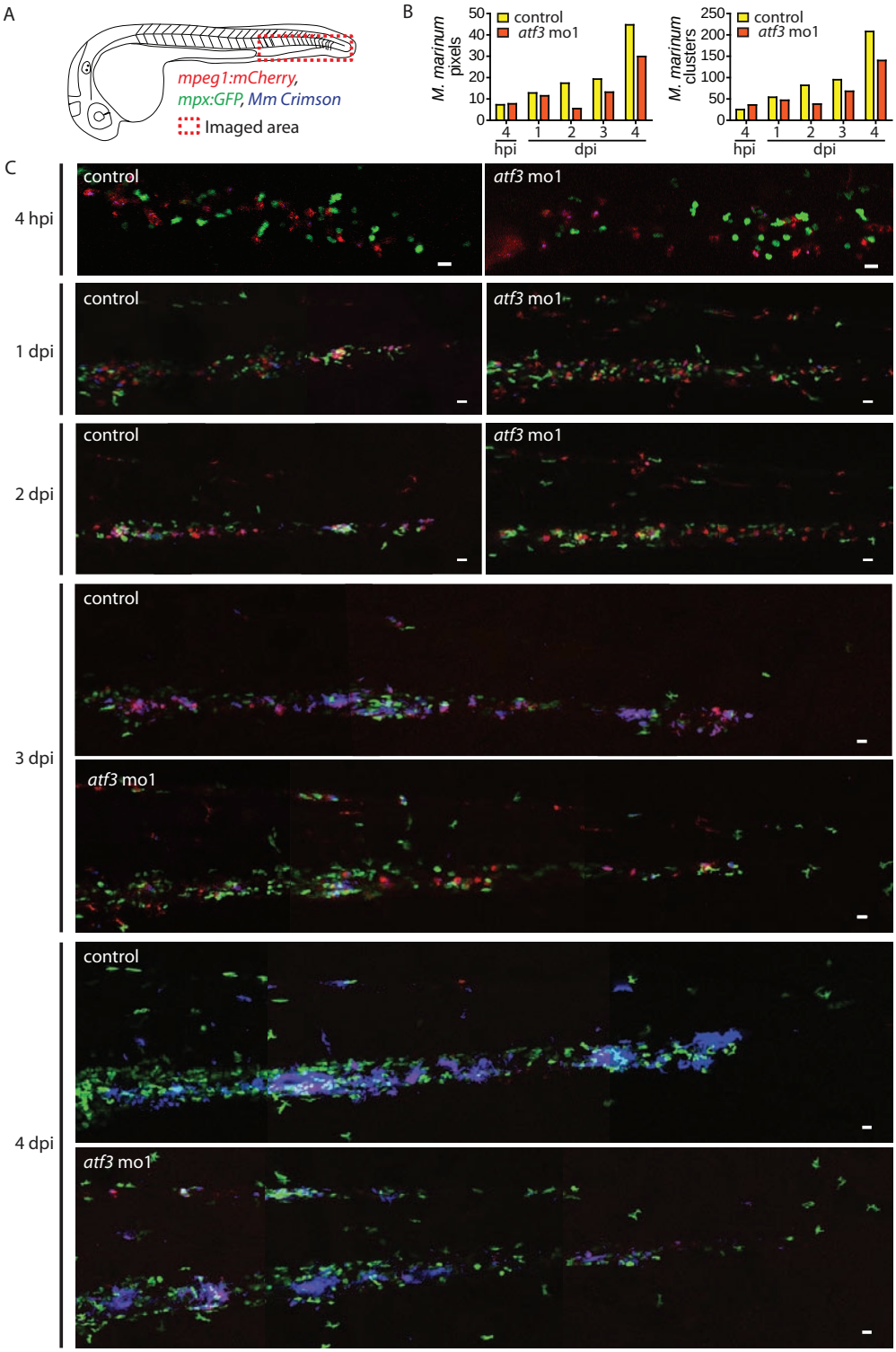
A
mpeg1:mCherry,
mpx:GFP, Mm Crimson
Imaged area
B
M. marinum pixels
control
atf3 mo1
hpi
dpi
M. marinum clusters
C
4 hpi
1 dpi
2 dpi
3 dpi
4 dpi
control
atf3 mo1

with *atf3* morpholino 1 or a control morpholino. The infection process was imaged in the tail region posterior to the urogenital opening (fig. 6A) over a time course starting at 4 hpi and continuing daily from 1 dpi until 4 dpi. Consistent with our previous results (Fig. 4), we observed that despite both embryos starting with an equal dose of infection, the *atf3* morphant had less *M. marinum* pixels and clusters in the tail at 4 dpi compared to the control embryo (fig. 6B). Both embryos showed macrophages containing *M. marinum* and an evenly spread leukocyte pattern at 4 hpi (fig. 6C). This changed at 1 dpi when the distribution of leukocytes appeared to be different in the *atf3* morphant compared to the control embryo: higher numbers of leukocytes were observed in the infected tail region of the *atf3* morphant, although both embryos showed leukocyte accumulation around the *M. marinum* bacteria. A similar difference in leukocyte accumulation was observed at 2 dpi when for the first time a difference in bacterial load was also apparent, reflected by less *M. marinum* fluorescent pixels in the *atf3* morphant (fig. 6B). At 3 dpi spreading of infection to the dorsal side of the tail could be observed in both the control embryo and the *atf3* morphant and at 4 dpi the control embryo had higher *M. marinum* infection. This is also the stage when both embryos no longer had detectible levels of *mpeg1*-promoter driven mCherry fluorescence, however the highly infected control embryo now seemed to have more neutrophils (*mpx*-promoter driven GFP fluorescence) surrounding the granulomas. In conclusion, increased leukocyte attraction at the stage when granuloma formation is first initiated (1-2 dpi) and prior to the inflammatory gene expression response at the later stage of granuloma formation (4-5 dpi), might be the explanation for the better ability of *atf3* morphants to control *M. marinum* infection.

Discussion

Distinct phases in the host response to *M. marinum* infection

The zebrafish *M. marinum* infection model has provided new insights into the development and function of granuloma-like structures, which are the hallmark of infection with pathogenic mycobacteria, including the human pathogen *M. tuberculosis* [17]. Despite the wide use of this model, the innate immune response of zebrafish embryos to *M. marinum* infection, especially during the early stages of infection, had not yet been well characterised. Previous microarray data had shown that early after infection (8 hpi), the host response to *M. marinum* is minimal, in sharp contrast with the strong pro-inflammatory response of zebrafish embryos to other pathogens like *Edwardsiella tarda* and *Salmonella typhimurium*, which cause acute disease [56]. As reported in here, detection of more subtle changes in gene expression during *M. marinum* infection required RNA deep sequencing with four biological replicates. We performed this RNA-Seq analysis over a time course from 2 hpi up to 5 dpi and visualised the host-pathogen interactions throughout the infection process until granuloma formation in order to interrelate the infection stages with the host gene expression profiles. As summarised in figure 7, our gene expression profiles reveal three main phases in the host response: early-phase: induction of complement and transcription factors followed by induction of pro-inflammatory cytokines within hours after phagocytosis of *M. marinum*; mid-phase: minimal response between 6 hpi to 1 dpi when the tissue dissemination of *M. marinum* has begun, except for the induction of complement and apolipoprotein genes; late-phase: progressively increasing induction of complement, transcription factors, pro-inflammatory cytokines, matrix metalloproteinases, and other defence and inflammation related gene groups, along with the expansion of granulomas.

Mycobacterial recognition is an essential step for phagocytosis by macrophages and this process is mediated by pattern recognition receptors (PRRs) [57-59]. In response to recognising *M. marinum*, macrophages rapidly phagocytose the bacteria (fig. 1A) and transcription factors with well-established functions in immunity (for example *atf3*, *jun* and *fos*, and the *irf* family members) are significantly up-regulated at 2 hpi (fig. 3A). Directly after the early peak of transcription factor induction, an induction of pro-inflammatory cytokines and chemokines (*il1b*, *tnfa*, *il8,* and *cxcl-c1c*) occurs at 4 hpi (fig. 3B). During this early-phase response between 2 and 4 hpi, the matrix metalloproteinases *mmp9* and *mmp13a* are also induced (fig. 3C). The timing of this early induction is not surprising because Mmps are known to function in cleaving cytokines and chemokines to augment or to inhibit their functional activity [60, 61]. A second function of Mmps is to degrade components of the extracellular matrix [62], thereby allowing immune cells to migrate to sites of inflammation from the bloodstream. In this infection model, macrophages do not need to migrate towards the infection site because they phagocytose *M. marinum* following injection into the blood circulation; however, after phagocytosis the infected cells migrate outside the vascular system by traversing

endothelial barrier and migrate into tissue (fig. 1C-E and supplementary movie S1) [18] which requires proteolysis of the basement membrane by metalloproteinases. At 2 dpi and 3 dpi, when uninfected macrophages (fig. 1M) and neutrophils (fig. 1N) are first attracted to the forming granulomas (which requires cytokine dependent leukocyte attraction and extracellular matrix degradation), pro-inflammatory cytokines (fig. 3B) and *mmp9* and *mmp13a* (fig. 3C) are once again up-regulated. This induction increases over time until 5 dpi, the time point when the granuloma structures start protruding the epithelial layer (supplementary fig. 1B) and infected macrophages can leave the granuloma to form new granulomas [20]. The increasing expression of *mmp9* during this period is consistent with its proposed function in facilitating the recruitment of macrophages during granuloma formation [45].

A proper balance in immune regulation is essential for the host to suppress bacterial growth. It has been shown that an imbalance in MMP production can also be host-damaging during mycobacterial infection [63-69]. Therefore, it is coherent that the *tissue inhibitor of metalloproteinase 2b* (*timp2b*) is also induced together with *mmp9* and *mmp13a* (fig. 3C). In addition, susceptibility to *M. marinum* in zebrafish can result from either inadequate or excessive acute inflammation [36, 70], therefore it is not surprising that concomitant with the induction of pro-inflammatory genes and transcriptional activators, numerous negative regulators of the TLR pathway (*irak3*, *socs3a*, and a group of NFκB inhibitors) are up-regulated during early- and late-phase infection (supplementary fig. 2D). We have shown that a similar induction of negative regulators occurs during *S. typhimurium* infection [32, 36].

When mycobacteria are intracellular, they can release mycobacterial lipids which are incorporated into exocytosing vesicles of macrophages [71] which allows the mycobacterial lipids to be transferred between cells. This process is mediated by host apolipoprotein E [72], one of the group of apolipoproteins that is also found to be differentially regulated during *M. marinum* infection (fig. 3D). By transferring antigenic lipids from cell to cell, such as TDM, the pathogen can extend its area of influence beyond its own host cell such as attracting cells to form a granuloma-like structure in a myd88-dependent manner in mice [73], similarly to the effect that secreted virulence factor ESAT-6 has on enhancing recruitment of macrophages in a Mmp9-dependent manner in zebrafish [45]. When studying the response of apolipoprotein genes during *M. marinum* infection, we observed a collective regulation of lipoproteins (fig. 3D). Not only are they collectively regulated, they also show a strong fluctuation between up-and down-regulation during the infection process and are the only group of genes, besides complement, that are up-regulated during the mid-phase of infection. This rapid fluctuation in regulation makes the apolipoprotein family intriguing to investigate further. It is not yet known whether these apolipoproteins function similarly in zebrafish and whether *M. marinum* is also capable of modulating cell function via apolipoproteins.

Numerous complement components in zebrafish are transferred from mother to egg as proteins or mRNA [47], thus, protecting the embryo before it is capable of synthesizing

immune-relevant molecules. As mentioned previously, complement is slightly up-regulated during early- and mid-phase infection and is highly induced during late-phase infection when the granuloma matures (fig. 3E). This indicates that already at 1 dpf, the zebrafish embryo itself is capable of inducing complement components in response to *M. marinum* infection. It has been shown that complement component C3 on the surface of *M. tuberculosis* mediates phagocytosis of this bacterium [58] and recently, all the homologs of the mammalian complement fundamental components were found to be present in zebrafish as revealed by phylogenetic analysis [74]. Therefore, it is possible that zebrafish c3a and c3c function in the same manner to assist phagocytosis of *M. marinum*, a process which occurs progressively during granuloma maturation.

During the granuloma maturation, infected cells containing high numbers of *M. marinum* undergo cell death and are phagocytosed by multiple newly recruited macrophages [20]. This process seems beneficial for the mycobacteria because the granuloma expands in this manner. However, dead macrophages also attract neutrophils which are capable of exerting antimicrobial functions against *M. marinum* via inducible Nitric Oxide Synthase (iNOS) signalling [75] and are capable of phagocytosing dying infected macrophages after which they can kill internalised mycobacteria through NADPH-oxidase dependent mechanisms [76]. We observe neutrophils containing *M. marinum* as soon as 1 dpi around the injection site (fig. 1B) and at 3 dpi within the granuloma-like structures (supplementary fig. 1A). In addition, genes of the phagocyte oxidase complex are induced significantly at 4 and 5 dpi (supplementary fig. 2E), which correlates with the infection stage where infected macrophages start dying and increasing numbers of neutrophils are attracted to the maturing granuloma (fig. 1S and T). These results support that neutrophils play an important role during this stage of infection when macrophages are no longer capable of containing mycobacterial growth. Many other defence related genes are induced at this stage of granuloma expansion and the host transcriptome response now has a clear pro-inflammatory signature similar to that observed within hours after infection with the acute pathogens *E. tarda a*nd *S. typhimurium* [56]. In contrast, our time course analysis suggests that during the first days of infection *M. marinum* is capable of suppressing host pro-inflammatory signalling, allowing its replication in macrophages and the initiation of granulomas.

The infection-inducible host transcription factor Atf3 antagonises the control of *M. marinum* growth after acute infection

The RNA sequencing expression profiles allow us to hypothesise which genes play a role during infection with *M. marinum*. We chose to study *atf3* because it is one of the transcription factor genes that is up-regulated during the early- and late-phase host response (fig. 3A). ATF3 is a member of the CREB/ATF family of basic leucine zipper transcription factors. It has been shown to act primarily as a repressor, but splice forms that are unable to bind DNA can also stimulate transcription presumably by sequestration of inhibitory co-factors [77]. In mice, ATF3 is used as an ER stress marker that is expressed in the macrophage-rich area of *M. tuberculosis*-induced granulomas [78]. When analysing

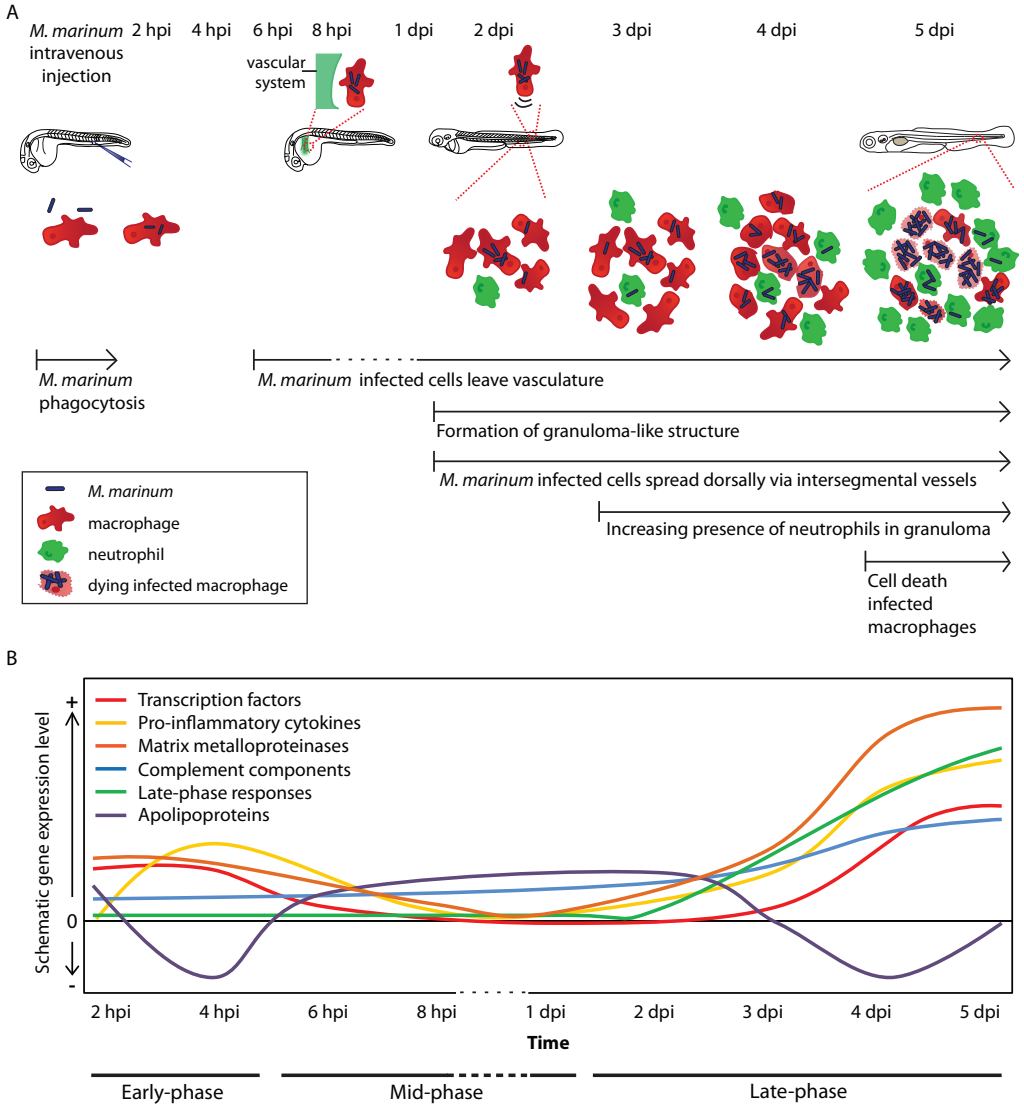

Figure 7. Infection process of *M. marinum*. A schematic overview representing (A) the observed host-pathogen interactions and (B) the gene expression profiles of transcription factors (red line), pro-inflammatory cytokines (yellow line), matrix metalloproteinases (orange line), complement components (blue line), late-phase responses (green line), and apolipoproteins (purple line).

GEO profiles in the NCBI database we find that *Atf3* expression is gradually induced in mice during early lung immune response to *M. tuberculosis* (GDS4257) and *ATF3* expression is induced in human macrophages in response to hypoxia (GDS2036). Hypoxia occurs in the environment of the human tuberculous granulomas and it may be responsible for *M. tuberculosis* dormancy in humans [79]. It was recently shown in mice that ROS-mediated super-induction of *ATF3* causes high susceptibility to bacterial infections through the suppression of interleukin 6 (IL-6) and that *ATF3*-/- mice are protected against bacterial infections [80]. Atf3 can also be induced by LPS in bone-marrow derived from mice and this induction was suggested to regulate TLR-stimulated inflammatory responses as part of a negative-feedback loop [2]. Similarly, we observe less *M. marinum* infection in *atf3* morphant zebrafish embryos (fig. 4), but we did not observe a strong effect of *atf3* knockdown on the transcriptional signature. However, we did observe a general down-regulation trend of a group of apolipoproteins (supplementary fig. 4) which is interesting because it was previously shown that apolipoprotein E for example can inhibit cell migration of smooth muscle cells [81]. In addition, we found that Atf3 functions in suppressing macrophage and neutrophil migration towards local damage-induced inflammation sites (fig. 5), a process that is also important in the *M. marinum*-granuloma environment. To determine whether such increased attraction of leukocytes to inflammatory sites also occurs during granuloma formation in the *atf3* morphants, we imaged this process in a double transgenic zebrafish line with fluorescent macrophages and neutrophils. Knockdown of *atf3* resulted in an attenuated infection level as soon as 2 dpi and leukocyte numbers seemed to be increased around the infection locations at 1 and 2 dpi. Although differences in granuloma structure are difficult to quantify due to high variation between individual granulomas within single embryos, these observations suggest that increased leukocyte recruitment during the early stage of infection might be responsible for better restriction of *M. marinum* growth in *atf3* morphants. In contrast, attenuated *M. marinum* infection under knockdown conditions of *mmp9* has been associated with impaired rather than enhanced macrophage recruitment [45]. This difference between the *atf3* and *mmp9* knockdown phenotypes might be explained by the timing of leukocyte recruitment. It is possible that enhanced early recruitment of neutrophils to the initiating granuloma in *atf3* morphants helps restricting *M. marinum* growth. In contrast, *mmp9*, which is induced by the mycobacterial secreted protein ESAT-6 [45], is probably more important at later stages, when macrophage recruitment promotes granuloma expansion. Further research is necessary to determine the precise function of Atf3 during *M. marinum* infection.

In summary, this study provides a detailed description of the observed host-pathogen interactions during *M. marinum* infection in zebrafish embryos and interrelates this with gene expression profiles obtained from RNA sequencing. We also demonstrate that Atf3, one of the transcription factors induced during the early- and late-phase of infection, antagonises the host control of *M. marinum* acute infections, indicating the strength of using gene expression profiles to identify key host genes involved in mycobacterial pathogenesis.

Acknowledgements

The authors would like to thank Georges Lutfalla (University Montpellier 2) for the kind gift of *Tg(mpeg1:mCherry-F)* fish, Ulrike Nehrdich, Laura van Hulst and Davy de Witt for fish care, and other lab members for helpful discussions. EB, HPS, and AHM were supported by the Smart Mix Program of the Netherlands Ministry of Economic Affairs and the Ministry of Education, Culture and Science, JR by a Marie Curie Fellowship of the European 7th Framework Initial Training Network FishForPharma (PITG-GA-2011-289209), and PIR by a Marie Curie Intra-European Fellowship (PIEF-GA-2010-274389).

References

1. Whitmore, M.M. *et al.* Negative regulation of TLR-signaling pathways by activating transcription factor-3. *Journal of immunology* **179**, 3622-3630 (2007).

2. Gilchrist, M. *et al.* Systems biology approaches identify ATF3 as a negative regulator of Toll-like receptor 4. *Nature* **441**, 173-178 (2006).

3. Ottenhoff, T.H. New pathways of protective and pathological host defense to mycobacteria. *Trends in microbiology* **20**, 419-428 (2012).

4. Cooper, A.M. & Torrado, E. Protection versus pathology in tuberculosis: recent insights. *Current opinion in immunology* **24**, 431-437 (2012).

5. Stinear, T.P. *et al.* Insights from the complete genome sequence of Mycobacterium marinum on the evolution of Mycobacterium tuberculosis. *Genome Res* **18**, 729-741 (2008).

6. Ruley, K.M. *et al.* Identification of Mycobacterium marinum virulence genes using signature-tagged mutagenesis and the goldfish model of mycobacterial pathogenesis. *FEMS microbiology letters* **232**, 75-81 (2004).

7. Tobin, D.M. & Ramakrishnan, L. Comparative pathogenesis of Mycobacterium marinum and Mycobacterium tuberculosis. *Cellular microbiology* **10**, 1027-1039 (2008).

8. Stamm, L.M. *et al.* Mycobacterium marinum escapes from phagosomes and is propelled by actin-based motility. *The Journal of experimental medicine* **198**, 1361-1368 (2003).

9. Leake, E.S., Myrvik, Q.N. & Wright, M.J. Phagosomal membranes of Mycobacterium bovis BCG-immune alveolar macrophages are resistant to disruption by Mycobacterium tuberculosis H37Rv. *Infection and immunity* **45**, 443-446 (1984).

10. Vergne, I., Chua, J., Singh, S.B. & Deretic, V. Cell biology of mycobacterium tuberculosis phagosome. *Annu Rev Cell Dev Biol* **20**, 367-394 (2004).

11. Simeone, R. *et al.* Phagosomal rupture by Mycobacterium tuberculosis results in toxicity and host cell death. *PLoS pathogens* **8**, e1002507 (2012).

12. van der Wel, N. *et al.* M. tuberculosis and M. leprae translocate from the phagolysosome to the cytosol in myeloid cells. *Cell* **129**, 1287-1298 (2007).

13. Ramakrishnan, L. Revisiting the role of the granuloma in tuberculosis. *Nat Rev Immunol* **12**, 352-366 (2012).

14. Parikka, M. *et al.* Mycobacterium marinum causes a latent infection that can be reactivated by gamma irradiation in adult zebrafish. *PLoS pathogens* **8**, e1002944 (2012).

15. Swaim, L.E. *et al.* Mycobacterium marinum Infection of Adult Zebrafish Causes Caseating Granulomatous Tuberculosis and Is Moderated by Adaptive Immunity. *Infection and Immunity* **74**, 6108-6117 (2006).

16. Davis, J.M. *et al.* Real-time visualization of mycobacterium-macrophage interactions leading to initiation of granuloma formation in zebrafish embryos. *Immunity* **17**, 693-702 (2002).

17. Berg, R.D. & Ramakrishnan, L. Insights into tuberculosis from the zebrafish model. *Trends Mol Med* **18**, 689-690 (2012).

18. Clay, H. *et al.* Dichotomous Role of the Macrophage in Early Mycobacterium marinum Infection of the Zebrafish. *Cell Host & Microbe* **2**, 29-39 (2007).

19. Volkman, H.E. *et al.* Tuberculous granuloma formation is enhanced by a mycobacterium virulence determinant. *PLoS Biol* **2**, e367 (2004).

20. Davis, J.M. & Ramakrishnan, L. The Role of the Granuloma in Expansion and Dissemination of Early Tuberculous Infection. *Cell* **136**, 37-49 (2009).

21. Traver, D. *et al.* The Zebrafish as a Model Organism to Study Development of the Immune System. **81**, 254-330 (2003).

22. Clay, H., Volkman, H.E. & Ramakrishnan, L. Tumor Necrosis Factor Signaling Mediates Resistance to Mycobacteria by Inhibiting Bacterial Growth and Macrophage Death. *Immunity* **29**, 283-294 (2008).

23. van der Vaart, M., van Soest, J.J., Spaink, H.P. & Meijer, A.H. Functional analysis of a zebrafish myd88 mutant identifies key transcriptional components of the innate immune system. *Dis Model Mech* **6**, 841-854 (2013).

24. Lawson, N.D. & Weinstein, B.M. In vivo imaging of embryonic vascular development using transgenic zebrafish. *Dev Biol* **248**, 307-318 (2002).

25. Renshaw, S.A. *et al.* A transgenic zebrafish model of neutrophilic inflammation. *Blood* **108**, 3976-3978 (2006).

26. Bernut, A. *et al.* Mycobacterium abscessus cording prevents phagocytosis and promotes abscess formation. *Proc Natl Acad Sci U S A* (2014).

27. d'Alençon, C.A. *et al.* A high-throughput chemically induced inflammation assay in zebrafish. *BMC Biology* **8**, 151 (2010).

28. van der Sar, A.M. *et al.* Mycobacterium marinum Strains Can Be Divided into Two Distinct Types Based on Genetic Diversity and Virulence. *Infection and Immunity* **72**, 6306-6312 (2004).

29. Kimmel, C.B., Ballard, W.W., Kimmel, S.R., Ullmann, B. & Schilling, T.F. Stages of embryonic development of the zebrafish. *Dev Dyn* **203**, 253-310 (1995).

30. Benard, E.L. *et al.* Infection of zebrafish embryos with intracellular bacterial pathogens. *J Vis Exp* **pii: 3781. doi: 10.3791/3781** (2012).

31. Veneman, W.J. *et al.* A zebrafish high throughput screening system used for Staphylococcus epidermidis infection marker discovery. *BMC Genomics* **14**, 255 (2013).

32. Stockhammer, O.W., Zakrzewska, A., Hegedus, Z., Spaink, H.P. & Meijer, A.H. Transcriptome profiling and functional analyses of the zebrafish embryonic innate immune response to Salmonella infection. *J Immunol* **182**, 5641-5653 (2009).

33. Zakrzewska, A. *et al.* Macrophage-specific gene functions in Spi1-directed innate immunity. *Blood* **116**, e1-11 (2010).

34. Ordas, A. *et al.* MicroRNA-146 function in the innate immune transcriptome response of zebrafish embryos to Salmonella typhimurium infection. *BMC genomics* **14**, 696 (2013).

35. Huang da, W., Sherman, B.T. & Lempicki, R.A. Systematic and integrative analysis of large gene lists using DAVID bioinformatics resources. *Nat Protoc* **4**, 44-57 (2009).

36. Kanwal, Z. *et al.* Deficiency in hematopoietic phosphatase ptpn6/Shp1 hyperactivates the innate immune system and impairs control of bacterial infections in zebrafish embryos. *J Immunol* **190**, 1631-1645 (2013).

37. Anders, S. & Huber, W. Differential expression analysis for sequence count data. *Genome biology* **11**, R106 (2010).

38. Mariathasan, S. & Monack, D.M. Inflammasome adaptors and sensors: intracellular regulators of infection and inflammation. *Nat Rev Immunol* **7**, 31-40 (2007).

39. Mayer-Barber, K.D. *et al.* Caspase-1 independent IL-1beta production is critical for host resistance to mycobacterium tuberculosis and does not require TLR signaling in vivo. *Journal of immunology* **184**, 3326-3330 (2010).

40. Kinoshita, S., Biswas, G., Kono, T., Hikima, J. & Sakai, M. Presence of two tumor necrosis factor (tnf)-alpha homologs on different chromosomes of zebrafish (Danio rerio) and medaka (Oryzias latipes). *Mar Genomics* **13**, 1-9 (2014).

41. Tobin, D.M. *et al.* The lta4h Locus Modulates Susceptibility to Mycobacterial Infection in Zebrafish and Humans. *Cell* **140**, 717-730 (2010).

42. Deng, Q. *et al.* Localized bacterial infection induces systemic activation of neutrophils through Cxcr2 signaling in zebrafish. *Journal of leukocyte biology* **93**, 761-769 (2013).

43. de Oliveira, S. *et al.* Cxcl8 (IL-8) mediates neutrophil recruitment and behavior in the zebrafish inflammatory response. *Journal of immunology* **190**, 4349-4359 (2013).

44. Elkington, P.T., O'Kane, C.M. & Friedland, J.S. The paradox of matrix metalloproteinases in infectious disease. *Clin Exp Immunol* **142**, 12-20 (2005).

45. Volkman, H.E. *et al.* Tuberculous granuloma induction via interaction of a bacterial secreted protein with host epithelium. *Science* **327**, 466-469 (2010).

46. Brew, K., Dinakarpandian, D. & Nagase, H. Tissue inhibitors of metalloproteinases: evolution, structure and function. *Biochim Biophys Acta* **1477**, 267-283 (2000).

47. Wang, Z., Zhang, S., Tong, Z., Li, L. & Wang, G. Maternal transfer and protective role of the alternative complement components in zebrafish Danio rerio. *PloS one* **4**, e4498 (2009).

48. Hall, C.J. *et al.* Immunoresponsive gene 1 augments bactericidal activity of macrophage-lineage cells by regulating beta-oxidation-dependent mitochondrial ROS production. *Cell Metab* **18**, 265-278 (2013).

49. Urieli-Shoval, S., Linke, R.P. & Matzner, Y. Expression and function of serum amyloid A, a major acute-phase protein, in normal and disease states. *Curr Opin Hematol* **7**, 64-69 (2000).

50. Hegedus, Z. *et al.* Deep sequencing of the zebrafish transcriptome response to mycobacterium infection. *Molecular immunology* **46**, 2918-2930 (2009).

51. Stockhammer, O.W. *et al.* Transcriptome analysis of Traf6 function in the innate immune response of zebrafish embryos. *Mol Immunol* **48**, 179-190 (2010).

52. Wellen, K.E. *et al.* Coordinated regulation of nutrient and inflammatory responses by STAMP2 is essential for metabolic homeostasis. *Cell* **129**, 537-548 (2007).

53. Zhang, J., Yu, L.P., Li, M.F. & Sun, L. Turbot (Scophthalmus maximus) hepcidin-1 and hepcidin-2 possess antimicrobial activity and promote resistance against bacterial and viral infection. *Fish & shellfish immunology* (2014).

54. van der Vaart, M. *et al.* The DNA Damage-Regulated Autophagy Modulator DRAM1 Links Mycobacterial Recognition via TLP-MYD88 to Authophagic Defense. *Cell host & microbe* **15**, 753-767 (2014).

55. Zhang, C. *et al.* Transcriptional activation of the human stress-inducible transcriptional repressor ATF3 gene promoter by p53. *Biochemical and biophysical research communications* **297**, 1302-1310 (2002).

56. van der Vaart, M., Spaink, H.P. & Meijer, A.H. Pathogen recognition and activation of the innate immune response in zebrafish. *Adv Hematol* **2012**, 159807 (2012).

57. Schlesinger, L.S. Macrophage phagocytosis of virulent but not attenuated strains of Mycobacterium tuberculosis is mediated by mannose receptors in addition to complement receptors. *J Immunol* **150**, 2920-2930 (1993).

58. Schlesinger, L.S., Bellinger-Kawahara, C.G., Payne, N.R. & Horwitz, M.A. Phagocytosis of Mycobacterium tuberculosis is mediated by human monocyte complement receptors and complement component C3. *J Immunol* **144**, 2771-2780 (1990).

59. Maeda, N. *et al.* The cell surface receptor DC-SIGN discriminates between Mycobacterium species through selective recognition of the mannose caps on lipoarabinomannan. *The Journal of biological chemistry* **278**, 5513-5516 (2003).

60. Schonbeck, U., Mach, F. & Libby, P. Generation of biologically active IL-1 beta by matrix metalloproteinases: a novel caspase-1-independent pathway of IL-1 beta processing. *Journal of immunology* **161**, 3340-3346 (1998).

61. Ito, A. *et al.* Degradation of interleukin 1beta by matrix metalloproteinases. *The Journal of biological chemistry* **271**, 14657-14660 (1996).

62. Sternlicht, M.D. & Werb, Z. How matrix metalloproteinases regulate cell behavior. *Annu Rev Cell Dev Biol* **17**, 463-516 (2001).

63. Chang, J.C. *et al.* Effect of Mycobacterium tuberculosis and its components on macrophages and the release of matrix metalloproteinases. *Thorax* **51**, 306-311 (1996).

64. Rivera-Marrero, C.A., Schuyler, W., Roser, S. & Roman, J. Induction of MMP-9 mediated gelatinolytic activity in human monocytic cells by cell wall components of Mycobacterium tuberculosis. *Microbial pathogenesis* **29**, 231-244 (2000).

65. Quiding-Jarbrink, M., Smith, D.A. & Bancroft, G.J. Production of matrix metalloproteinases in response to mycobacterial infection. *Infection and immunity* **69**, 5661-5670 (2001).

66. Hrabec, E., Strek, M., Zieba, M., Kwiatkowska, S. & Hrabec, Z. Circulation level of matrix metalloproteinase-9 is correlated with disease severity in tuberculosis patients. *Int J Tuberc Lung Dis* **6**, 713-719 (2002).

67. Price, N.M. *et al.* Identification of a matrix-degrading phenotype in human tuberculosis in vitro and in vivo. *Journal of immunology* **166**, 4223-4230 (2001).

68. Price, N.M., Gilman, R.H., Uddin, J., Recavarren, S. & Friedland, J.S. Unopposed matrix metalloproteinase-9 expression in human tuberculous granuloma and the role of TNF-alpha-dependent monocyte networks. *Journal of immunology* **171**, 5579-5586 (2003).

69. Izzo, A.A., Izzo, L.S., Kasimos, J. & Majka, S. A matrix metalloproteinase inhibitor promotes granuloma formation during the early phase of Mycobacterium tuberculosis pulmonary infection. *Tuberculosis (Edinb)* **84**, 387-396 (2004).

70. Tobin, D.M. *et al.* Host genotype-specific therapies can optimize the inflammatory response to mycobacterial infections. *Cell* **148**, 434-446 (2012).

71. Beatty, W.L., Ullrich, H.J. & Russell, D.G. Mycobacterial surface moieties are released from infected macrophages by a constitutive exocytic event. *Eur J Cell Biol* **80**, 31-40 (2001).

72. van den Elzen, P. *et al.* Apolipoprotein-mediated pathways of lipid antigen presentation. *Nature* **437**, 906-910 (2005).

73. Geisel, R.E., Sakamoto, K., Russell, D.G. & Rhoades, E.R. In vivo activity of released cell wall lipids of Mycobacterium bovis bacillus Calmette-Guerin is due principally to trehalose mycolates. *Journal of immunology* **174**, 5007-5015 (2005).

74. Zhang, S. & Cui, P. Complement system in zebrafish. *Developmental and comparative immunology* (2014).

75. Elks, P.M. *et al.* Hypoxia inducible factor signaling modulates susceptibility to mycobacterial infection via a nitric oxide dependent mechanism. *PLoS pathogens* **9**, e1003789 (2013).

76. Yang, C.T. *et al.* Neutrophils exert protection in the early tuberculous granuloma by oxidative killing of mycobacteria phagocytosed from infected macrophages. *Cell Host Microbe* **12**, 301-312 (2012).

77. Chen, B.P., Liang, G., Whelan, J. & Hai, T. ATF3 and ATF3 delta Zip. Transcriptional repression versus activation by alternatively spliced isoforms. *The Journal of biological chemistry* **269**, 15819-15826 (1994).

78. Seimon, T.A. *et al.* Induction of ER stress in macrophages of tuberculosis granulomas. *PloS one* **5**, e12772 (2010).

79. Boshoff, H.I. & Barry, C.E., 3rd Tuberculosis - metabolism and respiration in the absence of growth. *Nat Rev Microbiol* **3**, 70-80 (2005).

80. Hoetzenecker, W. *et al.* ROS-induced ATF3 causes susceptibility to secondary infections during sepsis-associated immunosuppression. *Nat Med* **18**, 128-134 (2012).

81. Hui, D.Y. & Basford, J.E. Distinct signaling mechanisms for apoE inhibition of cell migration and proliferation. *Neurobiol Aging* **26**, 317-323 (2005).

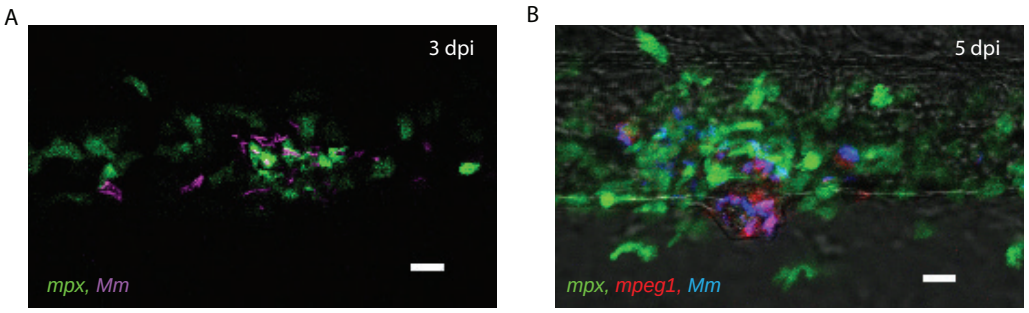

Supplementary figure 1. Granuloma contains infected neutrophils at 3 dpi and grows outside the vasculature at 5 dpi. (A) Neutrophils (*Tg(mpx:GFP)*) containing *M. marinum* (mCherry-expressing Mma20 depicted in magenta) at 3 dpi in granuloma of infected embryo from figure 1R. Z-stack maximum intensity projection of slices 9-18 of 27 total. (B) Granuloma from E2-Crimson-expressing *M. marinum* M-strain (depicted in blue) infected *Tg(mpx:GFP)/Tg(mpeg1:mCherry-F)* embryo at 5 dpi from figure 1T. Bacterial infection can be seen in cluster extending outwards from the tail region of the embryo. Scale bars: 20 µm.

Supplementary figure 2. Overview of expression profiles during *M. marinum* infection of gene groups additional to those shown in Fig. 3. Gene expression levels of groups of selected genes during a time course of *M. marinum* infection are represented as log2 fold change values. Groups of genes represented are: (A) ADAM metalloproteinases; (B) acute phase response, other than complement; (C) prostaglandin biosynthetic genes and receptors (late response); (D) negative regulators (late response); (E) NADPH oxidase complex genes. Statistically significant data points (adjusted P-value <0.1) are indicated below the x-axis as the shape filled with the colour of the specific gene (see legend for gene shape and colour). Only genes are shown for which differential expression was significant in at least one time point (F-I) qPCR validation of expression levels of (F) *il1b*, (G) *il8*, (H) *mmp9*, and (I) *apoa4*.

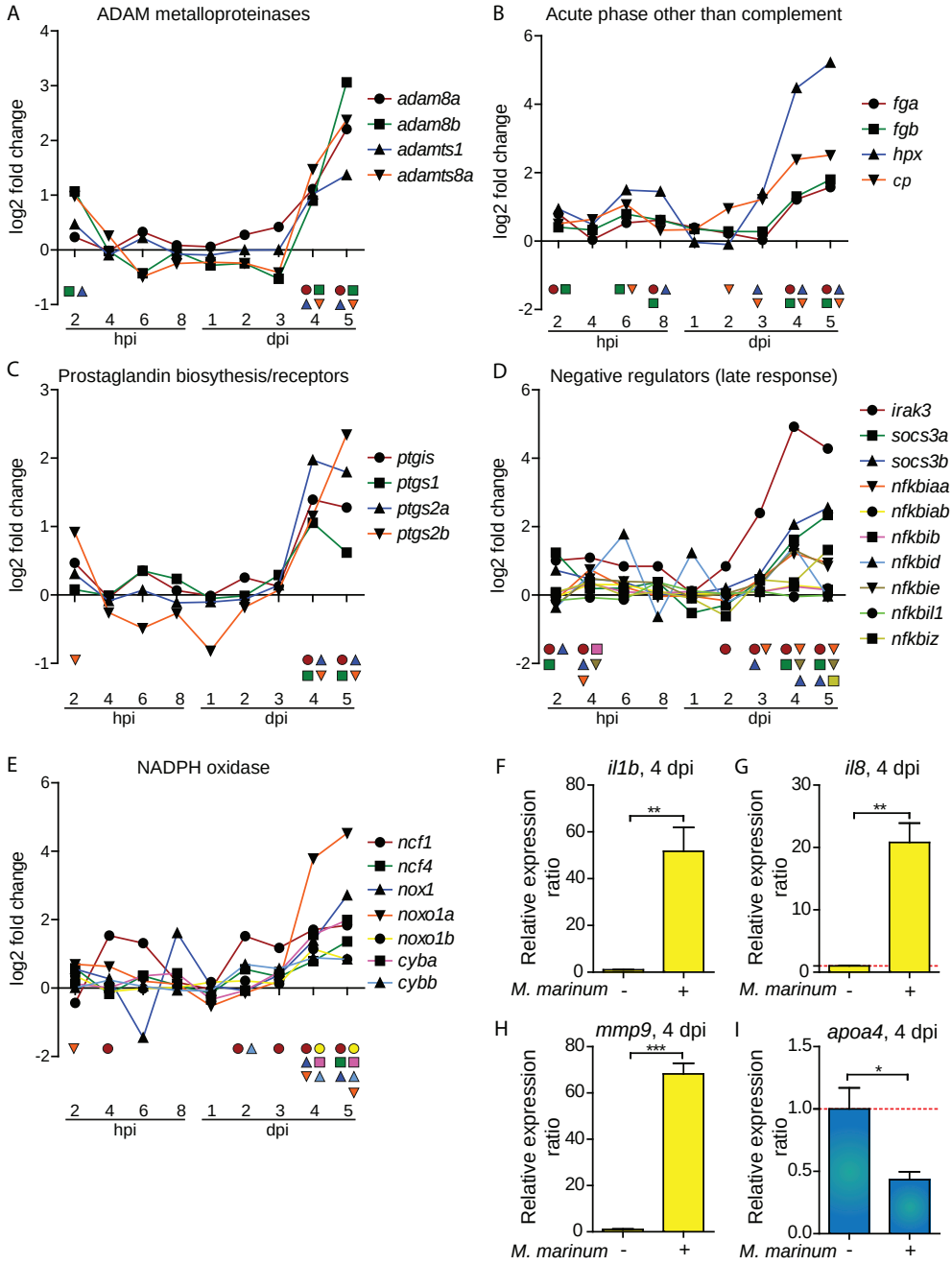
A
ADAM metalloproteinases
log2 fold change
adam8a
adam8b
adamts1
adamts8a
hpi
dpi
B
Acute phase other than complement
fga
fgb
hpx
cp
C
Prostaglandin biosythesis/receptors
ptgis
ptgs1
ptgs2a
ptgs2b
D
Negative regulators (late response)
irak3
socs3a
socs3b
nfkbiaa
nfkbiab
nfkbib
nfkbid
nfkbie
nfkbil1
nfkbiz
E
NADPH oxidase
ncf1
ncf4
nox1
noxo1a
noxo1b
cyba
cybb
F
il1b, 4 dpi
Relative expression ratio
M. marinum
G
il8, 4 dpi
H
mmp9, 4 dpi
I
apoa4, 4 dpi

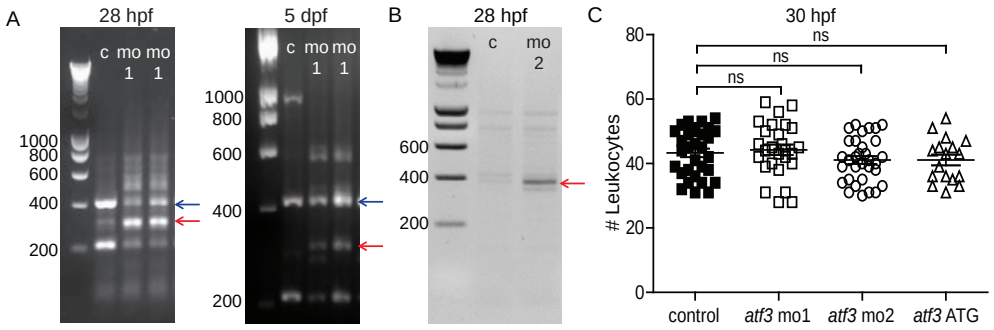

Supplementary figure 3. Validation of *atf3* morpholino knockdown. (A-B) Knockdown of *atf3*. Expression of *atf3* was determined by RT-PCR using RNA from embryos injected with (A) *atf3* morpholino 1 (Mo1) or control morpholino (c) at 28 hpf and 5 dpf or with (B) *atf3* morpholino 2 (Mo2) or control morpholino (c) at 28 hpf. (A) Blue arrow indicates control RT-PCR product size (425 bp) and red arrow indicates morpholino 1 knockdown predicted product size (317 bp). (B) Red arrow indicates RT-PCR product designed to amplify included intron during atf3 morpholino 2 knockdown (374 bp) on the right. (C) Normal leukocyte numbers in *atf3* morphants. *atf3* morphants and control embryos were fixed at 30 hpf and were immuno-labelled with Ab against the general leukocyte marker L-plastin. Leukocyte numbers were counted blinded in the tail (ns = not significant).

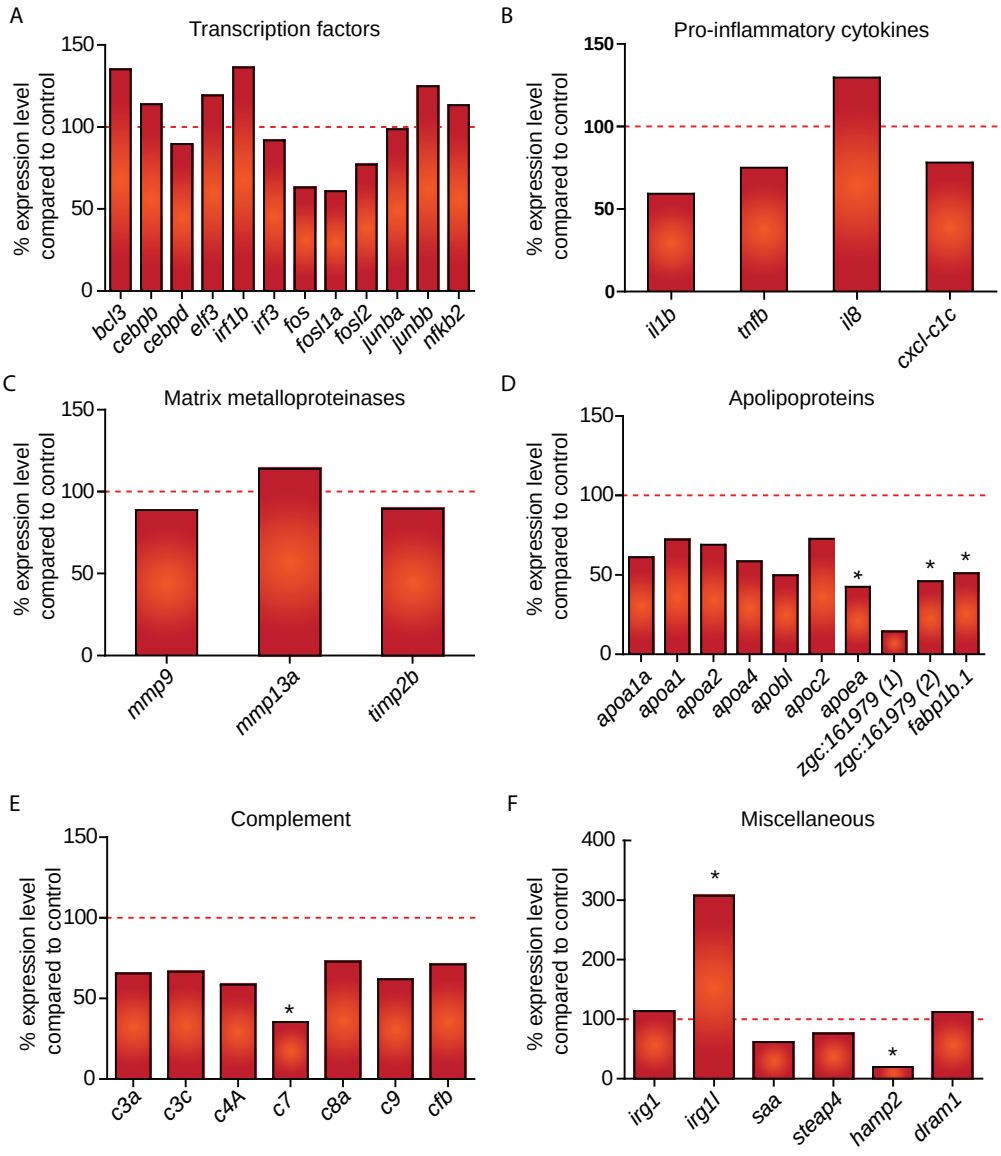

Supplementary figure 4. Effect of *atf3* knockdown on immune response at 4 dpi. The expression level of selected genes (identical to those in fig. 3) under conditions of *atf3* deficiency is expressed as the percentage of the expression level in the corresponding control. Results are based on RNA-Seq analysis of pools of 30 infected and 30 uninfected embryos for each group. Embryos were injected with *M. marinum* Mma20 (250 cfu) or mock injected with 2% PVP, and RNA-Seq analysis was performed at 4 dpi. Asterisks indicate significant difference.

Supplementary table 1: Gene ontology and KEGG pathways enriched in infected embryos

Gene ID	Gene name	Description
Matrix metalloproteinases and inhibitors		
ENSDARG00000042816	*mmp9*	matrix metalloproteinase 9
ENSDARG00000012395	*mmp13a*	matrix metalloproteinase 13a
ENSDARG00000075261	*timp2b*	tissue inhibitor of metalloproteinase 2b
Cytokines		
ENSDARG00000005419	*il1b*	interleukin 1, beta
ENSDARG00000009511	*tnfa*	tumor necrosis factor a (TNF superfamily, member 2)
ENSDARG00000013598	*tnfb*	tumor necrosis factor b (TNF superfamily, member 2)
ENSDARG00000100007	*il8*	interleukin 8
CXCL chemokines		
ENSDARG00000075045	*cxcl-c1c*	chemokine (C-X-C motif) ligand C1c
Transcription factors		
ENSDARG00000007823	*atf3*	activating transcription factor 3
ENSDARG00000087832	*bcl3*	B-cell CLL/lymphoma 3
ENSDARG00000042725	*cebpb*	CCAAT/enhancer binding protein (C/EBP), beta
ENSDARG00000087303	*cebpd*	CCAAT/enhancer binding protein (C/EBP), delta
ENSDARG00000077982	*elf3*	E74-like factor 3 (ets domain transcription factor, epithelial-specific)
ENSDARG00000032768	*irf1b*	interferon regulatory factor 1b
ENSDARG00000076251	*irf3*	interferon regulatory factor 3
ENSDARG00000031683	*fos*	v-fos FBJ murine osteosarcoma viral oncogene homolog
ENSDARG00000015355	*fosl1*	FOS-like antigen 1
ENSDARG00000040623	*fosl2*	fos-like antigen 2
ENSDARG00000074378	*junba*	jun B proto-oncogene a
ENSDARG00000088371	*junbb*	jun B proto-oncogene b
ENSDARG00000038687	*nfkb2*	nuclear factor of kappa light polypeptide gene enhancer in B-cells 2, p49/p100
Lipid transport		
ENSDARG00000012076	*apoa1a*	apolipoprotein A-Ia
ENSDARG00000086583	*apoa1 (2 of 2)*	apolipoprotein A-I
ENSDARG00000015866	*apoa2*	apolipoprotein A-II
ENSDARG00000040298	*apoa4*	apolipoprotein A-IV
ENSDARG00000022767	*apobl/apobb*	apolipoprotein B, like
ENSDARG00000092155	*apoc2*	apolipoprotein C-II
ENSDARG00000086370	*apoea*	apolipoprotein Ea
ENSDARG00000041490	*zgc:161979 (1)*	apolipoprotein A-II family
ENSDARG00000095863	*zgc:161979 (2)*	apolipoprotein A-II family
ENSDARG00000059227	*fabp1b.1*	fatty acid binding protein 1b, tandem duplicate 1
Complement		
ENSDARG00000012694	*c3a*	complement component c3a
ENSDARG00000052207	*c3c*	complement component c3c
ENSDARG00000038424	*c4a*	complement component 4A (Rodgers blood group)
ENSDARG00000057121	*c7 (2 of 2)*	complement component 7
ENSDARG00000039516	*c8a*	complement component 8, alpha polypeptide
ENSDARG00000016319	*c9*	complement component 9
ENSDARG00000055278	*cfb*	complement factor B
irg1 and irg1l		
ENSDARG00000069844	*irg1*	immunoresponsive gene 1
ENSDARG00000062788	*irg1l*	immunoresponsive gene 1, like
Miscellaneous		
ENSDARG00000045999	*saa*	serum amyloid A
ENSDARG00000055901	*steap4*	STEAP family member 4
ENSDARG00000053227	*hamp2*	hepcidin antimicrobial peptide 2
Autophagy		
ENSDARG00000045561	*dram1*	DNA-damage regulated autophagy modulator 1

ADAM metalloproteinases		
ENSDARG00000001452	*adam8a*	a disintegrin and metalloproteinase domain 8a
ENSDARG00000057644	*adam8b*	a disintegrin and metalloproteinase domain 8b
ENSDARG00000041566	*adamts1*	ADAM metallopeptidase with thrombospondin type 1 motif, 1
ENSDARG00000007709	*adamts8a*	ADAM metallopeptidase with thrombospondin type 1 motif, 8a
Acute phase other than complement		
ENSDARG00000020741	*fga*	fibrinogen alpha chain
ENSDARG00000008969	*fgb*	fibrinogen, B beta polypeptide
ENSDARG00000051912	*hpx (1 of 2)*	hemopexin
ENSDARG00000010312	*cp*	ceruloplasmin
prostaglandin biosythesis/receptors		
ENSDARG00000060094	*ptgis*	prostaglandin I2 (prostacyclin) synthase
ENSDARG00000052148	*ptgs1*	prostaglandin-endoperoxide synthase 1
ENSDARG00000004539	*ptgs2a*	prostaglandin-endoperoxide synthase 2a
ENSDARG00000010276	*ptgs2b*	prostaglandin-endoperoxide synthase 2b
negative regulators (late response)		
ENSDARG00000053131	*irak3*	interleukin-1 receptor-associated kinase 3
ENSDARG00000025428	*socs3a*	suppressor of cytokine signaling 3a
ENSDARG00000026611	*socs3b*	suppressor of cytokine signaling 3b
ENSDARG00000005481	*nfkbiaa*	nuclear factor of kappa light polypeptide gene enhancer in B-cells inhibitor, alpha a
ENSDARG00000007693	*nfkbiab*	nuclear factor of kappa light polypeptide gene enhancer in B-cells inhibitor, alpha b
ENSDARG00000030087	*nfkbib*	nuclear factor of kappa light polypeptide gene enhancer in B-cells inhibitor, beta
ENSDARG00000077001	*nfkbid*	nuclear factor of kappa light polypeptide gene enhancer in B-cells inhibitor, delta
ENSDARG00000068367	*nfkbie*	nuclear factor of kappa light polypeptide gene enhancer in B-cells inhibitor, epsilon
ENSDARG00000003157	*nfkbil1*	nuclear factor of kappa light polypeptide gene enhancer in B-cells inhibitor-like 1
ENSDARG00000095117	*nfkbiz*	nuclear factor of kappa light polypeptide gene enhancer in B-cells inhibitor, zeta
NADPH oxidase		
ENSDARG00000033735	*ncf1*	neutrophil cytosolic factor 1 (p47phox)
ENSDARG00000040812	*ncf4*	neutrophil cytosolic factor 4 (p40phox)
ENSDARG00000070062	*nox1*	NADPH oxidase 1
ENSDARG00000041294	*noxo1a*	NADPH oxidase organizer 1a
ENSDARG00000056374	*noxo1b*	NADPH oxidase organizer 1b
ENSDARG00000018283	*cyba*	cytochrome b-245, alpha polypeptide (p22phox)
ENSDARG00000056615	*cybb*	cytochrome b-245, beta polypeptide (p91phox, chronic granulomatous disease)

Footnote: table of gene IDs, names and descriptions of selected genes that are presented in this research (fig. 3 and supplementary fig. 2). * *zgc:161979* (1) and (2) are two paralogues of an apolipoprotein A-II family gene on chromosome 16.

Supplementary movie S1. E2-Crimson-expressing *M. marinum* bacterial infection in *Tg(fli1a:EGFP)/Tg(mpeg1:mCherry-F)*. A z-stack was imaged every 20 minutes at the caudal vein from 180 minutes post infection (mpi) to 820 mpi and is presented as a maximum intensity z-stack projection of the merged E2-Crimson, EGFP and mCherry channels. At 400 minutes an infected macrophage (purple: overlapping E2-Crimson and mCherry) can be seen outside the vasculature. Supplementary movie can be viewed at: https://www.dropbox.com/sh/1zwu4b6f1uzeuap/Ftc9uFKwpG?n=26155020

Chapter 5

Phagocytosis of mycobacteria by zebrafish macrophages is dependent on the scavenger receptor Marco, a key control factor of pro-inflammatory signalling

Erica L. Benard, Stefan J. Roobol, Herman P. Spaink, Annemarie H. Meijer

Developmental and Comparative Immunology, In press

Abstract

Scavenger receptors on the cell surface of macrophages play an important role in host defence through their ability to bind microbial ligands and induce phagocytosis. Concurrently, signal transduction pathways are initiated that aid in defence mechanisms against the invading microbe. Here we report on the function of scavenger receptor Marco (*Ma*crophage *r*eceptor with *co*llagenous structure) during infection of zebrafish embryos with *Mycobacterium marinum,* a close relative of *M. tuberculosis.* Morpholino knockdown demonstrates that Marco is required for the rapid phagocytosis of *M. marinum* following intravenous infection. Furthermore, gene expression analysis shows that Marco controls the initial transient pro-inflammatory response to *M. marinum* and remains a determining factor for the immune response signature at later stages of infection. Increased bacterial burden following *marco* knockdown indicates that this scavenger receptor is important for control of *M. marinum* growth, likely due to delayed phagocytosis and reduced pro-inflammatory signalling observed under conditions of Marco deficiency.

Introduction

Scavenger receptors (SRs) comprise a large family of transmembrane cell surface glycoproteins and are mainly expressed in macrophages, dendritic cells and endothelial cells [1]. Originally these receptors were characterised by their ability to recognise and internalise modified low-density lipoproteins (LDLs), such as oxidised LDL and acetylated LDL, thereby making these susceptible to degradation [2]. For this reason they have been extensively studied in relation to development of atherosclerosis [3]. However, SRs also have many other important functions, for example in pathogen clearance, in transport of cargo within the cell, and in lipid transport [4-6].

Class A SRs in vertebrates consist of three proteins: SR-AI, SR-AII and MARCO (*ma*crophage *r*eceptor with *co*llagenous structure). SR-AI and SR-AII are both encoded by the macrophage scavenger receptor 1 (*MSR1*) gene [7] but differ in structure due to alternative splicing of the gene product. SR-AI contains a C-terminal cysteine-rich domain which is lacking in SR-AII [8]. The trimeric membrane-bound MARCO protein has short intracellular and transmembrane domains, as well as a large extracellular domain that consists of a spacer domain, a long collagenous domain, and a C-terminal scavenger receptor cysteine-rich domain (SRCR domain V) [9]. In un-inflamed tissues, expression of mouse and human *MARCO* is restricted to macrophages of the splenic marginal zone, medullary cords of the lymph nodes, and alveolar macrophages of the lung [9-11]. Under inflammatory conditions caused by bacterial infection or lipopolysaccharide (LPS) injection, *MARCO* expression can be rapidly up-regulated [12, 13] and its expression profile extends to the splenic macrophages of both red and white pulp, dendritic cells [14], and Kupfer cells in the liver [10]. Deficiency of MARCO in mouse models and patients is

linked with autoimmune diseases such as systemic lupus erythematosus (SLE), which is most likely due to its role in the binding to and clearance of apoptotic cells, which are considered to be a major source for auto-antigens [15-18]. The first indication for a role of MARCO in anti-bacterial defence was that monoclonal antibodies inhibited capturing of heat-killed bacteria by macrophages in the marginal zone areas of the spleen in mice [13].

Recent findings supporting the immunological role of MARCO in human infections are that single nucleotide polymorphisms (SNPs) in *MARCO* are associated with increased susceptibility to pulmonary tuberculosis (TB) in humans [19, 20]. *Mycobacterium tuberculosis* is the causative agent of TB, a common and frequently lethal infectious disease. After being phagocytosed by macrophages, mycobacteria are capable of inhibiting the phagosome-lysosome fusion by interfering with the Rab-controlled membrane trafficking, allowing them to reside and proliferate in a safe environment [21]. Increased phagocytic activity of *M. tuberculosis* has been observed in mouse macrophages deficient in autophagy-related gene 7 (ATG7), which display higher expression levels of *MARCO* and *MSR1* [22]. MARCO has been shown to assist in the phagocytosis of *M. tuberculosis* in mice via specific binding to the cell wall glycolipid trehalose 6,69-dimycolate (TDM) of this bacteria and to cooperate with TLR2/CD14 signalling in activating cytokine responses [23]. TDM is capable of inducing many elements of *M. tuberculosis* pathogenesis and is predicted to be present in *M. marinum*, a natural fish pathogen and a close relative of *M. tuberculosis* [24]. *M. marinum* causes an infection in zebrafish (*Danio rerio*) that shares pathological hallmarks with human TB disease, including the formation of caseating granulomas and development of latency [25, 26].

The early life stages of the zebrafish, which are transparent, have proven extremely useful to study the early events in mycobacteria-host interactions, from phagocytosis to early granuloma formation [27-30]. We have previously shown that a zebrafish homologue of *MARCO* is expressed in embryos, downstream of the transcription factor Spi1/Pu.1 that is required for myeloid cell development [31]. Furthermore, others have demonstrated expression of *marco* in macrophages and dendritic cells of adult zebrafish [32]. Here we report on a functional study of the zebrafish *marco* gene.

We demonstrate that Marco is required for the rapid phagocytosis of *M. marinum* in zebrafish and is an essential player in the establishment of an initial transient pro-inflammatory response to this pathogen. Furthermore, we show that Marco is important for mycobacterial growth control.

Materials and methods

Zebrafish husbandry

Zebrafish were handled in compliance with the local animal welfare regulations and were maintained according to standard protocols (zfin.org). The culture was approved

by the local animal welfare committee (DEC) of the University of Leiden and all protocols adhered to the international guidelines specified by the EU Animal Protection Directive 2010/63/EU. Zebrafish lines used in this study included AB/TL, *Tg(mpeg1:EGFP)*^{gl22} [33], *Tg(mpeg1:mCherry)*^{UMSF00134}, *Tg(mpeg1:Gal4-VP16)*^{gl24} [33], *Tg*(*mpx*:*GFP*)^{i114} [35], and *Tg(UAS-E1b:NTR-mCherry)*^{i149} [36]. Embryos were grown at 28.5°C in egg water (60 µg/ml Instant Ocean sea salts). For the duration of bacterial injections and imaging, embryos were kept under anaesthesia in egg water containing 200 µg/ml tricaine (Sigma-Aldrich). Embryos used for stereo fluorescence imaging were kept in egg water containing 0.003% 1-phenyl-2-thiourea (Sigma-Aldrich) to prevent melanisation.

Marco sequence and morpholino knockdown

A cDNA clone of *marco* (EST CO929777) was obtained from GenomeCube. The full length sequence was determined by the sequencing service of BaseClear (Leiden, Netherlands) and submitted to GenBank (accession number BankIt1734081 Marco KJ955494). Protein domains were detected with SMART analysis. Amino acid identity and similarity percentages were determined using UniProt CLUSTAL O(1.2.0) multiple sequence alignment. Splice blocking morpholino oligonucleotides were designed based on the alignment of the cDNA sequence with the genomic sequence from Ensembl gene ENSDARG00000059294 (Supplementary fig 1A). Two morpholinos were obtained from Gene Tools, morpholino 1 targeting the intron 15-exon 16 boundary and morpholino 2 targeting the exon 9-intron 9 boundary (Mo1: 5'ACGGACCACTGATGAAGAAAAACAA3'; 0.02 mM and Mo2: 5'TAACTAAAAGTACCTTGGCTTCCAC3'; 0.3 mM). Morpholinos were diluted to the desired concentration in 1x Danieau buffer (58 mM NaCl, 0.7 mM KCl, 0.4 mM $MgSO_4$, 0.6 mM $Ca(NO_3)_2$, 5.0 mM HEPES; pH 7.6) containing 1% phenol red (Sigma-Aldrich) and 1 nl was injected into the yolk at the 1-2 cell stage using a Femtojet injector (Eppendorf). As a control the standard control oligonucleotide from Gene Tools was used.

Chemical treatments

For nitroreductase-dependent macrophage ablation, metronidazole, (10 mM, 2 hours treatment, Sigma-Aldrich, M3761) was administered via the egg water to 3 days post fertilisation (dpf) embryos. Copper sulphate ($CuSO_4$, 10 uM, 2 hours treatment, Merck, #1027910250) was administered via the egg water to induce cell death of neuromast hair cells and a subsequent inflammatory response [37]. After copper sulphate treatment the embryos were briefly washed three times with egg water and fixed in 4% paraformaldehyde in PBS.

Infection experiments

Mycobacterium marinum infections were performed using the Mma20 strain expressing mCherry in a pSMT3 vector [38] or the *Salmonella typhimurium* strain SL1027 carrying the DsRed expression vector pGMDs3 [39]. Embryos were staged at 24 hours post fertilisation

(hpf) by morphological criteria [40] and manually dechorionated. Bacteria were prepared and injected into the blood circulation at 28 hpf [41] and PBS or 2% Polyvinylpyrrolidone (PVP40) in PBS (w/v) was used as a mock injection. In experiments for fluorescent bacterial pixel count and qPCR analysis, 200 colony forming units (cfu) of *M. marinum* was used. In experiments for phagocytosis analysis, 180 cfu *M. marinum* or *S. typhimurium* was injected into the blood circulation at 30 hpf. This stage of development was used because the Duct of Cuvier is located more laterally over the yolk sac compared to 28 hpf which facilitates imaging purposes for quantification. Infected embryos were fixed at 5, 10, 20 and 30 minutes post infection (mpi) in 4°C 4% paraformaldehyde in PBS. Leukocytes were immuno-labelled and the number of intra- and extra-cellular bacteria was counted over the yolk sac.

Fluorescence-activated cell sorting

Macrophages and neutrophils were isolated by FACS from 6 dpf *Tg(mpeg1:mCherry)^{UMSF001}* [34] and *Tg*(*mpx*:GFP)^{i114} [35] zebrafish larvae, respectively. The procedure is described in detail in [42]. In short, larvae were dechorionated using pronase treatment, rinsed in calcium-free Ringer solution, and digested with 0.25% trypsin. The obtained cell suspension was centrifuged, rinsed with PBS and resuspended in Leibovitz medium L15 without phenol red, 1% fetal calf serum, 0.8mM CaCl2, penicillin 50 U/ml and streptomycin 0.05 mg/ml. The single cell suspension was subjected to FACS at room temperature using a FACSAria (Becton Dickinson) with the BD FACSDiva software version 5.0.3 and a Coherent Sapphire solid state laser 488 nm with 13 mW power. The GFP+ and GFP- cell fractions were collected as above but with 10% fetal calf serum and RNA was isolated using the RNAaqueous Micro Kit (Ambion).

RNA isolation, cDNA synthesis, and expression analyses

Whole embryo RNA isolation, removal of residual genomic DNA, cDNA synthesis and quantitative RT-PCR (qPCR) analysis was performed as described in [43]. qPCR results were analysed using the ΔΔCt method. All reactions were performed as technical duplicates and data were normalised to the expression of peptidylprolyl isomerase A like (*ppial*) for whole embryo samples and to *eukaryotic translation initiation factor 4A, isoform 1B* (*eif4a1b*) for cells isolated by FACS. Primer sequences for *ppial* and *marco* are described in [31], primer sequences for *mmp9* and *il1b* are described in [43], and primer sequence for *eif4a1b* are: FW: 5'TTCAGAAACTCAGTACTAGCATACA3'; REV: 5'GTGACATCCAACACCTCTGC3'. Knockdown of *marco* with morpholino 1 was verified by qPCR and to validate the knockdown of morpholino 2, the SuperScript® One-Step RT-PCR System (Invitrogen, #10928-034) was used with 50ng DNAse treated RNA template. RT-PCR primers for *marco* knockdown verification were FW: 5'GACAGACAGGAGATCCTGG3'; REV: 5'CTCCACGCTCACCTTTGAGAC3'. The following adjustments were made to the PCR settings: 59.4°C for 30 seconds for the annealing step of the PCR amplification with 30 cycles.

RNA for deep sequencing analysis was isolated using QIAzol lysis reagent and purified using the Rneasy MinElute Cleanup kit (QIAGEN Benelux B.V., Venlo, Netherlands). RNA sequencing was performed as previously described [44]. Gene Expression Omnibus (GEO) database accession for RNASeq: GSE58230.

Immunohistochemistry

Identification of neutrophils and macrophages was done by immuno-labelling with a leukocyte specific L-plastin antibody and Alexa568/488-conjugated secondary antibody, combined with neutrophil specific staining for myeloperoxidase activity [45].

Imaging

Stereo fluorescence images were taken with a Leica MZ16FA stereo fluorescence microscope equipped with a DFC420C digital colour camera. Overlay images of bright field and fluorescence stereomicroscopy were made using Fiji [46]. Bacterial pixel counts were obtained on stereo fluorescence images and analysed using dedicated software [47]. Quantification of phagocytosis was performed on an Axiovert 100M microscope with a W Plan-APOCHROMAT 40x 1.0 NA objective. Confocal images were taken on a Leica TCS SPE with an HCX APO 40x 1.0 NA objective and the Nikon Ti Eclipse with a plan apo 20x NA 0.75 WD 1mm with V (violet) correction.

Statistical analysis

All data (mean ± SEM) were analysed using unpaired, two-tailed t-tests for comparisons between two groups and one-way ANOVA with Tukey's Multiple Comparison method as a post-hoc test for other data (*, $p<0.05$; **, $p<0.01$; ***, $p<0.001$).

Results

The zebrafish *marco* gene is expressed in larval macrophages and is up-regulated during infection

Sequencing of a cDNA clone of the zebrafish *marco* gene revealed that the predicted protein shows more than 60% similarity with murine and human MARCO and has a highly conserved protein domain structure (fig. 1A-C, Supplementary table 1A). The similarity is highest (ca. 85%) in the C-terminal cysteine-rich domain, which is essential for the binding of bacteria [48] (Supplementary table 1B). To confirm the expression of *marco* in macrophages of zebrafish larvae, we used a transgenic macrophage reporter line, *Tg(mpeg1:mCherry)* to isolate macrophages by FACS at 6 days post fertilisation (dpf). We found the expression of *marco* to be highly enriched in the fluorescent macrophage cell fraction compared to the fluorescent-negative background (fig. 1D). In addition, *marco* expression is lowly expressed in neutrophils sorted from 6 dpf *Tg*(*mpx*:*GFP*) transgenic larvae (fig. 1E). We previously observed that *marco* is induced during *S. typhimurium*

infection in zebrafish embryos [49], therefore, we sought to determine whether zebrafish *marco* is regulated in a similar manner during infection with *M. marinum*, the natural mycobacterial pathogen for fish. qPCR analysis showed that *marco* is induced at 4 hours post infection (hpi) (fig. 1F), however, no difference in expression level could be observed at 4 days post infection (dpi) (fig. 1G), a time point when the embryos are severely infected and contain granuloma-like structures.

Marco functions in the phagocytosis of *M. marinum*

The conserved protein domain structure of zebrafish Marco allows us to hypothesise that it functions as a phagocytic scavenger receptor, similar to mammalian MARCO. To test this hypothesis, we set up an *in vivo* assay to determine the percentage of phagocytosed *M. marinum* at various time points. The assay consists of microinjecting a single cell suspension of fluorescently labelled *M. marinum* into the blood circulation at the site of the blood island, fixing the embryos at 5, 10, 20 and 30 mpi, immuno-labelling leukocytes with L-plastin antibody [50], and counting of intra- and extra-cellular *M. marinum* at the site of the Duct of Cuvier under a fluorescence microscope (fig. 2A). Following intravenous injection *M. marinum* is phagocytosed specifically by macrophages [27, 51] and neutrophils are known to be unable to efficiently phagocytose bacteria in liquid compartments such as the blood circulation [52], Therefore, we considered the L-plastin labelled leukocytes with internalised *M. marinum* as macrophages. The Duct of Cuvier was used as the counting site because it is distant from the site of injection, thereby avoiding interfering wounding effects, and it is located close to the surface, which facilitates imaging. Two sources of *M. marinum* can be used for this assay: a glycerol stock or a 7H9 liquid culture stock grown to logarithmic phase [41]. By injecting aliquots of a glycerol stock of *M. marinum* the dose could be kept constant throughout experiments, however, the injected glycerol stock bacteria showed a faster rate of phagocytosis (97% at 30 mpi) (fig. 2B+C) compared to the liquid culture bacteria (65% at 30 mpi) (fig. 2D) in the control embryos.

We used an antisense morpholino oligonucleotide approach to block intron-exon splicing events for zebrafish *marco* (Supplementary fig 1B+C). Morpholino-mediated knockdown of *marco* did not affect leukocyte development (Supplementary fig 1D and E). The ability of leukocytes to migrate towards a local inflammation site was also not affected. This was verified by performing a chemically induced inflammation (ChIN) assay [37] in which copper-induced damage of neuromast hair cells was capable of attracting both macrophages and neutrophils in the *marco* morphants similar as in the control group (Supplementary fig 1F). Injection with equal numbers of glycerol stock bacteria in the *marco* morphants (Supplementary fig 1G) showed that the morphants showed a significant reduction in the phagocytosis of *M. marinum* (fig. 2B) at time points up to 20 min after injection. By 30 min after injection the difference was no longer significant, indicating that phagocytosis of *M. marinum* in *marco* morphants is delayed but not abolished. This delay in phagocytosis of *M. marinum* was phenocopied with a second morpholino targeting another intron-exon boundary (fig. 2C). In addition, a delay in

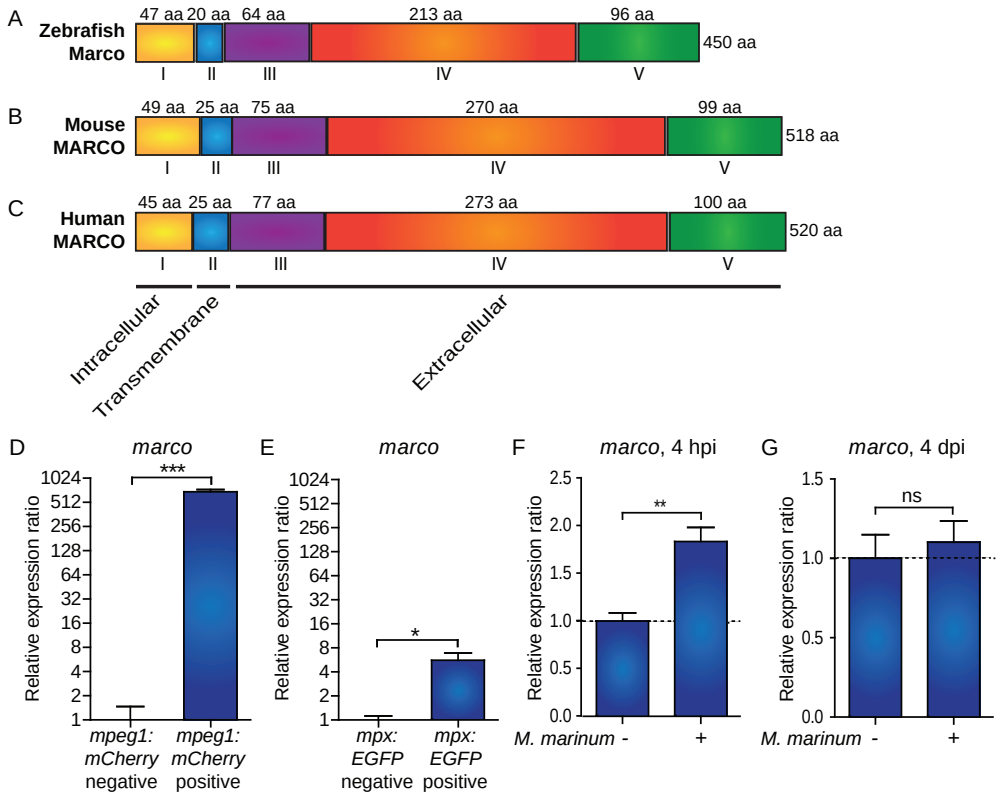

Figure 1. Zebrafish *marco* encodes a macrophage specific protein with conserved domains and is induced during early *M. marinum* infection. Comparison of the predicted (A) zebrafish Marco protein structures with (B) murine and (C) human MARCO. The cytoplasmic domain (I), transmembrane domain (II), short spacer domain (III), collagenous domain (IV), and C-terminal cysteine-rich domain (V) are conserved domains detected by SMART analysis. The domains are indicated by Roman numbers; the amino acid (aa) residue lengths of the subunit chains are indicated above their corresponding domains; and the total protein lengths are indicated to the right. The predicted cellular location of each region is indicated below. (D-E) Zebrafish *marco* is expressed in macrophages. Expression of *marco* in (D) macrophages and (E) neutrophils. qPCR analysis was performed on RNA from fluorescence-positive cell fractions obtained by cell sorting of 6 dpf larvae transgenic reporter lines for macrophages (*Tg(mpeg1:mCherry)*) and neutrophils (*Tg(mpx:EGFP)*). Expression was compared against the fluorescence-negative cell fraction of each transgenic line. (F-G) *marco* is up-regulated during early *M. marinum* infection. qPCR analysis was performed on RNA from (F) 4 hpi and (G) 4 dpi mock injected and *M. marinum* (200 cfu) injected AB/TL embryos. All graphs show data combined from three biological replicates (n=15 per group, pooled per replicate).

phagocytosis was also observed in the *marco* morphants injected with *M. marinum* from liquid culture (fig. 2A and D). In this experiment, the reduction of phagocytosis was significant at time points between 10 and 30 min after injection.

To investigate whether other scavenger receptors have a similar function in aiding phagocytosis of *M. marinum* we chose to knock down *cd36*, a class B scavenger receptor that is down-regulated during *M. marinum* infection at 4 days post infection (dpi) (data not published) and is shown to play a role in phagocytosis of bacteria such as *Staphylococcus aureus* [53]. The results showed that Cd36 does not influence the phagocytosis of *M. marinum* in zebrafish embryos (fig. 2A and E). Furthermore, in another study we similarly knocked down *mpeg1*, a different macrophage specific gene with no suggested function in phagocytosis and found that this gene also does not influence the phagocytosis of *M. marinum* [54]. To test whether Marco plays a role in the phagocytosis of other intracellular pathogens we performed the phagocytosis assay with *Salmonella typhimurium*. A significant reduction of phagocytosed bacteria was observed in *marco* morphants at 30 and 60 min post injection (Supplementary fig 2), indicating that Marco is not merely specific for phagocytosis of *M. marinum*. At 2 h post injection the complete dose of injected bacteria had been phagocytosed both in *marco* morphants and in the control embryos, indicating that Marco deficiency delays but does not abolish phagocytosis of *S. typhimurium*, similar as observed for *M. marinum* (Supplementary fig 2). Since both the scavenger receptor Cd36 and the macrophage specific Mpeg1 do not affect phagocytosis, we conclude that Marco plays a specific role in bacterial phagocytosis by macrophages.

marco knockdown has no detectable effect on the phagocytosis of ablated cells

After identifying a direct antimicrobial phagocytic function of Marco, we further sought to define whether Marco also plays a role in a different phagocytic process, namely phagocytosis of dying cells. Previous research has shown that murine MARCO is capable of binding to apoptotic cells, indicating a function in the phagocytosis and clearance of dead cells [15, 16]. Specific collective cell death at a controlled time-point can be achieved in zebrafish larvae by using nitroreductase-mediated ablation. We created a double transgenic line of *Tg(mpeg1:EGFP)* and *Tg(mpeg1:Gal4-VP16)/Tg(UAS-E1b:NTR-mCherry)* in which all macrophages express GFP and a subpopulation expresses nitroreductase mCherry. Not all GFP-positive macrophages in this line express mCherry due to silencing of the UAS promoter [55]. Cell death was induced in this subpopulation of macrophages expressing nitroreductase by treating the embryos with metronidazole, which is metabolised into a toxic product [36, 56]. At 120 minutes post treatment (mpt) the nitroreductase-positive subpopulation of macrophages started dying, between approximately 150 and 260 mpt the dead cells became phagocytosed by healthy GFP-positive macrophages, which then continued to migrate away from the site of phagocytosis between 260 and 280 mpt (fig. 3). In simultaneously time lapse recordings of 4 embryos per group, we detected 4-6 phagocytosis events in each of the *marco* morphants and control embryos (Supplementary fig 2B). Therefore, this analysis did not reveal a significant effect of *marco* knockdown on phagocytosis of chemically ablated cells.

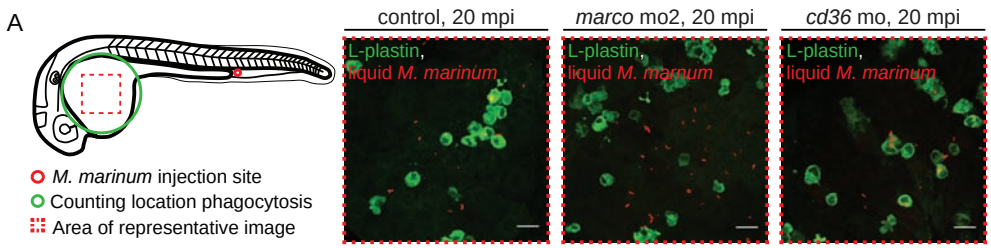
A
control, 20 mpi
marco mo2, 20 mpi
cd36 mo, 20 mpi
L-plastin,
liquid M. marinum
M. marinum injection site
Counting location phagocytosis
Area of representative image

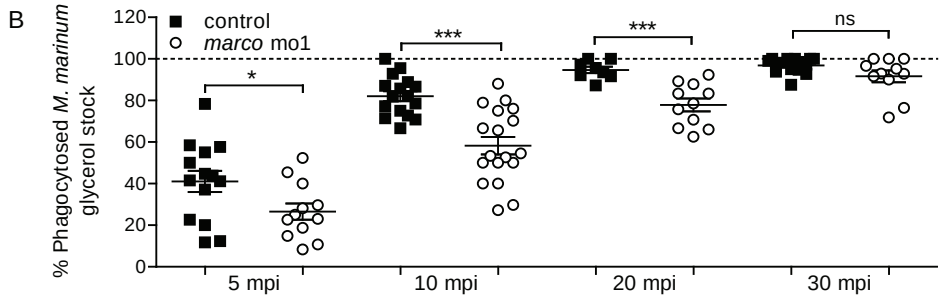
B
% Phagocytosed M. marinum glycerol stock
control
marco mo1
5 mpi
10 mpi
20 mpi
30 mpi
ns

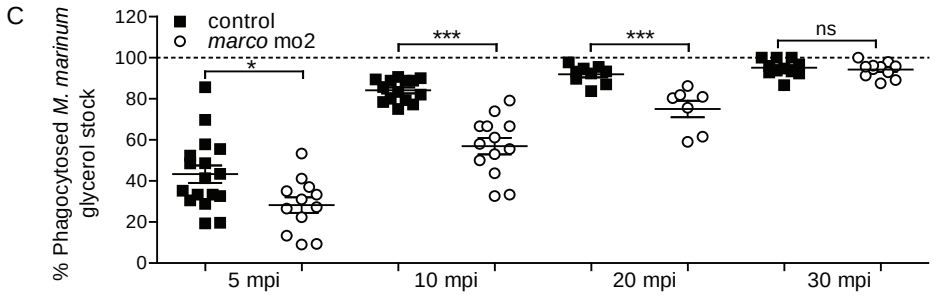
C
% Phagocytosed M. marinum glycerol stock
control
marco mo2
5 mpi
10 mpi
20 mpi
30 mpi
ns

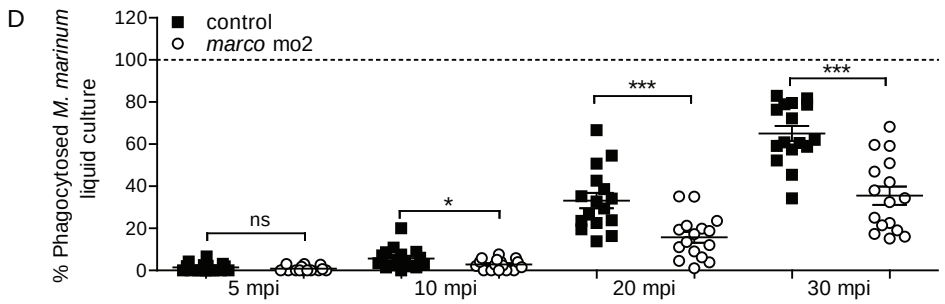
D
% Phagocytosed M. marinum liquid culture
control
marco mo2
5 mpi
10 mpi
20 mpi
30 mpi
ns

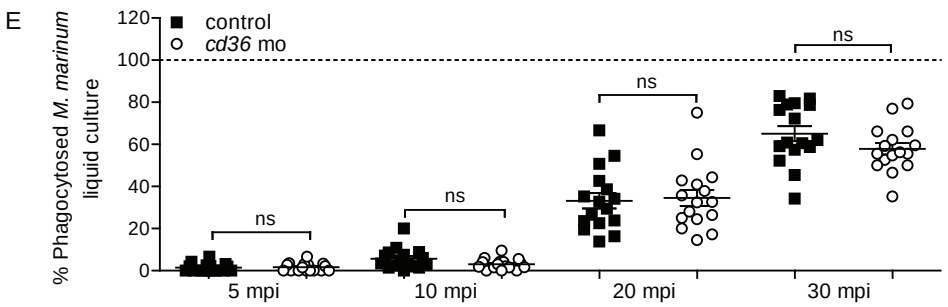
E
% Phagocytosed M. marinum liquid culture
control
cd36 mo
5 mpi
10 mpi
20 mpi
30 mpi
ns

Figure 2. Marco functions in the phagocytosis of *M. marinum*. Quantification of *M. marinum* phagocytosis. (A) Schematic overview of the phagocytosis quantification process and representative images of infected control embryos, *marco* morphants (mo2), and *cd36* morphants at 20 mpi. (B-D) Morphants of *marco* ((B) morpholino 1 and (C-D) morpholino 2) show a delayed phagocytosis of *M. marinum* (B-C) glycerol stock and (D) 7H9 liquid culture. (E) Morphants of *cd36* show no difference in phagocytosis of *M. marinum*. Each data point represents the percentage of phagocytosed *M. marinum* in an individual embryo.

Marco is required for a pro-inflammatory response following phagocytosis of *M. marinum*

The host immune response to mycobacteria includes production of pro-inflammatory cytokines induced by TLR2 detection of pathogen-associated molecular patterns (PAMPs), and MARCO has been proposed to function cooperatively with this receptor [23]. After identifying that Marco facilitates bacterial phagocytosis, we then investigated whether zebrafish Marco also plays a role in inducing a pro-inflammatory cytokine response to *M. marinum.* Therefore, we analysed the gene expression levels of *il1b*, *il8* and *mmp9* to *M. marinum* at 4 hpi based on a time-course analysis that showed significant up-regulation of cytokine and matrix metalloproteinase gene expression in our infection model (data not shown). As expected, all the genes were significantly up-regulated in the control embryos at 4 hpi; however, upon knockdown of *marco*, these genes were no longer significantly up-regulated at this time-point (fig. 4A-C). Subsequently, we investigated whether the *marco* morphants completely lacked this pro-inflammatory response during time or whether there was merely a delay in response, similar to the delay in phagocytosis of *M. marinum*. Expression levels of *il1b* were determined every hour from 2 hpi until 6 hpi (fig. 4D). As expected, the control embryos showed significant *il1b* up-regulation, of which the peak (5-fold) was at 3 hpi in this experiment. At this time-point the *marco* morphants had a significantly lower level of *il1b* up-regulation (2-fold). After the peak at 3 hpi, the *il1b* expression response in the controls declined and became non-significant at 6 hpi. At none of the time point tested, did *marco* morphants reach the same peak level of *il1b* up-regulation as observed in the control group. This led us to conclude that Marco is an essential player in the establishment of an initial transient pro-inflammatory response to *M. marinum* infection.

Marco deficiency also leads to an altered immune response at the granuloma stage of *M. marinum* infection

Since *marco* morphants showed a reduced pro-inflammatory response in the first hours after infection, we next studied whether the morphants have a differently regulated immune response to *M. marinum* at a later stage of infection, when characteristic granulomatous lesions have formed. For this purpose we analysed RNA sequencing (RNA-Seq) profiles of pools of uninfected and infected *marco* morphants and controls at 4 dpi. Although the morpholino effect is likely to have diluted out over time, an

RNA-Seq profile at this stage should reveal if *marco* knockdown has a longer lasting effect. We had previously identified a gene set showing robust and reproducible up-regulation at this stage of the infection {Benard, In press #430}. As shown in figure 5A (and Supplementary table 2), several genes from this signature set display an altered response in infected *marco* morphants compared to infection in the control group. Under conditions of *marco* knockdown we observed a significantly higher up-regulation (2-fold or higher) of genes such as *mmp9, mmp13a, moxd1, steap4, tcap,* and *timp2b.* In addition, a non-coding RNA (*si:ch211-243g18.3*) showed approximately 20-fold higher up-regulation. Conversely, expression levels of other genes, such as *cyp1a*, *cyp24a*, and *hmox1*, appeared to be significantly lower in infected *marco* morphants compared with infected controls. The level of *il1b* up-regulation was similar in both infected groups, in contrast to the reduced up-regulation of this gene in *marco* morphants during the first hours of infection. In conclusion, at the late stage of infection, knockdown of *marco* causes an altered immune response, but pro-inflammatory signalling is not impaired.

Marco is important for mycobacterial growth control

Our observations that knockdown of *marco* (i) delays phagocytosis of *M. marinum*, (ii) suppresses the initial pro-inflammatory response to this infection, and (iii) affects the expression signature of larvae with mycobacterial granulomas, suggest that Marco contributes to controlling *M. marinum* growth. We therefore investigated the bacterial burden of *marco* morphants during *M. marinum* infection. Control embryos and *marco* morphants were infected with *M. marinum* at 28 hpf and the bacterial fluorescent pixels per embryo were analysed at 4 dpi. The results show that Marco deficiency leads to a significant increase in *M. marinum* bacterial burden (fig. 5B+D) and this effect could be verified by using a second splice-blocking morpholino of *marco* (fig. 5C+E). This increased infection level of *marco* morphants indicates that Marco plays a protective role in innate host defence against mycobacterial infection.

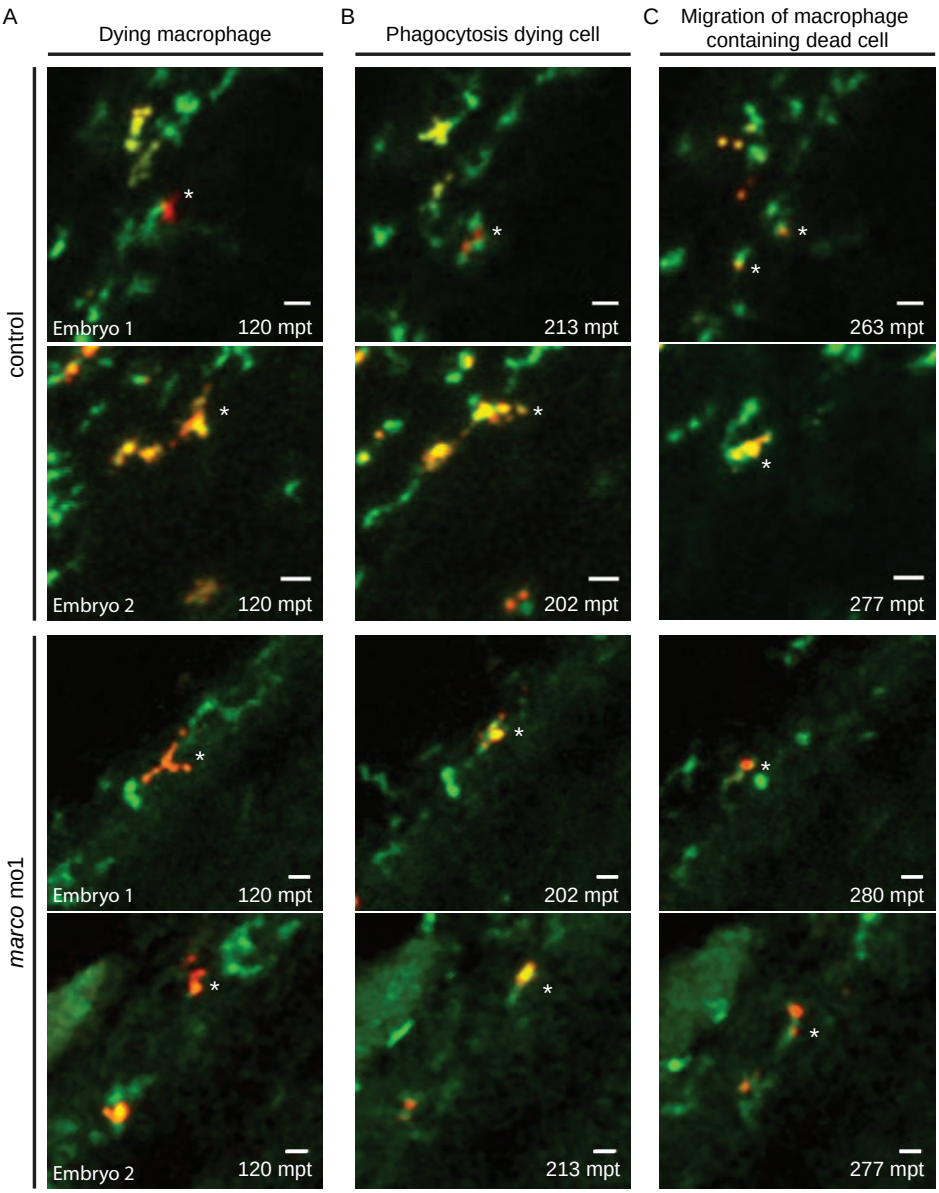

Figure 3. Morphants of *marco* are capable of phagocytosing dead cells. Phagocytosis of dying cells by macrophages was monitored in time. *marco* morphants and their controls were imaged after metronidazole treatment which induces nitroreductase-mediated cell ablation in a subpopulation of macrophages (mCherry positive cells). All macrophages express GFP. Time points represented are (A) time of nitroreductase-positive cells undergoing cell death, (B) phagocytosis of the dying cells by healthy GFP-positive macrophages and (C) migration of the macrophage containing the dead cell. Time lapse recordings were made of 4 embryos per group and examples of phagocytosis are shown for 2 control embryos en 2 *marco* morphants. Quantification of phagocytosis events are shown in Supplementary fig 2B. Asterisks indicate the phagocytosing macrophage; mpt: minutes post treatment.

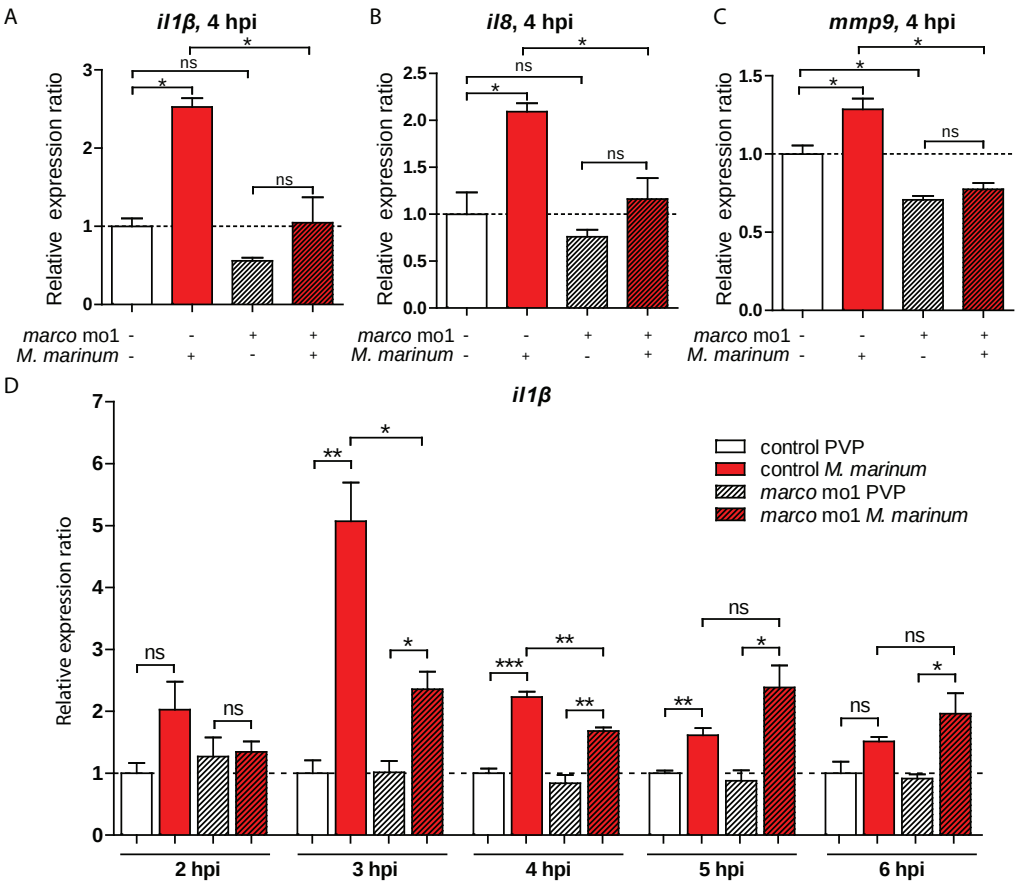

Figure 4. Morphants of *marco* have suppressed induction of pro-inflammatory cytokine response to *M. marinum*. (A-C) Effect of *marco* knockdown on the response of *il1b*, *il8* and *mmp9* to *M. marinum* infection. Expression levels of (A) *il1b*, (B) *il8* and (C) *mmp9* were determined by qPCR for marco morphants and their control embryos at 4 hpi after infection with *M. marinum* (200 cfu) and mock PVP injected controls; (D) Effect of *marco* knockdown on *il1b* expression in time (2-6 hpi). Expression was compared against the control PVP sample of each time point. All graphs show data combined from three biological replicates (n=15 per group, pooled per replicate).

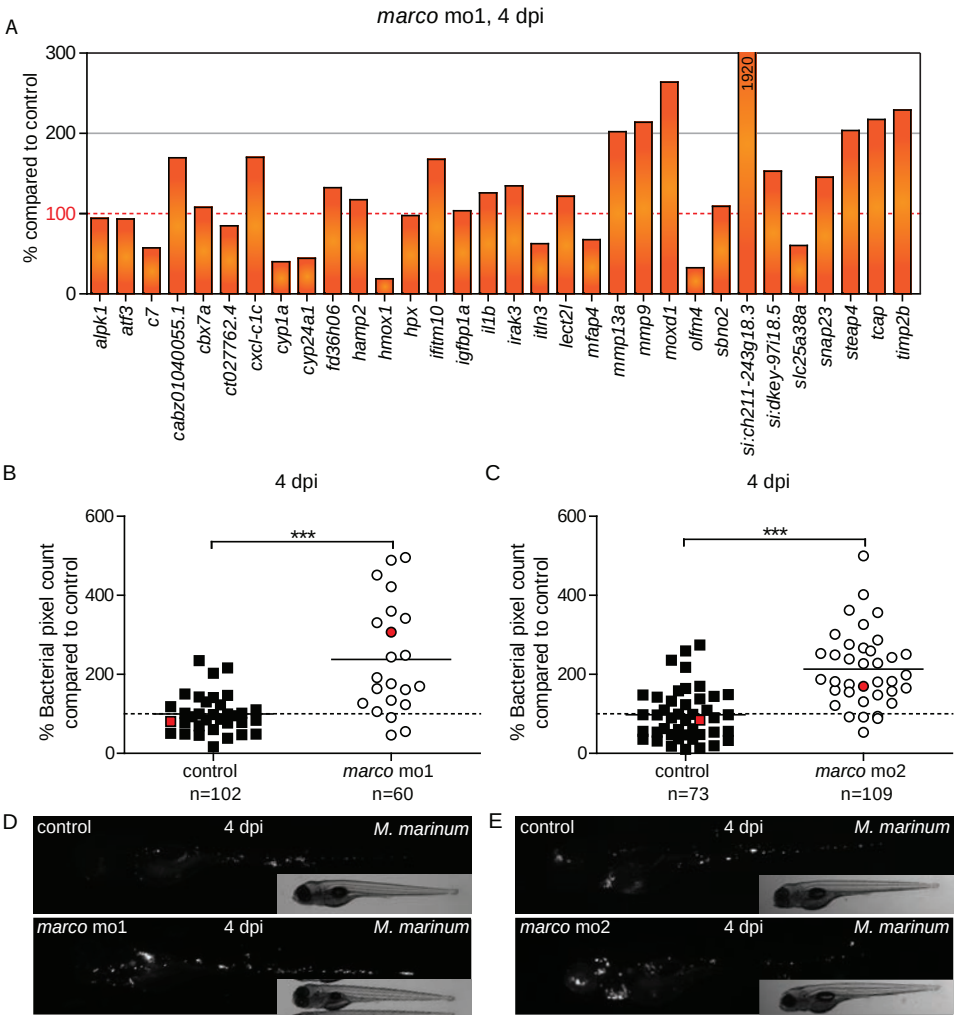

Figure 5. Effect of *marco* knockdown on the innate immune response and control of *M. marinum* infection. (A) Graph of the percentage of expression levels of infected *marco* mo1 morphants compared to infected control embryos on a set of 32 genes that showed reproducible induction by *M. marinum* infection in control embryos. The expression level of these genes under conditions of *marco* deficiency is expressed as the percentage of the expression level in the corresponding control. Results are based on RNA-Seq analysis of pools of 30 infected and 30 uninfected embryos for each group. Embryos were injected with *M. marinum* (200 cfu) or mock injected with 2% PVP, and RNA-Seq analysis was performed at 4 dpi. (B-E) *marco* knockdown impairs control of *M. marinum* infection. AB/TL embryos were injected with two different splice blocking morpholinos against (A-D) *marco* or with control morpholino, subsequently injected with mCherry-expressing *M. marinum*, and infected embryos were imaged at 4 dpi. (B-C) Bacterial burden was quantified by determining the number of fluorescent bacterial pixels and (D-E) representative stereo fluorescent images are shown below the graph of each experiment. Red symbols indicate which individuals are shown below as representative images. Graphs show combined results of 3 repeated independent experiments. Each data point represents an individual embryo.

Discussion

Phagocytosis of bacteria is an essential host defence mechanism carried out by macrophages and scavenger receptors are a key component of this process. MARCO is a scavenger receptor that has been shown to bind the cell wall component TDM of *M. tuberculosis* [23]. Here we have used a zebrafish model for tuberculosis and show that Marco mediates phagocytosis of *M. marinum* and that the initial pro-inflammatory response to this infection is dependent on Marco. We also observed a higher bacterial burden of *M. marinum* infection under conditions of *marco* knockdown.

M. marinum circulating in the blood of zebrafish embryos is rapidly phagocytosed by macrophages [57]. When *marco* was knocked down with a targeted morpholino oligonucleotide approach we observed a delay in phagocytosis of *M. marinum*. Similarly, we found that phagocytosis of intravenously injected *S. typhimurium* bacteria is also delayed under *marco* knockdown conditions. This *M. marinum* phagocytosis delay is specific for *marco* deficiency because it was repeatedly observed with two morpholinos targeting different exon-intron boundary sites and knockdown of control genes *cd36*, encoding a class B scavenger receptor, and *mpeg1,* encoding a macrophage-specific perforin*,* has no effect on phagocytosis. That *marco* deficiency does not completely abolish phagocytosis was not unexpected. One explanation might be that we used morpholinos, which generally produce a partial knockdown. A second explanation is that there are multiple receptors that can initiate phagocytosis of mycobacteria, such as the complement receptors (CRs) CR1, CR3, and CR4 that phagocytose opsonised *M. tuberculosis* [58-60], and the mannose receptors that interact with lipoarabinomannan (LAM) in the mycobacterial cell wall [61, 62]. Therefore, it is remarkable that knockdown of a single scavenger receptor, Marco, causes a significant delay in the phagocytosis of *M. marinum*. This indicates that apparently other receptors cannot fully compensate for the reduction of Marco.

When trying to establish whether Marco also plays a role in the phagocytosis of apoptotic or necrotic macrophages infected with *M. marinum*, we found image quantification of this process extremely difficult due to the sporadic occurrence and the varying location of these events. This prompted us to create an inducible system in which we could provoke cell death of a subpopulation of macrophages. Using this system, we found no evidence for a function of Marco in phagocytosis of dead cells resulting from toxification. However, it is possible that a null mutant of *marco,* which is currently not available, might reveal a stronger phenotype. Furthermore, we cannot exclude that Marco may still play a scavenging role during infection-induced cell death.

Studies using macrophages isolated from MARCO$^{-/-}$ mice have demonstrated that MARCO is preferentially utilised to "tether" mycobacterial TDM to the macrophage and to activate the TLR2 signalling pathway in response to this virulence factor [23]. This signalling not only requires MARCO and TLR2 but also CD14, which functions as a co-receptor.

CD14 is suggested to enhance the physical proximity of bacterial lipopeptides to the TLR1/2 heterodimers, without binding directly to the receptor complex [63-65]. However, CD14 alone cannot facilitate the TLR1/2-mediated response to bacterial lipopeptides because an additional co-receptor, such as MARCO, is needed [23]. Macrophages from MARCO-/- mice also produced markedly lower levels of pro-inflammatory cytokines in response to infection with virulent *M. tuberculosis*. In addition, MARCO has been shown to function in the non-opsonic recognition of *Streptococcus pneumoniae*, which leads to increased Nod2- and TLR2/CD14-dependent chemokine and cytokine production and, ultimately, the recruitment of effector monocytes/macrophages [4]. Here we confirm the finding that Marco functions as an essential player in the establishment of a pro-inflammatory response to mycobacteria in an *in vivo* infection model. However, the accessory molecule CD14 that is shown to interact with MARCO during this signalling process in mice, does not exist in the zebrafish genome [66]. Our results therefore indicate that zebrafish Marco is capable of functioning independently of the co-receptor CD14 in mediating a pro-inflammatory response to *M. marinum*. Since Tlr2 is conserved within fish and is capable of recognising (myco)bacterial ligands [67, 68], it is still likely that Marco functions as a co-receptor of Tlr2 in the recognition and phagocytosis of *M. marinum*.

Conclusion

Other interactions between scavenger receptors and TLR signalling are also known. Macrophages of mice have been shown to up-regulate *Marco* via LPS-induced TLR4 signalling, which can be a mechanism to increase phagocytic activity [69]. Similarly, when we infect zebrafish with *S. typhimurium*, an LPS-containing pathogen, we observe induction of *marco* [49]. In the present study, we have demonstrated that *marco* is also induced during the early stage (4 hpi) of *M. marinum* infection. The up-regulation of *marco* at this stage coincides with the time point during which the host produces a Marco-dependent pro-inflammatory response to *M. marinum*.

In this study we show that Marco is important for rapid phagocytosis of *M. marinum*, a process that most likely reoccurs during the development of granuloma-like structures when bacteria are released from necrotic cells. Marco is also is essential for the maximum induction of the initial pro-inflammatory response towards *M. marinum* infection, and remains a determining factor for the immune response signature at later stages of infection. All these factors probably contribute to the fact that *marco* deficiency leads to increased *M. marinum* growth in the zebrafish infection model. The broad range of functions that scavenger receptors have is not only a result of the many ligands that they recognise, but also of the various co-receptors that they partner with. This combination enables them to mount a highly versatile response. The fact that CD14, one of the co-receptors of MARCO that has been proposed to aid in the cytokine response regulation, is missing in zebrafish highlights the necessity of future work to unravel the signal transduction pathway associated with Marco in zebrafish.

Acknowledgements

We thank Julien Rougeot for help with RNA deep sequencing analysis, and other group members for helpful discussions. We further thank Steven Renshaw (University of Sheffield) for the *Tg(mpx:GFP)* line, George Lutfalla (University Montpellier 2) for the *Tg(mpeg1:mCherry)* line, Graham Lieschke (Monash University) for the *Tg(mpeg1:EGFP)* and *Tg(mpeg1:Gal4-VP16)* lines, Anna Huttenlocher (University of Wisconsin) for L-plastin Ab, Astrid van der Sar (VU Medical Center, Amsterdam) for bacterial strains and plasmids, and Alex Nezhinsky and Fons Verbeek for making their Pixel count software available prior to publication. This work was supported by the Smart Mix Program of the Netherlands Ministry of Economic Affairs and the Ministry of Education, Culture and Science.

References

1. Murphy, J.E., Tedbury, P.R., Homer-Vanniasinkam, S., Walker, J.H. & Ponnambalam, S. Biochemistry and cell biology of mammalian scavenger receptors. *Atherosclerosis* **182**, 1-15 (2005).

2. Goldstein, J.L., Ho, Y.K., Basu, S.K. & Brown, M.S. Binding site on macrophages that mediates uptake and degradation of acetylated low density lipoprotein, producing massive cholesterol deposition. *Proc Natl Acad Sci U S A* **76**, 333-337 (1979).

3. Kzhyshkowska, J., Neyen, C. & Gordon, S. Role of macrophage scavenger receptors in atherosclerosis. *Immunobiology* **217**, 492-502 (2012).

4. Dorrington, M.G. *et al.* MARCO is required for TLR2- and Nod2-mediated responses to Streptococcus pneumoniae and clearance of pneumococcal colonization in the murine nasopharynx. *Journal of immunology* **190**, 250-258 (2013).

5. Pollock, S. *et al.* Uptake and trafficking of liposomes to the endoplasmic reticulum. *Faseb J* **24**, 1866-1878 (2010).

6. Xu, S. *et al.* Apolipoproteins of HDL can directly mediate binding to the scavenger receptor SR-BI, an HDL receptor that mediates selective lipid uptake. *Journal of lipid research* **38**, 1289-1298 (1997).

7. Emi, M. *et al.* Structure, organization, and chromosomal mapping of the human macrophage scavenger receptor gene. *J Biol Chem* **268**, 2120-2125 (1993).

8. Krieger, M. & Herz, J. Structures and functions of multiligand lipoprotein receptors: macrophage scavenger receptors and LDL receptor-related protein (LRP). *Annu Rev Biochem* **63**, 601-637 (1994).

9. Elomaa, O. *et al.* Cloning of a novel bacteria-binding receptor structurally related to scavenger receptors and expressed in a subset of macrophages. *Cell* **80**, 603-609 (1995).

10. Kraal, G., van der Laan, L.J., Elomaa, O. & Tryggvason, K. The macrophage receptor MARCO. *Microbes Infect* **2**, 313-316 (2000).

11. Palecanda, A. *et al.* Role of the scavenger receptor MARCO in alveolar macrophage binding of unopsonized environmental particles. *J Exp Med* **189**, 1497-1506 (1999).

12. van der Laan, L.J. *et al.* Macrophage scavenger receptor MARCO: in vitro and in vivo regulation and involvement in the anti-bacterial host defense. *Immunol Lett* **57**, 203-208 (1997).

13. van der Laan, L.J. *et al.* Regulation and functional involvement of macrophage scavenger receptor MARCO in clearance of bacteria in vivo. *J Immunol* **162**, 939-947 (1999).

14. Granucci, F. *et al.* The scavenger receptor MARCO mediates cytoskeleton rearrangements in dendritic cells and microglia. *Blood* **102**, 2940-2947 (2003).

15. Wermeling, F. *et al.* Class A scavenger receptors regulate tolerance against apoptotic cells, and autoantibodies against these receptors are predictive of systemic lupus. *J Exp Med* **204**, 2259-2265 (2007).

16. Rogers, N.J. *et al.* A defect in Marco expression contributes to systemic lupus erythematosus development via failure to clear apoptotic cells. *J Immunol* **182**, 1982-1990 (2009).

17. Tas, S.W., Quartier, P., Botto, M. & Fossati-Jimack, L. Macrophages from patients with SLE and rheumatoid arthritis have defective adhesion in vitro, while only SLE macrophages have impaired uptake of apoptotic cells. *Ann Rheum Dis* **65**, 216-221 (2006).

18. Podack, E.R., Deyev, V. & Shiratsuchi, M. Pore formers of the immune system. *Adv Exp Med Biol* **598**, 325-341 (2007).

19. Bowdish, D.M. *et al.* Genetic variants of MARCO are associated with susceptibility to pulmonary tuberculosis in a Gambian population. *BMC Med Genet* **14**, 47 (2013).

20. Ma, M.J. *et al.* Genetic variants in MARCO are associated with the susceptibility to pulmonary tuberculosis in Chinese Han population. *PLoS One* **6**, e24069 (2011).

21. Vergne, I., Chua, J., Singh, S.B. & Deretic, V. Cell biology of mycobacterium tuberculosis phagosome. *Annu Rev Cell Dev Biol* **20**, 367-394 (2004).

22. Bonilla, D.L. *et al.* Autophagy regulates phagocytosis by modulating the expression of scavenger receptors. *Immunity* **39**, 537-547 (2013).

23. Bowdish, D.M. *et al.* MARCO, TLR2, and CD14 are required for macrophage cytokine responses to mycobacterial trehalose dimycolate and Mycobacterium tuberculosis. *PLoS Pathog* **5**, e1000474 (2009).

24. Tobin, D.M. & Ramakrishnan, L. Comparative pathogenesis of Mycobacterium marinum and Mycobacterium tuberculosis. *Cellular microbiology* **10**, 1027-1039 (2008).

25. Parikka, M. *et al.* Mycobacterium marinum causes a latent infection that can be reactivated by gamma irradiation in adult zebrafish. *PLoS pathogens* **8**, e1002944 (2012).

26. Swaim, L.E. *et al.* Mycobacterium marinum Infection of Adult Zebrafish Causes Caseating Granulomatous Tuberculosis and Is Moderated by Adaptive Immunity. *Infection and Immunity* **74**, 6108-6117 (2006).

27. Clay, H. *et al.* Dichotomous Role of the Macrophage in Early Mycobacterium marinum Infection of the Zebrafish. *Cell Host & Microbe* **2**, 29-39 (2007).

28. Tobin, D.M. *et al.* The lta4h Locus Modulates Susceptibility to Mycobacterial Infection in Zebrafish and Humans. *Cell* **140**, 717-730 (2010).

29. van der Vaart, M., van Soest, J.J., Spaink, H.P. & Meijer, A.H. Functional analysis of a zebrafish myd88 mutant identifies key transcriptional components of the innate immune system. *Dis Model Mech* **6**, 841-854 (2013).

30. Cambier, C.J. *et al.* Mycobacteria manipulate macrophage recruitment through coordinated use of membrane lipids. *Nature* **505**, 218-222 (2014).

31. Zakrzewska, A. *et al.* Macrophage-specific gene functions in Spi1-directed innate immunity. *Blood* **116**, e1-11 (2010).

32. Wittamer, V., Bertrand, J.Y., Gutschow, P.W. & Traver, D. Characterization of the mononuclear phagocyte system in zebrafish. *Blood* **117**, 7126-7135 (2011).

33. Ellett, F., Pase, L., Hayman, J.W., Andrianopoulos, A. & Lieschke, G.J. mpeg1 promoter transgenes direct macrophage-lineage expression in zebrafish. *Blood* **117**, e49-e56 (2010).

34. Bernut, A. *et al.* Mycobacterium abscessus cording prevents phagocytosis and promotes abscess formation. *Proc Natl Acad Sci U S A* **111**, E943-952 (2014).

35. Renshaw, S.A. *et al.* A transgenic zebrafish model of neutrophilic inflammation. *Blood* **108**, 3976-3978 (2006).

36. Gray, C. *et al.* Simultaneous intravital imaging of macrophage and neutrophil behaviour during inflammation using a novel transgenic zebrafish. *Thromb Haemost* **105**, 811-819 (2011).

37. d'Alençon, C.A. *et al.* A high-throughput chemically induced inflammation assay in zebrafish. *BMC Biology* **8**, 151 (2010).

38. van der Sar, A.M. *et al.* Mycobacterium marinum Strains Can Be Divided into Two Distinct Types Based on Genetic Diversity and Virulence. *Infection and Immunity* **72**, 6306-6312 (2004).

39. van der Sar, A.M. *et al.* Zebrafish embryos as a model host for the real time analysis of Salmonella typhimurium infections. *Cellular Microbiology* **5**, 601-611 (2003).

40. Kimmel, C.B., Ballard, W.W., Kimmel, S.R., Ullmann, B. & Schilling, T.F. Stages of embryonic development of the zebrafish. *Dev Dyn* **203**, 253-310 (1995).

41. Benard, E.L. *et al.* Infection of zebrafish embryos with intracellular bacterial pathogens. *J Vis Exp* **61** pii: 3781. doi: 10.3791/3781 (2012).

42. Rougeot, J. *et al.* RNA sequencing of FACS-sorted immune cell populations from zebrafish infection models to identify cell specific responses to intracellular pathogens. *Methods in Molecular Biology* (In press).

43. Stockhammer, O.W., Zakrzewska, A., Hegedus, Z., Spaink, H.P. & Meijer, A.H. Transcriptome profiling and functional analyses of the zebrafish embryonic innate immune response to Salmonella infection. *J Immunol* **182**, 5641-5653 (2009).

44. Veneman, W.J. *et al.* A zebrafish high throughput screening system used for Staphylococcus epidermidis infection marker discovery. *BMC Genomics* **14**, 255 (2013).

45. Cui, C. *et al.* Infectious disease modeling and innate immune function in zebrafish embryos. *Methods Cell Biol* **105**, 273-308 (2011).

46. Schindelin, J. *et al.* Fiji: an open-source platform for biological-image analysis. *Nat Methods* **9**, 676-682 (2012).

47. Nezhinsky A.E., V.F.J. Efficient and Robust Shape Retrieval from Deformable Templates. *International Symposium on Leveraging Applications of Formal Methods* Part II, LNCS 7610 (T. Margaria, B. Steffen, and M. Merten (Eds.)), 42-55 (2012).

48. Elomaa, O. *et al.* Structure of the human macrophage MARCO receptor and characterization of its bacteria-binding region. *J Biol Chem* **273**, 4530-4538 (1998).

49. Kanwal, Z. *et al.* Deficiency in hematopoietic phosphatase ptpn6/Shp1 hyperactivates the innate immune system and impairs control of bacterial infections in zebrafish embryos. *J Immunol* **190**, 1631-1645 (2013).

50. Mathias, J.R. *et al.* Live imaging of chronic inflammation caused by mutation of zebrafish Hai1. *Journal of Cell Science* **120**, 3372-3383 (2007).

51. Yang, C.T. *et al.* Neutrophils exert protection in the early tuberculous granuloma by oxidative killing of mycobacteria phagocytosed from infected macrophages. *Cell Host Microbe* **12**, 301-312 (2012).

52. Colucci-Guyon, E., Tinevez, J.Y., Renshaw, S.A. & Herbomel, P. Strategies of professional phagocytes in vivo: unlike macrophages, neutrophils engulf only surface-associated microbes. *Journal of Cell Science* **124**, 3053-3059 (2011).

53. Sharif, O. *et al.* The scavenger receptor CD36 downmodulates the early inflammatory response while enhancing bacterial phagocytosis during pneumococcal pneumonia. *J Immunol* **190**, 5640-5648 (2013).

54. Benard, E.L. *et al.* The macrophage-expressed perforins Mpeg1 and Mpeg1.2 have anti-bacterial function in zebrafish. *Journal of Innate Immunity* (In press).

55. Akitake, C.M., Macurak, M., Halpern, M.E. & Goll, M.G. Transgenerational analysis of transcriptional silencing in zebrafish. *Developmental biology* **352**, 191-201 (2011).

56. Pisharath, H. & Parsons, M.J. Nitroreductase-mediated cell ablation in transgenic zebrafish embryos. *Methods Mol Biol* **546**, 133-143 (2009).

57. Davis, J.M. *et al.* Real-time visualization of mycobacterium-macrophage interactions leading to initiation of granuloma formation in zebrafish embryos. *Immunity* **17**, 693-702 (2002).

58. Hirsch, C.S., Ellner, J.J., Russell, D.G. & Rich, E.A. Complement receptor-mediated uptake and tumor necrosis factor-alpha-mediated growth inhibition of Mycobacterium tuberculosis by human alveolar macrophages. *J Immunol* **152**, 743-753 (1994).

59. Schlesinger, L.S., Bellinger-Kawahara, C.G., Payne, N.R. & Horwitz, M.A. Phagocytosis of Mycobacterium tuberculosis is mediated by human monocyte complement receptors and complement component C3. *J Immunol* **144**, 2771-2780 (1990).

60. Schlesinger, L.S. Macrophage phagocytosis of virulent but not attenuated strains of Mycobacterium tuberculosis is mediated by mannose receptors in addition to complement receptors. *J Immunol* **150**, 2920-2930 (1993).

61. Schlesinger, L.S., Hull, S.R. & Kaufman, T.M. Binding of the terminal mannosyl units of lipoarabinomannan from a virulent strain of Mycobacterium tuberculosis to human macrophages. *J Immunol* **152**, 4070-4079 (1994).

62. Schlesinger, L.S., Kaufman, T.M., Iyer, S., Hull, S.R. & Marchiando, L.K. Differences in mannose receptor-mediated uptake of lipoarabinomannan from virulent and attenuated strains of Mycobacterium tuberculosis by human macrophages. *J Immunol* **157**, 4568-4575 (1996).

63. Nakata, T. *et al.* CD14 directly binds to triacylated lipopeptides and facilitates recognition of the lipopeptides by the receptor complex of Toll-like receptors 2 and 1 without binding to the complex. *Cellular microbiology* **8**, 1899-1909 (2006).

64. Brightbill, H.D. *et al.* Host defense mechanisms triggered by microbial lipoproteins through toll-like receptors. *Science* **285**, 732-736 (1999).

65. Manukyan, M. *et al.* Binding of lipopeptide to CD14 induces physical proximity of CD14, TLR2 and TLR1. *Eur J Immunol* **35**, 911-921 (2005).

66. Iliev, D.B., Roach, J.C., Mackenzie, S., Planas, J.V. & Goetz, F.W. Endotoxin recognition: in fish or not in fish? *FEBS Lett* **579**, 6519-6528 (2005).

67. Meijer, A.H. *et al.* Expression analysis of the Toll-like receptor and TIR domain adaptor families of zebrafish. *Molecular immunology* **40**, 773-783 (2004).

68. Ribeiro, C.M., Hermsen, T., Taverne-Thiele, A.J., Savelkoul, H.F. & Wiegertjes, G.F. Evolution of recognition of ligands from Gram-positive bacteria: similarities and differences in the TLR2-mediated response between mammalian vertebrates and teleost fish. *Journal of immunology* **184**, 2355-2368 (2010).

69. Chen, Y. *et al.* A regulatory role for macrophage class A scavenger receptors in TLR4-mediated LPS responses. *Eur J Immunol* **40**, 1451-1460 (2010).

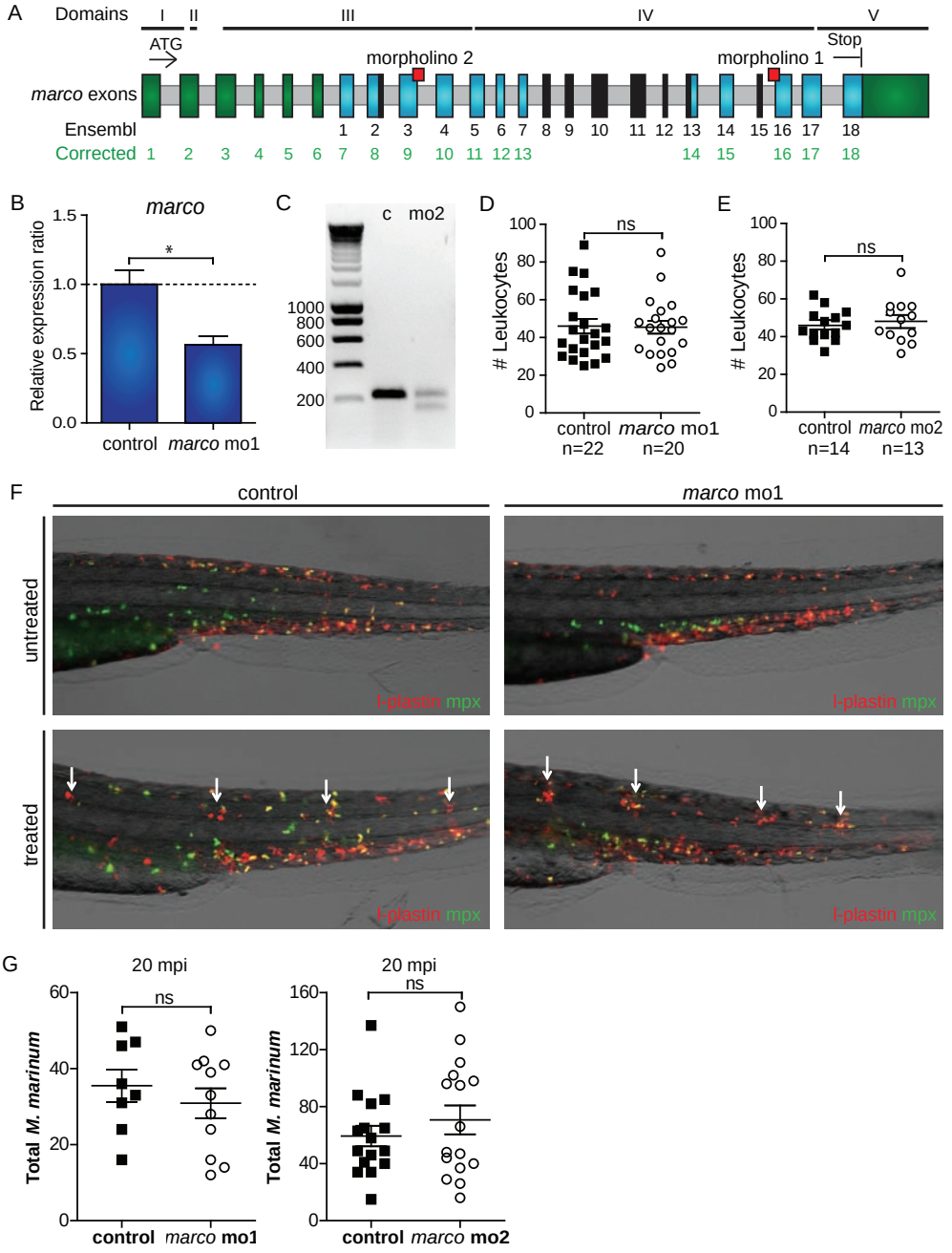

Supplementary figure 1. Validation of morpholino knockdown. (A) Corrected annotation of *marco* exons. The sequenced cDNA clone of *marco* shows that there are 6 additional exons (shown in green) prior to exon 1 in the current annotation in Ensembl (Zv9, ENSDARG00000059294), which was based on a predicted gene, LOC571584. Furthermore, the cDNA shows partial absence of Ensembl exons 2 and 13 and complete absence of exons 8 – 12 and 15 (shown in black), and an extended final exon (shown in green). Exons that are not different between the

Supplementary figure 1 continued: Ensembl annotation and the corrected annotation are shown in blue and introns are shown in grey. Exon-intron boundary sites targeted by morpholinos (red squares), the ATG and stop codon sites, and the conserved protein domains (I to V corresponding with fig. 1) are indicated. (B-C) Knockdown of *marco*. The predicted effect of splice blocking morpholinos 1 is deletion of exon 16 in the collagenous domain and the predicted effect of morpholino 2 is deletion of exon 9 in the spacer domain. The exon deletion effect of morpholino 1 could not be confirmed by RT-PCR, but qPCR analysis (28 hpf) demonstrated that the *marco* mRNA level was effectively reduced (B). Deletion of exon 9 following knockdown of *marco* with morpholino 2 was confirmed by RT-PCR (C) using RNA from embryos injected with *marco* morpholino 2 (mo2) or control morpholino (c). The expected RT-PCR product size for the control embryos is 228 bp and for *marco* mo2 morphants is 143 bp. (D-E) Normal leukocyte numbers in *marco* morphants. *marco* (D) morpholino 1 and (E) morpholino 2 morphants and control embryos were fixed at 30 hpf and were immuno-labelled with Ab against the general leukocyte marker L-plastin. Leukocyte numbers were counted blinded over the Duct of Cuvier, (ns = not significant). (F) Marco does not affect migration of leukocytes towards local inflammation sites. Representative images of copper sulphate treated control and *marco* morphant 3 dpf embryos. Embryos were immuno-labelled with Ab against the general leukocyte marker L-plastin (red signal) in combination with a neutrophil-specific Mpx TSA-staining (green signal) at 3 dpf. White arrows indicate accumulation of leukocytes at the local inflammation sites at the neuromasts. (G) Total number of *M. marinum* counted over Duct of Cuvier at 20 mpi for *marco* mo1 and mo2 morphants.

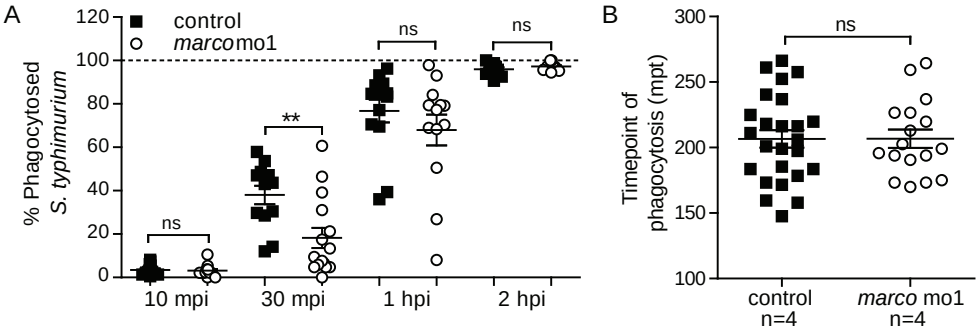

Supplementary figure 2. *marco* knockdown affects phagocytosis of *S. typhimurium* but not phagocytosis of dead cells. (A) An injected dose of 180 cfu of Ds-Red labelled *S. typhimurium* SL1027 is completely phagocytosed in wild type embryos at 2 hpi and *marco* knockdown leads to a delay in phagocytosis at 30 mpi. Each data point represents the percentage of phagocytosed *S. typhimurium* in an individual embryo and the mean ± SEM is indicated. (B) Phagocytosis of dead cells by healthy macrophages was not affected by knockdown of *marco.* Phagocytosis events of chemically ablated macrophages by healthy macrophages were quantified from time lapse movies of 4 embryos per group (representative images in fig. 3). Each data point represents a single phagocytosis event and the mean ± SEM is indicated.

Supplementary table 1. Zebrafish Marco homology compared to murine and human MARCO

A Protein homology

Identical / Similar	z-Marco	m-MARCO	h-MARCO
z-Marco	**100**	35	32
m-MARCO	62	**100**	66
h-MARCO	64	84	**100**

B Cysteine-rich domain V homology

Identical / Similar	z-Marco	m-MARCO	h-MARCO
z-Marco	**100**	52	50
m-MARCO	84	**100**	70
h-MARCO	86	90	**100**

***** Homology for (A) whole protein sequences and (B) Cysteine-rich domain V was determined between zebrafish Marco (z-Marco), murine MARCO (m-MARCO) and human MARCO (h-MARCO).

Supplementary table 2. Comparison of expression levels of selected infection inducible genes

			control uninf vs control inf		marco inf vs control inf	
Ensembl ID	**Description**	**Gene name**	**fold change**	**Adj P-value**	**fold change**	**Adj P-value**
ENSDARG00000059741	alpha-kinase 1	*alpk1*	2.8	0.00	0.9	1
ENSDARG00000007823	activating transcription factor 3	*atf3*	2.6	0.04	0.9	1
ENSDARG00000057121	complement component 7	*c7 (2 of 2)*	3.5	6.1E-05	0.6	0.38
ENSDARG00000086869	three-finger protein 5 (LOC100003647 precursor)	*cabz01040055.1*	16.0	3.2E-17	1.7	0.38
ENSDARG00000038025	chromobox homolog 7a	*cbx7a*	2.6	0.00	1.1	1
ENSDARG00000086654	Uncharacterized protein	*ct027762.4*	50.1	2.3E-21	0.8	1
ENSDARG00000075045	chemokine (C-X-C motif) ligand c1c	*cxcl-c1c*	16.8	8.9E-08	1.7	0.88
ENSDARG00000026039	cytochrome P450, family 1, subfamily A	*cyp1a*	13.3	2.1E-22	0.4	0.01
ENSDARG00000070420	cytochrome P450, family 24, subfamily A, polypeptide 1	*cyp24a1*	4.3	2.3E-07	0.4	0.01
ENSDARG00000092858	non-coding RNA	*fd36h06*	4.7	5.5E-06	1.3	1
ENSDARG00000053227	hepcidin antimicrobial peptide 2	*hamp2*	40.5	2.7E-13	1.2	1
ENSDARG00000027529	heme oxygenase (decycling) 1	*hmox1*	4.6	3.1E-07	0.2	1.6E-09
ENSDARG00000051912	hemopexin	*hpx (1 of 2)*	18.8	1.9E-30	1.0	1
ENSDARG00000093303	interferon induced transmembrane protein 10	*ifitm10*	2.3	0.09	1.7	0.49
ENSDARG00000014947	insulin-like growth factor binding protein 1a	*igfbp1a*	3.1	0.00	1.0	1
ENSDARG00000005419	interleukin 1, beta	*il1b*	10.5	0.00	1.3	1
ENSDARG00000053131	interleukin-1 receptor-associated kinase 3	*irak3*	26.9	2.9E-08	1.3	1
ENSDARG00000003523	intelectin 3	*itln3*	19.7	5.6E-26	0.6	0.60
ENSDARG00000033227	leukocyte cell-derived chemotaxin 2 like	*lect2l*	11.1	2.2E-22	1.2	1
ENSDARG00000090557	microfibrillar-associated protein 4	*mfap4 (6 of 13)*	62.8	5.6E-26	0.7	1
ENSDARG00000012395	matrix metalloproteinase 13a	*mmp13a*	6.3	5.5E-06	2.0	0.09
ENSDARG00000042816	matrix metalloproteinase 9	*mmp9*	19.4	1.4E-28	2.1	0.02
ENSDARG00000031136	monooxygenase, DBH-like 1	*moxd1*	5.1	0.00	2.6	0.00
ENSDARG00000074322	olfactomedin 4	*olfn4 (3 of 8)*	6.1	6.1E-06	0.3	0.01
ENSDARG00000016188	strawberry notch homolog 2 (Drosophila)	*sbno2 (2 of 3)*	2.2	0.04	1.1	1
ENSDARG00000092826	non-coding RNA	*si:ch211-243g18.3*	0.9	1	19.2	0.06
ENSDARG00000090352	non-coding RNA	*si:dkey-97i18.5*	34.9	1.4E-39	1.5	1
ENSDARG00000059805	solute carrier family 25, member 38a	*slc25a38a*	3.8	0.08	0.6	1
ENSDARG00000055252	synaptosomal-associated protein, 23kDa	*snap23 (2 of 2)*	4.2	0.01	1.5	1
ENSDARG00000055901	steap family member 4	*steap4*	2.7	0.00	2.0	0.03
ENSDARG00000007344	titin-cap (telethonin)	*tcap*	4.0	2.6E-06	2.2	0.01
ENSDARG00000075261	tissue inhibitor of metalloproteinase 2b	*timp2b*	3.5	3.8E-05	2.3	0.00

* All genes differentially regulated in *marco* infected morphants compared to infected control embryos (adjusted P-value <0.1) showed no significant change in uninfected *marco* morphants compared to uninfected control embryos with exception of *steap4* (fold change 2.1, adjusted P-value 0.04).

Chapter 6

The macrophage-expressed perforins Mpeg1 and Mpeg1.2 have anti-bacterial function in zebrafish

Erica L. Benard[1], Peter I. Racz[1], Julien Rougeot[1], Alexander E. Nezhinsky[2], Fons J. Verbeek[2], Herman P. Spaink[1], Annemarie H. Meijer[1]

[1]Institute of Biology Leiden, Leiden University
[2]Leiden Institute for Advanced Computer Science, Leiden University

Journal of Innate Immunity, In press

Abstract

Macrophage expressed gene 1 (*MPEG1*) encodes an evolutionary conserved protein with a predicted Membrane Attack Complex/Perforin domain associated with host defence against invading pathogens. In vertebrates, MPEG1/Perforin-2 is an integral membrane protein of macrophages, suspected to be involved in killing of intracellular bacteria by pore-forming activity. Zebrafish have three copies of *MPEG1*, two of which are expressed in macrophages, whereas the third could be a pseudogene. The *mpeg1* and *mpeg1.2* genes show differential regulation during infection of zebrafish embryos with the bacterial pathogens, *Mycobacterium marinum* and *Salmonella typhimurium*. While *mpeg1* is down-regulated during infection with both pathogens, *mpeg1.2* is infection inducible. Up-regulation of *mpeg1.2* is partially dependent on the presence of functional Mpeg1, and requires the Toll-like receptor adaptor molecule MyD88 and transcription factor NFκB. Knockdown of *mpeg1* alters the immune response to *M. marinum* infection and results in increased bacterial burden. In *S. typhimurium* infection, both *mpeg1* and *mpeg1.2* knockdown increase bacterial burdens, but *mpeg1* morphants show increased survival time. The combined results of these two *in vivo* infection models support the anti-bacterial function of the MPEG1/Perforin-2 family and indicate that the intricate cross-regulation of the two *mpeg1* copies aids the zebrafish host in combatting infection of various pathogens.

Introduction

Membrane Attack Complex/Perforin (MACPF) proteins belong to a large superfamily of pore forming molecules present in almost all living organisms [1, 2]. In vertebrates, MACPF proteins perform crucial roles in immune defence against both extracellular and intracellular infections [3, 4]. The MACPF domain is present in the components of the terminal complement pathway (C6, C7, C8, and C9), which form the membrane attack complex (MAC) targeting gram-negative bacteria and certain pathogenic parasites directly by forming pores on their cell membranes [1]. The MACPF domain is also present in the perforins released by cytotoxic T lymphocytes and natural killer cells, which create pores in the plasma membranes of infected and transformed host cells, allowing the entry of cytolytic proteins [4].

In addition to the complement proteins and the perforins, there is another MACPF domain-containing membrane protein involved in the immune system, named Macrophage expressed gene 1 (MPEG1) or Perforin-2 [3]. *MPEG1* was first identified as a macrophage-specific gene in human and mice, but how it contributes mechanistically to macrophage defence remains to be elucidated [3, 5]. Homologs of *MPEG1* are found in marine metazoans, such as the sea sponge [6], the pacific oyster [7], and abalone shellfish [8], and evolutionary reconstruction suggests that an ancestral *MPEG1* gene gave rise to the vertebrate perforin genes [9]. Expression of *MPEG1* homologs in the invertebrates is up-

regulated by viral and bacterial infections or by exposure to bacterial lipopolysaccharide (LPS) [6-8]. Furthermore, recombinant sea sponge Mpeg has been shown to inhibit bacterial growth *in vitro* [6]. In mice, *Mpeg1* (also named *Perforin-2*) is up-regulated during prion infection and its expression could be induced in primary mouse embryonic fibroblasts by several types of bacterial infections [10, 11]. Mouse embryonic fibroblasts rapidly induce expression of *Mpeg1* in response to infection with *Mycobacterium smegmatis*, and these fibroblasts lose their ability to kill this non-pathogenic mycobacterium species when *Mpeg1* is knocked down with siRNA [11]. Furthermore, this study showed that *M. smegmatis* bacteria are sensitive to the bacteriolytic activity of lysozyme when they are recovered from *Mpeg1*-expressing fibroblasts but not when they are recovered from *Mpeg1*-deficient cells, suggesting physical attack of the bacterial membrane by the MACPF domain of Mpeg1 [11]. It has also been shown that Mpeg1 restricts growth of *Chlamydia trachomatis* in macrophages, while studies in HeLa cells suggest that chlamydiae are protected from Mpeg1-mediated killing in epithelial cells by prevention of *Mpeg1* transcription [12]. Following ectopic expression of *Mpeg1* in HeLa cells, the protein concentrated around the chlamydia-containing vacuoles and inhibited chlamydial growth. It has been proposed that the MACPF domain of Mpeg1 is oriented inside membrane vesicles and that upon bacterial infection these vesicles traffic and fuse with bacteria-containing endosomes to mediate bacterial killing by pore formation[3].

The zebrafish genome contains an *mpeg1* gene that like its human and murine counterpart is expressed by macrophages and encodes a protein with the conserved MACPF domain as well as the characteristic transmembrane region [13, 14]. There are several advantages for using zebrafish as a model to study host-pathogen interactions. Firstly, the free-living zebrafish embryos and early larval stages are optically transparent and *in vivo* visualization of infectious disease processes is facilitated by various transgenic lines, including reporter lines using the *mpeg1* promoter to drive fluorescent protein expression in macrophages [14]. Secondly, genetic approaches are easily applicable, such as the efficient inactivation of gene functions achieved by injection of antisense morpholino oligonucleotides. Thirdly, it is possible to study the innate immune response in the absence of an adaptive immune contribution. Already at 1 day post fertilisation (dpf) the innate immune system of the zebrafish embryo is capable of defence against microbial infections [15], while the adaptive immune system does not mature before three weeks of age [16]. Differentiated myeloid cells of the innate immune system are able to phagocytose apoptotic cell corpses [15] and adhere and phagocytose bacteria injected into the blood [15, 17, 18]. These properties led to the development of zebrafish infection models for a wide variety of pathogens [19].

In this study, we used well-established zebrafish embryo models for *Mycobacterium marinum* and *Salmonella enterica* serovar Typhimurium (*S. typhimurium*) infections to investigate the function of *mpeg1* and one of its paralogues named *mpeg1.2*. We show that these two MPEG1 homologues are differentially regulated during infection and provide *in vivo* evidence for the function of both genes in anti-bacterial defence.

Materials and methods

Zebrafish lines and handling of embryos

Zebrafish were handled in compliance with the local animal welfare regulations and were maintained according to standard protocols (zfin.org). The culture was approved by the local animal welfare committee (DEC) of the University of Leiden and all protocols adhered to the international guidelines specified by the EU Animal Protection Directive 2010/63/EU. Adult zebrafish were not sacrificed for this study. All experiments in this study were performed on embryos/larvae before the free-feeding stage and did not fall under animal experimentation law according to the EU Animal Protection Directive 2010/63/EU. Zebrafish lines used in this study included AB/TL, *myd88*^{hu3568} [20], *Tg(mpx:gfp)*^{i114} [21], *Tg(mpeg1:EGFP)*^{gl22} [14], and *Tg(mpeg1:mCherry-F)*^{UMSF001} [22]. Embryos were grown at 28.5-30°C in egg water (60 µg/ml Instant Ocean sea salts). For the duration of bacterial injections and imaging, embryos were kept under anaesthesia in egg water containing 200 µg/ml tricaine (Sigma-Aldrich). Embryos used for stereo fluorescence imaging were kept in egg water containing 0.003% 1-phenyl-2-thiourea (Sigma-Aldrich) to prevent melanisation.

Morpholino knockdown

Morpholino oligonucleotides (Gene Tools) were diluted to the desired concentration in 1x Danieau buffer (58 mM NaCl, 0.7 mM KCl, 0.4 mM $MgSO_4$, 0.6 mM $Ca(NO_3)_2$, 5.0 mM HEPES; pH 7.6) containing 1% phenol red (Sigma-Aldrich) and 1 ηL was injected into the yolk at the 1-2 cell stage using a Femtojet injector (Eppendorf). For knockdown of *mpeg1* or *mpeg1.2*, two morpholinos each were used, one targeting the exon 1-intron 1 splice junction (*mpeg1* Mo1: 5'ATTTTGTACTTACTTGAACCCGTGC3', 0.3 mM; *mpeg 1.2* Mo1: 5'ACTTTTCTGTCTTACCTGAACTCGT3', 0.1 mM), and the other targeting the intron 1-exon 2 splice junction (*mpeg1* Mo2: 5'GGTTACGGACCTGAGAAACAAATTT3', 0.1 mM; *mpeg 1.2* Mo2: 5'TGCGTACCTGAGAAGATAACACAAA3', 0.1 mM). For knockdown of *ptpn6* the splice junction morpholino 1 (*ptpn6* Mo1: 5'ACTCATTCCTTACCCGATGCGGAGC3') was used as described previously [23]. As a control, the standard control morpholino from Gene Tools was used at the same concentrations as the other morpholinos.

Chemical treatments

NFκB activation inhibitor (NAI, 50 nM, 4 hours total treatment, including 2 hours pre-treatment, Calbiochem, #481406) and copper sulphate ($CuSO_4$, 10 uM, 2 hours treatment) Merck, #1027910250) [24] were administered via the egg water. After copper sulphate treatment the embryos were briefly washed three times with egg water and fixed in 4% paraformaldehyde in PBS.

Infection experiments

Mycobacterium marinum infections were performed using the Mma20 strain expressing mCherry in a pSMT3 vector [25] or the M strain expressing GFP in a pMSP12 vector [26]. *M. marinum* was heat-killed by incubation in 80°C for 20 min and plated during injections to control for bacterial growth. *S. typhimurium* infections were performed using the *S. typhimurium* strain SL1027 and its isogenic LPS Ra mutant derivative SF1592, carrying the DsRed expression vector pGMDs3 [18], and *Staphylococcus epidermidis* infections were performed using strain O-47 [27]. Embryos were staged at 24 hpf by morphological criteria and manually dechorionated. Bacteria were prepared and injected into the blood circulation at 28 hpf, and PBS or 2% PVP was injected as a control [28]. The same conditions were used for injection of 1 nl of LPS from *S. typhimurium* dissolved in PBS (10 µg/ml, Sigma, #L6511). For *S. typhimurium* plating assays, groups of 5 infected embryos (150 cfu) were homogenised using a Bullet blender (Next advance) for 3 minutes, speed 4 with 5 1.0 mm Zirconium Oxide beads, density is 5.5g/cc and a dilutions series was plated at 1 and 16 hpi.

Fluorescence-activated cell sorting

Macrophages and neutrophils were isolated by FACS from 6 dpf *Tg(mpeg1:mCherry-F)*^{UMSF001} [22] and *Tg*(*mpx*:*egfp*)^{i114} [21] zebrafish larvae, respectively, and the RNA was extracted as described [13].

RNA isolation, cDNA synthesis, and expression analyses

Whole embryo RNA isolation, removal of residual genomic DNA, cDNA synthesis and quantitative RT-PCR (qPCR) analysis was performed as described in [29]. qPCR results were analysed using the ΔΔCt method. All reactions were performed as technical duplicates and data were normalised to the expression of peptidylprolyl isomerase A like (*ppial*) for whole embryo samples and to (*eif4*) for cells isolated by FACS. Primer sequences for *ppial* and *mpeg1* are described in [13], primer sequences for *mmp9* and *il1b* are described in [29], primer sequences for *mpeg1.2* were: FW: 5'TCAGGCCAATGTGAACGACA3'; REV: 5'GGTGACTCAGGAGTGCATGT3', and primer sequences for *eif4a1b* were: FW: 5'TTCAGAAACTCAGTACTAGCATACA3'; REV: 5'GTGACATCCAACACCTCTGC3'. Knockdown of mpeg1 with both morpholinos was verified by qPCR and to validate the knockdown of *mpeg1.2* with both morpholinos, the SuperScript® One-Step RT-PCR System (Invitrogen, #10928-034) was used with 50ng DNAse treated RNA template. RT-PCR primers for *mpeg1.2* Mo1 knockdown verification were FW: 5'CTGCGCAATTTAGACGTGGG3'; REV: 5'GACGTGTCGTTCACATTGGC3', and for Mo2 were FW: as Mo1 primer; REV: 5'TTAATGCCTGCGGATGCAGA3'. The following adjustments were made to the PCR settings: 59.4°C for 30 seconds for the annealing step of the PCR amplification with 40 cycles.

RNA for deep sequencing analysis was isolated using QIAzol lysis reagent and purified

using the Rneasy MinElute Cleanup kit (QIAGEN Benelux B.V., Venlo, Netherlands). RNA sequencing was performed as previously described [27]. Gene Expression Omnibus (GEO) database accession for RNASeq: GSE49188 and GSE54885.

Immunohistochemistry and enzyme histochemistry

For simultaneous identification of *S. typhimurium*, neutrophils and macrophages a combination of immuno-labelling and enzymatic staining was used. First a neutrophil specific staining for myeloperoxidase (mpx) activity was performed. This was achieved by fixing embryos in 4% PFA in 4 °C overnight, washing three times briefly in PBSTx (PBS with 0.05% Triton X100 (Sigma Aldrich)), washing briefly in amp diluent from the TSA Plus Fluorescein System kit (Perkin Elmer) and incubating in 1:50 of Fluorescein in amp diluent at 28 °C for 10 minutes. The embryos were then washed again three times in PBSTx and fixed in 4% PFA for 20 minutes at room temperature. Next, the embryos were immuno-labelled with an anti-*Salmonella* polyclonal antibody with an Alexa 568-conjugated secondary antibody as described [30]. Finally, total leukocytes were immuno-labelled with an L-plastin antibody and Alexa 633-conjugated secondary antibody [31]. Macrophages were identified as L-plastin-positive, mpx-negative cells.

Image analysis

Fluorescence images were taken with a Leica MZ16FA stereo fluorescence microscope equipped with a DFC420C digital colour camera. In *M. marinum* infection experiments, bacterial pixel counts were obtained with stereo fluorescence images and analysed using dedicated pixel quantification software [32]. Each image contains two channels: bright field and fluorescence. Image recognition software identifies the location of each embryo (each image can contain up to 3 embryos) and links the outline and orientation per embryo in the bright field channel to the fluorescence channel. Each fluorescent pixel is quantified and allocated to a location in the embryo (background is determined by a non-infected control) and the software provides the value of total amount of fluorescent pixels per embryo. This is done for all groups of embryos and the results are written to a comma-separated file for statistical analysis. Leukocyte counts were performed on a Zeiss AxioObserver confocal microscope with an EC PlnN 10x 0.3 NA objective and all other confocal images were taken on a Leica TCS SPE with HCX APO 40x 0.8 NA objective. Maximum intensity projections of merged channel confocal images were made in Fiji.

Statistical Analysis

Data (mean ± SEM) were analysed (Prism 5.0, GraphPad Software, San Diego, CA) using unpaired, two-tailed t-tests for comparisons between two groups and one-way ANOVA with Tukey's Multiple Comparison method as a post-hoc test for other data (*, $p<0.05$; **, $p<0.01$; ***, $p<0.001$). Statistical significance in survival curves was determined by a logrank test.

Results

The zebrafish genome contains a conserved family of *mpeg1* genes

The zebrafish *mpeg1* gene (Chromosome 8: ENSDARG00000055290) was previously described as a macrophage-specific marker [13 14]. Inspection of the zebrafish reference genome sequence showed that two paralogues of the *mpeg1* gene are present on the same chromosome (fig. 1A). In consultation with the zebrafish nomenclature committee (ZFIN) the three *mpeg1* genes have been named *mpeg1.1* (hereafter referred to as *mpeg1* for consistency with previous publications and nomenclature of derived transgenic lines), *mpeg1.2* (Chromosome 8: ENSDARG00000043093), and *mpeg1.3* (Chromosome 8: ENSDARG00000078569). All three of the predicted Mpeg1 proteins contain conserved regions also found in mouse and human MPEG1, including a signal peptide, a Membrane Attack Complex/Perforin (MACPF) domain, and a transmembrane region (fig. 1B). Amino acid alignment of Mpeg1 and Mpeg1.2 reveals that these domains are located in the same positions (supplementary fig. 1). The three zebrafish Mpeg1 isoforms show around 80-90% amino acid similarity (with ca. 60-70% identity) among each other and their similarity with murine and human MPEG1 (overall and within the MACPF domain) is around 70-80% (with between 43 and 50% identity) (supplementary table 1A, B).

The *mpeg1* promoter region has been successfully used to drive macrophage-specific expression in zebrafish transgenic reporter lines [14, 22]. We determined RNAseq profiles of macrophages isolated from 5 day old *Tg(mpeg1:mCherry-F)*^{UMSF001} zebrafish larvae by FACS and found expression of both *mpeg1* and *mpeg1.2* to be enriched in the fluorescent macrophage cell fraction compared to the fluorescent-negative background (data not shown). The macrophage-specific expression of these two genes was confirmed by qPCR analysis on the same cell fractions and their expression was not enriched in neutrophils sorted from *Tg*(*mpx*:*egfp*)^{i114} [21] transgenic larvae (fig. 1C+D). Expression of *mpeg1.3* was not observed in any of our RNAseq deep sequencing data sets of larval leukocyte populations or of different bacterial infection experiments in various embryonic, larval and adult stages, and it is well possible that this is a pseudogene. Therefore, we focussed this study on *mpeg1* and *mpeg1.2*.

Mpeg1 expressing macrophages participate in the formation of granuloma-like structures

The development of the *mpeg1*-driven transgenic lines has opened a new window of opportunity for detailed visualisation of host-pathogen interactions. We have previously shown that *mpeg1*-expressing macrophages are capable of phagocytosing both *S. typhimurium* and *M. marinum* bacteria [28]. The hallmark of infection with pathogenic mycobacteria is the clustering of infected macrophages into granuloma-like aggregates [17]. We used the *Tg(mpeg1:mCherry-F)*^{UMSF001} line to study the behaviour

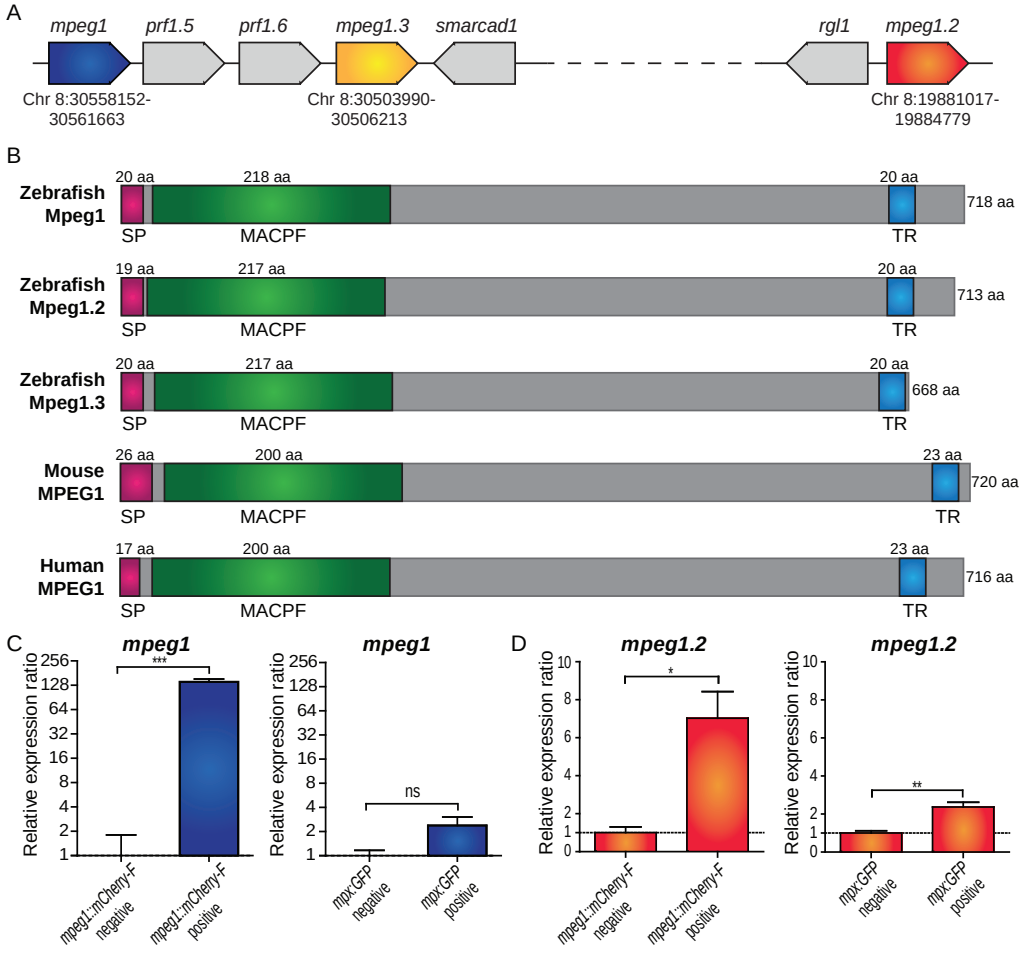

Figure 1. Zebrafish *mpeg1* genes encode proteins with conserved transmembrane and Membrane Attack Complex/Perforin domains and are expressed in macrophages. (A) Schematic representation of the region containing the genes *mpeg1*, *mpeg1.2* and *mpeg1.3* on zebrafish chromosome 8 (Chr 8). Coding direction of the genes is indicated by the pointed end and the exact location is indicated in digits below the gene. (B) Comparison of the predicted Mpeg1, Mpeg1.2, and Mpeg1.3 protein structures with murine and human MPEG1. The Signal Peptide (SP), Membrane Attack Complex/Perforin (MACPF), and Transmembrane Region (TR) are conserved domains detected by SMART analysis. (C-D) Expression of zebrafish *mpeg1* and *mpeg1.2* in (C) macrophages and (D) neutrophils. qPCR analysis was performed on RNA from fluorescence-positive cell fractions obtained by cell sorting of 6 dpf larvae of transgenic reporter lines for macrophages (mpeg1: *Tg(mpeg1:mCherry-F)*) and neutrophils (mpx: *Tg(mpx:EGFP)*). Expression was compared against the fluorescence-negative cell fraction of each transgenic line. Graphs show data combined of three biological replicates ((C) log2 scale).

of *mpeg1*-expressing macrophages during infection with GFP-expressing *M. marinum*. Imaging the same site of infection over a 0-5 days post infection (dpi) time course clearly showed that *mpeg1*-positive macrophages contribute to the formation of the tight granuloma-like structure (fig. 2). At 8 hours post infection (hpi) the majority of phagocytosed *M. marinum* bacteria were contained within *mpeg1*-positive cells. By 3 dpi *mpeg1*-positive infected cells had formed a compact centre of a growing granuloma-like aggregate, to which many uninfected *mpeg1*-macrophages were attracted. The *M. marinum*-containing *mpeg1*-positive cells showed a rounded morphology at this stage, while *mpeg1*-positive cells attracted to the border of granulomas showed a branched morphology similar to that of *mpeg1*-positive cells in uninfected embryos. At 4 dpi the granuloma structures had become more compact. At 5 dpi, cording of *M. marinum* was observed in granulomas indicative of extracellular growth, while less mCherry-fluorescent macrophages were present compared to 4 dpi, consistent with the occurrence of infected macrophage cell death at this stage [33]. The remaining mCherry-fluorescent cells all showed a rounded morphology, markedly different from the extensively branched morphology of mCherry-fluorescent macrophages in uninfected embryos (fig. 2A). While these data do not exclude the possible presence of other macrophage subpopulations, it shows that the majority of macrophages contributing to granuloma formation can be traced using the *mpeg1* marker.

Opposite regulation of *mpeg1* and *mpeg1.2* during infection

Analysis of the *Tg(mpeg1:mCherry-F)*^{UMSF001} reporter line indicated that the *mpeg1* promoter version driving the expression of mCherry in this transgenic line is active over the entire time course of *M. marinum* infection, from the 1 day old embryo up to the larval stage. However, in *S. typhimurium* infection of embryos we had previously observed that *mpeg1* expression is down-regulated [23, 29]. These observations prompted us to further investigate the regulation of *mpeg1* expression during different infections and compare this with the expression of the closely related *mpeg1.2* gene. First, we examined *mpeg1* and *mpeg1.2* expression by qPCR during a time course of *M. marinum* infection ranging from 2 hpi up to 5 dpi (fig. 3A). Within several hours after the intravenous injection of *M. marinum,* the expression level of *mpeg1* declined as compared to the mock-injected controls and this resulted in a significant down-regulation of approximately 3-fold at 8 hpi (fig. 3B). A similar trend, although not significant, was observed at 8 hpi in embryos infected with the attenuated *M. marinum* ΔRD1 strain (supplementary fig. 2A) as well as in embryos infected with heat-killed *M. marinum* (supplementary fig. 2B). This indicates that the *mpeg1* down-regulation response results from the presence of *M. marinum* and is independent of the virulence or viability of the bacteria. Between 1 to 3 dpi, the level of expression returned to control levels, but at 4 dpi a minor but significant down-regulation was observed again (fig. 3C). In contrast, expression of *mpeg1.2* was unaffected up to 3 dpi and was significantly up-regulated at 4 and 5 dpi (fig. 3C).

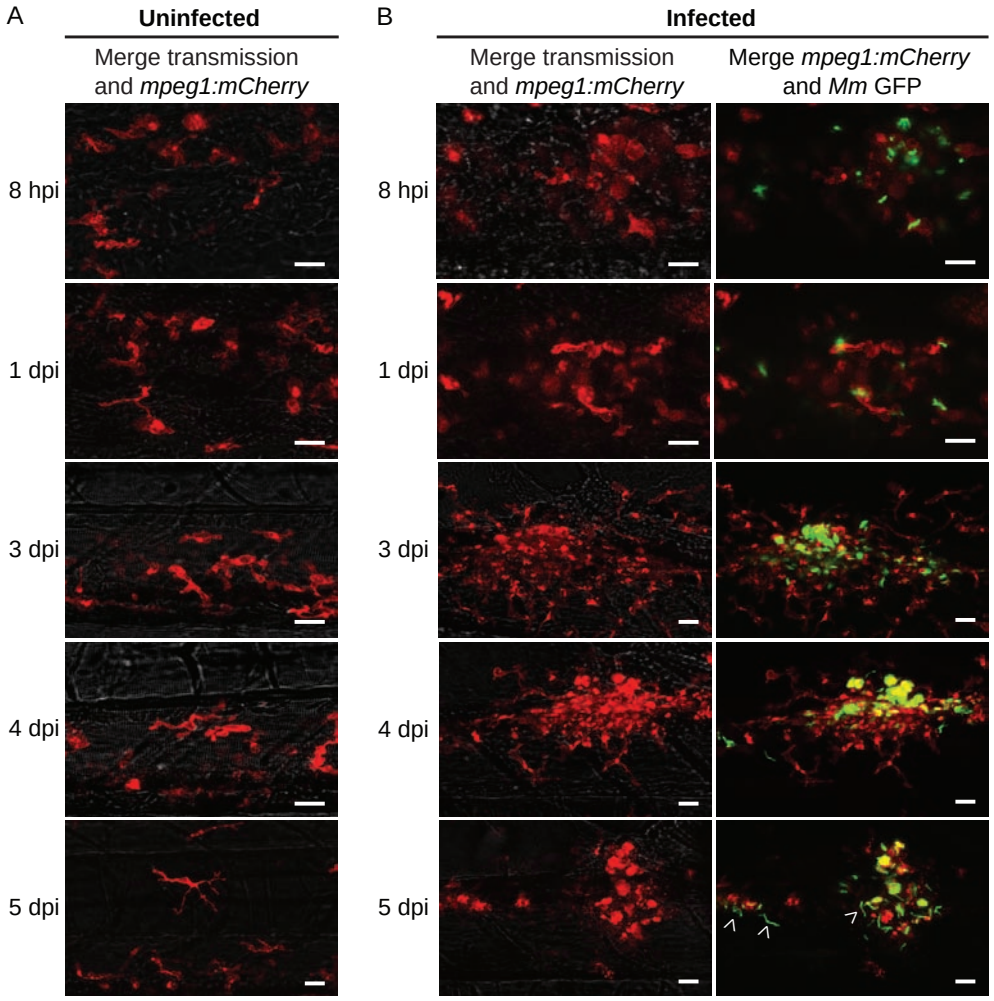

Figure 2. Tg(*mpeg1*)-positive macrophages are involved in formation of *M. marinum* granuloma-like aggregates. GFP-expressing *M. marinum* M-strain (150 cfu) bacterial infection in *Tg(mpeg1:mCherry-F)* zebrafish embryos. Confocal z-stack projections showing identical locations in the posterior region of the caudal haematopoietic tissue in (A) an uninfected embryo and (B) an infected embryo developing a granuloma-like aggregate (same infection site followed over time). Images were taken at 8 hours post injection (hpi), 1 dpi, 2 dpi (not shown), 3 dpi, 4 dpi and 5 dpi. Arrowheads indicate cording of *M. marinum*. Scale bar: 20 µm.

Next, we investigated if *mpeg1* and *mpeg1.2* were also differentially regulated during *S. typhimurium* infection. Intravenous *S. typhimurium* infection in zebrafish embryos is acute and lethal within one day [18]. We have previously reported a robust induction of pro-inflammatory gene expression at 8 hpi [23, 29] and therefore investigated *mpeg1* and *mpeg1.2* expression at this time point. While *mpeg1* showed approximately 4-fold down-regulation, *mpeg1.2* was up-regulated more than 10-fold (fig. 3D). The uninfected and *S. typhimurium* infected embryos at 8 hpi contained similar numbers

of macrophages (uninfected 54 ± 4.5 s.e.m., n=16 embryos; infected 51 ± 3.6 s.e.m., n = 15 embryos). Furthermore, as previously shown, expression of other markers for zebrafish embryonic macrophages, including *csf1r*, *cxcr3.2*, and *mfap4*, is unchanged at this time point of infection, indicating the specificity of the alterations in *mpeg1* and *mpeg1.2* expression [23]. Infection with an attenuated lipopolysaccharide (LPS) mutant of *S. typhimurium* (Ra) [18] also led to significant down-regulation of *mpeg1*, but *mpeg1.2* showed only a slight and non-significant up-regulation (supplementary fig. 2C). We also observed down-regulation of *mpeg1* and up-regulation of *mpeg1.2* in infection models for *Staphylococcus epidermidis* (supplementary fig. 2D-E), indicating that the differential regulation of these genes is a more general phenomenon in response to bacterial infections.

The opposite regulation of *mpeg1* and *mpeg1.2* raised the question if these two genes might influence each other's expression levels. To address this question we used the *S. typhimurium* infection model and knocked down *mpeg1* or *mpeg1.2* by injecting morpholinos specific for each gene (supplementary fig. 3A-D). When *mpeg1* was knocked down, the expression of *mpeg1.2* was up-regulated to a lower extent than in the control infected group (fig. 3E). In contrast, when *mpeg1.2* was knocked down the down-regulation of *mpeg1* was unchanged during *S. typhimurium* infection (fig. 3F). Since the *mpeg1* morpholino sequence did not overlap with the sequence of *mpeg1.2*, the *mpeg1* knockdown effect on *mpeg1.2* gene expression is unlikely to be due to a cross-reaction between the *mpeg1* morpholino and the *mpeg1.2* mRNA. Furthermore, we excluded that morpholino treatments might have affected macrophage or neutrophil numbers (supplementary fig. 3E). Therefore, our results suggest that the infection-dependent up-regulation of *mpeg1.2* is partially dependent on the presence of a functional Mpeg1.

The innate immune response is initiated by detection of microbes through pattern recognition receptors, including Toll-like receptors (TLRs), which signal via both Myd88-dependent and Myd88-independent pathways [34]. Our previous analysis of a Myd88-deficient zebrafish mutant showed that a major part of the innate immune response of zebrafish embryos to bacterial infections is dependent on this central TLR signalling adaptor [20]. To determine whether the regulation of *mpeg1* and *mpeg1.2* in response to infection is Myd88–dependent, we injected *S. typhimurium* into *myd88* mutants and their wildtype siblings. Down-regulation of *mpeg1* at 8 hpi was observed in *myd88* mutants similar to the wild type (fig. 4A). In contrast, *mpeg1.2* up-regulation was reduced to approximately 30% of the level observed for wild type infected embryos (fig. 4B). The TLR ligand LPS was sufficient to induce *mpeg1.2* up-regulation (fig. 4C), but did not lead to *mpeg1* down-regulation (data not shown). LPS-mediated up-regulation of *mpeg1.2* was abolished by *myd88* mutation or by inhibition of transcription factor NFκB, which functions downstream of TLR-Myd88 signalling (fig. 4C). In conclusion, up-regulation of *mpeg1.2* expression is partly dependent on MyD88-NFκB signalling, while down-regulation of *mpeg1* appears to be mediated by a Myd88-independent mechanism.

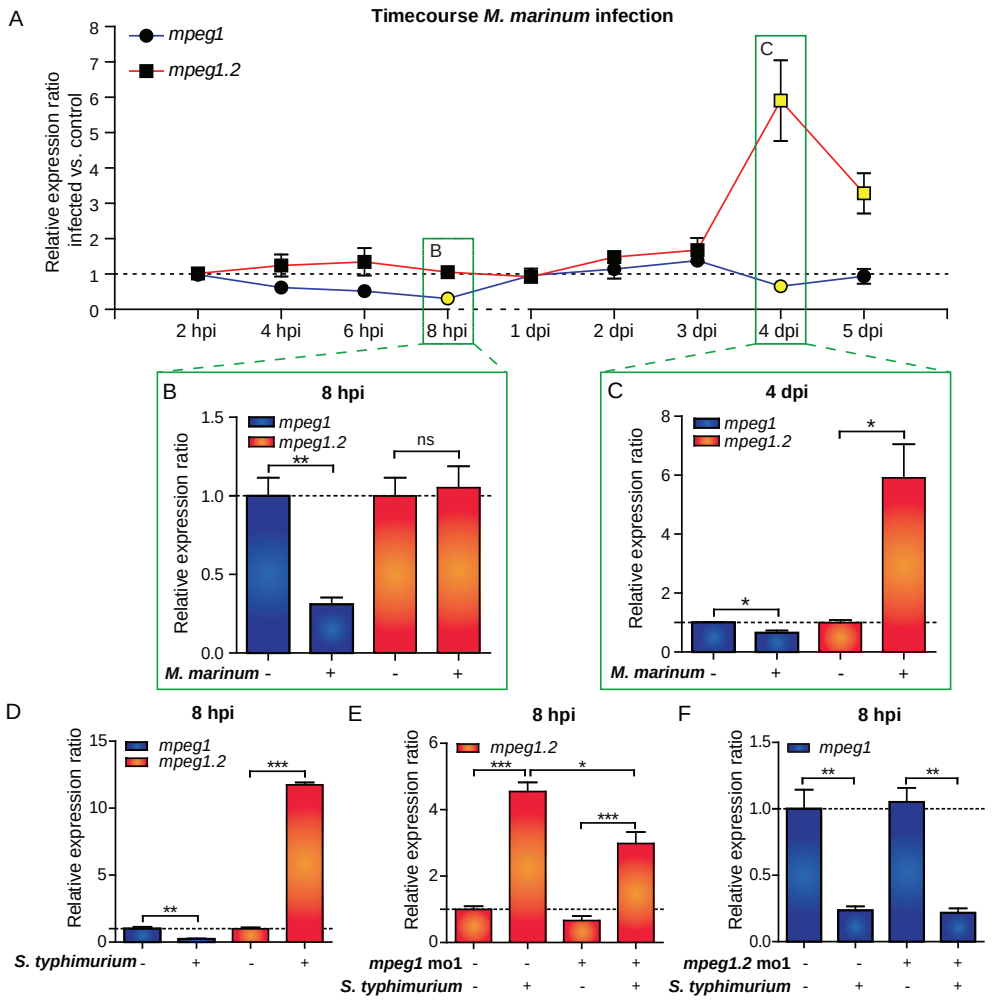

Figure 3. *mpeg1* is down-regulated and *mpeg1.2* is up-regulated upon bacterial infections. (A-C) *mpeg1* and *mpeg1.2* expression during *M. marinum* infection. AB/TL embryos were injected with *M. marinum* Mma20 bacteria (200 cfu) or 2% PVP as a mock control. Expression of *mpeg1* (round data points) and *mpeg1.2* (square data points) was analysed by qPCR at 2, 4, 6 and 8 hpi and at 1, 2, 3, 4 and 5 dpi. Light colouring of the data point in A indicates that expression in infected embryos was significantly different from uninfected controls, and in B and C the full data sets are shown for the time point indicated with boxes in A. (D) *mpeg1* and *mpeg1.2* expression in response to *S. typhimurium* SL1027 infection. AB/TL embryos were injected with 200 cfu of bacteria or mock injected with PBS, and qPCR was performed at 8 hpi. (E, F) Effect of *mpeg1* and *mpeg1.2* morpholino knockdown on each other's gene expression. AB/TL embryos were injected with (F) *mpeg1* or (G) *mpeg1.2* morpholino and subsequently infected with *S. typhimurium* SL1027 as in D. Note that *mpeg1* knockdown had a reducing effect on the up-regulation of *mpeg1.2* expression by *S. typhimurium* infection, while *mpeg1.2* knockdown did not affect the infection-dependent down-regulation of *mpeg1*. Verification of the knockdown effects is shown in supplementary fig. 4A-D. qPCR results are presented as relative ratios of three biological replicates of the infected groups compared to the relevant mock injected control groups (n=18 per group).

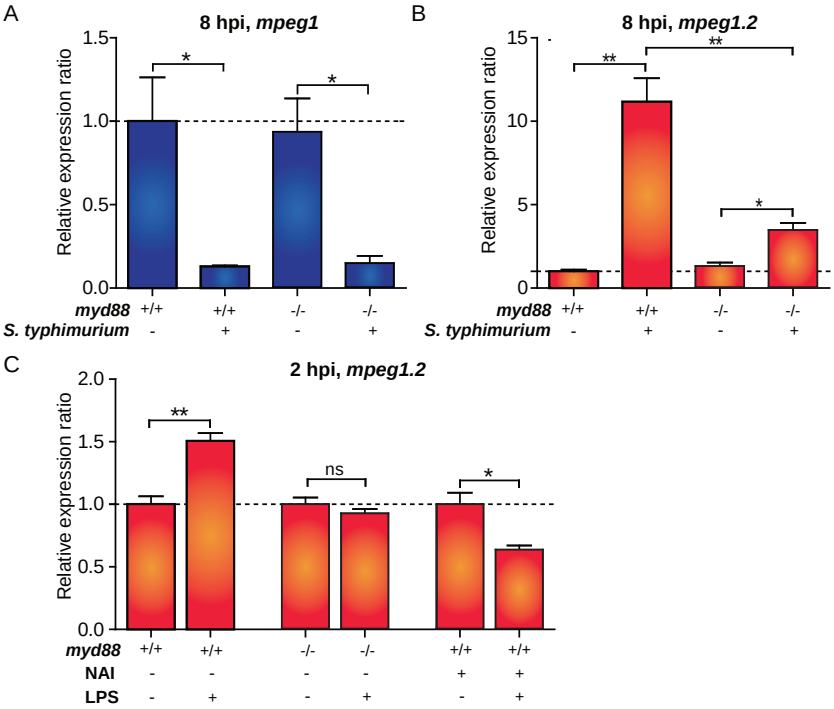

Figure 4. *mpeg1.2* up-regulation but not mpeg1 down-regulation is Myd88 and NFκB dependent. (A-B) Effect of *myd88* mutation on the response of *mpeg1* and *mpeg1.2* to *S. typhimurium* infection. Expression levels of (A) *mpeg1* and (B) *mpeg1.2* were determined by qPCR for *myd88+/+* and *myd88*$^{-/-}$ embryos at 8 hpi after infection with *S. typhimurium* SL1027 bacteria (150 cfu) and mock PBS injected controls; (C) Effect of *myd88* mutation and NFκB inhibition on the response of *mpeg1.2* to LPS treatment. *mpeg1.2* expression in *myd88+/+, myd88*$^{-/-}$ and NFκB activation inhibitor (NAI) treated embryos in response to injection with purified LPS (100 µg/ml) or PBS as a control was determined at 2 hpi. All graphs show data combined from three biological replicates (*n*=20 per group, pooled per replicate).

Knockdown of *mpeg1* leads to impaired control of *M. marinum* infection

To study the function of Mpeg1 and Mpeg1.2 during bacterial infection we used splice morpholinos targeting each gene. First, we investigated the effect of knocking down *mpeg1* on *M. marinum* infection. The morphants and their controls were injected with mCherry-expressing *M. marinum* at 28 hpf and the bacterial fluorescent pixels per embryo were analysed at 4 dpi, when granuloma-like aggregates are formed (fig. 2). *mpeg1* morphants showed higher levels of infection with *M. marinum* compared to their controls (fig. 5A+C). The higher bacterial load in the *mpeg1* morphants was phenocopied with a second morpholino (fig. 5B+D). *M. marinum* infection experiments were terminated at 5 dpi before larvae reached the free-feeding stage and *mpeg1* morphants did not die from the increased bacterial load during this period. We did not expect to see an effect on bacterial load in the *mpeg1.2* morphants since the expression of this gene is barely detectable during the first days of development and only becomes

induced at 4 dpi. As expected, *mpeg1.2* knockdown with two different morpholinos did not have an effect on *M. marinum* infection (fig. 5E-H). While *mpeg1.2* may be important at later larval stages that cannot be analysed by morpholino knockdown, we conclude that only Mpeg1 plays an important role in controlling the early pathogenesis of *M. marinum* infection.

The observation that embryos deficient in Mpeg1 develop increased infection is consistent with the expected anti-bacterial function of Mpeg1 proteins as members of the MACPF superfamily. We next investigated if, other than such a direct anti-bacterial role, Mpeg1 might be important for macrophage functions such as phagocytosis or migration. A phagocytosis assay was performed using both morpholinos targeting *mpeg1*. The morphants and their controls were injected with 180 cfu of mCherry-expressing Mma20 at 30 hpf and these embryos were fixed at the time points 5, 10, 20, 30 and 40 minutes post infection (mpi). Leukocytes were immuno-labelled with L-plastin antibody and Alexa488-conjugated secondary antibody [31] and all intracellular and extracellular Mma20 were counted over the yolk sac of each embryo to determine the percentage of phagocytosis. The yolk sac is an ideal location for analysing phagocytosis due to the superficial position of the blood circulation, which enables easy imaging, and this location is distant from the injection site, thereby minimizing possible wounding effects on the behaviour of macrophages. We observed normal levels of phagocytosis in both *mpeg1* morphants at all stages post infection (fig. 6A), demonstrating that Mpeg1 does not play a role in the phagocytosis of *M. marinum*. Since inflammation plays an important role in *M. marinum*-granuloma environment, we also investigated of *mpeg1* deficiency might have a general effect on leukocyte recruitment. We therefore performed the chemically induced inflammation (ChIN) assay [24] on *mpeg1* morphants and their controls. The copper-induced damage of neuromast hair cells in this assay was capable of attracting both macrophages and neutrophils in the *mpeg1* morphants similar as in the control group (fig. 6B). In summary, Mpeg1 does not affect the basal response of macrophages to infection, such as phagocytosis of *M. marinum*, or migration of leukocytes towards local inflammation sites.

We next sought out to identify whether the *mpeg1* morphants have a differently regulated immune response to *M. marinum.* To this end, we subjected pools of approximately 30 infected and uninfected *mpeg1* morphants to RNA sequencing analysis at 4 dpi and compared the infection response with that of embryos treated with control morpholino. We focused this comparison on a preselected set of 33 genes that showed robust and reproducible up-regulation by *M. marinum* infection at 4 dpi in four independent experiments (supplementary table 2). Approximately one third of the genes in this set, including pro-inflammatory markers such as *il1b*, *mmp9*, and *mmp13a*, showed a similar level of *M. marinum*-induced up-regulation in *mpeg1* morphants as in control embryos (fig. 7A). Other genes showed approximately 2-3-fold higher up-regulation in the *mpeg1* morphant group, including *hamp2*, *hpx*, *steap4*, and genes for a non-coding RNA (*si:dkey-97i18.5*) or uncharacterised proteins

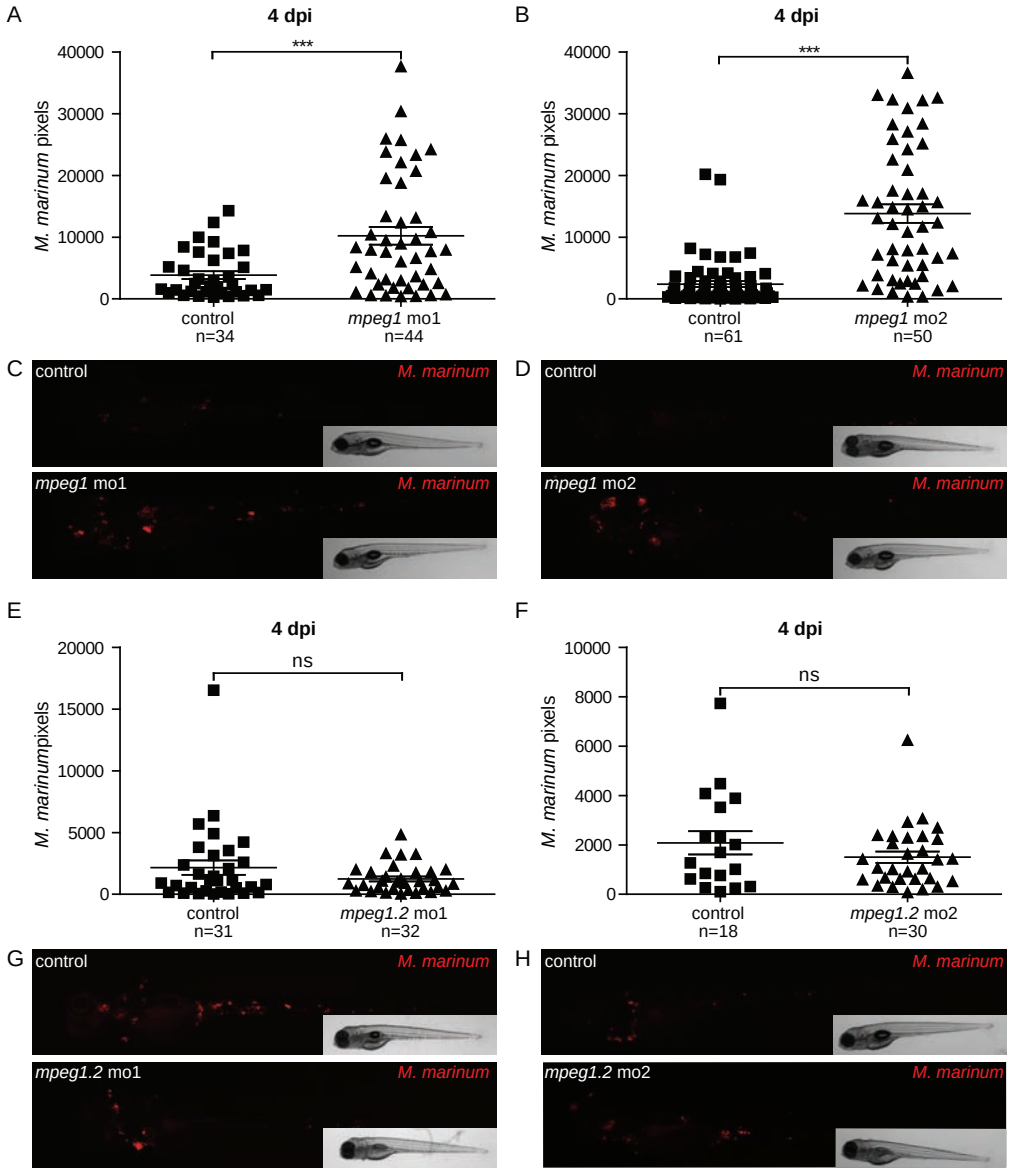

Figure 5. *mpeg1* knockdown impairs control of *M. marinum* infection. AB/TL embryos were injected with two different splice blocking morpholinos against (A-D) *mpeg1* or (E-H) *mpeg1.2* or with control morpholino, subsequently injected with mCherry-expressing *M. marinum* Mma20 strain and infected embryos were imaged at 4 dpi. (A, B, E, F) Bacterial burden was quantified by determining the number of fluorescent bacterial pixels with dedicated software and (C, D, G, H) representative stereo fluorescent images are shown below the graph of each experiment. Graphs show one representative result of five (A) or three (B, E, and F) repeated independent experiments. Each data point represents an individual embryo.

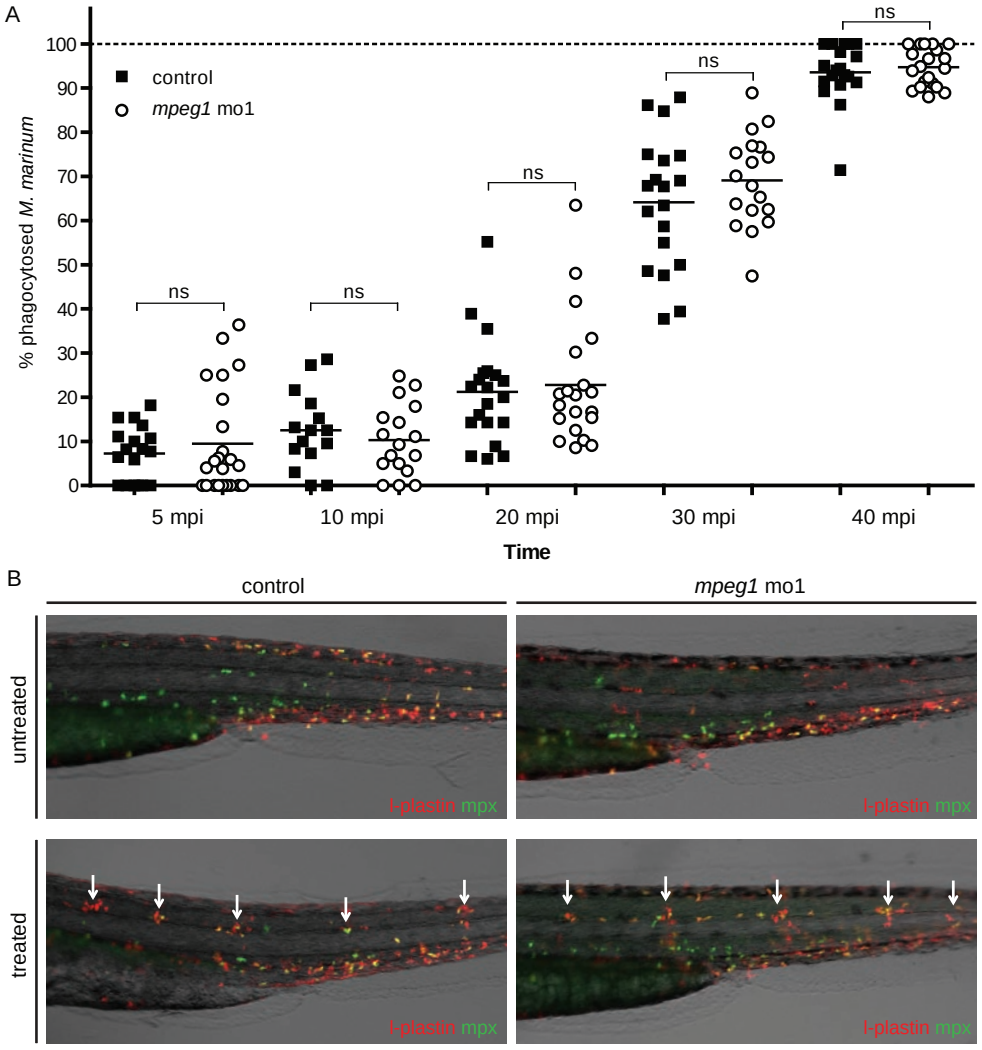

Figure 6. *mpeg1* does not play a role in phagocytosis of *M. marinum* or in leukocyte migration towards local inflammation. (A) Quantification of *M. marinum* phagocytosis. *mpeg1* morphants and their controls were injected with mCherry-expressing *M. marinum* Mma20 strain (180 cfu), fixed at 5, 10, 20, 30 and 40 mpi, and stained with L-plastin Ab to label leukocytes. Intra- and extra-cellular bacteria were counted over the yolk sac and results are presented as percentage of phagocytosed Mma20. (B) Representative images of untreated and copper sulphate treated control and *mpeg1* morphant 3 dpf embryos. Embryos were immuno-labelled with Ab against the general leukocyte marker L-plastin (red signal) in combination with a neutrophil-specific Mpx TSA-staining (green signal). White arrows indicate accumulation of leukocytes at the local inflammation sites at the neuromasts.

(*cabz01040055.1 ct027762.4*). Additionally there was a group of genes with notably lower expression in infected *mpeg1* morphants (less than 28% of the expression level in infected control embryos), which included *cyp24a1*, *hmox1*, *igfbp1a*, *slc25a38a*, and another non-coding RNA gene (*si:ch211-243g18.3*). The effect of *mpeg1* knockdown on the *M. marinum*-induced gene expression profile was markedly different from the effects of two other genes that we analysed for comparison: *ptpn6* and *myd88*. Knockdown of *ptpn6*, previously shown to function as a negative regulator of the innate immune response [23], led to a hyper-induction of approximately two third of the genes in the same gene set, including the inflammatory markers *il1b*, *mmp9*, and *mmp13a* (fig. 7B). In contrast, these inflammatory markers and the majority of other genes in the gene set showed a strongly reduced expression in *M. marinum*-infected *myd88* mutants (fig. 7C), consistent with the function of MyD88 protein as an adaptor in Toll-like and Interleukin receptor signalling [20]. We have previously shown that both the hyper-induced immune response in *ptpn6* morphants and the immunodeficiency of *myd88* mutants are associated with an increased susceptibility to *M. marinum* [20, 23]. Since the *mpeg1* knockdown effect on the *M. marinum*-dependent gene set is clearly different from both phenotypes, there is no indication that a general hyper-induction of the immune response or a general immunodeficiency could be the underlying cause of the increased bacterial burden under *mpeg1* knockdown conditions.

Mpeg1 and Mpeg1.2 both function in controlling *S. typhimurium* infection

As described above, the more acute phenotype of *S. typhimurium* infection led to rapid up-regulation of *mpeg1.2* gene expression, while *mpeg1* was simultaneously down-regulated (fig. 4A-B). To determine whether Mpeg1 and Mpeg1.2 play an anti-bacterial role during this acute infection, we injected *S. typhimurium* in *mpeg1* and *mpeg1.2* morphants at 28 hpf and assessed bacterial burden by cfu counts. Plating embryos for cfu counts showed that at 1 hpi all groups started with equal levels of *S. typhimurium* and that at 16 hpi morphants of *mpeg1* and *mpeg1.2* both had approximately 6-fold higher cfu counts than the control group (fig. 8A). Increased cfu counts were also observed with a second set of morpholinos for *mpeg1* and *mpeg1.2* (fig. 8B). This striking difference in the cfu counts indicates that both genes play a role in controlling the *S. typhimurium* infection in zebrafish embryos.

Next, we aimed to determine whether the higher cfu numbers in the morphants was associated with a decreased survival rate. Morphants of *mpeg1* and *mpeg1.2* and control embryos were injected with *S. typhimurium*, screened for equal level of infection under a stereo fluorescence microscope directly after injection, and monitored for heart beat from 14 hpi onwards. *mpeg1.2* deficiency caused a similar or decreased survival time compared to the control group (fig. 8C-D) and unexpectedly, *mpeg1* morphants survived significantly longer than the control embryos (fig. 8C-D), despite that these morphants showed increased cfu counts similar to *mpeg1.2* morphants. This opposing effect on survival could not be attributed to a difference in intracellular or extracellular location of *S. typhimurium* between the two morphants because both

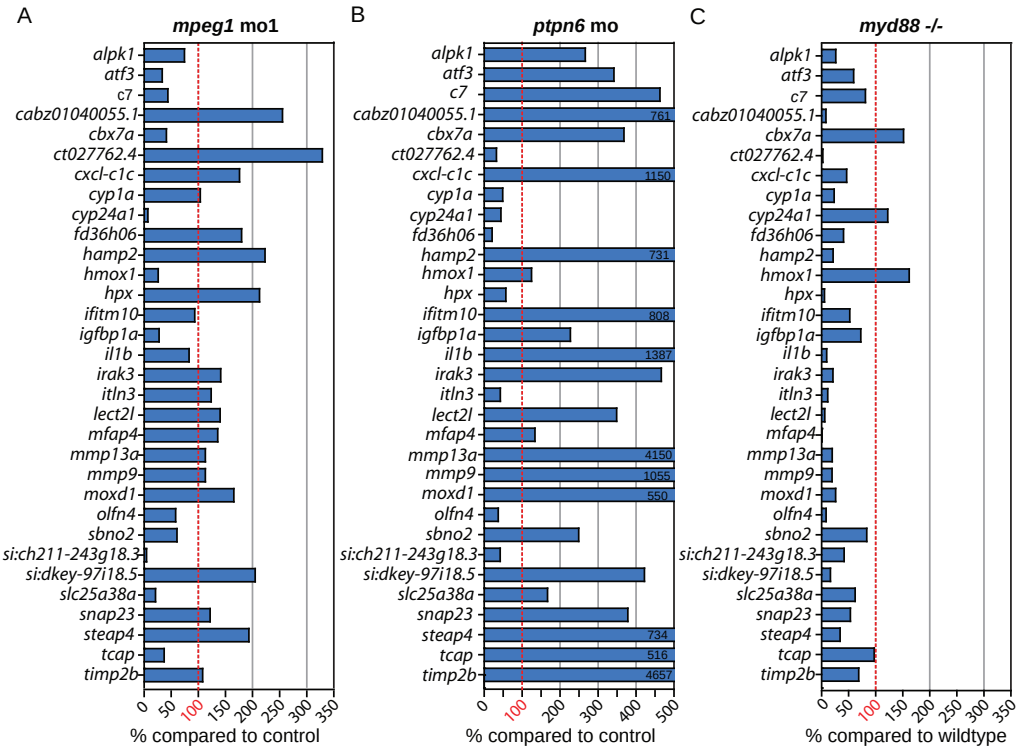

Figure 7. Effect of *mpeg1* knockdown on the innate immune response during *M. marinum* infection in comparison with known effects of *ptpn6* and *myd88* deficiencies. Graphs show the effects of (A) *mpeg1* mo1 knockdown, (B) *ptpn6* morpholino knockdown and (C) *myd88* mutation on a set of genes that showed reproducible induction by *M. marinum* infection in control embryos. The expression level of these genes under conditions of *mpeg1*, *ptpn6* or *myd88* deficiency is expressed as the percentage of the expression level in the corresponding control. Results are based on RNAseq analysis of pools of 30 infected and 30 uninfected embryos for each group. Embryos were injected with *M. marinum* Mma20 (300 cfu) or mock injected with 2% PVP, and RNAseq analysis was performed at 4 dpi.

Figure 8. *mpeg1* and *mpeg1.2* knockdown increase bacterial burden and pro-inflammatory gene expression, but have opposite effects on host survival during *S. typhimurium* infection. (A-B) Quantification of bacterial burden. *mpeg1* and *mpeg1.2* morphants ((A) morpholinos 1 and (B) morpholinos 2) and control embryos were injected with Ds-Red-expressing *S. typhimurium* SL1027 bacteria (200 cfu) and PBS as mock control. Embryos were homogenised and plated at 1 and 16 hpi to determine *S. typhimurium* cfu counts (n=5 per group, 2 biological replicates, log2 scale). (C-D) Survival rates. The percentage of survival of infected *mpeg1* morphants, *mpeg1.2* morphants ((C) morpholinos 1 and (D) morpholinos 2) and control embryos was determined over a time course of 32 hpi. DsRed-expressing *S. typhimurium* SL1027 bacteria were injected into the blood circulation (150 cfu). Survival curves of *mpeg1* morphants (red line), *mpeg1.2* morphants (green line) and control embryos (blue line) are shown of one representative experiment of three individual experiments. (E) Quantification of intracellular and extracellular *S. typhimurium* over the Duct of Cuvier in control embryos, *mpeg1* morphants and *mpeg1.2* morphants at 4 and 8 hpi (representative confocal images in supplementary fig.4). Statistical significance is indicated for intracellular *S. typhimurium* (red letters) and extracellular *S. typhimurium* (blue letters) (calculated from confocal images of n=6-8 embryos per group).

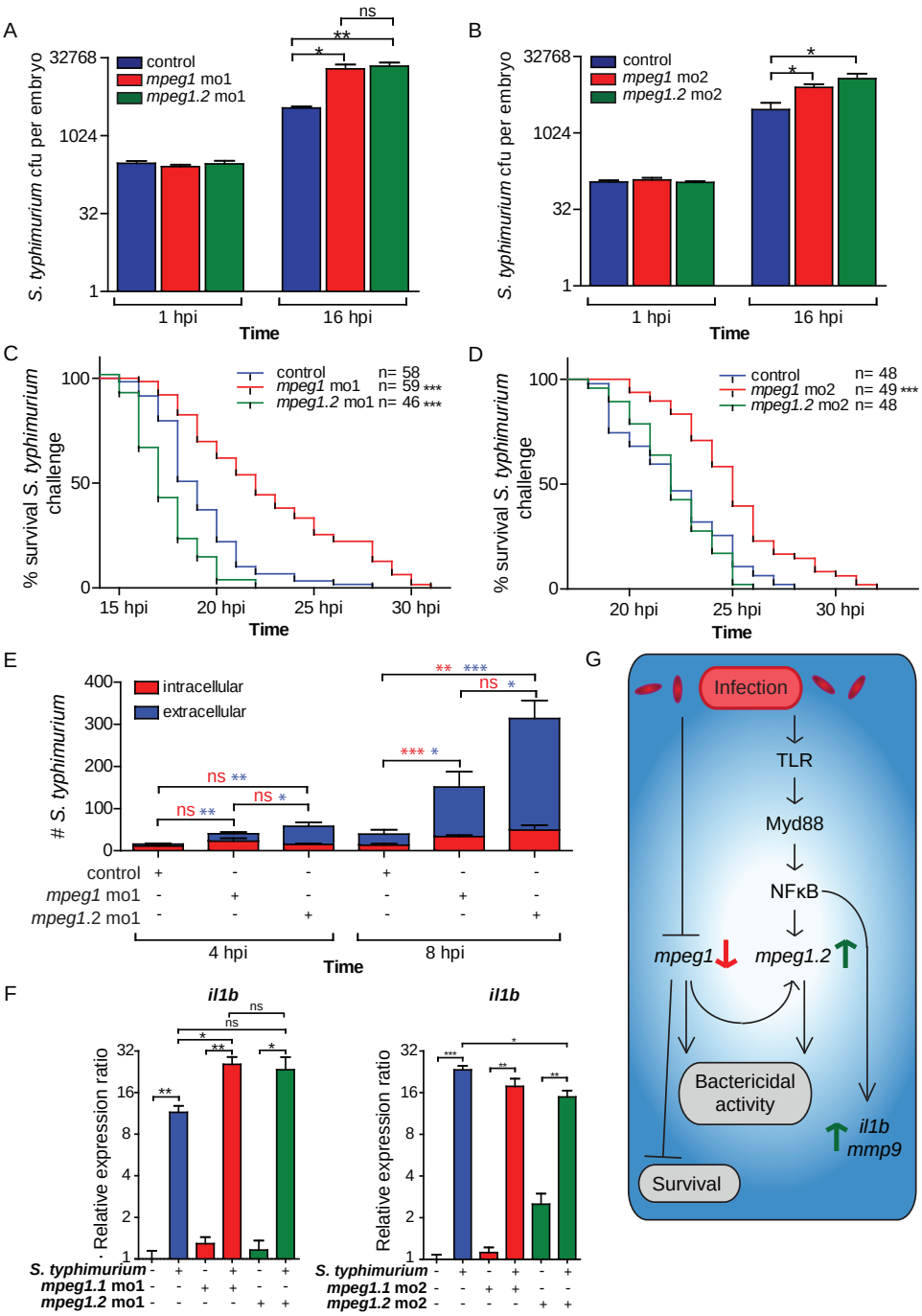

Figure 8 continued: (F) Pro-inflammatory gene expression of *il1b* under the same experimental conditions as in A-B was analysed by qPCR at 16 hpi (*n*=15 per group, pooled per replicate, 3 biological replicates, log2 scale). (G) A schematic representation of *mpeg1* and *mpeg1.2* regulation and their function.

mpeg1 and *mpeg1.2* morphants showed a significantly higher number of extracellular *S. typhimurium* compared to the control embryos at 8 hpi (fig. 8E and supplementary fig. 4). Furthermore, the opposing survival effect could also not be attributed to a difference in expression of the major *S. typhimurium* responsive pro-inflammatory genes, *il1b* (fig. 8F) and *mmp9* (supplementary fig. 5), which showed clear induction in *mpeg1* and *mpeg1.2* morphants. While the increased survival rate of *mpeg1* morphants remains unexplained, our results suggest that the up-regulation of *mpeg1.2* with concomitant down-regulation of *mpeg1* aids the host in combatting *S. typhimurium* infection (fig. 8G).

Discussion

The perforins of cytotoxic T-cells and natural killer cells and the membrane attack complex proteins of the complement system share the ability to form pores in membranes [1, 2]. While the roles of these proteins in host defence are well understood, the function of the structurally related MPEG1/Perforin-2 family in macrophages remains to be fully elucidated [3, 9]. In zebrafish an *mpeg1*-expressing population of macrophages develops during the first day of embryogenesis [13]. The availability of well-established infection models for zebrafish embryos enabled us to study the function of *mpeg1* in innate host defence. We show that *mpeg1* is down-regulated during infection in a Myd88-independent manner, while a close homolog, *mpeg1.2*, is up-regulated partially by a Myd88-NFκB-dependent mechanism. Notwithstanding this opposite regulation pattern, we found that both *mpeg1* and *mpeg1.2* are important for controlling infections with intracellular bacterial pathogens.

The close chromosomal location of the different *mpeg1* genes in zebrafish suggests that these are the result of recent gene duplication events, after which *mpeg1* and *mpeg1.2* appear to have developed specialised functions and *mpeg1.3* may have become a pseudogene. A similar situation is found in mice and other rodents, where a gene named pore forming protein-like (*Pfpl*) is most likely paralogous to *Mpeg1*, since it is located in close vicinity and encodes a protein with 66% amino acid identity. Whereas *Mpeg1* is inducible by infection both in macrophages and other cell types [11, 12] the expression pattern of *Pfpl* in trophoblasts indicates a developmental function of this gene [35] and EST profiles in the NCBI database provide no indication for significant expression of *Pfpl* in cells or organs related to the immune system. EST profiles of the single *MPEG1* gene in human support its possible function in the immune system, but to the best of our knowledge, functional studies of the human gene have not yet been reported. Studies of murine *Mpeg1* in cultured fibroblasts, macrophages, and HeLa cells led to the hypothesis that upon bacterial infection Mpeg1/Perforin-2 vesicles traffic to and fuse with bacteria-containing compartments, where attack and pore formation on the bacterial surface is subsequently initiated [3, 11, 12]. To further investigate the correlation of *MPEG1* with infectious diseases, we inspected curated microarray datasets in the NextBio database (http://www.nextbio.com/b/nextbioCorp.nb). This analysis shows

that *MPEG1* is frequently regulated during infection, both in studies using cultured macrophages and in studies using mouse infection models. For example, *MPEG1* shows significant down-regulation in human macrophages exposed to *Staphylococcus aureus* [36] and in human monocytes infected with *Francisella tularensis* [37]. In contrast, up-regulation has been observed in for example the lungs of mice infected with these pathogens [38, 39]. Thus, in human and mouse different infection conditions are associated either with up- or down-regulation of *MPEG1,* while in zebrafish *mpeg1* and *mpeg1.2* are regulated in opposite directions under the same infection conditions.

Using the zebrafish-*M. marinum* infection model we found that knockdown of *mpeg1* results in increased bacterial burden, consistent with the proposed bactericidal function of Mpeg1 as a pore forming molecule [11]. However, there might be a broader effect as we observed an altered immune response expression signature in infected *mpeg1* morphants that might also have an impact on the ability to control infection. The function of *mpeg1.2*, which has extremely low basal expression level, could only be assessed using an *S. typhimurium* infection model, where this gene is rapidly up-regulated. In this model, knockdown of *mpeg1* attenuated the up-regulation of *mpeg1.2*, indicating a broader effect of *mpeg1* on the innate immune response consistent with the results of *M. marinum* infection. Knockdown of either *mpeg1* or the inducible *mpeg1*.2 gene led to increased bacterial burden of *S. typhimurium* infection, providing *in vivo* support for the anti-bacterial function of both genes. Due to toxicity effects of combining the morpholinos we were unable to investigate possible synergism between the anti-bacterial functions of *mpeg1* and *mpeg1.2*. However, a remarkable difference between the separate knockdown of *mpeg1* and *mpeg1.2* was observed in that the survival time of *mpeg1* morphants was prolonged despite the increase in cfu numbers. This suggests that the survival advantage of *mpeg1* morphants could be due to an altered immune response and that, during the normal course of *S. typhimurium* infection, embryos might die from host damaging effects of the immune response rather than as a direct effect of the bacterial load. That *S. typhimurium*-infected zebrafish embryos die primarily from a host damaging immune response is supported by our previous study of the regulatory phosphatase Ptpn6. Deficiency in Ptpn6 leads to a decreased survival rate during *S. typhimurium* infection, which correlates with a hyper-induced expression of many pro-inflammatory genes [23]. Two of the main pro-inflammatory marker genes, *il1b* and *mmp9*, were highly up-regulated in both *mpeg1* and *mpeg1.2* morphants, similar to infected control embryos. A difference in the expression of these marker genes therefore does not explain the survival advantage of *mpeg1* morphants and the underlying cause of this effect currently remains unknown. Together, this first study of the MPEG1/Perforin-2 family in a whole organism model enables us to present a scheme that summarises the regulatory mechanisms of both *mpeg1* and *mpeg1.2* and links this to the biological effects of the two genes (fig. 8G). The specialised function of the two *mpeg1* paralogues in zebrafish indicated by our morpholino knockdown study can be seen as a motivation to develop zebrafish or mouse knockout models for further investigation of the mechanisms by which Mpeg1/Perforin-2 proteins exert their immunological function.

Acknowledgements

The authors would like to thank Georges Lutfalla (University Montpellier 2) for the kind gift of *Tg(mpeg1:mCherry-F)* fish, Michiel van der Vaart for providing RNA of LPS injected myd88 mutant embryos, Ulrike Nehrdich, Laura van Hulst and Davy de Witt for fish care, and other lab members for helpful discussions. EB, AEN, FJV, HPS, and AHM were supported by the Smart Mix Program of the Netherlands Ministry of Economic Affairs and the Ministry of Education, Culture and Science, PIR by a Marie Curie Intra-European Fellowship (PIEF-GA-2010-274389), and JR by a Marie Curie Fellowship of the European 7th Framework Initial Training Network FishForPharma (PITG-GA-2011-289209).

References

1. Kondos, S.C. et al. The structure and function of mammalian membrane-attack complex/perforin-like proteins. Tissue Antigens 76, 341-351 (2010).

2. Rosado, C.J. et al. The MACPF/CDC family of pore-forming toxins. Cell Microbiol 10, 1765-1774 (2008).

3. McCormack, R., de Armas, L., Shiratsuchi, M. & Podack, E.R. Killing machines: three pore-forming proteins of the immune system. Immunol Res 57, 268-278 (2013).

4. Voskoboinik, I., Dunstone, M.A., Baran, K., Whisstock, J.C. & Trapani, J.A. Perforin: structure, function, and role in human immunopathology. Immunol Rev 235, 35-54 (2010).

5. Spilsbury, K. et al. Isolation of a novel macrophage-specific gene by differential cDNA analysis. Blood 85, 1620-1629 (1995).

6. Wiens, M. Innate Immune Defense of the Sponge Suberites domuncula against Bacteria Involves a MyD88-dependent Signaling Pathway: INDUCTION OF A PERFORIN-LIKE MOLECULE. Journal of Biological Chemistry 280, 27949-27959 (2005).

7. Renault, T., Faury, N., Barbosa-Solomieu, V. & Moreau, K. Suppression substractive hybridisation (SSH) and real time PCR reveal differential gene expression in the Pacific cupped oyster, Crassostrea gigas, challenged with Ostreid herpesvirus 1. Dev Comp Immunol 35, 725-735 (2011).

8. Kemp, I.K. & Coyne, V.E. Identification and characterisation of the Mpeg1 homologue in the South African abalone, Haliotis midae. Fish & Shellfish Immunology 31, 754-764 (2011).

9. D'Angelo, M.E., Dunstone, M.A., Whisstock, J.C., Trapani, J.A. & Bird, P.I. Perforin evolved from a gene duplication of MPEG1, followed by a complex pattern of gene gain and loss within Euteleostomi. BMC Evol Biol 12, 59 (2012).

10. Kopacek, J. et al. Upregulation of the genes encoding lysosomal hydrolases, a perforin-like protein, and peroxidases in the brains of mice affected with an experimental prion disease. J Virol 74, 411-417 (2000).

11. McCormack, R., de Armas, L.R., Shiratsuchi, M., Ramos, J.E. & Podack, E.R. Inhibition of intracellular bacterial replication in fibroblasts is dependent on the perforin-like protein (perforin-2) encoded by macrophage-expressed gene 1. J Innate Immun 5, 185-194 (2013).

12. Fields, K.A., McCormack, R., de Armas, L.R. & Podack, E.R. Perforin-2 restricts growth of Chlamydia trachomatis in macrophages. Infect Immun 81, 3045-3054 (2013).

13. Zakrzewska, A. et al. Macrophage-specific gene functions in Spi1-directed innate immunity. Blood 116, e1-11 (2010).

14. Ellett, F., Pase, L., Hayman, J.W., Andrianopoulos, A. & Lieschke, G.J. mpeg1 promoter transgenes direct macrophage-lineage expression in zebrafish. Blood 117, e49-e56 (2010).

15. Herbomel, P., Thisse, B. & Thisse, C. Ontogeny and behaviour of early macrophages in the zebrafish embryo. Development 126, 3735-3745 (1999).

16. Trede, N.S., Langenau, D.M., Traver, D., Look, A.T. & Zon, L.I. The use of zebrafish to understand immunity. Immunity 20, 367-379 (2004).

17. Davis, J.M. et al. Real-time visualization of mycobacterium-macrophage interactions leading to initiation of granuloma formation in zebrafish embryos. Immunity 17, 693-702 (2002).

18. van der Sar, A.M. et al. Zebrafish embryos as a model host for the real time analysis of Salmonella typhimurium infections. Cellular Microbiology 5, 601-611 (2003).

19. Meijer, A.H. & Spaink, H.P. Host-pathogen interactions made transparent with the zebrafish model. Curr Drug Targets 12, 1000-1017 (2011).

20. van der Vaart, M., van Soest, J.J., Spaink, H.P. & Meijer, A.H. Functional analysis of a zebrafish myd88 mutant identifies key transcriptional components of the innate immune system. Dis Model Mech 6, 841-854 (2013).

21. Renshaw, S.A. et al. A transgenic zebrafish model of neutrophilic inflammation. Blood 108, 3976-3978 (2006).

22. Bernuta, A. et al. Mycobacterium abscessus cording prevents phagocytosis and promotes abscess formation. PNAS in press (2014).

23. Kanwal, Z. et al. Deficiency in hematopoietic phosphatase ptpn6/Shp1 hyperactivates the innate immune system and impairs control of bacterial infections in zebrafish embryos. J Immunol 190, 1631-1645 (2013).

24. d'Alençon, C.A. et al. A high-throughput chemically induced inflammation assay in zebrafish. BMC Biology 8, 151 (2010).

25. van der Sar, A.M. et al. Mycobacterium marinum Strains Can Be Divided into Two Distinct Types Based on Genetic Diversity and Virulence. Infection and Immunity 72, 6306-6312 (2004).

26. Cosma, C.L., Humbert, O., Sherman, D.R. & Ramakrishnan, L. Trafficking of superinfecting Mycobacterium organisms into established granulomas occurs in mammals and is independent of the Erp and ESX-1 mycobacterial virulence loci. J Infect Dis 198, 1851-1855 (2008).

27. Veneman, W.J. et al. A zebrafish high throughput screening system used for Staphylococcus epidermidis infection marker discovery. BMC Genomics 14, 255 (2013).

28. Benard, E.L. et al. Infection of zebrafish embryos with intracellular bacterial pathogens. J Vis Exp pii: 3781. doi: 10.3791/3781 (2012).

29. Stockhammer, O.W., Zakrzewska, A., Hegedus, Z., Spaink, H.P. & Meijer, A.H. Transcriptome profiling and functional analyses of the zebrafish embryonic innate immune response to Salmonella infection. J Immunol 182, 5641-5653 (2009).

30. Meijer, A.H. et al. Identification and real-time imaging of a myc-expressing neutrophil population involved in inflammation and mycobacterial granuloma formation in zebrafish. Developmental and comparative immunology 32, 36-49 (2008).

31. Mathias, J.R. et al. Live imaging of chronic inflammation caused by mutation of zebrafish Hai1. Journal of Cell Science 120, 3372-3383 (2007).

32. Nezhinsky A.E., V.F.J. Efficient and Robust Shape Retrieval from Deformable Templates. International Symposium on Leveraging Applications of Formal Methods Part II, LNCS 7610 (T. Margaria, B. Steffen, and M. Merten (Eds.)), 42-55 (2012).

33. Clay, H., Volkman, H.E. & Ramakrishnan, L. Tumor Necrosis Factor Signaling Mediates Resistance to Mycobacteria by Inhibiting Bacterial Growth and Macrophage Death. Immunity 29, 283-294 (2008).

34. O'Neill, L.A. & Bowie, A.G. The family of five: TIR-domain-containing adaptors in Toll-like receptor signalling. Nat Rev Immunol 7, 353-364 (2007).

35. Hemberger, M., Himmelbauer, H., Ruschmann, J., Zeitz, C. & Fundele, R. cDNA subtraction cloning reveals novel genes whose temporal and spatial expression indicates association with trophoblast invasion. Dev Biol 222, 158-169 (2000).

36. Koziel, J. et al. Phagocytosis of Staphylococcus aureus by macrophages exerts cytoprotective effects manifested by the upregulation of antiapoptotic factors. PLoS One 4, e5210 (2009).

37. Butchar, J.P. et al. Microarray analysis of human monocytes infected with Francisella tularensis identifies new targets of host response subversion. PLoS One 3, e2924 (2008).

38. Frank, K.M. et al. Host response signature to Staphylococcus aureus alpha-hemolysin implicates pulmonary Th17 response. Infection and immunity 80, 3161-3169 (2012).

39. Walters, K.A. et al. Francisella tularensis subsp. tularensis induces a unique pulmonary inflammatory response: role of bacterial gene expression in temporal regulation of host defense responses. PLoS One 8, e62412 (2013).

40. Volkman, H.E. et al. Tuberculous granuloma formation is enhanced by a mycobacterium virulence determinant. PLoS Biol 2, e367 (2004).

A Protein homology

Similar \ Identical	z-Mpeg1	z-Mpeg1.2	z-Mpeg1.3	m-MPEG1	h-MPEG1
z-Mpeg1	100	66	69	45	48
z-Mpeg1.2	89	100	56	44	46
z-Mpeg1.3	85	81	100	43	43
m-MPEG1	77	74	75	100	75
h-MPEG1	75	73	73	91	100

B MACPF domain homology

Similar \ Identical	z-Mpeg1	z-Mpeg1.2	z-Mpeg1.3	m-MPEG1	h-MPEG1
z-Mpeg1	100	72	70	45	50
z-Mpeg1.2	92	100	59	45	47
z-Mpeg1.3	83	82	100	49	50
m-MPEG1	78	74	84	100	77
h-MPEG1	74	74	82	93	100

Supplementary table 1. Homology between zebrafish Mpeg1 proteins, murine MPEG1 and human MPEG1. Homology for (A) whole protein sequences and (B) MACPF domains was determined between zebrafish Mpeg1 (z-Mpeg1, NP_997902.1), Mpeg1.2 (z-Mpeg1.2, ENSDARP00000063271), Mpeg1.3 (z-Mpeg1.3, ENSDARP00000098563), murine MPEG1 (m-MPEG1, NP_034951.1) and human MPEG1 (h-MPEG1, NP_001034485.1). Amino acid identity and similarity percentages were determined using UniProt CLUSTAL O(1.2.0) multiple sequence alignment.

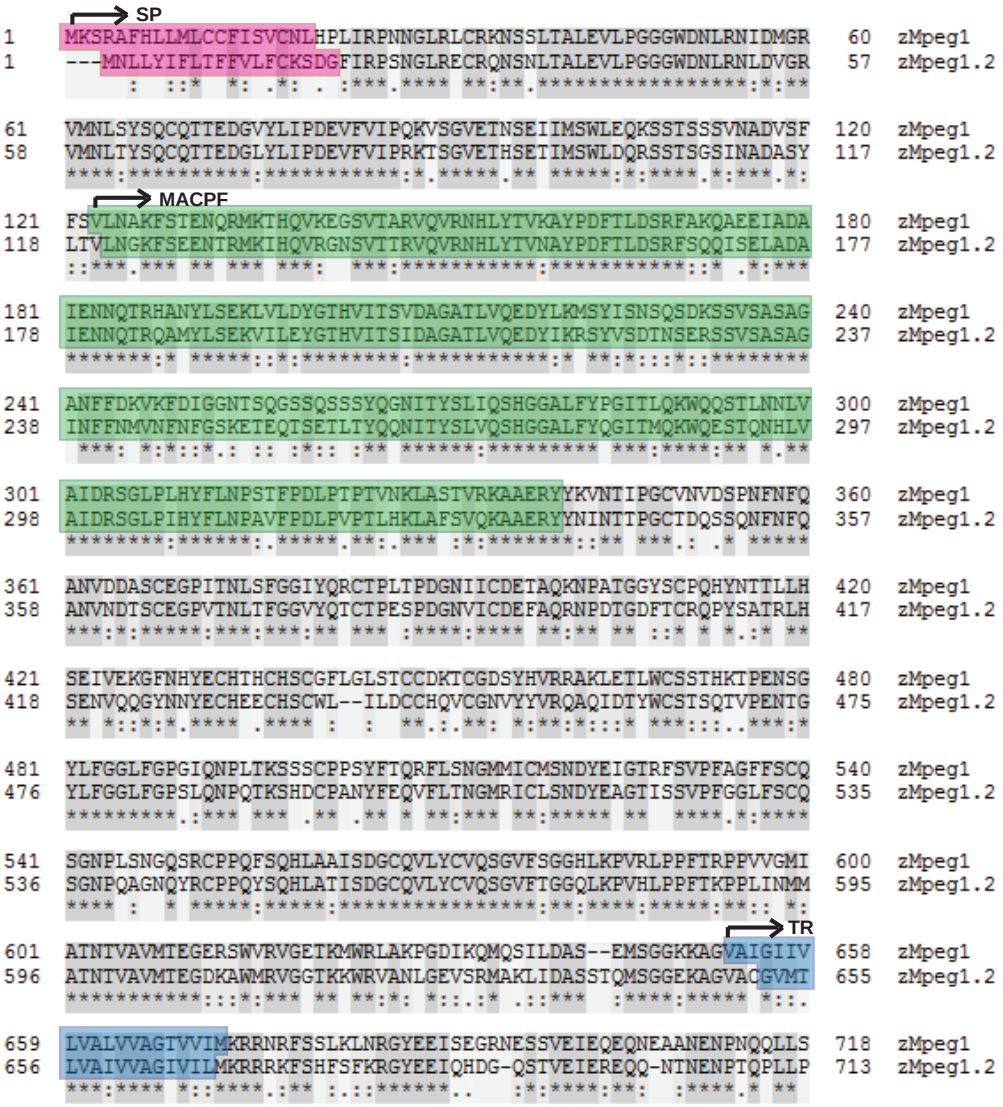

Supplementary figure 1. Mpeg1 and Mpeg1.2 protein alignment. The Signal Peptide (SP), Membrane Attack Complex/Perforin (MACPF), and Transmembrane Region (TR) are located in the same position in Mpeg1 and Mpeg1.2.

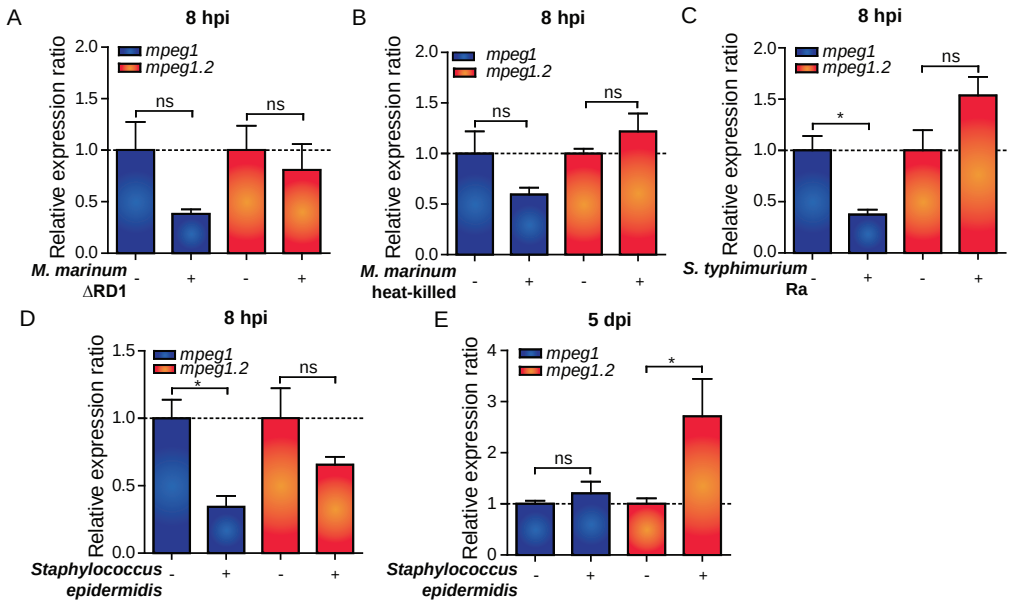

Supplementary figure 2. Expression analysis of *mpeg1* and *mpeg1.2* during different bacterial infections. Expression at 8 hpi following intravenous infection with (A) *M. marinum ΔRD1* [40] (800 cfu), (B) heat-killed *M. marinum* (300 cfu), (C) *S. typhimurium* LPS mutant strain Ra (200 cfu), and (D) *Staphylococcus epidermidis* strain O-47 (800 cfu). (E) Expression at 5 dpi following yolk infection at 2 hpf with *Staphylococcus epidermidis* strain O-47 (20 cfu). Expression levels of *mpeg1* and *mpeg1.2* were determined by qPCR. All graphs show data combined from three biological replicates (*n*=20 per group, pooled per replicate).

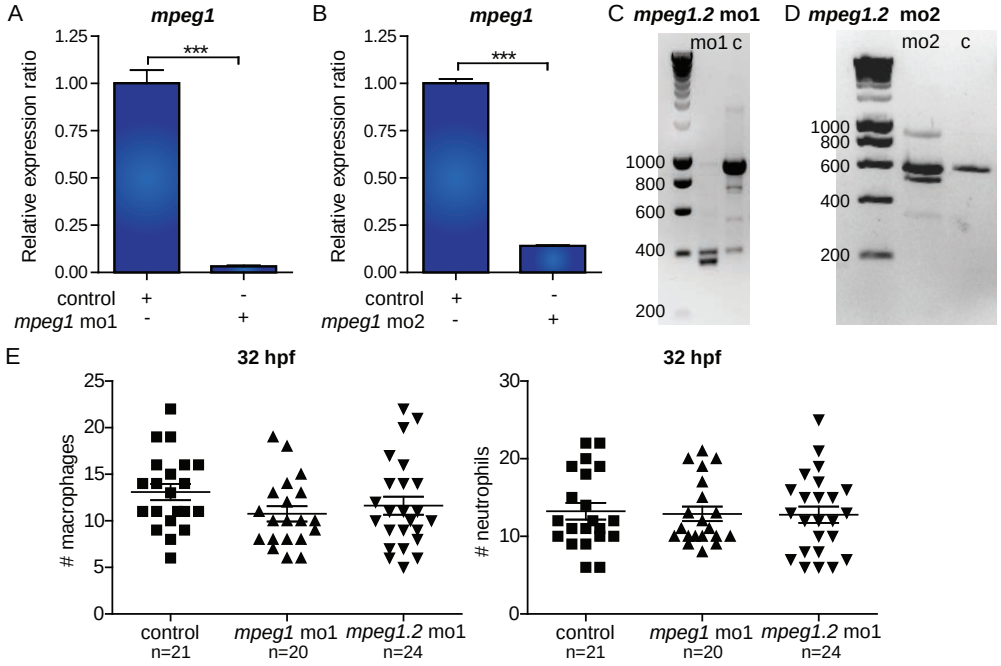

Supplementary figure 3. Verification of *mpeg1* and *mpeg1.2* knockdown. (A-B) Knockdown of *mpeg1*. Expression of *mpeg1* was determined by qPCR at 28 hpf after knockdown with (A) *mpeg1* morpholino 1 (B) *mpeg1* morpholino 2 and in embryos injected with control morpholino. Both forward and reverse qPCR primers target exon 2 of *mpeg1*.(C-D) Knockdown of *mpeg1.2*. Because of the low basal expression level of *mpeg1.2*, the knockdown effect on this gene was assessed under infection conditions (8 hpi). Expression of *mpeg1.2* was determined by RT-PCR using RNA from embryos injected with (C) *mpeg1.2* morpholino 1 (mo1) or control morpholino (c) (D) *mpeg1.2* morpholino 2 (mo2) or control morpholino (c) and infected with *S. typhimurium.* Digits in C and D indicate smart ladder base pair size. For both *mpeg1.2* morphants, the RT-PCR product (944 bp for mo1 and 569 bp in size for mo2) is disrupted upon morpholino injection. The RT-PCR forward primer for *mpeg1.2* targets exon 1 and both RT-PCR reverse primers for *mpeg1.2* target exon 2. (E) Normal leukocyte numbers in *mpeg1* and *mpeg1.2* morphants. *mpeg1* and *mpeg1.2* morphants and control embryos were fixed at 32 hpf and were stained with the neutrophil mpx-TSA staining and immuno-labelled with Ab against the general leukocyte marker L-plastin. Macrophage (L-plastin-positive, mpx negative) and neutrophil (L-plastin/mpx double positive) numbers were counted blinded in the tail (ns = not significant).

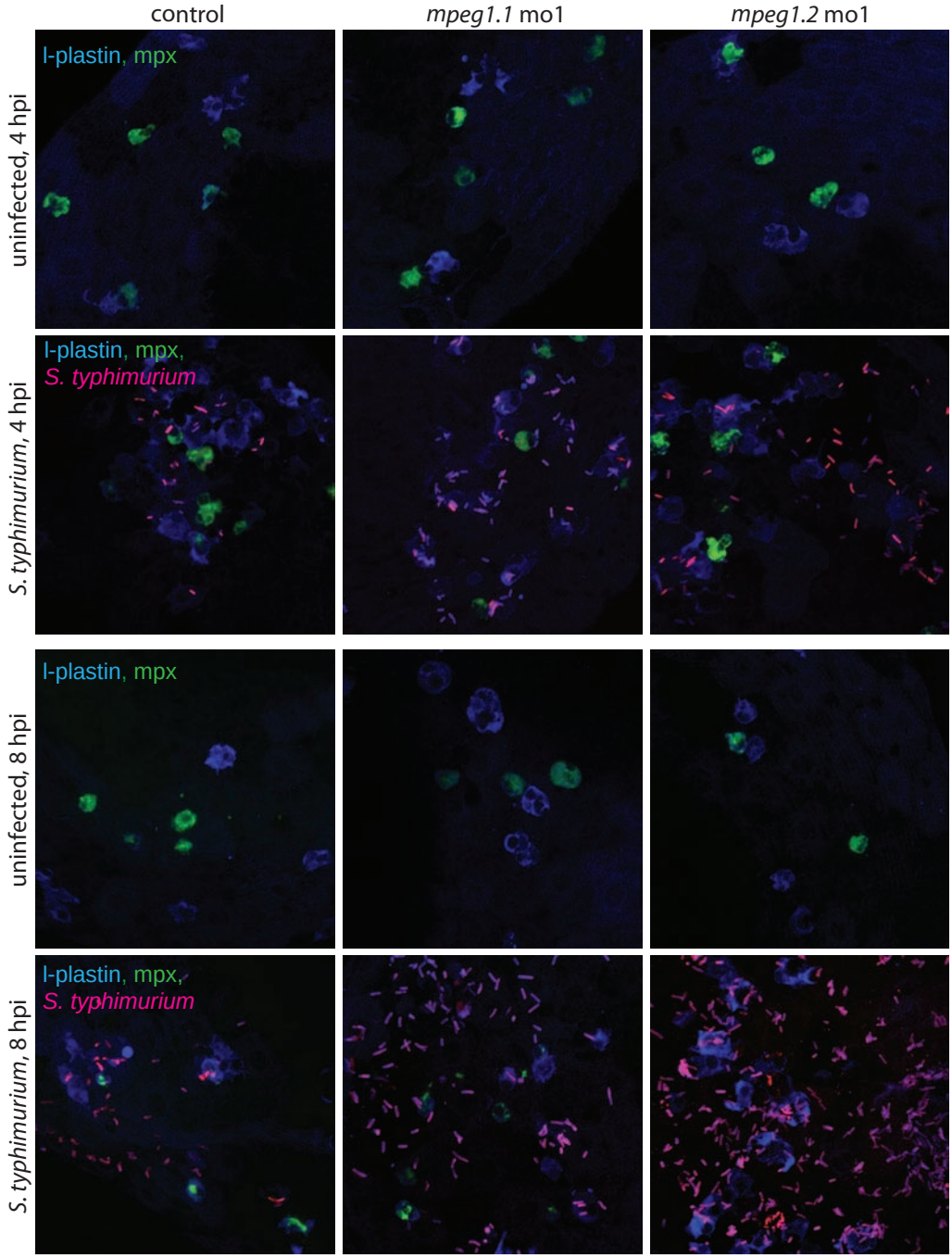

Supplementary figure 4. Representative images of the *S. typhimurium* infection process during *mpeg1* and *mpeg1.2* knockdown. *S. typhimurium* SL1027 bacteria (150 cfu) were injected into the caudal vein of AB/TL embryos. Embryos were fixed at 4 and 8 hpi and stained for mpx activity in neutrophils (green) followed by double antibody staining against *S. typhimurium* (red) and L-plastin (blue). Macrophages are identified as L-plastin-positive, mpx-negative cells

Supplementary figure 4 continued: and no differences in macrophage numbers were observed between the different groups. Confocal z-stack projections show identical locations in the Duct of Cuvier in uninfected and infected control embryos, *mpeg1* (mo1) morphants, and *mpeg1.2* (mo1) morphants. Numbers of *S. typhimurium* bacteria contained within macrophages or extracellular were quantified from images of 6-8 embryos per group and data are shown in Fig. 8E.

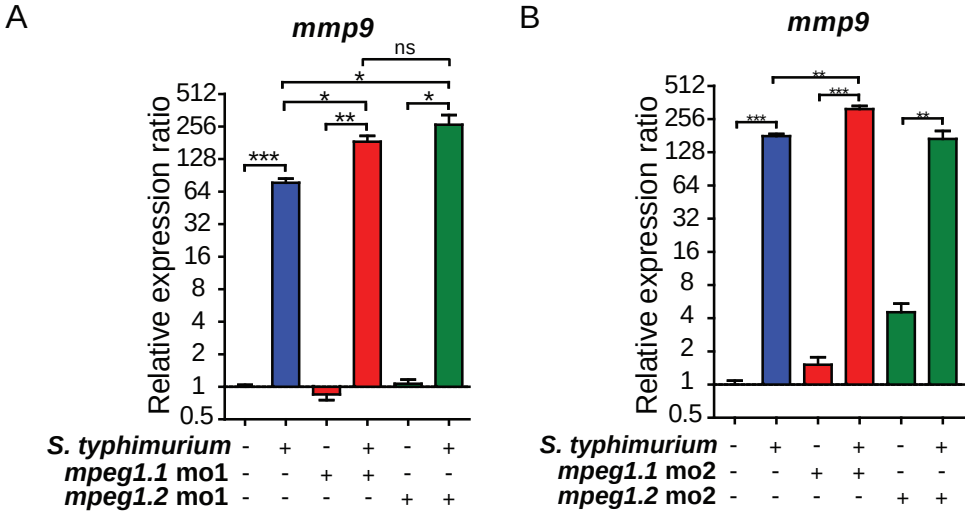

Supplementary figure 5. Expression of *mmp9* during *S. typhimurium* infection of *mpeg1* and *mpeg1.2* knockdown embryos. (A-B) Gene expression of *mmp9* under the same experimental conditions as in fig. 8A-B were analysed by qPCR at 16 hpi (*n*=15 per group, pooled per replicate, 3 biological replicates, log2 scale).

Supplementary table 2. Overview top induced genes *M. marinum* infection.

Ensembl ID	Gene name	Description	log2 fold change	Adjusted P-value
ENSDARG00000059741	*alpk1*	alpha-kinase 1	1.2	4.8E-04
ENSDARG00000007823	*atf3*	activating transcription factor 3	1.7	1.4E-08
ENSDARG00000057121	*c7 (2 of 2)*	complement component 7	1.7	2.0E-06
ENSDARG00000086869	*cabz01040055.1*	three-finger protein 5 (LOC100003647 precursor)	3.1	3.1E-22
ENSDARG00000038025	*cbx7a*	chromobox homolog 7a	1.8	3.9E-10
ENSDARG00000086654	*ct027762.4*	Uncharacterized protein	2.1	5.1E-07
ENSDARG00000075045	*cxcl-c1c*	chemokine (C-X-C motif) ligand c1c	1.7	5.6E-04
ENSDARG00000026039	*cyp1a*	cytochrome P450, family 1, subfamily A	2.5	3.3E-17
ENSDARG00000070420	*cyp24a1*	cytochrome P450, family 24, subfamily A, polypeptide 1	2.2	5.0E-14
ENSDARG00000092858	*fd36h06*	non-coding RNA	2.4	2.2E-10
ENSDARG00000053227	*hamp2*	hepcidin antimicrobial peptide 2	3.0	1.3E-12
ENSDARG00000027529	*hmox1*	heme oxygenase (decycling) 1	1.5	1.9E-04
ENSDARG00000051912	*hpx (1 of 2)*	hemopexin	2.2	1.2E-12
ENSDARG00000093303	*ifitm10*	interferon induced transmembrane protein 10	1.4	1.5E-03
ENSDARG00000014947	*igfbp1a*	insulin-like growth factor binding protein 1a	1.9	1.1E-10
ENSDARG00000005419	*il1b*	interleukin 1, beta	2.4	1.2E-07
ENSDARG00000053131	*irak3*	interleukin-1 receptor-associated kinase 3	2.6	3.0E-08
ENSDARG00000003523	*itln3*	intelectin 3	3.3	3.6E-24
ENSDARG00000033227	*lect2l*	leukocyte cell-derived chemotaxin 2 like	2.3	1.3E-14
ENSDARG00000090557	*mfap4 (6 of 13)*	microfibrillar-associated protein 4	1.9	2.5E-06
ENSDARG00000012395	*mmp13a*	matrix metalloproteinase 13a	2.0	2.8E-09
ENSDARG00000042816	*mmp9*	matrix metalloproteinase 9	2.7	1.6E-23
ENSDARG00000031136	*moxd1*	monooxygenase, DBH-like 1	1.6	3.3E-06
ENSDARG00000074322	*olfn4 (3 of 8)*	olfactomedin 4	1.5	6.0E-04
ENSDARG00000016188	*sbno2 (2 of 3)*	strawberry notch homolog 2 (Drosophila)	1.3	6.6E-05
ENSDARG00000092826	*si:ch211-243g18.3*	non-coding RNA	4.3	3.7E-06
ENSDARG00000090352	*si:dkey-97i18.5*	non-coding RNA	2.4	2.4E-16
ENSDARG00000059805	*slc25a38a*	solute carrier family 25, member 38a	2.0	1.2E-04
ENSDARG00000055252	*snap23 (2 of 2)*	synaptosomal-associated protein, 23kDa	1.6	7.6E-04
ENSDARG00000055901	*steap4*	steap family member 4	1.4	5.8E-05
ENSDARG00000007344	*tcap*	titin-cap (telethonin)	2.2	1.2E-13
ENSDARG00000075261	*timp2b*	tissue inhibitor of metalloproteinase 2b	1.4	4.9E-05

* List of 33 genes that consistently showed significant up-regulation during *M. marinum* infection in at least three out of four independent experiments (adjusted P-value <0.01). AB/TL embryos were injected with control morpholino, subsequently injected with mCherry-expressing *M. marinum* Mma20 strain, and infected embryos and uninfected controls were subjected to RNAseq analysis at 4 dpi.

Chapter 7

Summary and discussion

Tuberculosis is a life-threatening disease caused by infection with the bacterial pathogen *Mycobacterium tuberculosis*. Approximately one third of the world population is infected with *M. tuberculosis* and research of the World Health Organisation demonstrates that tuberculosis is second only to human immunodeficiency virus infection/acquired immunodeficiency syndrome (HIV/AIDS) as the greatest killer worldwide due to a single infectious agent. Although tuberculosis can be treated with four antimicrobial drugs, multidrug resistant strains are emerging world-wide. This highlights the need to increase our knowledge on how the host's immune system contributes to combating the mycobacterial infection. *M. tuberculosis* is a pathogen that is able to subvert the killing mechanisms of macrophages and can replicate intra-cellularly in this cell type. Central to the pathology of tuberculosis is the formation of granulomatous aggregates of infected and non-infected macrophages and other immune cells [1]. These granulomas provide a niche for the long-term survival of the pathogen inside its host. Studying this pathological hallmark of the disease requires whole organism models. Many animal models for tuberculosis are used, each having specific advantages as well as limitations [2, 3]. For example, a wealth of immunological tools is available for research in mice, but *M. tuberculosis* is not a natural pathogen of rodent species, and mice do not form the highly structured granulomas that are seen in human patients. In the recent years, the zebrafish has emerged as a new animal model for tuberculosis. Zebrafish develop tuberculosis following infection with a close relative of *M. tuberculosis*, namely *Mycobacterium marinum*. Granulomas in the zebrafish structurally resemble the human tuberculous granuloma and the transparent early life stages of the zebrafish proved to be a highly versatile model system to study the early events in granuloma formation [4-7] (**chapter 2**).

Morpholino screen identified candidate innate immune genes involved in *M. marinum* infection

To identify innate immune host genes involved in controlling mycobacterial growth during early stages of infection when granulomas are being formed we set up a morpholino-based knockdown screen. This screen identified 5 reproducible hits out of the 17 candidate genes analysed that demonstrated either an increased or decreased infection of *M. marinum* after knockdown (**chapter 3**). These hits provided a basis for further in-depth analysis to identify which step of the infection process is affected and which genes and pathways are influenced, as demonstrated subsequently in chapters 4, 5, and 6 for the hit genes *marco*, *mpeg1*, and *atf3*, respectively.

Time-resolved transcriptome analysis of *M. marinum* infection and the function of the inducible transcription factor Atf3

To increase our knowledge about the infection process of *M. marinum* we analysed RNA sequencing gene expression profiles throughout a time course of *M. marinum* infection every 2 hours until 8 hours post infection and daily from 1 until 5 days post infection,

and interrelated these to the observed characteristic host-pathogen interactions at specific time points (**chapter 4**). This analysis revealed that there is an early-, mid-, and late-phase response during *M. marinum* infection (fig. 1). The early-phase response is observed until 4 hpi during which macrophages phagocytose the *M. marinum* and travel through the vascular system. This phase was characterised by rapid induction of transcription factors and a subsequent transient peak of pro-inflammatory gene expression. This is followed by a mid-phase response between 6 hpi and 1 dpi during which infected macrophages could be seen to still travel through and occasionally leave the vascular system and the expression levels of most genes return to uninfected control levels. Such a 'silent' mid-phase is in sharp contrast with the response to an acute pathogen, like *S. typhimurium*, where expression levels of pro-inflammatory genes strongly increase over the same time frame [8]. Finally, there is a late-phase response with a progressive increase in differential gene expression between 2 dpi and 5 dpi when granuloma-like aggregates start forming containing increasing numbers of uninfected and infected macrophages with an occasional infected neutrophil. It was clear that the transition between the mid-phase and late-phase (2 dpi) is associated with strong metabolic changes. At 4 dpi many infected macrophages start dying and at 5 dpi the granuloma contains high numbers of infected and uninfected neutrophils. This period was characterised by increasing expression levels of the same genes that were induced during the early-phase response and many other inflammation-associated genes. The zebrafish infection model has previously shown that susceptibility to *M. marinum* can result from either inadequate or excessive acute inflammation balance in immune response [9]. Therefore it is not surprising that concomitant with the induction of pro-inflammatory genes and transcriptional activators, we found numerous negative regulators of innate immunity signalling pathways to be up-regulated during early- and late-phase infection. Of interest is the expression profile of complement components because they are up-regulated consistently throughout the infection, even at the mid-phase when other immune related genes show baseline levels. Similar to other expression profiles, the complement components are also increasingly induced during the late-phase. Furthermore, a striking regulatory pattern was observed of a group of apolipoprotein genes that is the exact opposite of that of pro-inflammatory genes, showing down-regulation during the early- and late-phase and up-regulation during the mid-phase. This could be an interesting group of genes to study further in more detail because they have previously been linked to mycobacterial infection by their suggested function in transferring antigenic lipids from cell to cell, thereby enabling the mycobacteria to elicit their influence beyond the cell that contains them [10, 11].

One of the transcription factor genes up-regulated during the early- and late-phase of infection is *activating transcription factor 3* (*atf3*), which in mice is known to function as a transcriptional repressor of genes involved in the immune response [12, 13] and is used as an ER stress marker that is expressed in the macrophage-rich area of *M. tuberculosis*-induced granulomas [14]. Embryos in which *atf3* is knocked down have a decreased *M. marinum* infection (**chapter 4**), however, we did not observe a strong effect on the

transcriptional signature in these morphants. Instead, we found that Atf3 functions in suppressing macrophage and neutrophil migration towards local damage-induced inflammation sites. To determine whether *atf3* morphants also recruit higher numbers of macrophages and neutrophils to the forming *M. marinum* granuloma, an important process in granuloma formation, we imaged this process in a double transgenic zebrafish line with fluorescent macrophages and neutrophils. Knockdown of *atf3* resulted in an attenuated infection level as soon as 2 dpi and leukocyte numbers seemed to be increased around the infection locations at 1 and 2 dpi. This suggests that increased leukocyte recruitment during the early stage of infection might be responsible for better restriction of *M. marinum* growth in *atf3* morphants. Although further research is necessary to determine the mechanism of Atf3 function during *M. marinum* infection our results indicate that the induction of *atf3* during *M. marinum* infection antagonises an effective innate immune control of this pathogen.

Marco functions in phagocytosis of *M. marinum* and controls the hosts pro-inflammatory signalling response to *M. marinum* infection

The first line of defence against *M. tuberculosis* is phagocytosis by macrophages and it has been shown in mice that the Scavenger receptor MARCO plays an assisting role in this process by binding to the cell wall component glycolipid trehalose 6,69-dimycolate (TDM) of this pathogen [15]. Furthermore, recent studies on single nucleotide polymorphisms (SNPs) in humans have identified MARCO to be associated with increased susceptibility to tuberculosis [16, 17]. We used the zebrafish tuberculosis model to study the function of Marco during *M. marinum* infection. Using two independent morpholinos we demonstrated that Marco is a key player in the rapid phagocytosis of *M. marinum* following intravenous injection of the pathogen (**chapter 5**, fig. 1). This response was specific because knockdown of a second scavenger receptor, *cd36*, had no effect on phagocytosis. The presence of multiple other receptors that can initiate phagocytosis of mycobacteria [18-20] indicates how remarkable it is that knockdown of a single receptor leads to a significant delay in phagocytosis.

After TDM binding to MARCO in mice, it was demonstrated that TLR2 signalling pathways were activated in response to the mycobacteria. This response also required the co-receptor CD14 which is suggested to enhance the proximity of mycobacteria to the receptor complex [21-23]. We showed that Marco in zebrafish functions as an essential player in the establishment of an initial transient pro-inflammatory response to mycobacteria at 4 hours after infection (**chapter 5**, fig. 1); however, it is likely that a parallel Marco-independent signalling route exists because knockdown of *marco* did not block the *M. marinum*-induced pro-inflammatory response completely. In addition, the accessory molecule CD14 does not exist in the zebrafish genome indicating that Marco is capable of functioning independently of the co-receptor CD14 in mediating a pro-inflammatory response to *M. marinum.* Further research is therefore necessary to identify the exact signal transduction pathway associated with Marco in zebrafish.

In addition to the immediate effects on phagocytosis and cytokine induction, knockdown of *marco* lead to a significant increase in mycobacterial burden during development of infected larvae. The delayed phagocytosis of *M. marinum* in *marco* morphants could be a reoccurring process because highly infected macrophages are known to die and be phagocytosed by newly recruited macrophages, a process in which Marco may also play a role (fig. 1). We hypothesise that the accumulated delay in reoccurring phagocytosis of *M. marinum* in combination with the dampened initial pro-inflammatory response to *M. marinum* infection leads to an inability of the embryos to control the infection sufficiently which leads to the observed higher bacterial infection in the *marco* morphants.

Mpeg1 and Mpeg1.2 have anti-bacterial functions in zebrafish

Membrane Attack Complex/Perforin (MACPF) proteins play a crucial role against phagocytosed pathogens by forming pores either directly on the surface of invading bacteria or in the plasma membranes of infected and transformed host cells, allowing the entry of cytolytic proteins. Macrophage expressed gene 1 (*MPEG1*) belongs to the superfamily of MACPF containing proteins and is conserved between human, mouse and zebrafish. In addition to *mpeg1*, the zebrafish genome also contains an *mpeg1.2* and *mpeg1*.3 gene as a result of gene duplication, although based on our expression data *mpeg1.3* seems to be a pseudogene.

The *mpeg1* and *mpeg1.2* genes are differentially regulated during infection with *M. marinum* and with *Salmonella typhimurium,* another intracellular pathogen that we used as a comparative model in our studies. At different time points after infection with either of these pathogens we observed that *mpeg1* is down-regulated and *mpeg1.2* is up-regulated (**chapter 6**). While our results of increased *M. marinum* infection during knockdown of *mpeg1* are consistent with the expected anti-bacterial function (fig. 1), we also observed an altered immune response to *M. marinum* infection indicating that Mpeg1 might have a broader effect on controlling infection. Knockdown of *mpeg1.2* did not lead to any difference in controlling *M. marinum* infection, which might be explained by the late time point (four days after infection) during which we first observed up-regulation of this gene during *M. marinum* infection. This suggests that Mpeg1.2 functions during the later stages of infection (fig. 1) when the knockdown effects of the *mpeg1.2* morpholino have diminished. To still be able to study the functionality of both Mpeg1 and Mpeg1.2 we used the more acute *S. typhimurium* infection model, in which we observed down-regulation of *mpeg1* and up-regulation of *mpeg1.2* within eight hours after infection. We showed this process to be partially dependent on the presence of functional Mpeg1, and to require the Toll-like receptor adaptor molecule MyD88 and transcription factor NFκB. Knockdown of both *mpeg1* and *mpeg1.2* increased *S. typhimurium* bacterial burdens, but unexpectedly *mpeg1* morphants showed prolonged survival. We hypothesised that the survival advantage of *mpeg1* morphants might be explained by a difference in expression of pro-inflammatory markers, but this was not the case and therefore the underlying cause of this phenotype currently remains

unknown. The combined results of the *M. marinum* and *S. typhimurium* infection models provide *in vivo* support for the anti-bacterial function of the MPEG1 family and indicate that the intricate cross-regulation of the two *mpeg1* copies aids the zebrafish host in combatting infection of various pathogens.

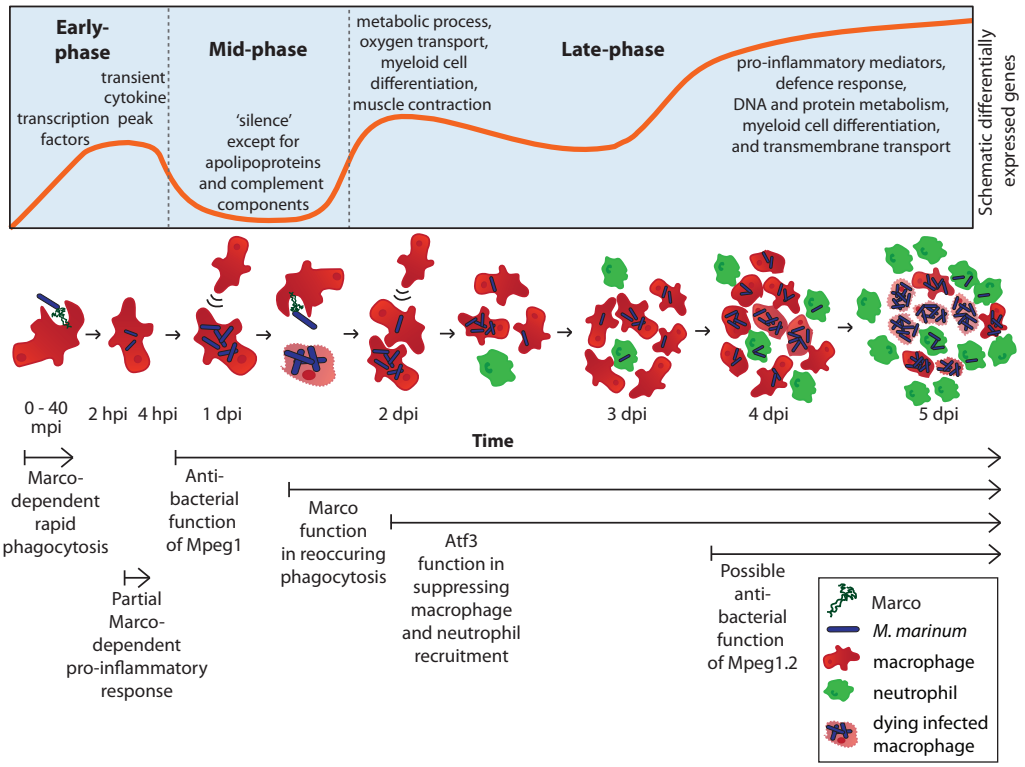

Figure 1: Schematic representation of the host immune response to *M. marinum* infection and function of Marco, Mpeg1 and Atf3 during *M. marinum* infection in zebrafish embryos. A schematic overview representing observed gene expression profile responses (orange line represents total genes up- and down-regulated during infection) and observed host-pathogen interactions. Functional properties of Marco, Mpeg1 and Atf3 are indicated below the time scale of infection.

Conclusion

The work presented in this thesis provides a great amount of information on mycobacterial infection processes which will be of great value for future studies. Providing a better framework for studying innate immune defence in the zebrafish – *M. marinum* model, we have combined a detailed time-resolved description of the host transcriptome response with confocal imaging of the precise events that take place during the process of pathogenesis. Furthermore, a successful morpholino knockdown screen revealed functions for scavenger receptor Marco in phagocytosis and initiation of the innate immune response, anti-bacterial functions for perforins of the Mpeg1

family, and a regulatory role for transcription factor Atf3 in leukocyte recruitment. Thereby, as summarised in figure 1, we have provided new insights into mechanisms involved in processes that either counteract or support the innate immune control of *M. marinum* infection.

References

1. Guirado, E. & Schlesinger, L.S. Modeling the Mycobacterium tuberculosis Granuloma - the Critical Battlefield in Host Immunity and Disease. *Front Immunol* **4**, 98 (2013).

2. Apt, A. & Kramnik, I. Man and mouse TB: contradictions and solutions. *Tuberculosis (Edinb)* **89**, 195-198 (2009).

3. Baldwin, S.L. *et al.* Evaluation of new vaccines in the mouse and guinea pig model of tuberculosis. *Infection and immunity* **66**, 2951-2959 (1998).

4. Davis, J.M. *et al.* Real-time visualization of mycobacterium-macrophage interactions leading to initiation of granuloma formation in zebrafish embryos. *Immunity* **17**, 693-702 (2002).

5. Cosma, C.L., Humbert, O., Sherman, D.R. & Ramakrishnan, L. Trafficking of superinfecting Mycobacterium organisms into established granulomas occurs in mammals and is independent of the Erp and ESX-1 mycobacterial virulence loci. *J Infect Dis* **198**, 1851-1855 (2008).

6. Clay, H. *et al.* Dichotomous Role of the Macrophage in Early Mycobacterium marinum Infection of the Zebrafish. *Cell Host & Microbe* **2**, 29-39 (2007).

7. Volkman, H.E. *et al.* Tuberculous granuloma formation is enhanced by a mycobacterium virulence determinant. *PLoS Biol* **2**, e367 (2004).

8. Stockhammer, O.W., Zakrzewska, A., Hegedus, Z., Spaink, H.P. & Meijer, A.H. Transcriptome profiling and functional analyses of the zebrafish embryonic innate immune response to Salmonella infection. *J Immunol* **182**, 5641-5653 (2009).

9. Tobin, D.M. *et al.* Host genotype-specific therapies can optimize the inflammatory response to mycobacterial infections. *Cell* **148**, 434-446 (2012).

10. Beatty, W.L., Ullrich, H.J. & Russell, D.G. Mycobacterial surface moieties are released from infected macrophages by a constitutive exocytic event. *Eur J Cell Biol* **80**, 31-40 (2001).

11. van den Elzen, P. *et al.* Apolipoprotein-mediated pathways of lipid antigen presentation. *Nature* **437**, 906-910 (2005).

12. Gilchrist, M. *et al.* Systems biology approaches identify ATF3 as a negative regulator of Toll-like receptor 4. *Nature* **441**, 173-178 (2006).

13. Whitmore, M.M. *et al.* Negative regulation of TLR-signaling pathways by activating transcription factor-3. *Journal of immunology* **179**, 3622-3630 (2007).

14. Seimon, T.A. *et al.* Induction of ER stress in macrophages of tuberculosis granulomas. *PloS one* **5**, e12772 (2010).

15. Bowdish, D.M. *et al.* MARCO, TLR2, and CD14 are required for macrophage cytokine responses to mycobacterial trehalose dimycolate and Mycobacterium tuberculosis. *PLoS Pathog* **5**, e1000474 (2009).

16. Ma, M.J. *et al.* Genetic variants in MARCO are associated with the susceptibility to pulmonary tuberculosis in Chinese Han population. *PLoS One* **6**, e24069 (2011).

17. Bowdish, D.M. *et al.* Genetic variants of MARCO are associated with susceptibility to pulmonary tuberculosis in a Gambian population. *BMC Med Genet* **14**, 47 (2013).

18. Schlesinger, L.S. Macrophage phagocytosis of virulent but not attenuated strains of Mycobacterium tuberculosis is mediated by mannose receptors in addition to complement receptors. *J Immunol* **150**, 2920-2930 (1993).

19. Schlesinger, L.S., Bellinger-Kawahara, C.G., Payne, N.R. & Horwitz, M.A. Phagocytosis of Mycobacterium tuberculosis is mediated by human monocyte complement receptors and complement component C3. *J Immunol* **144**, 2771-2780 (1990).

20. Hirsch, C.S., Ellner, J.J., Russell, D.G. & Rich, E.A. Complement receptor-mediated uptake and tumor necrosis factor-alpha-mediated growth inhibition of Mycobacterium tuberculosis by human alveolar macrophages. *J Immunol* **152**, 743-753 (1994).

21. Brightbill, H.D. *et al.* Host defense mechanisms triggered by microbial lipoproteins through toll-like receptors. *Science* **285**, 732-736 (1999).

22. Manukyan, M. *et al.* Binding of lipopeptide to CD14 induces physical proximity of CD14, TLR2 and TLR1. *Eur J Immunol* **35**, 911-921 (2005).

23. Nakata, T. *et al.* CD14 directly binds to triacylated lipopeptides and facilitates recognition of the lipopeptides by the receptor complex of Toll-like receptors 2 and 1 without binding to the complex. *Cellular microbiology* **8**, 1899-1909 (2006).

Samenvatting

Verdediging tegen bacteriële infecties door het aangeboren immuunsysteem

Het immuunsysteem speelt een belangrijke rol in de snelle bestrijding van ziekteverwekkers die het lichaam zijn binnengedrongen. Het immuunsysteem is onder te verdelen in twee componenten: het aangeboren immuunsysteem en het adaptieve immuunsysteem. Het aangeboren immuunsysteem is al vanaf de geboorte aanwezig terwijl het adaptieve immuunsysteem zich pas later begint te ontwikkelen. Het zebravisembryo is een uitstekend model om het aangeboren immuunsysteem te bestuderen omdat de embryo's tijdens de eerste ontwikkelingsdagen al actieve gespecialiseerde aangeboren immuuncellen bevatten: macrofagen en neutrofielen, twee belangrijke typen van witte bloedcellen. Hierdoor kunnen specifiek de functies van het aangeboren immuunsysteem bestudeerd worden zonder dat deze beïnvloed worden door het adaptieve immuunsysteem. Bovendien ontwikkelen de embryo's zich buiten de ouderlijke vis en zijn ze doorzichtig waardoor er gemakkelijk kan worden waargenomen wat zich in het binnenste van het embryo afspeelt.

Het zebravisembryo wordt veel gebruikt als model voor onderzoek naar mycobacteriële infectie. Mycobacteriën veroorzaken levensbedreigende menselijke ziekten, waaronder tuberculose en lepra. In het zebravisonderzoeksmodel wordt de bacterie *Mycobacterium marinum* gebruikt, een natuurlijke ziekteverwekker van vissen en nauw verwant aan de menselijke variant ervan: *Mycobacterium tuberculosis*. De meest kenmerkende infectiestructuur van tuberculose is het zogenaamde granuloom, een opeenhoping van geïnfecteerde en niet geïnfecteerde cellen. Het zebravisonderzoeksmodel is erg belangrijk geweest om aan te tonen dat het aangeboren immuunsysteem zelf in staat is om granulomen te laten ontstaan. Voorheen dacht men dat dit alleen plaats kon vinden in aanwezigheid van het adaptieve immuunsysteem. Daarnaast veronderstelde men vroeger ook dat granuloomontwikkeling in gang werd gezet door het immuunsysteem om daarmee de infectie af te schermen van de rest van het lichaam. Zebravisonderzoek heeft inmiddels echter aangetoond dat deze veronderstelling maar ten dele klopt: het is gebleken dat het de bacterie is die het begin van de granuloomvorming aanstuurt en de vroege stadia van de granulomen helpen juist in het verspreiden van de infectie. Deze voorbeelden laten zien hoe belangrijk het is om verschillende modellen te gebruiken om onze kennis van infectieprocessen compleet te maken.

Dit proefschrift is gericht op verdedigingsmechanismen van het aangeboren immuunsysteem die verantwoordelijk zijn voor de controle van mycobacteriële groei na infectie in een zebravisembryo. Daarnaast is ook een andere intracellulaire bacterie, *Salmonella typhimurium*, gebruikt om de rol van immuungenen in verschillende infectieprocessen te vergelijken. Om zebravisembryo's te infecteren met bacteriën

worden speciale injectietechnieken gebruikt die in hoofdstuk 2 en in een videoartikel (www.jove.com/video/3781) verder beschreven zijn. In dit hoofdstuk wordt tevens toegelicht hoe de geïnfecteerde embryo's met geavanceerde microscopen bekeken worden en welke resultaten men kan verkrijgen door toepassing van de verschillende injectietechnieken.

Om te kunnen vastleggen welke immuungenen een rol spelen in het controleren van mycobacteriële groei tijdens de vroege fase van infectie (wanneer granulomen ontstaan), werden verschillende genen die een rol spelen in macrofagen geselecteerd voor nader onderzoek. De macrofaag is een belangrijke cel aangezien deze sterk bijdraagt aan de vorming van granulomen tijdens infectie. Daarnaast werden ook genen geselecteerd waarvan tijdens eerder onderzoek naar voren kwam dat hun expressieniveau gereguleerd wordt tijdens het infectieproces; dit suggereert dat ze in dit proces een rol zouden kunnen spelen. Om te kunnen onderzoeken welke rol dit precies zou kunnen zijn, werd een techniek toegepast waarmee de aanmaak van functionerende eiwitten van deze genen tijdelijk werd uitgeschakeld. Zodoende kon het effect hiervan op de infectie worden bestudeerd. De resultaten van deze experimenten worden verder omschreven in **hoofdstuk 3**. Wanneer bleek dat uitschakeling van één van deze eiwitten leidde tot reproduceerbare resultaten waarbij de zebravisembryo's een ernstigere of juist een verminderde infectie ontwikkelden, werd dit gen beschouwd als veelbelovend voor verder onderzoek naar de exacte functie ervan.

Om een uitgebreide omschrijving te kunnen geven hoe een gastheer reageert op infectie met *Mycobacterium marinum* werd een techniek toegepast genaamd 'RNA sequencing'. Tijdens toepassing van deze techniek wordt het expressieniveau van alle genen waargenomen tijdens opeenvolgende tijdspunten van infectie. De gekozen tijdspunten varieerden van het moment direct na infectie (2 uur na infectie) tot aan latere infectiestadia wanneer de embryo's al granulomen ontwikkeld hebben (5 dagen na infectie). In **hoofdstuk 4** worden deze expressieniveaus vergeleken met opgenomen microscopiebeelden van de infectie in een embryo. Zo kan een link worden gelegd tussen opvallende expressiepatronen enerzijds en anderzijds het zichtbare beeld van interacties tussen bacteriën en immuuncellen op datzelfde tijdspunt. Eén van de opvallende expressiepatronen is dat van *atf3*, een gen dat codeert voor een transcriptiefactor, een eiwit dat de expressie van andere genen reguleert. De inductie van deze transcriptiefactor tijdens infectie met *M. marinum* lijkt gunstig te zijn voor de bacterie maar niet voor de gastheer, aangezien uitschakeling van *atf3* de zebravisembryo's beter beschermt tegen infectie.

In **hoofdstuk 5** wordt de functie van één van de genen die een rol speelt in macrofagen tijdens infectie, nader bestudeerd: de scavenger-receptor 'Marco' (**ma**crophage **r**eceptor with **co**llagenous structure). Scavenger-receptoren spelen een belangrijke rol in het herkennen van bacteriën en het opnemen hiervan door macrofagen. Tijdelijke uitschakeling van *marco* in de zebravisembryo laat zien dat deze receptor niet alleen essentieel is voor het snel opnemen van *M. marinum* door de macrofaag, maar tevens

essentieel is voor de daaropvolgende ontstekingsreactie.

Nadat de macrofaag *M. marinum* heeft opgegeten is de bacterie in staat om de natuurlijke vernietigingsmechanismen van de macrofaag te ontlopen. Zodoende kan de bacterie door blijven groeien binnenin deze cel. Op dat moment komt een ander verdedigingsmechanisme van de macrofaag in actie, namelijk de porie-vormende Mpeg1 en Mpeg1.2 eiwitten (**ma**cro**p**hage **e**xpressed gene 1). **Hoofdstuk 6** laat zien dat beide Mpeg1 eiwitten antibacteriële functies hebben, zowel tijdens infectie met *M. marinum* als met *S. typhimurium*.

In **hoofdstuk 7** worden de bevindingen uit dit proefschrift samengevat en bediscussieerd. De nieuwe inzichten die verkregen werden door toepassing van het zebravismodel, en betrekking hebben op gunstige én ongunstige mechanismen tijdens infectie, dragen bij aan een sterke uitbreiding van onze kennis over het aangeboren immuunsysteem.

List of publications

Zakrzewska A, Cui C, Stockhammer OW, **Benard EL**, Spaink HP, Meijer AH. Macrophage-specific gene functions in Spi1-directed innate immunity. *Blood,* 2010.

Cui C, **Benard EL**, Kanwal Z, Stockhammer OW, van der Vaart M, Zakrzewska A, Spaink HP, Meijer AH. Infectious disease modelling and innate immune function in zebrafish embryos. *Methods in Cell Biology*, 2011.

Benard EL, van der Sar AM, Ellett F, Lieschke GJ, Spaink HP, Meijer AH. Infection of zebrafish embryos with intracellular bacterial pathogens. *Journal of Visualized Experiments*, 2012.

Benard EL, Racz PI, Rougeot J, Nezhinsky AE, Verbeek FJ, Spaink HP, Meijer AH. The macrophage-expressed perforins Mpeg1 and Mpeg1.2 have specialised functions in controlling bacterial infections in zebrafish. *Journal of Innate Immunity,* 2014. In press.

Benard EL, Roobol SJ, Spaink HP, Meijer AH. Phagocytosis of mycobacteria by zebrafish macrophages is dependent on the scavenger receptor Marco, a key control factor of pro-inflammatory signalling. *Developmental and comparative Immunology*, 2014. In press.

Fink IR, **Benard EL**, Hermsen T, Meijer AH, Forlenza M, Wiegertjes GF. Molecular and functional characterization of the scavenger receptor CD36 in zebrafish and common carp. *Molecular Immunology*. Manuscript under revision.

Ellett F, Pase L, **Benard EL**, Azabdaftari D, Andrianopoulos A, Lieschke GJ. An *in vivo P. marneffei* infection model reveals neutrophil-to-macrophage pathogen shuttling between viable leukocytes during infection establishment. Manuscript under revision.

Benard EL, Rougeot J, Racz PI, Spaink HP, Meijer AH. Time-resolved transcriptome profiling of the zebrafish host innate immune response to mycobacterium infection. Manuscript in preparation.

Curriculum vitae

Erica Benard was born on March 5th, 1986 in Westville, South Africa. After moving to Dordrecht, The Netherlands, she completed her high school education at the Insula College Dordrecht. In 2004 she started studying for her BSc in Biology at Leiden University, during which she performed an internship at the Microbiology department (under supervision of Ing. Mark Arentshorst and Dr. Arthur F.J. Ram). During her MSc studies at the same university, she completed two internships, one at the Leiden University at the department of Molecular Cell Biology (under supervision of Dr. Annemarie H. Meijer), and one at the Walter and Eliza Hall Institute of Medical Research, Melbourne, Australia at the Cancer and Haematology Department (under supervision of Dr. Felix Ellett and Prof. Graham J. Lieschke). Shortly after obtaining her MSc degree in 2009 (*cum laude*) she started as a PhD-student in the infectious disease group of Dr. Annemarie H. Meijer at the Molecular Cell Biology department headed by Prof. Dr. Herman P. Spaink. During her PhD-training she studied the innate immune response against intracellular bacterial pathogens, using the zebrafish embryo as a model organism, which resulted in the work before you. In July 2014 she started her postdoctoral research in the laboratory of Prof. Dr. Matthias Hammerschmidt at the Institute for Developmental Biology, University of Cologne, Germany.